Pattern Corotation Radii from Potential-Density Phase-Shifts for 153 OSUBGS Sample Galaxies

Ronald J. Buta

Department of Physics and Astronomy, University of Alabama, Tuscaloosa, AL 35487, USA

Xiaolei Zhang

Department of Physics and Astronomy, George Mason University, Fairfax, VA 22030, USA

Received _____; accepted _____

ABSTRACT

The potential-density phase-shift method is an effective new tool for investigating the structure and evolution of galaxies. In this paper, we apply the method to 153 galaxies in the Ohio State University Bright Galaxy Survey (OSUBGS) to study the general relationship between pattern corotation radii and the morphology of spiral galaxies. The analysis is based on near-infrared H-band images that have been deprojected and decomposed assuming a spherical bulge. We find that multiple pattern speeds are common in disk galaxies. By selecting those corotation radii close to or slightly larger than the bar radius as being the bar corotation (CR) radius, we find that the average and standard deviation of the ratio $\mathcal{R} = r(CR)/r(bar)$, is 1.20±0.52 for 101 galaxies having well-defined bars. There is an indication that this ratio depends weakly on galaxy type in the sense that the average ranges from 1.03±0.37 for 65 galaxies of type Sbc and earlier, to 1.50±0.63 for 36 galaxies of type Sc and later. Our bar corotation radii are on average smaller than those estimated from single-pattern-speed numerical simulations, most likely because these simulations tend to find the pattern speed which generates a density response in the gas that best matches the morphology of the outer spiral structure. Although we find CR radii in most of the sample galaxies that satisfy conventional ideas about the extent of bars, we also consider the alternative interpretation that in many cases the bar CR is actually inside the bar and that the bar ends close to its outer Lindblad resonance instead of its CR. These "super-fast" bars are the most controversial finding from our study. We see evidence in the phase-shift distributions for ongoing decoupling of patterns, which hints at the formation pathways of nested patterns, and which in turn further hints at the longevity of the density wave patterns in galaxies. We also examine how uncertainties in the orientation parameters of galaxies and in

the shapes of bulges affect our results.

Subject headings: galaxies: spiral; galaxies: photometry; galaxies: kinematics and dynamics; galaxies: structure

1. Introduction

There is considerable evidence at this time that internal secular evolution is an important physical process in disk galaxies. Kormendy & Kennicutt (2004) have argued that such evolution accounts for the disk-like "pseudobulges" seen in late-type galaxies, and evidence of bulges built through secular evolution has been found to be present across the entire Hubble-de Vaucouleurs sequence (Laurikainen et al. 2007). Secular evolution can also explain the transformation of galaxy morphological features other than bulges along this sequence. An important engine for the evolution in many cases appears to be the presence of bars, ovals, and spiral structure in disk galaxies. The ability of a bar or oval to drive gas to the central regions of galaxies is often argued as the dominant process involved (Kormendy & Kennicutt 2004), although gas accretion alone is not adequate to produce the significant mass-flow rate needed to transform a galaxy's Hubble type from late to early, nor will it be able to produce the observed stellar content of most bulges (Zhang 2003).

The rate at which a pattern rotates (the "pattern speed") is an important feature in secular evolutionary processes. The pattern speed, together with the rotation curve of the parent galaxy, determines the location of all wave-particle resonances, which in turn influences how a wave interacts with the basic state of a galactic disk.[1] It had been argued by Lynden-Bell & Kalnajs (1972, hereafter LBK) that the wave/basic-state interaction which loads and unloads the angular momentum onto the density wave train for its outward transport can only happen at wave-particle resonances for a quasi-steady wave pattern. This angular momentum transport is believed to be necessary for the generation of spirals,[2], but

[1]The term basic state refers to the axisymmetric disk when the density-wave modal density distribution is subtracted.

[2]Thus, the reason for the title of the original LBK paper "On the Generating Mechanism of the Spiral Structure."

wave/basic-state interaction across the entire galactic disk, and the role of this wide-spread interaction to the maintenance of a quasi-steady spiral structure and to the long-term evolution of the basic state, were not addressed in LBK.

Zhang (1996, 1998, 1999) showed that stars must also be involved in the secular evolutionary process of a galaxy and furthermore should be a major part of the mass redistribution process which grows bulges and transforms galaxy morphologies. To enable the participation of stars, which were traditionally thought to be adiabatic and non-dissipative, required a significant breakthrough in our understanding of the physical processes occurring in so-called self-organized large scale structures of which spirals and bars are examples. The new secular dynamical evolution mechanism discovered in Zhang (1996, 1998, 1999) operates mainly through spontaneously formed quasi-steady spiral and bar *modes* which, when interacting with the basic state of the galactic disk, slowly transforms a galaxy's morphology over its lifetime due to a collective dissipation process[3] enabled by an azimuthal phase-shift between the density-wave modal density distribution and the potential distribution implied by that density. In spite of the importance of the potential-density phase-shift for studies of galactic evolution, the topic is not discussed even

[3]The "collective dissipation" process in a galaxy possessing a spontaneously formed density wave pattern leads to the "graininess" effect of the stellar potential, which breaks the conservation of the Jacobi integral or the adiabatic condition of a single stellar orbit, and enables the secular orbital decay or increase needed for secular evolution. Since this process involves the coordinated motion of all the individual stars on the disk, it could not be regarded as a kind of "broadening of resonances" effect due to fluctuating wave amplitudes because the latter effect is due to the single orbit's *passive* response to an *applied*, smooth, large-scale perturbation potential. Other evidences that these two points of view are incompatible are given later in the Discussion section of the current paper.

in the latest edition of *Galactic Dynamics* (Binney & Tremaine 2008). S. Tremaine (private communication, 2008) stated that the reason for this omission is that the Zhang papers argue that there must be wave/basic-state interaction all across the disk of a spiral galaxy, and not just at the resonances, which is contrary to the widely-accepted claim of the LBK paper. Without this wide-spread angular momentum exchange between the basic state and the wave, however, it is unlikely there could be the continuous mass flow and basic state change needed to gradually transform galaxy morphologies across the Hubble time[4].

---

[4]Note that what LBK derive, and the Binney and Tremaine book (equation [6.56] or Appendix J) insists on, is that the outward angular momentum flux is a constant across the disk for a steady wave, and this conclusion is also consistent with (in fact equivalent to) their other claim that the angular momentum exchange between the wave and the basic state happens only at the wave-particle resonances. This means the wave does not pick up angular momentum from most of the disk stars *en route* of its outward transport, and therefore the stars over most of the disk area cannot lose/gain their angular momentum and accrete/excrete. These conclusions of LBK and Binney and Tremaine were all derived for a steady *wave train* under the tightly wrapped WKBJ approximation. Zhang (1998) on the other hand has shown that the *total* (gravitational *plus* advective) angular momentum flux for a spontaneously-formed, open spiral *mode* is NOT a constant, but rather of the shape of a bell peaked at corotation. Thus the gradient of this flux, which is proportional to the angular momentum exchange rate of the wave with the basic state, is no longer zero across most of the area of the disk, which enables galaxy-wide mass accretion and excretion. Evidence for the bell-shaped angular momentum flux was also seen in the Gnedin, Goodman & Frei (1995) calculation for M100, though there only the gravitational angular momentum flux contribution (or gravitational torque couple) was calculated and not the advective contribution, so the shape of the total angular momentum flux could not be inferred. Plus, since

In a previous paper (Zhang & Buta 2007, hereafter paper I; see also Zhang 1996), we showed that the theoretically-expected potential-density phase-shifts for spiral/bar modes can be measured from near-infrared images of galaxies; furthermore, the corotation radii determined through the zero-crossings of the radial distribution of phase-shift are arrived at without need of the measurement of actual kinematics. The idea is that the sign of the phase-shift tells us in what sense angular momentum is exchanged between a density wave mode and the basic state of a galaxy, and the sign of the phase-shift has to change across corotation because the sense of angular momentum density itself changes sign across corotation. Without the mutual consistency of these two sets of signs, a spiral/bar mode will not be able to spontaneously emerge out of an originally featureless disk, as shown in Zhang (1998). We confirmed in paper I that if a single steady pattern with a well-defined pattern speed actually exists in a galaxy disk, then the radius where the phase-shift changes from positive to negative appears to be the location of that pattern's corotation radius. If instead multiple patterns with differing pattern speeds exist in a single disk galaxy, then multiple positive-to-negative (P/N) crossings would be seen marking the locations of corotation radii for the individual modes, and the radii where patterns with different

---

these authors deliberately chose not to adopt any dynamical model for the interpretation of their results, Gnedin et al. (1995) made no comments (and apparently had no realization) of the significance of this peak. We have found recently, however, that the radial location of this peak, at about 135-140" (see Figure 7 of Gnedin et al. 1995), coincides almost exactly with that found by Zhang & Buta (2007) for the outer CR location of this galaxy, (see Figure 8, left frame of Zhang & Buta 2007). This near coincidence of our CR location derived using the phase shift method, and the peak of the bell-shaped gravitational torque couple derived independently by Gnedin et al. is a strong support for the arguments presented in Zhang (1998), which was also confirmed by the N-body simulations presented there.

pattern speeds decouple would be seen as negative-to-positive (N/P) crossings – once again using the sign of angular momentum density argument. N/P crossings are further discussed in section 2.1.

In practice, we have to exercise considerable judgment in interpreting phase-shift distributions. Our working assumption is that we are dealing with quasi-steady wave modes. If the modes are not steady (e.g., out of equilibrium, transient, or too young and unsettled) the method will not give a reliable corotation radius. Nevertheless, we found that we can identify those galaxies for which our working assumption is likely to be incorrect, through signatures of the lack of pattern and phase shift coherence. Pattern coherence and phase-shift-plot coherence seem to be well correlated, and both of them usually tell the same story of whether the pattern is likely to be steady or not, or else in the process of decoupling. Also, less steady patterns should introduce more noise into the phase-shift plots.

In this paper, we apply the phase-shift method to a much larger sample of galaxies than in paper I: the Ohio State University Bright Galaxy Survey (OSUBGS; Eskridge et al. 2002). This survey includes all RC3 (de Vaucouleurs et al. 1991) galaxies having a type in the range S0/a to Sm (or stage index $0 \leq T \leq 9$), total blue magnitude $B_T \leq 12.0$, blue light isophotal diameter $D_{25} \leq 6'.5$, and declination in the range $-80^\circ < \delta < +50^\circ$. The whole OSUBGS has 205 galaxies, but our analysis is based on a subset of 153 OSUBGS galaxies having inclinations less than 65^o (Buta, Laurikainen, & Salo 2004). Several close pairs were excluded from our analysis. The images we used were obtained with the 1.65μm H-band filter, and were deprojected by Laurikainen et al. (2004) assuming the bulges are spherical. Our goals are to examine the statistics of the density wave patterns in normal, massive galaxies, and to get a general picture of the role these patterns are actually playing on the morphological evolution of the disks of the galaxies. We also seek to demonstrate the

robustness of the phase-shift method by examining the impact of deprojection uncertainties on the phase-shift distributions, and by correlating the coherence of the phase-shift distribution with the coherence of the density wave pattern itself.

2. Comments on the Physical Basis of the Method and the Calculation Procedure

A fair questioning of the validity of the potential-density phase-shift method is that it is used to determine a partially kinematic feature, i.e. the corotation radii, in the absence of any direct kinematic data. The reason this is possible is because there are two kinds of phase-shifts: one is predicted by the Poisson equation after integrating the density, while the other is predicted by the equations of motion. *For a self-sustained mode, these two have to give a phase-shift distribution across the galactic radii that agree*, i.e., the density distribution and the velocity field distribution have to achieve global self-consistency to lead to a single phase-shift distribution. This means that neither the density distribution nor the velocity field of a mode can be of an arbitrary shape. It is why we can predict a partially kinematic quantity such as corotation radii from the density field alone, because *in physical galaxies the requirement of global self-consistency has presumably already been satisfied.*

The explicit demonstration that stellar orbital motion for a spiral mode requires that the phase-shift changes sign at corotation is from Zhang (1996, second Appendix). There the orbital solution itself diverges at exactly the corotation radius due to the passive-orbit resonance condition. The fact that for collective modes the phase shift actually goes through zero-crossing at corotation, as well as changes sign, is demonstrated in Zhang (1998), where the relation of the phase-shift to the flux of total angular momentum across the disk is established. Since the angular momentum flux is of the shape of a bell with the top of the bell at corotation, and the sine of the phase-shift is shown to be proportional to the angular

momentum flux gradient (derivative), then the phase-shift distribution both changes sign and goes through zero at CR because this is exactly the behavior of the derivative of the bell-shaped angular momentum flux.

Kalnajs (1971) showed that for a pure logarithmic spiral, the phase-shift is actually a constant across all disk radii – a well-known result of the potential theory which has been reviewed in the book by Snow (1952). The fact that even though the potential theory predicts a constant phase-shift value whereas a spiral *mode* has a variable phase-shift, changing sign and crossing zero at CR, is because the modal density distribution is not that of a single logarithmic spiral of a constant trend of radial density falloff. The modal shape is carefully balanced globally during the self-organization process to allow all the required properties, including phase-shift distributions, to be satisfied simultaneously. In fact, Zhang (1998) showed that a phase-shift distribution that has such a changing shape across the disk is the only possible one which allows the mode to spontaneously emerge. No other phase-shift distribution would be compatible with the mode creating itself from nothingness.

The phase-shift for any galaxy is defined by equation (3) in paper 1, which was first obtained in Zhang (1996, 1998), and this definition involves the integral of the product of the density and the derivative of the gravitational potential. Our analysis begins with a deprojected near-infrared image sampled into a square array with dimension chosen a power of 2. This array is most often assumed to be proportional to the density distribution for a constant mass-to-light ratio (we have verified in Paper 1 that a variable mass-to-light ratio does not significantly change the corotation radii determined by the phase-shift method). The density array is then used to calculate a gravitational potential array using an approach similar to that of Quillen, Frogel, & González (1994). The phase-shift distribution ϕ_o versus galactic radius is derived using these density and potential square arrays re-sampled

onto a polar grid, and the graph is analyzed for P/N crossings. As noted in paper I, the phase-shift does not "know" the sense of rotation of a galaxy, but we deduce this by noting the sense of winding of the spiral pattern, S or Z, assuming the arms are trailing (this is generally a safe assumption, but exceptions to this rule do exist, such as the case NGC 4622 treated in Paper I). Furthermore, in practice we limit the phase-shift analysis to $r < r_o(25) \equiv D_o(25)/2$, where $D_o(25)$ is the extinction-corrected isophotal diameter at the surface brightness μ_B=25.0 mag arcsec^{-2} from RC3.

The appearance of a phase-shift distribution can be smooth or noisy. A noisy distribution does *not* necessarily result from a poor or noisy image, but often appears to indicate the presence of unsteady patterns. At large radii, image noise can also contribute. Ideally, we visualize a smooth curve through the distribution. To evaluate the significance of all suspected CR radii, we overplot circles on the deprojected near-IR (and, if available, optical) images. We deduce which radii are likely to be real CRs by comparing actual density wave patterns like bars, ovals, and different spirals on the images with the P/N crossing radii on the phase-shift plot. In cases of potential multiple pattern speeds, we sometimes see in the phase-shift plots evidence for ongoing pattern decoupling which doesn't have a clear P/N crossing (or only a weak/shallow crossing) but which shows some form of "bumpy" feature, the location of which corresponds to an actual morphological feature on the image.

The reason we might see "near-crossings" for some features rather than full crossings is that decoupling is likely to be a gradual process that occurs in stages. We do not expect a strong P/N crossing until a pattern has completely distinguished itself. In fact, we suggest that the formation of multiple zero crossings in the phase-shift distribution can be understood in terms of an evolutionary sequence, such as is shown in Figure 1. In Phase 1, a bar and spiral share the same pattern speed and have a single CR which has been

arbitrarily set at $r/r_o(25)$=0.5 (arrow). Except for a small inner pattern, the bar extends from $r/r_o(25)\approx$0.1 to the beginning of the spiral at 0.5. Over time, the inner part of the bar begins to decouple from the spiral, as shown in Phase 2. This leads to a near-crossing at $r/r_o(25)\approx$0.3-0.4. Eventually, the inner part of the bar decouples more completely from the spiral and a well-defined crossing is seen (Phase 3), again at $r/r_o(25)\approx$0.3-0.4. The three curves in Figure 1 are based on NGC 7479 (Phase 1), NGC 613 (Phase 2), and NGC 4593 (Phase 3). The curves have all been scaled to give the main CR at $r/r_o(25)$=0.5. Besides the possibility depicted here, other pathways for the formation of nested patterns are possible.

2.1. N/P Crossings and Mode-Decoupling

In the case of nested patterns, we have argued that N/P crossings indicate where an inner pattern and an outer pattern decouple, i.e., where they start to have different pattern speeds. For some galaxies, there is evidence that these N/P crossings could extend as far as the outer Lindblad resonance (OLR) of the inner mode, although this has not been found to be universal. For a bar and a spiral, this seems at odds with conventional thoughts on mode couplings, where the inner Lindblad resonance (ILR) of an outer spiral mode coincides with the CR of an inner bar mode (e.g., Massett & Tagger 1987), although Rautiainen & Salo (1999) have shown that other matchings of resonance locations of the inner and outer modes (such as CR-inner 4:1 or OLR-ILR) are possible. The reason an N/P crossing could be at a location outside the CR of the inner mode and possibly extend all the way to its OLR is that the complete mode usually has negative angular momentum density inside CR, and positive angular momentum density outside CR until the OLR is reached. A positive phase-shift distribution supports the growth of the portion of the mode inside CR, and a negative phase-shift distribution supports the growth of the portion of the mode outside

CR (both these phase-shift senses allow the torquing of the density by the potential in the right direction to remove/inject angular momentum from/to the mode to enhance its growth). The negative portion of the phase-shift distribution thus definitely belongs to the inner mode and not the outer one, and it ought to have the same pattern speed as the inner one. Whether it extends all the way to the OLR of the mode or not is found to vary for individual galaxies, and this should be studied in detail in galaxies where kinematic data as well as good images are both available. But in principle, if a mode sustains itself between its ILR and OLR, the phase-shift distribution should be one-positive/one-negative hump and the corresponding radial angular momentum flux is shaped like a bell.

3. Phase-Shift Distributions

We have examined the phase-shift distributions for 153 OSUBGS galaxies (see Eskridge et al. 2002 for details about the survey) based on the publicly-available H-band (1.65μm) images. The deprojected versions of these images were kindly made available to us by E. Laurikainen (see Laurikainen et al. 2004). The images were prepared by cleaning the originals of foreground and background objects, assessing the sky background subtraction, fitting ellipses to optical isophotes where possible and matching these fits to the H-band, using two-dimensional decomposition to characterize the bulges and derive disk radial scale-lengths, and finally deprojecting the galaxies using mean orientation parameters from the ellipse fits and assuming a spherical shape for the bulge. The latter assumption is incorrect in many galaxies and when applied causes light to be oversubtracted from the minor axis. This leads to what we refer to as "decomposition pinch" or "spherical bulge pinch" in the inner regions of the deprojected images. We found that this has some effect on our analysis, especially for the most inclined galaxies in the sample. To minimize its impact, we use what we call an "average bulge image", that is, an image based on an average of

the deprojected image we get assuming a spherical bulge and the deprojected image we get assuming the bulge is as flat as the disk. Most bulges have a flattening intermediate between these two extremes, and this approach provides a better approximation than either extreme does. This is discussed in more detail in section 5.2.

For each galaxy, we illustrate the phase-shift distribution versus the normalized radius, $r/r_o(25)$, as given in the left-hand-side plots of Figures 2.1 to 2.153. On each plot, slanted arrows indicate phase-shift zero crossings we believe to be significant. There are some zero crossings that we believe to be due to image noise, or are otherwise insignificant due to the non-steady nature of the patterns. These we have not compiled. Also, almost half the plots show negative phase differences just outside a crossing having $r{\approx}0''$, with no corresponding inner positive phase differences, possibly indicating nuclear patterns unresolved by our current images/analyses. We have also not compiled most of these. The significant zero crossings are taken to be corotation radii and all are compiled in Table 1 in arcseconds. For some galaxies, only a single crossing is found, while for others we can identify as many as five likely significant crossings. In general, we gave a code to each crossing as a judgment of its significance: code 3 crossings are taken to be most significant. Code 1 crossings are less secure, and we tended to ignore any crossings close to the outer r_o unless we could identify an actual pattern at such radii. Table 1 also summarizes some of the scatter in crossing positions. Sharp crossings have no error indicated, while for noisy crossings, the number under the column "err" is a standard deviation of several close crossings. The reason we cannot assign a general error bar for our approach (even for sharp crossings) is the difficulty of judging (quantitatively) how self-consistent and how steady a given mode is. We can only judge by eye how coherent the pattern and the phase-shift plot are, and how well the features correspond to one another. However, one trend we do find is that for very straight bars, because of the smallness of the resulting phase shift values, the absolute values of the determined CR locations are more prone to deprojection error than those for more open or

skewed patterns.

Table 1 also includes judgments of the bar corotation radii, indicated by an asterisk following the value. In some cases, an alternative interpretation is indicated by the value in boldface. These choices are discussed further in section 5.1.

To the right of each phase-shift plot, we show the deprojected H-band image of the galaxy with red circles overlaid showing how the corotation radii relate to features seen in the galaxies. Code 3 radii are shown by full red circles while code 1 radii are shown by dotted circles. In several cases, a significant N/P crossing is indicated by a green circle. In many cases, we can see clear relationships to observed patterns, such as bars or different spiral patterns. These are discussed individually for each galaxy.

Almost all of our phase-shift distributions are calculated using the Laurikainen et al. (2004) deprojected images, Fourier-smoothed by 21 terms to reduce some of the image noise (Buta et al. 2005). The phase shift calculations are made using a numerical procedure originally developed in Zhang (1996), and adapted to the current project during the work on Paper I.

4. Description of Individual Galaxies

Note: radii discussed are given in arcseconds, but to facilitate comparisons with the phase-shift plots, the normalized radius is also given in parentheses.

NGC 150 (Figure 2.1) - A galaxy with a well-defined bar and spiral pattern. The best defined P/N crossing is at r=38″ (0.33, solid red circle), which mostly encircles the bar ends. A second crossing at r=72″ (0.62, dotted red circle) is less certain and could signify a decoupling of the main spiral from the bar. Also, at r=13″ (0.11), the inflection in the positive phase-shift indicates the decoupling of an inner pattern (the bar-like feature in the

image) in progress. We show in section 5.2 that the "spike" seen at r/r_o=0.06 is likely due to decomposition pinch (see section 3).

NGC 157 (Figure 2.2)- The phase-shift distribution shows three well-defined P/N crossings, suggesting all patterns are fully decoupled and have reached quasi-steady state. The CR for the main inner pattern is at r=40″ (0.31) and for the outer pattern is at r=73″ (0.57). The graph in Figure 8 shows that these radii each correspond to a peak in the amplitude of the m=2 component of the H-band light distribution. For comparison, the dynamical model of Sempere & Rozas (1997) gave a single corotation radius of 50″, intermediate between our two values.

NGC 210 (Figure 2.3)- Classified in the de Vaucouleurs Atlas of Galaxies (deVA, Buta et al. 2007) as (R'_2)SAB(s)b, the implication is that NGC 210 has an OLR subclass feature in its outer regions. In the H-band, the outer pseudoring is mainly an R_1 component. The phase-shift distribution is complicated but we can identify several features. First, there is a likely decoupling inner pattern at r=6.″4 (0.04). In fact, in blue light there is a nuclear feature of approximately this size (Buta & Crocker 1993). The main nonaxisymmetric feature in NGC 210 is a large oval which is associated with two crossings: one at 37″ ±4″ (0.25), and a second crossing at 81″ (0.54). There is isophote twisting in this feature, which could be the result of two pattern speeds or else continuous pattern shearing. The larger crossing appears to circle through the lower density regions perpendicular to the oval axis, and from this CR two spiral arms appear to be emanating. This seems to support the idea of an OLR subclass feature since the outer pseudoring lies outside the larger CR. Neither crossing is cleanly-defined, which might be an indication of residual on-going decoupling and pattern shearing.

NGC 278 (Figure 2.4) - This high surface brightness galaxy has an inner spiral pattern that has been interpreted as a nuclear ring (Knapen et al. 2004). We find a well-defined

P/N crossing at r=25″ (0.34) that just encompasses this feature.

NGC 289 (Figure 2.5) - The complicated phase-shift plot shows several P/N crossings. The first, at $r\approx$4″ (0.03), is ill-defined, but we believe it is real because there is a prominent N/P crossing at $r\approx$12″ (0.08). The overlay image shows that the crossing at r=21″ (0.13) encircles the ends of an inner oval. Another major crossing near r=66″ (0.42) signifies a decoupled outer spiral pattern. This galaxy has extensive spiral structure at large radii (deVA), which could account for the outermost crossing near r_o.

Rautiainen et al. (2008; hereafter RSL08; see also Rautiainen et al. 2005, hereafter RSL05) obtained a fairly good representation of the inner spiral structure of NGC 289 for a pattern speed placing $r(CR)$ at 61″ (0.39), which is very close to our third CR. Their estimated bar radius of 23.″8 (0.15) is very close to our second CR. Thus, it is likely that Rautiainen et al. have derived the spiral pattern speed and not the bar pattern speed.

NGC 428 (Figure 2.6) - A very late-type galaxy whose sense of unwinding is uncertain but which appears to be "Z" in optical images. The phase-shift distribution shows a well-defined crossing at r=55″ (0.45) that circles around the ends of an oval bar feature.

NGC 488 (Figure 2.7) - there is a well-defined crossing at r=70″ (0.43) that could be associated with a tightly-wrapped spiral. The crossing at r=34″ (0.21) could be associated with a weak inner oval. There is also the evidence of a decoupled nuclear pattern. Other crossings are of uncertain significance and could be an indication of on-going pattern decoupling.

NGC 578 (Figure 2.8) - The two innermost P/N crossings for this galaxy are most likely to be significant. The first, at r=19″ (0.13), encircles just beyond the ends of the bar of the galaxy. The second, at r=39″ (0.27), is associated with a bright inner spiral. The crossings at r=80″ (0.54) and 135″ (0.92) are uncertain because they occur either near the

RC3 isophotal radius or are associated with an indistinct pattern of large patches.

The RSL08 survey gave $r(CR)$=78.″9 (0.54), which corresponds almost exactly with our third CR. Their bar radius of 23″ (0.16) is close to our first CR.

NGC 613 (Figure 2.9) - We believe this galaxy is a strong case of a pattern evolving from a bar-driven spiral to a decoupled inner bar and outer spiral. The phase-shift plot shows first of all that there is a pattern in the central regions that is almost decoupled from the outer regions. In the near-IR image, there is in fact a small central bar nearly aligned with the main bar in this region. This feature is also interpreted as a nuclear ring by Mazzuca et al. (2008.) Well outside this area are two more crossings, the one at r=55″ (0.33) being shallow while the one at r=88″ (0.53) is well-defined. The shallowness of crossing 2 is what suggests on-going decoupling. The r=55″ crossing encircles the inner part of the apparent bar, while the r=88″ crossing encircles the whole bar and part of the main spiral pattern. We suspect the galaxy started out as a pure spiral, and that the inner part of the bar could be speeding up and decoupling from the spiral. Other evidence in support of the decoupling hypothesis for this galaxy include the spur spiral arms between the two CRs which are disconnected from the outer arms. Since the different segments of the pattern may not be steady, the pattern speeds inferred from the CR radii for the two patterns should be understood as average values.

RSL08 were unable to get a very good fit to the structure of this galaxy with a single pattern speed. Their value of $r(CR)$=126″ (0.76) is much larger than any of our CR radii.

NGC 685 (Figure 2.10) - The main crossing at r=19″ (0.17) appears to circle the ends of the bar. The pattern is ill-defined beyond the bar ends and none of the crossings in the outer region may be significant.

NGC 864 (Figure 2.11) - The galaxy shows three well-defined P/N crossings within

r_o. The innermost circle lies within the bar while the next crossing circles slightly outside the bar ends. The third crossing lies within the inner spiral arms. All three could be fully decoupled patterns each with a distinct pattern speed. Although we have selected the second CR in Table 1 as the bar CR (asterisk), the negative phase-shifts in the bar region suggest that the inner crossing could be the bar CR.

NGC 908 (Figure 2.12) - The assumption of a perfectly spherical bulge in this case leads to strong decomposition pinch. Hence, we use the average bulge image (section 3) for our analysis. The phase-shift distribution for this grand-design spiral shows one strong outer P/N crossing and two possibly significant inner crossings that are not necessarily artifacts of residual pinch. In particular, the second crossing, if significant, could indicate another on-going decoupling pattern. The main crossing at r=79″ (0.44) lies in the middle of the spiral pattern and just inside the peak of the m=2 Fourier intensity amplitudes (Figure 8).

NGC 1042 (Figure 2.13) - The strong N/P crossing at $r\approx$14″ (0.10) suggests there is an inner pattern, but the P/N crossing associated with it is not very well defined. The two larger crossings are much better defined. The innermost of these encircles around the very open inner spiral, which is almost barlike. The third circle lies within the outer arms.

NGC 1058 (Figure 2.14) - The shallow crossing at r=30″ (0.31) encircles the ends of a weak inner oval.

NGC 1073 (Figure 2.15) - The phase-shift distribution for this galaxy, already described in paper 1, shows two well-defined crossings. The one at r=38″ (0.26) lies just inside the ends of the prominent bar. In fact, the bar ends very near the radius of a strong N/P crossing, suggesting that the bar extends to near its OLR. The crossing at r=89″ (0.61) lies within the outer spiral arms.

Interestingly, the best-fitting simulation of RSL08 gave $r(CR)$=48.″7 (0.33), intermediate between our two CRs but closer to the inner one. Consistent with our results, these authors get $r(CR)/r(bar) < 1$. The best-fitting simulation, however, fails to represent the spiral structure well.

NGC 1084 (Figure 2.16) - Both crossings seem to be associated with the bright inner structure. The strongest crossing at r=22″ (0.23) may be associated with an inner oval.

NGC 1087 (Figure 2.17) - The main P/N crossing at r=35″ (0.31) lies well beyond the ends of the prominent (but asymmetric) bar. There is the indication of a nuclear bar but the crossing is not well defined.

NGC 1187 (Figure 2.18) - The main crossing at r=55″ (0.33) lies within the bright inner spiral pattern, while the crossing near r_o may be associated with the outer spiral pattern. The innermost crossing lies within the weak-looking bar, and encircles an inner oval. This suggests that CR_1 in Table 1 is the actual corotation radius for the bar of this galaxy.

The best-fitting RSL08 simulation of this galaxy gave $r(CR)$=74.″1 (0.45), intermediate between our two larger CR radii. Although the simulation reproduces the inner arms fairly well, the outer spiral is likely too complicated to be described by a single pattern speed.

NGC 1241 (Figure 2.19) - This bright barred spiral shows only one significant P/N crossing within r_o. This CR lies within the ends of the bar, and appears associated with a small inner pattern. The prominent N/P crossing is shown as the green circle in Figure 2.19. indicating that the entire pattern may end at close to its OLR. There is, however, some indication of a local peak in the negative portion of the phase-shift plot near $r/r_o = 0.24$, which, if real, could signify an ongoing mode-decoupling process. Furthermore, there is the indication of some decomposition pinch in the central regions.

An RSL08 simulation which does not represent the spiral structure of this galaxy well gives $r(CR) = 41\farcs5$ (0.47). This value is surprisingly close to the N/P crossing we find.

NGC 1300 (Figure 2.20) - The galaxy fits tightly into the image field, and the phase-shift analysis suggests two significant crossings, one at r=55″ (0.29) lying just inside the bright ansae of the primary bar, and one at r=142″ (0.75) lying in the bright spiral arms. The image is displayed to emphasize how the inner CR encircles a part of the bar that is slightly twisted relative to the ansae. The bar appears to extend well beyond its CR into the negative-to-positive crossing, which should be close to the OLR of the bar pattern. The shocked arm segment near the OLR radius could be a kind of OLR ring for the inner mode, and the shock itself might be related to the shearing of material due to the sharply-varying pattern speeds for the two modes.

NGC 1302 (Figure 2.21) - The main crossing at r=31″ (0.27) encircles the ends of a strong inner oval. Two outer crossings are weak but there is strong optical structure in this outer region.

The best-fitting simulation of RSL08 gave $r(CR) = 50\farcs4$ (0.43), which is very close to our second CR at 55″ (0.47). The bar radius of $30\farcs7$ (0.26) estimated by RSL08 is almost identical to our first CR.

NGC 1309 (Figure 2.22)- The crossing at r=15″ (0.23) appears to encircle an inner oval. The crossing at r=48″ (0.73) is of uncertain significance. There is also a near crossing at 8″ (0.12) that could indicate a decoupling pattern in the bulge.

NGC 1317 (Figure 2.23) - The P/N crossing at r=18″ (0.22) is inside the main outer oval and circles at about twice the radius of the prominent nuclear bar which is aligned perpendicular to the primary oval. The nuclear ring surrounding this bar has dimensions 26″× 20″ and is also aligned perpendicular to the bar. The second crossing at r=43″

(0.52) circles just inside the ends of the main oval. A third crossing at r=105″ (1.27) is of uncertain significance but could be associated with an outer spiral.

The simulation of RSL08 gave $r(CR) = 54\farcs5$ (0.66), outside our second CR but still well inside the radius of the primary oval, which has $r(bar) = 61\farcs1$ (0.74), also according to RSL08. Thus, we are in agreement with RSL08 that NGC 1317 has $\mathcal{R} < 1$.

NGC 1350 (Figure 2.24) - Our analysis for this galaxy is based on an average bulge image to minimize the strong pinch provided by the spherical bulge assumption. The phase-shift distribution shows a significant crossing at r=135″ (0.86), well outside the bar ends but not beyond the galaxy's well-defined outer R_1' pseudoring. This CR instead encompasses an extended oval, much larger than the apparent ansae-type bar. The prominent N/P crossing near $r/r_o(25)$ passes within these ansae. The noisy crossing at r=12″ (0.08) also suggests an inner pattern is present, and at least the inner oval part of the bar could belong to that crossing.

NGC 1371 (Figure 2.25) - The crossing at r=19″ (0.11) appears to encircle an inner oval. This oval shows isophote twisting further out and makes the bar appear to spill over the CR circle. The second crossing is near the outer edge of a fainter spiral pattern, although the noisiness of the second and the third crossings could imply a continuous shearing spiral pattern in this region.

NGC 1385 (Figure 2.26) - The most significant crossing, at r=32″, (0.31) circles well beyond the ends of the galaxy's bar. There may be crossings within 5″ (0.05) and at ≈51″ (0.50), but these are uncertain, especially the latter which occurs in a region of irregular and likely unsteady structure.

NGC 1493 (Figure 2.27) - There is only a single strong crossing inside r_o for this galaxy. This crossing circles well beyond the apparent ends of the bar with faint spiral arms

emanating from it. A weak crossing near r=10″ (0.10) could signify decoupling within the main bar itself.

NGC 1559 (Figure 2.28) - There is only a single major crossing, and this circles the ends of the galaxy's bar. The outer pattern is complicated and may be unsteady.

NGC 1617 (Figure 2.29) - Based on an average bulge image (section 3), we find two likely significant crossings at r=14″ (0.11) and 38″ (0.30), although the latter crossing is weak. The deprojected image shows two misaligned ovals (Figure 2.29a,b), although the effects of deprojection are still uncertain as this galaxy is highly inclined. Each circle lies within the ends of an oval.

NGC 1637 (Figure 2.30) - The crossing at r=23″ (0.19) circles around the ends of the galaxy's bar with two spiral arms emanating from it. The crossing at r=51″ (0.42) also looks significant and is associated with the main spiral pattern, which is dominated by a single bright arm. There may also be a small inner crossing.

NGC 1703 (Figure 2.31) - The crossing at r=25″ (0.28) appears associated with the bright inner spiral pattern. The outer crossing may be associated with the outer, poorly organized spiral pattern. There may also be a pattern, an inner oval, at $r\approx$10″ (0.11) that is not fully decoupled from the main spiral.

NGC 1792 (Figure 2.32) - The morphology of this galaxy suggests an unsteady pattern defined by scattered star-forming regions. Nevertheless, the phase-shift distribution indicates at least 2 relatively well-defined P/N crossings within r_o, due probably to the skewed distribution of the density. The analysis is based on an average bulge image. A nuclear crossing is suggested but is poorly defined.

NGC 1808 (Figure 2.33) - This galaxy overflows the field of view of the H-band image. The main crossing at r=74″ (0.38) lies just inside the ends of the apparent bar. The small

inner pattern at r=7″ could be associated with the galaxy's well-known nuclear structure. The outermost crossing is of uncertain significance.

NGC 1832 (Figure 2.34) - The main P/N crossing at r=23″ (0.28) appears to be associated with the galaxy's bar with emanating spirals. The next crossing at r=39″ (0.48) could be associated with the outer spiral. Other crossings inside and outside these radii are uncertain, but a possibly decoupling pattern at $r\approx$6″ (0.07) is evident.

RSL08 found a reasonably good simulation of this galaxy that places CR at 32.″8 (0.41), which is very close to our second CR and is likely to be the pattern speed of the spiral, not the bar. Our first crossing is close to the bar radius of 18.″9 (0.23) estimated by RSL08. Thus, while RSL08 placed NGC 1832 in the slow bar domain, we place it in the fast bar domain.

NGC 2090 (Figure 2.35) - The galaxy shows two main P/N crossings inside r_o. The crossing at r=25″ (0.17) is at about twice the radius of the ends of an inner oval and includes a bright inner spiral. There is also an indication of a small inner pattern decoupling at $r\approx$11″ (0.08), as well as a nuclear pattern.

NGC 2139 (Figure 2.36) - The spiral pattern in this galaxy is largely chaotic, but there is a well-defined bar. The main P/N crossing at r=22″ (0.27) encircles at more than twice the apparent bar radius.

NGC 2196 (Figure 2.37) - The phase-shift distribution shows two possibly significant crossings, the main pattern appearing to be a large, broad oval (Figure 2.37b).

NGC 2442 (Figure 2.38) - Although the phase-shift distribution is fairly simple in having mainly a single major crossing, the galaxy itself is complicated and may be interacting (Mihos & Bothun 1997). Thus, we are unsure that all pattern features are in the same plane. The main P/N crossing encircles just outside the ends of a large bar-like

feature. There is a small inner pattern that could be associated with the noisy crossing near r=11″ (0.06). The presence of an even smaller nuclear pattern is also indicated but not resolved.

NGC 2559 (Figure 2.39) - The single strong P/N crossing encircles just outside the ends of the prominent bar of this galaxy. The spiral appears to be bar-driven, but the dip in phase-shift near r=16″ (0.09) could imply an inner decoupling bar.

NGC 2566 (Figure 2.40)- An interesting case where the apparent bar in the near-IR shows two clearly misaligned components. The phase-shift distribution shows two P/N crossings, but only the outer one is strong. The crossing at r=56″ (0.40) appears to encircle the ends of the inner part of the bar, while the crossing at r=99″ (0.71) circles just outside the ends of the outer part of the bar. The weakness of the inner crossing could signify a newly decoupled pattern. This galaxy has very faint outer structure.

NGC 2775 (Figure 2.41) - The weak crossing at r=64″ (0.49) appears associated with a large, broad oval. The crossing at r=104″ (0.79) is of uncertain significance.

NGC 2964 (Figure 2.42) - The P/N crossing at r=37″ (0.42) appears to circle just outside the ends of the galaxy's main bar. At least two separate spiral patterns break from the bar region, but neither shows its own crossing, suggesting the system is defined mostly by a single pattern speed. The phase-shift distribution also suggests a small inner pattern near r=3″ (0.03; not shown on the overlay image). The N/P crossing associated with this inner pattern actually comes close to but just inside the ends of the bar, and we cannot rule out this galaxy as a possible bar extending well beyond its CR.

NGC 3059 (Figure 2.43) - The single main P/N crossing at r=26″ (0.20) encircles around the ends of the strong apparent bar. A second crossing near r=102″ (0.78) is close to r_o and of uncertain significance.

NGC 3166 (Figure 2.44) - The main crossing at $r{\approx}55''$ (0.39) is broad and somewhat ill-defined, but appears to circle the ends of the strong inner oval. There is also the indication of an unresolved nuclear pattern.

NGC 3223 (Figure 2.45) - The crossing at $r{=}23''$ (0.17) could be associated with a small inner oval. The crossing at $r{=}62''$ (0.45) is likely to be associated with the spiral arms.

NGC 3227 (Figure 2.46) - This galaxy is the spiral component of an E-S pair with NGC 3226. The phase-shift distribution suggests two significant crossings. The one at $r{=}47''$ (0.29) is noisy but circles just outside the ends of an inner boxy bar zone. The crossing at $108''$ (0.66) lies outside the main spiral arms but still well inside r_o. There is the suggestion of a nuclear crossing as well.

NGC 3261 (Figure 2.47) - A multi-armed barred spiral showing three possibly significant P/N crossings within r_o. The crossing at $r{=}29''$ (0.23) circles around the ends of the prominent bar. The crossings at $r{=}38''$ (0.30) and $52''$ (0.41) could indicate non-steady spirals, since they are so close together, but we do see different spiral patterns in this region and these two CRs could be real.

RSL08 obtained a good simulation representation of NGC 3261 with $r(CR) = 44\farcs1$ (0.34), intermediate between our second and third CRs and likely associated with the spiral and not the bar. Our first CR is comparable to their estimate of the bar radius, $28\farcs3$ (0.22).

NGC 3275 (Figure 2.48) - Two clear crossings can be identified in the phase-shift plot. The larger radius, at $r{=}26''$ (0.29), circles near the ends of the bar while the smaller radius is well inside the bar ends. In this case, the suggestion is that the bar may extend to near its OLR radius, or else the outer portion is in the process of evolving into a bar-driven spiral. None of the crossings at larger radii looks significant.

The RSL08 simulation of this galaxy gives $r(CR) = 44\farcs2$ (0.50), much larger than our second CR which is close to the bar radius of $28\farcs9$ (0.33) estimated by those authors.

NGC 3319 (Figure 2.49) - The phase-shift distribution for this late-type galaxy shows three likely significant P/N crossings. The crossing at r=38″ (0.21) circles the ends of the prominent bar, but the much larger crossing at r=126″ (0.68) lies near the outer extent of the main spiral pattern. The crossing at r=9.″ 5 (0.05) lies well inside the bar ends as does its associated N/P crossing.

NGC 3338 (Figure 2.50) - This galaxy has clear patterns on different scales. The three indicated crossings are all likely to be significant.

NGC 3423 (Figure 2.51) - A late-type galaxy with weak features. There is a possibly significant but noisy P/N crossing near r=18″ (0.15), and there may also be one at smaller radii, but there is no clearly-defined pattern in the outer disk and the outer crossings may not be significant.

NGC 3504 (Figure 2.52) - The single P/N crossing at r=24″ (0.30) circles well inside the apparent bar ends of this relatively normal-looking barred spiral. The primary bar is noticeably twisted (Figure 2.52a) and the 24″ crossing appears to circle an inner oval. However, the near-crossing at r≈42″ (0.52) coincides with the ends of the main bar/oval (Figure 2.52b) and could indicate a nearly decoupled pattern. The 42″ near-crossing also passes through the gap regions of the prominent R_1' outer pseudoring and seems to support the idea that the feature is linked to an OLR.

RSL08 were able to obtain a good simulation of this galaxy that gave $r(CR) = 44\farcs5$ (0.55), which is very close to our second CR. Their bar radius of $37\farcs4$ (0.46) is intermediate between our two CRs.

NGC 3507 (Figure 2.53) - The crossing at r=26″ (0.26) appears to circle just outside

the bar ends, while the one at r=52″ (0.51) circles just outside the bright spiral pattern.

An RSL08 simulation model that best matches the B-band spiral morphology gave $r(CR) = 34\farcs2$ (0.34), which is well inside our second CR but close to our first CR. Nevertheless, our first CR matches well the bar radius of $28\farcs1$ (0.28) estimated by RSL08. The RSL08 model makes the outer spiral more prominent than the inner spiral, while the near-IR image indicates a stronger inner spiral.

NGC 3513 (Figure 2.54) - The single major P/N crossing circles far outside the ends of the bar, close to the outer edge of a strong spiral. The ends of the bar are delineated in this case by the N/P crossing at r≈31″ (0.34). Although we have selected the main P/N crossing as the bar CR in Table 1, the galaxy appears to be a transition type where an inner pattern is decoupling from the outer pattern as indicated by the hump in the negative-valued inner portion of the phase-shift curve. The bar may then be ending at close to its OLR after decoupling, not its CR.

An excellent RSL08 model gives $r(CR) = 43\farcs5$ (0.48), which is well inside our single main CR of 60″ (0.66).

NGC 3583 (Figure 2.55) - The main P/N crossing at r=30″ (0.35) circles around the ends of the bar in this galaxy. The outer crossing appears to be associated with the outer spiral arms.

The RSL08 model of this galaxy reproduces the shape of the inner pseudoring well for $r(CR) = 32\farcs1$ (0.38), which is very close to our main CR crossing.

NGC 3593 (Figure 2.56) - The phase-shift distribution is based on an average bulge image (section 3) since the inclination of this galaxy is high. The plot shows three crossings of uncertain significance. Deprojection based on outer isophote shapes still leaves an extended oval distribution in the galaxy's inner regions.

NGC 3596 (Figure 2.57) - The innermost crossing at r=12″ (0.10) appears related to a small inner oval. The crossing at r=32″ (0.27) lies in the middle of the main spiral pattern and its weakness could indicate an ongoing decoupling. The remaining two CRs lie near the edge of the near-IR disk, but an optical color image of NGC 3596 from the Sloan Digital Sky Survey (SDSS) shows considerable structure at larger radii. From comparisons of the optical image, the NIR image, and the phase-shift plot we consider all four individual crossings to be significant; they appear to refer to different density wave patterns.

NGC 3646 (Figure 2.58) - The inner CR at r=15″ (0.13) appears to encircle an area strongly affected by decomposition pinch. The crossing at r=74″ (0.63) lies in the outer spiral. There are also indications from both the phase-shift plot and the image of a decoupling bar in the intermediate-radius region.

NGC 3675 (Figure 2.59) - The third crossing at r=82″ (0.46) encircles a broad oval with tightly wrapped spiral structure emerging. The near-crossing at r=27″ (0.15) could be associated with a decoupling inner oval. The central crossing is not resolved in the NIR image.

NGC 3681 (Figure 2.60) - The main crossing lies just beyond the ends of a well-defined inner oval. An unresolved nuclear crossing is also indicated.

NGC 3684 (Figure 2.61) - The crossing at r=28″ (0.30) encircles an inner oval. The outer crossing is likely related to the faint outer structure.

NGC 3686 (Figure 2.62) - The main crossing at 42″ (0.43) lies largely outside a prominent bar and inner spiral. This could be an example of a genuine bar-driven spiral, but the prominent N/P crossing near r=27″ (0.28), and the undulations in the phase-shift curve in that region suggest that the inner bar pattern is going through a decoupling process.

The best-fitting RSL08 model for this galaxy gives $r(CR) = 35\farcs6$ (0.37), which is close to our main CR. Our two studies are in agreement that this galaxy may be a slow bar case.

NGC 3726 (Figure 2.63) - The inner shallow-crossing suggests a nearly-decoupled inner bar. The main crossing at r=65″ (0.35) lies well outside the bar ends. An SDSS image shows a fragmentary outer spiral.

An RSL08 model of this galaxy has $r(CR) = 83\farcs5 \pm 13\farcs9$ (0.45±0.075), which is intermediate between our two outer CRs.

NGC 3810 (Figure 2.64) - The crossing at r=14″ (0.11) appears to encircle a small inner oval. The other two crossings are in the main spiral arms. The spiral is multi-armed and lacks bisymmetry but is still regular-looking.

NGC 3887 (Figure 2.65) - The crossing at r=28″ (0.28) circles outside a large, inner oval. The crossing at r=57″ (0.57) encircles the main spiral pattern. On an optical SDSS image, there is a well-defined two-armed spiral beyond 60″ (0.60).

NGC 3893 (Figure 2.66) - The phaseshift plot shows two fairly well-defined crossings. The crossing at r=21″ (0.16) encircles a small inner oval, while the crossing at r=61″ (0.46) lies in the middle of the main outer spiral.

NGC 3938 (Figure 2.67) - The inner crossing at r=25″ (0.16) appears to encompass a broad oval, outside of which there is a bright inner spiral emanating from this CR circle. The crossing at r=62″ (0.38) lies in the middle of the main spiral pattern.

NGC 3949 (Figure 2.68) - The crossing at 8″ (0.09) circles just inside the ends of a small oval. The near-crossing at 38″ (0.44) is just around the chaotic spiral.

NGC 4027 (Figure 2.69) - This small late-type spiral considered of Magellanic type by de Vaucouleurs shows a well-defined single crossing at r=24″ (0.25) that encircles just

outside the ends of the prominent bar. The second crossing is barely evident but could signify a decoupling of the outer, asymmetric spiral pattern.

NGC 4030 (Figure 2.70) - This galaxy shows several significant-looking P/N crossings. The one at r=10″ (0.08) appears to be associated with an inner oval. The other outer crossings are connected with the prominent, complex spiral pattern which has up to 6 arms. There may also be a significant pattern at very small radii. The outer crossings are not affected by the fact that the multiplicity is greater than 2.

NGC 4051 (Figure 2.71) - This galaxy has a single main crossing at r=70″ (0.44) and another possibly significant crossing at r=3″ (0.02). The main crossing circles beyond the ends of the apparent bar in the middle of the spiral pattern. In this case, the spiral and the bar should have the same pattern speed.

An RSL08 model gives $r(CR)$ = 98″± 14″ (0.62±0.09), which is larger than our single main CR crossing. For the RSL08 value of the bar radius of 54.″1 (0.34), our analysis makes NGC 4051 a fast bar case, while the RSL08 model makes it a possible slow bar case.

NGC 4123 (Figure 2.72) - The main crossing at r=55″ (0.42) circles around the ends of the bar. The near crossing at r=18″ (0.14) could be associated with an inner misaligned pattern (affected slightly by decomposition pinch). The outer crossing lies mostly outside the spiral structure.

RSL08 show that a simulation model having $r(CR)$ = 69.″1 (0.53) matches the spiral structure well. Our main CR at 55″ is closer to their estimate of the bar radius, 59.″2 (0.45).

NGC 4136 (Figure 2.73) - This is possibly an evolving, unsettled system. The inner crossing lies well inside the ends of the inner bar. The next crossing encircles around the galaxy's inner ring and is well outside the bar ends. The remaining crossings are in the spiral arms.

NGC 4145 (Figure 2.74) - This very late-type spiral has a conspicuous bar and two apparent P/N crossings. The one at r=47″ (0.27) circles well outside the ends of the bar, while the crossing at r = 122″ (0.69) lies in the outer arms.

NGC 4151 (Figure 2.75) - The main P/N crossing at r=99″ (0.52) appears to circle just outside the ends of the bright bar/oval. The crossing at r=70″ (0.37) could signify some decoupling of the inner part of the bar. However, there is no misalignment between the inner parts of the bar and the extent of the outer oval. The phase-shift curve also indicates an unresolved nuclear pattern, and the possible decoupling of the inner oval in progress.

NGC 4212 (Figure 2.76) - The main CR circle is connected with the spiral arms, but no crossing is seen for the small inner oval. This pattern may not yet be decoupled from the spiral, and a hump on the negative portion of the phase-shift plot near the central region may indicate potential future decoupling.

NGC 4242 (Figure 2.77) - The main inner crossing encompasses a weak, broad oval, but other than this the galaxy has no organized pattern in the near-IR.

NGC 4254 (Figure 2.78) - The phase-shift plot shows mostly weak P/N crossings. The one at r=21″ (0.12) is related to a small inner oval. The crossing at r=56″ (0.33) may be connected with the inner spiral arms, while that at r=91″ (0.54) could be connected with the outer arms. There is also a nuclear crossing.

NGC 4293 (Figure 2.79) - The crossing at r=79″ (0.48) circles near the ends of the bar. The innermost crossing is in an area affected by strong decomposition pinch. We used an average bulge image for the analysis, but the crossing is still of uncertain accuracy. The outermost crossing is well-defined but close to r_o.

NGC 4303 (Figure 2.80) - The phase-shift method yields 5 significant-looking crossings for this excellent face-on spiral. The smallest crossing encircles the ends of an inner oval,

the inner part of the bar of this galaxy. The second crossing encircles the ends of the whole bar and part of the inner spiral. The next two crossings appear to be related to the inner pseudoring spiral arms, while the largest crossing is related to the outer arms.

RSL08 obtained an excellent fit to the B-band spiral structure of this galaxy with a single pattern speed having $r(CR)$=89″ (0.46), which is very close to our 4th CR at 85″ (0.44). Their estimate of the bar radius, 52.″5 (0.27), is closer to our second CR radius at 49″ (0.25). Although their model gives a good match to the outer arms, there is a third arm beyond the inner pseudoring that is not reproduced at all. Thus, our finding of a CR at 134″ (0.69) could indicate that there is indeed an independent pattern in this region.

NGC 4314 (Figure 2.81) - As shown in paper 1, this galaxy has a well-defined P/N crossing at 77″ (0.61) that circles almost exactly around the ends of the bar. In paper 1, we also detected an inner crossing, but our revised analysis only weakly detects it. The N/P crossing at r=20″ (0.16) indicates the presence of an inner pattern in any case.

An excellent RSL08 model that reproduces this galaxy very well gives $r(CR)$ = 81.″7 (0.65), in good agreement not only with our main CR estimate but also with their estimate of the radius of the bar at 82.″9 (0.66).

NGC 4394 (Figure 2.82) - There are at least three possibly significant crossings for this galaxy. The one at r=42″ (0.38) is noisy but appears to circle around the ends of the bar. The crossing at r=17″ (0.15) encompasses a broad inner part of the bar, while the crossing at r=90″ (0.81) is close to r_o, just outside a faint outer ring, and may not be significant. The weak N/P crossing at r=33″(0.30) circles somewhat inside the bar ends, suggesting that much of the bar may actually belong to the inner mode. This galaxy is interesting in that its prominent bar is skewed slightly in a leading sense, opposite the winding of its main outer arms.

An RSL08 model gives $r(CR) = 76\farcs7 \pm 10\farcs0$ (0.69±0.09), which agrees within uncertainties with our third CR value.

NGC 4414 (Figure 2.83) - The innermost crossing encircles an inner oval. The pattern is weak in the outer regions, and the outer crossings are uncertain. There is also the indication of an unresolved nuclear pattern.

NGC 4450 (Figure 2.84) - The crossing at r=31″ (0.20) appears related to a broad inner oval, while the one at r=59″ (0.37) could be associated with the spiral emanating from the ends of this oval. There may also be a small inner crossing. The outermost crossing is near r_o and is of uncertain significance although it is well-defined.

An RSL08 model places CR in NGC 4450 at $52\farcs3$ (0.33), close to our third CR. RSL08 give a bar radius of $49\farcs7$ (0.32), considerably larger than the inner oval and probably affected by the inner arms.

NGC 4457 (Figure 2.85) - The main P/N crossing at r=44″ (0.55) is noisy but appears to circle almost exactly around the ends of the galaxy's prominent inner oval. The phase-shift plot also suggests pattern decoupling near r=18″ (0.22).

The best-fitting simulation of RSL08 places CR at $39\farcs9$ (0.49), close to our single crossing.

NGC 4487 (Figure 2.86) - The main crossing at r=20″ (0.16) is associated with a bright inner oval. The outer crossing is in an area where there is little coherent pattern and may not be significant.

NGC 4496 (Figure 2.87) - Surprisingly, the most significant crossing is the N/P at r=31″ (0.26), shown as a green circle in Figure 2.87. This crossing encircles just outside the bar ends, and could be close to the location of the OLR of the small inner pattern. The two outer crossings are of uncertain significance.

NGC 4504 (Figure 2.88) - The main crossing at r=27″ (0.21) lies just beyond the ends of a broad inner oval. There is an indication of a decoupling pattern near r=10″.

NGC 4527 (Figure 2.89) - The crossing at r=65″ (0.34) encircles a broad bar-like feature. The central area is affected by strong decomposition pinch, and our analysis is based on an average bulge image. The apparent crossing near r=10″ (0.05) is uncertain for this reason. Also, deprojection leaves an extensive oval zone beyond 65″ that may not be significant.

NGC 4548 (Figure 2.90) - The inner crossing at r=19″ (0.12) coincides with a small inner oval, seen as a nuclear ring in the optical, and the outer crossing coincides with the ends of the primary bar. In this case, the bar and the main spiral would have the same pattern speed, and the galaxy can be thought of as having a "bar-driven" spiral.

A very interesting RSL08 model reproduces the structure of NGC 4548 for a corotation radius of 95.″2 (0.58). The main phase-shift CR is at 75″ (0.45), which is closer to the RSL08 bar radius of 75.″8 (0.46).

NGC 4571 (Figure 2.91) - The main crossing at r=51″ (0.46) lies within a faint spiral pattern. The inner-most crossing is of uncertain significance. The inner negative portion of the phase-shift plot indicates a possible future decoupling pattern, which may correspond to the inner oval.

NGC 4579 (Figure 2.92) - Only two of the four P/N crossings are well-defined. The one at r=25″ (0.14) encompasses a broad oval inside the bar, while the crossing at r=81″ (0.44) passes through the bright outer two-armed pattern. The weak crossing at r=48″ (0.27) coincides with the approximate ends of the bar, but if this is just a noise blip, then the dotted circle should be green and NGC 4579 would be a case where the bar extends to close to the OLR of its inner pattern. The innermost crossing at r=9″ (0.05) coincides with

a small inner oval.

Garcia-Burillo et al. (2008) have made a detailed study of the gravitational potential in NGC 4579, using both gas observations and a K-band image. Their goal was to examine the possible mechanism of fueling of its LINER/Seyfert 1.9 nucleus. These authors also suggested the possibility of multiple pattern speeds in NGC 4579 because of the prominent bar and inner oval. They placed the CR of the primary bar at 6±1kpc by assuming the ends of the bar extend exactly to CR. They also assumed that a ring in the vicinity of the inner oval lies at the oval's inner 4:1 resonance, and placed the CR of the oval at 1kpc. In comparison to our findings, Garcia-Burillo et al.'s adopted bar CR is intermediate between our 3rd and 4th CRs in Table 1 (at 4.7 and 7.9 kpc, for an assumed distance of 20 Mpc). Our innermost CR lies close to their adopted oval CR. Based on azimuthally-averaged torques, Garcia-Burillo et al. also suggested that the corotation barrier of the bar has been overcome in NGC 4579 due to secular evolutionary processes, and that the spiral may be decoupled from the bar. This was concluded because the measured torques were found to still be negative just outside their adopted bar CR, allowing an efficient population of the bar's inner 4:1 resonance. Although there is some general agreement between our two studies, the phase-shift method makes no *a priori* assumptions about the correspondence of bar CR radii and resonance features on the image, and as we have noted, NGC 4579 could be a case where the bar extends to close to the OLR of its inner pattern.

An RSL08 model that reproduces the arm structure of NGC 4579 gives $r(CR) = 71\farcs1 \pm 8\farcs4$ (0.39±0.05). This is good agreement with our largest CR radius of 81″ (0.45), suggesting that their CR refers to the spiral and not the bar.

NGC 4580 (Figure 2.93) - The crossing at r=15″ (0.24) could be associated with a small inner oval. The crossing at r=39″ (0.62) could be associated with the main spiral arms.

NGC 4593 (Figure 2.94) - The three P/N crossings are all well-defined. The one at r=12″ (0.10) coincides with a small inner oval. The crossing at r=66″ (0.57) circles just around the ends of the bar, while the outermost crossing is within the outer arms. This could be a case where the spiral pattern is fully decoupled from the bar pattern (see Figure 1).

NGC 4618 (Figure 2.95) - The phase-shift plot is unusual in having a broad negative region. In the H-band, the apparent nucleus is not centered within the bar. The plot shows only one major crossing that lies well beyond the bar ends. An inner fast bar might be emerging under the background of an outer, slower-rotating chaotic spiral.

NGC 4643 (Figure 2.96) - None of the crossings for this galaxy appears well-defined. Although the bar is strong, the pattern is so straight that the phase-shift method has difficulty locating the corotation radii. Our CR at 50″ (0.54) is considerably less than that provided by a model of RSL08: 69.″1 (0.75). The overlay also shows that the bar extends outside our CR estimate.

NGC 4647 (Figure 2.97) - The crossing at r=17″ (0.20) circles directly around the ends of the main bar. There is no coherent outer pattern in the H-band image, and the outer crossing is uncertain. Although we have interpreted the r=17″ crossing as the bar CR in Table 1, the negative phase-shifts inside this crossing suggest that all or most of the bar may belong to the innermost mode.

NGC 4651 (Figure 2.98) - The strong crossing at r=37″ (0.30) appears associated with the well-defined inner spiral pseudoring of the galaxy. A deep optical SDSS image shows other patterns outside this pseudoring that could account for the other outer crossings. The exact location of the innermost crossing is uncertain although the trend of the phase-shift curve indicates that a nuclear pattern is likely to be present. There is also the possibility of another decoupling pattern just outside the nuclear pattern both from the image and from

the phase-shift plot.

NGC 4654 (Figure 2.99) - The crossing at r=20″ (0.14) encircles the ends of an inner oval. The outer crossing may be associated with the outer spiral arms. There is also the indication of a nuclear pattern.

NGC 4665 (Figure 2.100) - As shown in paper 1, the main crossing for this galaxy occurs just inside the ends of the very strong bar. In paper 1, we argued that this could be a genuine case where the bar extends to beyond its CR radius. A second crossing in the inner regions may be associated with a small inner oval.

An RSL08 model of this galaxy places CR at 55″.2 ± 11″.8 (0.48±0.10), comparable to our main CR radius of 47″.2 (0.41). In both cases, the CR radius is less than the RSL08 bar radius of 62″.5 (0.55).

NGC 4689 (Figure 2.101) - In an optical SDSS image, this galaxy has an inner pseudoring pattern, and intermediate pseudoring pattern, and an outer ring or pseudoring pattern. The three main crossings in the phase-shift plot could be related to these features. Further decouplings of patterns in the inner region are also possibly going on.

NGC 4691 (Figure 2.102) - This galaxy has one main crossing inside r_o, but the overlay of this circle on the images shows that the bar is asymmetric. The crossing circles near the ends of the bar in any case, but at low light levels, the bar gets less elliptical and extends well outside the circle.

NGC 4699 (Figure 2.103) - The main crossing for this galaxy circles around the ends of the prominent inner bar. A smaller crossing indicates an unresolved nuclear pattern.

NGC 4772 (Figure 2.104) - This galaxy could be related to polar ring systems. Most of the phase differences are negative, which is very unusual. The patterns in this galaxy might not have reached quasi-steady state. The weak crossing at r=53″ (0.52) is shown as the red

circle in Figure 2.104.

NGC 4775 (Figure 2.105) - This galaxy lacks a coherent spiral pattern in visible light, yet the phase-shift plot shows one very well-defined crossing. This crossing could be related to a small inner oval, although the circle lies well beyond this oval.

NGC 4781 (Figure 2.106) - The crossing at r=15″ (0.14) appears associated with a small inner oval. The next crossing lies within the spiral pattern, and well beyond the ends of the rest of the bar. The outer crossing lies in a region of chaotic pattern. There is also the indication of a nuclear pattern. Although we have interpreted the r=17″ crossing as the bar CR in Table 1, the negative phase-shifts inside this crossing suggest that all or most of the bar may belong to this innermost mode.

NGC 4900 (Figure 2.107) - The crossing at r=9″ (0.13) lies inside the bar and encompasses an inner oval. Although we have interpreted the r=35″ (0.52) crossing as the bar CR in Table 1, the negative phase-shifts inside this crossing suggest that all or most of the bar may belong to this innermost mode.

NGC 4902 (Figure 2.108) - The crossing at r=9″ (0.10) encircles the ends of a small inner oval that is slightly misaligned with the main bar. The crossing at r=39″ (0.43) lies well beyond the bar ends and encompasses the main inner spiral. The crossing at r=60″ (0.66) could be associated with the outer spiral arms, although this crossing is weak and may indicate an ongoing decoupling. Although we have interpreted the r=39″ (0.43) crossing as the bar CR in Table 1, the negative phase-shifts inside this crossing suggest that the bar may actually belong to this innermost mode. This is especially suggested by the fact that the strong N/P crossing between the two CRs circles almost exactly around the bar ends. We suspect that in this case, the bar extends to close to the OLR of the innermost pattern (see sections 5.1.3 and 6.1). A fourth crossing at r = 87″ (0.96) is close to r_o and not within the field of the overlay.

An excellent RSL08 model of this galaxy places CR at 44.″3 (0.49), close to our second CR.

NGC 4930 (Figure 2.109) - The crossing at r=46″ (0.31) encompasses the ends of the bar. The one at r=97″ (0.66) may be associated with the outer spiral arms. There is definitely also an inner oval, but the innermost crossing is mostly inside this oval. The phase-shift plot suggests ongoing decoupling in the inner parts of the bar that might eventually result in the oval and the bar having different pattern speeds.

An RSL08 model places CR at 46.″6 (0.32), close to our second crossing although the latter is weak.

NGC 4939 (Figure 2.110) - This galaxy has a strong and complicated spiral pattern that yields several P/N crossings in the phase-shift plot. The crossing at r=17″ (0.10) appears associated with a small inner oval or bar. The crossing at r=38″ (0.23) could be associated with two inner spiral arms, while that at r=69″ (0.41) could be associated with the intermediate, still tightly-wrapped pattern. The crossing at r=120″ (0.82) could refer to the outer, more open arms. An optical image on the NASA/IPAC Extragalactic Database (NED) website suggests all the crossings refer to distinct patterns. There is indication also of a nuclear pattern that is not well resolved.

NGC 4941 (Figure 2.111) - The phaseshift distribution is noisy for this galaxy which includes an ovally-distorted spiral zone surrounded by a well-defined outer ring. The crossing at r=57″ (0.52) could be associated with the broad oval disk and spiral. The analysis is based on an average bulge image.

NGC 4995 (Figure 2.112) - The crossing at r=22″ (0.29) encircles the ends of the bar of this galaxy. The other crossings may be associated with different parts of the spiral arms, a bright inner pseudoring and very faint outer arms. There is indication of a nuclear pattern

as well.

An RSL08 model places CR at 64.″2 (0.85), very close to our outermost CR of 64.″5 (0.86). Since we also find a crossing around the ends of the bar, it is likely that the RSL08 value refers only to the spiral, and that the galaxy is a fast bar case.

NGC 5005 (Figure 2.113) - The phase-shift distribution is based on an average bulge image, owing to a high inclination. The deprojected image shows an oval with a twisted inner region. The crossing at r=29″ (0.17) encircles the twisted inner oval, while that at r=52″ (0.30) lies just outside the ends of the oval/bar, and from this outer CR two spiral arms are seen emanating.

NGC 5054 (Figure 2.114) - Our analysis is based on an average bulge image. The apparent oval in the center of this galaxy could be an artifact of decomposition pinch. There is no strong P/N crossing in this region, although the phase-shifts curve of the positive hump indicates a decoupling process in progress. The main crossing at r=74″ (0.47) lies in the middle of the main spiral. Figure 8 shows that this radius lies near the maximum of the m=3 relative Fourier amplitudes of the H-band light distribution. There is also indication of an unresolved nuclear pattern.

NGC 5085 (Figure 2.115) - The galaxy shows several significant-looking crossings. The crossing at r=6″ (0.06) may be associated with a small inner oval. The crossing at r=22″ (0.20) seems associated with an oval that joins with the inner spiral, while the crossing at r=47″ (0.43) may correspond to a different, outer spiral pattern. The crossing at r=97″ (0.89) is of uncertain significance.

NGC 5101 (Figure 2.116) - The crossing at r=54″ (0.31) appears to encompass the ends of the bar. The crossing at r=94″ (0.54) could be associated with the main outer arms, while the innermost crossing could refer to a weak inner oval.

NGC 5121 (Figure 2.117) - The main crossing at r=37″ (0.60) could be related to a large, broad oval.

NGC 5247 (Figure 2.118) - The main crossing at r=87″ (0.47) lies in the middle of the bright spiral pattern. Figure 8 shows that this radius lies near the maximum of the m=2 relative Fourier amplitudes of the H-band light distribution. The innermost crossing appears associated with a small inner oval. There is also the indication of an unresolved nuclear pattern.

NGC 5248 (Figure 2.119) - The main crossing at r=70″ (0.38) lies in the middle of the main inner spiral, while the crossing at r=12″ (0.06) encompasses a small inner oval where the well-known nuclear ring of this galaxy is located. The two weak outer crossings seen in the phase-shift plot are close to r_o but may be associated with the faint outer pseudoring of the galaxy. Figure 8 shows that the main crossing lies near the maximum of the m=2 relative Fourier amplitudes of the H-band light distribution.

NGC 5334 (Figure 2.120) - The innermost crossing lies well inside the bar ends. The crossing at r=42″ (0.32) circles far outside the bar ends, in the main spiral pattern. The third crossing may be connected with outer spiral arms. Although we have interpreted the r=42″ crossing as the bar CR in Table 1, the negative phase-shifts inside this crossing suggest that the bar may belong to the innermost mode. There in indication from the phase-shift plot that the bar is in the process of decoupling. The spike at r/r_o=0.4 is of uncertain significance.

NGC 5427 (Figure 2.121) - A grand-design spiral with several P/N crossings. The innermost crossing appears to be connected with a small inner oval. The next crossing, at r=38″ (0.44), lies in the middle of the main spiral pattern. The outermost crossing at r=63″ (0.73) could be associated with faint outer spiral structure.

NGC 5483 (Figure 2.122) - The weak crossing at r=18″ (0.15) appears to encircle the ends of an oval bar feature. This is followed closely by a better-defined crossing at r=26″ (0.22) which circles through the main inner arms. The phase-shift distribution suggests that the spiral and the oval are still in the process of decoupling. The weak outer crossing at r=73″ (0.61) may indicate a non-steady pattern in this region. There is also the indication of an unresolved nuclear structure.

NGC 5643 (Figure 2.123) - The crossing at r=24″ (0.16) circles the inner broad oval zone of the prominent bar. The next crossing, at r=67″ (0.44), is very well-defined, and circles far beyond the ends of the rest of the bar. This intermediate crossing could be the CR of the broad inner bar/spiral feature, while the crossing at r=105″ (0.68) could be associated with the outer spiral pattern. On the other hand, the inner portion of the bar could be corotating with the inner oval, since the features are aligned, and there is a ring-like feature near the N/P crossing indicating possible shearing between two decoupled patterns at this radius. We consider this second scenario more likely, making NGC 5643 very much like NGC 4902. There is also the indication of an unresolved nuclear structure.

NGC 5676 (Figure 2.124) - The crossing at r=23″ (0.19) circles the ends of a prominent oval. The other crossings are connected to the spiral arms which in optical images extend well beyond the outer circle.

NGC 5701 (Figure 2.125) - The phase-shift values are small in this galaxy because the density wave features are only weakly skewed. The one at r=52″ (0.40) appears to circle closely around the bar ends, while that at r=87″ (0.66) could be associated with the outer spiral arms, which show an R_1R_2' morphology in optical images. This structure is barely detectable in the near-IR OSUBGS image. There is also an indication of an unresolved nuclear structure.

An RSL08 model of this galaxy places CR at 64.″6 (0.49), intermediate between our

two outer CR values.

NGC 5713 (Figure 2.126) - The crossing at r=29″ (0.34) circles the ends of the bar. The crossing at r=71″ (0.84) may be associated with the outer arms, which are peculiar in this object. There is also indication of an unresolved nuclear structure. Although we have interpreted the r=29″ crossing as the bar CR in Table 1, the negative phase-shifts inside this crossing suggest that all or most of the bar may belong to this innermost mode.

NGC 5850 (Figure 2.127) - This galaxy is interesting in that it has a weak N/P crossing that passes almost exactly through a minimum in the bar profile. The bar has ansae, but these ansae lie outside the N/P crossing in an area with positive phase-shift. If we take our "rules" literally, that modes should come with both positive and negative phase-differences, with the latter following the former in radius, this means everything inside the bar minimum belongs to the inner mode, while the ansae belong to the outer mode. The main crossing at r=81″ (0.62) circles just beyond the ansae. The inner crossing at r=30″ (0.23) encircles a broad inner oval and doesn't seem to be related to the galaxy's well-known nuclear bar which only shows a hint of decoupling in the phase-shift plot.

An interesting RSL08 model of this galaxy places CR at 105.″1 (0.80). Our main CR value is close to the RSL08 bar radius of 75.″8 (0.58).

NGC 5921 (Figure 2.128) - The crossing at r=58″ (0.39) circles just outside the bar ends, while the one at r=21″ (0.14) circles an inner oval aligned with the main bar. The crossing at r=137″ (0.93) may be associated with the outer spiral arms. The N/P crossing at r=39″ (0.27) lies just inside the bar ends. Although we have selected the r=58″ crossing as the bar CR in Table 1, the substantial negative phase-shifts in the bar region suggests that much of the bar may belong to the inner mode.

The RSL08 model of this galaxy places CR at 71.″4 (0.49), well outside our bar CR

value. Instead, our value corresponds with their bar radius of 57.″0 (0.39).

NGC 5962 (Figure 2.129) - The main crossing at r=27″ (0.30) circles just outside the ends of a broad inner oval. There is indication of an unresolved inner pattern.

NGC 6215 (Figure 2.130) - There is a small inner oval in this galaxy, but there is no P/N crossing associated with it apart from weak indication of a potential decoupling. Instead, the three main crossings are associated with the complex spiral arms.

NGC 6221 (Figure 2.131) - The crossing at r=14.″5 (0.11) is connected to a small inner oval which is barely decoupled. The one at r=42″ (0.33) circles the ends of the bar. The largest crossing at r=93″ (0.73) is probably associated with the outer arms. In optical light this galaxy is distorted and seems clearly interacting.

NGC 6300 (Figure 2.132) - This is a galaxy with clear multiple patterns. The crossing at r=39″ (0.27) appears to encircle the ends of the bar, which spill only a little outside. The crossing at r=69″ (0.47) circles just inside the ends of the prominent oval inner pseudoring. The innermost crossing could be associated with a small inner oval.

NGC 6384 (Figure 2.133) - The crossing at r=20″ (0.10) circles just inside the ends of a prominent bar/oval. The other two crossings are connected with the spiral arms.

The best-fitting RSL08 model for this galaxy places CR at 72.″5 (0.36), very close to our second CR at 69″ (0.34).

NGC 6753 (Figure 2.134) - The phase-shift distribution shows four likely significant crossings. The one at r=11″ (0.14) is associated with a small inner oval. The next one at r=19″ (0.25) seems associated with a small inner spiral. The remaining crossings are associated with intermediate spiral patterns, which show more prominently in an optical image.

NGC 6782 (Figure 2.135) - The phase-shifts are small in this galaxy because of the lack of skewness of the pattern. We identify two possibly significant but weak crossings at r=12″ (0.17) and 28″ (0.41). The latter circles just inside the ends of the main bar. The galaxy is also known to have a strong secondary bar (Buta & Crocker 1993). This feature lies well inside the innermost crossing.

An interesting RSL08 model places CR at 37.″1 (0.54), well outside our value which is closer to the RSL08 bar radius of 29.″6 (0.43).

NGC 6902 (Figure 2.136) - The crossing at r=22″ (0.13) circles just outside the ends of a weak inner oval. The crossing at r=39″ (0.23) is weak but may be associated with the inner ring or inner spiral arms. The spiral pattern is extensive in this galaxy, and the outer crossing may be connected to the outer arms. There appears to be pattern decoupling going on in the central region. Pattern decoupling or shearing also appears to be going on in the intermediate radius region.

NGC 6907 (Figure 2.137) - The strong spiral and bar blend smoothly in this galaxy. The main crossing lies just beyond the ends of the apparent bar. The inner crossing is associated with a small inner oval.

NGC 7083 (Figure 2.138) - The crossing at r=4″ (0.03) lies well inside an inner oval, while that at r=18″ (0.15) lies well outside the ends of this oval. The crossing at r=50″ (0.43) lies just outside the inner spiral and may be associated with the outer pattern.

NGC 7205 (Figure 2.139) - The main crossing at r=74″ (0.61) lies mainly outside the bright inner spiral pattern. The prominent inner oval does not have an associated crossing, but we see evidence in the phase-shift plot at $r\approx$12″ (0.10) for ongoing decoupling.

NGC 7213 (Figure 2.140) - There are no obvious density wave patterns in the H-band image, but still we see P/N crossings that might be significant.

NGC 7217 (Figure 2.141) - The H-band image shows a weak two-armed spiral outside the second CR at 43″ (0.34).

NGC 7412 (Figure 2.142) - The crossing at r=14″ (0.12) corresponds to a small inner oval. The other two crossings are in the outer spiral arms which may be shearing.

NGC 7418 (Figure 2.143) - Both of the main crossings are far beyond the ends of the bar. The innermost crossing may indicate an unresolved inner pattern. Although we have interpreted the r=38″ (0.38) crossing as the bar CR in Table 1, the negative phase-shifts inside this crossing suggest that the bar may actually belong to this innermost mode.

NGC 7479 (Figure 2.144) - Within r_o, there are only two significant crossings in this galaxy. The crossing at r=58″ (0.45) encircles the ends of the bar closely. The innermost crossing may be associated with a small inner oval. The galaxy can be thought of as having a bar-driven spiral. The spiral pattern outside the main CR may be shearing.

NGC 7552 (Figure 2.145) - The crossing at r=59″ (0.57) encircles the bar ends. The other inner crossings may signify different sub-patterns within the bar.

An excellent RSL08 model of this galaxy places CR at 65.″0 (0.62), close to our main CR radius.

NGC 7582 (Figure 2.146) - The inner crossing at r=44″ (0.29) encircles an area with strong decomposition-pinch, which may in reality correspond to an oval feature in the galaxy center. The crossing at r=74″ (0,49) encircles just inside the bar ends. Our analysis is based on an average bulge image (section 3).

NGC 7713 (Figure 2.147) - The two closely spaced crossings are not clearly related to any pattern. They lie well beyond the inner oval which might be going through a decoupling process from the outer pattern.

NGC 7723 (Figure 2.148) - The crossing at r=21″ (0.20) corresponds to the ends of the bar. The crossing at r=40″ (0.38) corresponds to the bright inner spiral. The innermost crossing may correspond to the small inner oval. There is also the indication of an unresolved inner pattern.

An RSL08 model of this galaxy places CR at 33.″5 (0.31), between our two outermost crossings.

NGC 7727 (Figure 2.149) - The crossing at r=29″ (0.20) encircles an inner oval. The significance of the outer crossing is uncertain. There is also the indication of an unresolved inner pattern.

NGC 7741 (Figure 2.150) - The crossings are weak and we have averaged crossings at 45″ (0.34) and 59″ (0.44) as our best CR estimate. This average circles around the ends of the bar. There is considerable asymmetry in the bar in any case.

IC 4444 (Figure 2.151) - The crossing at r=10″ (0.17) circles the ends of a small inner bar. The crossing at r=41″ (0.72) lies just beyond the main spiral arms.

IC 5325 (Figure 2.152) - The crossing at r=15″ (0.18) encircles a weak inner oval. The other two crossings seem to correspond to the two sets of outer spiral arms.

ESO 138−10 (Figure 2.153) - The crossing at r=17″ (0.08) may be associated with a small inner oval. There is another oval at twice the radius of this one, but it only extends about halfway to the next crossing. There is indication of ongoing decoupling at the location of the second oval. The outer crossings are of uncertain significance.

5. Analysis

Having summarized what the phase-shift distributions reveal for each individual galaxy, we now analyze the entire galaxy sample. Table 2 provides an inventory of the features seen as well as a general characterization of the phase-shift plot as either "well-defined" (low noise), or "noisy" (having many likely noise-induced crossings), or else "noisy/unsteady" (implying little coherence in both the pattern and the phase-shift plot). Some of the ovals recognized in col. 4 of Table 2 could be artifacts of deprojection, but in general deprojection effects should not produce false P/N crossings. Table 2 also gives an assessment of whether a galaxy has a grand-design spiral or a flocculent spiral. This can be difficult to judge from the near-IR images given the low depth of exposure of some of the images. Instead, we provide the blue-light Elmegreen Arm Class (AC; Elmegreen & Elmegreen 1982, 1987) as a judgment of the coherence and complexity of the spiral pattern. B-band spirals that are chaotic, fragmented, asymmetric, irregular, or dominated by only a single arm are classes AC 1-4, and are considered flocculent. Spirals with at least two symmetric inner or outer arms, or ring-like arms, are classes 5-12 and are considered grand-design. These classes do not perfectly translate to what one sees in the near-IR. It is possible for a galaxy to be "optically-flocculent" and show a grand-design spiral in the near-IR (Thornley 1996; Buta et al. 1995). Also, some grand-design spirals are weak in the near-IR. Nonetheless, the arm class is still an instructive measure of the general coherence of a pattern.

The arm classes are given in col. 5 of Table 2. Most are taken from Elmegreen & Elmegreen (1987). In a few cases where the sample galaxy was not included in this paper, Buta estimated the arm class from available images in the de Vaucouleurs Atlas of Galaxies (Buta et al. 2007) and other sources. For 13 of the galaxies, the Hubble-de Vaucouleurs type is too early to provide a reliable arm classification. Of the remaining 140 galaxies having an arm classification, 93 would be considered grand-design in blue light. Of these,

we independently judged 67% to have a "well-defined" phase-shift plot. In the same set, 47 galaxies would be considered flocculent, and of these we judged the phase-shift plot to be "well-defined" for only 28%. This confirms what we might have expected: a coherent grand-design pattern is likely to be more steady and self-consistent (in a modal sense) than a flocculent, disorganized pattern.

Table 2 also summarizes the number of CRs we have identified. Among the best-defined grand-design spirals (AC 9 and 12), the number of CRs ranges from 1-5. For the 46 AC 9 and 12 galaxies in Table 2, the mean number of CRs we have recognized is $< n_{CR} > = 2.8$. For this same subset, 78% were judged to have well-defined phase-shift plots. The 47 AC 1-4 galaxies have $< n_{CR} > = 2.1$. These values largely exclude the weak inner crossings found in many of the galaxies. These appear to be due to largely unresolved features and we have not compiled most of them in Table 1. We expect that higher resolution images would tell more about the reality of such features.

One of the first conclusions we can draw from the Table 2 analysis is that we see considerable evidence for steady patterns and genuine density wave modes in many galaxies. If this were not the case, most phase-shift distributions would be uninterpretable, since only for quasi-steady modes do the potential-density phase-shift zero crossings correspond to partially kinematic features such as corotation radii. Nevertheless, some phase-shift distributions are complicated enough to suggest that the patterns are unsteady. Secondly, bars and ovals in early-type disks frequently have phase-shift crossings near or just beyond their apparent ends, i.e., they appear as fast patterns. These fast patterns appear to correspond to mature density wave mode features that have completed the decoupling process and have reached quasi-steady state, whereas density wave features in late-type disks appear to be slower patterns (see also Elmegreen & Elmegreen 1985; RSL08). Thirdly, multiple pattern speeds appear to be common among spirals, with the bar and the spiral

often having different pattern speeds and hence different corotation radii. Nevertheless, we do find evidence for some galaxies where the bar and the spiral have the same pattern speed and the same corotation radius (i.e. the so-called "bar-driven spirals"), and many such galaxies have their spirals emanating from the end of the bar (which is often identical to the CR). Finally, we find that some galaxies apparently break the "rule" that bars cannot extend beyond their own CR radius. Especially among intermediate-type barred galaxies, we have found cases where the ends of the bar lie near a strong N/P crossing, which is likely to be close to its outer Lindblad resonance radius, not CR. The strongest grand design spirals in our sample all show major P/N crossings in the middle of the spiral pattern, and these spiral patterns clearly must extend well beyond their CR radii also. These issues are discussed further in the next subsection.

5.1. Bar Extent and Corotation

5.1.1. Fast and Slow Bars

Debattista & Sellwood (2000) defined a "fast" bar to have a ratio of corotation radius to bar radius $\mathcal{R}$=$r(CR)/r(bar) \leq 1.4$ while a "slow" bar has $\mathcal{R} > 1.4$. Laurikainen et al. (2004, their Table 3) compiled bar radii for about 100 OSUBGS galaxies which we can use, together with the CR values derived in the current work, to examine this ratio. [The Laurikainen et al. (2004) bar radii are generally consistent with those of RSL08, but are smaller on average by 10% (RSL08)]. The radii are given only for "Fourier" bars, that is, bars for which the relative m=2 Fourier amplitude maintains a relatively constant position angle out to a certain radius. In deriving $\mathcal{R}$ for phase-shift-derived CR radii, we are faced with a difficulty in that many of our sample galaxies show multiple CRs. The question is, which radius do we take for the actual CR radius of an apparent bar? As noted in section 3, we have made such a selection in Table 1 by placing an asterisk next to the adopted bar CR

radius. In many cases, this is a reasonable judgment: the radius lies near or just beyond the bar ends or is the most reasonable choice because other CRs are likely associated with other patterns. Nevertheless, there are ambiguities, and we cannot be completely certain that all of the asterisked choices for the bar-CRs are correct. For example, many of the phase-shift distributions show negative values in the bar regions, suggesting that the bar CR may in fact lie well inside the apparent bar. Some of these are discussed in section 5.1.3. Table 1 indicates these alternative interpretations with boldfaced values. Table 3 summarizes our values of $\mathcal{R}$, providing two values when two interpretations are considered.

Figure 3 shows plots of $\mathcal{R}$ versus RC3 stage index T, for both the Table 1 asterisk values (upper panels) and the alternative boldface values for some galaxies (lower panels). The left panels show the individual points, while the right panels show the means by type. For the asterisk interpretations, we find for 65 galaxies of types Sbc and earlier ($T \leq 4$), the mean ratio is 1.03±0.37 (standard deviation), indicating that the bars generally extend to CR almost exactly. However, for 36 galaxies of type Sc and later ($T \geq 5$), the mean ratio is 1.50±0.63(s.d.). A similar trend was first found by RSL08 and seems consistent with Elmegreen & Elmegreen's (1985) finding that late-type bars are smaller than early-type bars and may fall well short of their corotation radii. The suggestion is that fast bars are found mainly in earlier types while slow bars are found mainly in later types.

Figure 4 shows plots of $\mathcal{R}$ versus absolute blue magnitude based on RC3 parameters, again based on the asterisked values of the bar CR in Table 1 and based on the alternative boldfaced values for some galaxies. For the asterisked values, the plot shows a weak trend in the sense that $\mathcal{R}$ is smaller on average for the more luminous galaxies in the sample. This is consistent with Figure 3 in the sense that the later type galaxies in the sample have the fainter absolute magnitudes.

Buta et al. (2005) estimated relative maximum bar and spiral torque strengths for

many of our sample galaxies, based on the same set of images. If $\mathcal{R}$ has a type dependence, we might expect the ratio to also be sensitive to bar strength because of bulge dilution in earlier types. Figure 5 shows $\mathcal{R}$ versus Q_b and Q_s. Only weak trends with bar and spiral strengths are evident, in the sense that the ratio rises slightly with these parameters. This is consistent with the type dependence of Q_b (Buta et al. 2004) and Q_s (Buta et al. 2005). These plots are based only on the asterisked values in Table 1.

5.1.2. Comparison with RSL08

The RSL08 dataset provides us with an opportunity to compare a different CR determination method with the phase-shift method, although the analyses are not completely independent since both approaches use the same near-IR images to define the gravitational potential. Nevertheless, the simulation method assumes a single pattern speed and evolves a cloud-particle disk in the potential until the morphology of the model matches the B-band morphology of the galaxy. The authors argue that their method can narrow down the corotation radius to within 20%.

Figure 6a compares our Table 1 asterisked CR radii with those from RSL08. (Individual comparisons were discussed in section 4). Although there is some correlation between the two datasets, our values of the bar CR are systematically lower than those estimated by RSL08. However, since the numerical simulation method largely focusses on matching the spiral morphology to a model, it is worth comparing the Rautiainen et al. CR radii with other (mostly spiral) radii in our Table 1. Figure 6b shows a comparison between the CR radii in our Table 1 closest in absolute difference to the Rautiainen et al. values against these same values. This naturally improves the correlation somewhat because now our spiral CR radii are brought in. This improvement in agreement shows that a numerical simulation using a single pattern speed has the tendency to assign the pattern speed of the

spiral to the bar. Even after the incorporation of some spiral pattern speeds, the plot shows that the mean difference is still such that our radii average less than theirs.

5.1.3. Super-fast Bars

Probably the most important issue brought to light from this analysis is the identification of numerous cases having or possibly having $\mathcal{R} < 1$, confirming the initial evidence for this class found in Paper I. Some of these are likely due to uncertainties in the estimated bar radius and/or in the phase-shift-determined CR radius. We have suggested in Paper I, however, that not all cases are likely to be due to these uncertainties. If real, these cases would have to be classified as "super-fast" bars. The existence of bars extending beyond their CR goes against the common wisdom of what should be the bar orbit structure (Contopoulos 1980). In passive orbit analysis, the stellar orbits support the bar within CR, but not outside CR.

One of the best cases of a possible super-fast bar in our sample is NGC 4902 (Figure 2.108). This galaxy is almost face-on so that deprojection uncertainties are not seriously impacting the results. The phase-shift distribution plot shows successive P/N crossings at $9\farcs0$ and $38\farcs6$, each involving a positive phase-shift section followed by a negative phase-shift section. The prominent N/P crossing at $25\farcs5$ ($r/r_o(25)$=0.28) is very close to the bar radius of $22''$ - $26''$ estimated by Laurikainen et al. (2004) and RSL08. As we noted in section 2.1, the negative portion of a phase-shift distribution belongs to the inner mode, and since this covers most of the bar of NGC 4902, we suggest that the actual bar CR in this case is at $9\farcs0$ (boldfaced in Table 1), not at $38\farcs6$ (asterisked in Table 1). The latter CR would therefore most likely be associated with the prominent spiral forming a pseudoring around the bar.

Comparable cases to NGC 4902 include NGC 1187 (Figure 2.18) and NGC 5643 (Figure 2.123). In each, an N/P crossing occurs at the bar ends, indicating that the bar belongs to an inner mode. In each case also, a second crossing farther out is most likely associated with a bright inner spiral. Even the classical barred spiral NGC 1300 could be in this category.

Figures 3c,d show the impact of such unusual interpretations on $\mathcal{R}$ versus type T, while Figures 4c,d show the impact on $\mathcal{R}$ versus absolute blue magnitude, using in each case the bold-faced alternative bar CR values from Table 1 for 14 objects. This considerably weakens the type dependence in $\mathcal{R}$ and changes the means to 0.94±0.40 for types Sbc and earlier and 1.15±0.70 for types Sc and later. This suggests that "super-fast" bars may occur throughout the spiral sequence, not just among earlier types. Late-type examples we have pointed out in section 3 include NGC 4496, 5334, and 7418. Figure 4c shows that with these alternative interpretations, there are almost no slow bars having $M_B^o < -19.5$.

5.2. Effect of Orientation Parameters and Bulge Shape on Phase-Shift Distributions

We have noted in the above discussions that the assumption of a spherical bulge can lead to something called "decomposition pinch," where the inner isophotes of a galaxy show a pinched shape in a deprojected image due to over-correction for bulge light along the minor axis. We would like to know how this artifact affects what we see in the phase-shift plots. We are also interested in how uncertainties in the adopted orientation parameters for a galaxy affect the appearance of the plots. For this purpose, we have chosen the galaxy NGC 150, which has both a prominent bar and a spiral.

Figures 7a and b show the sensitivity of the phase-shift distribution to the assumption

of bulge shape. The test was made with non-Fourier-smoothed images, and hence the phase-shift plot in Figure 7b is slightly noisier than that in Figure 2.1, which used the Fourier-smoothed version of the same image. Panel (a) shows the results for an image of NGC 150 deprojected assuming the bulge is as flat as the disk, while panel (b) shows the results assuming the bulge is spherical. The main difference between these plots is the appearance of a spike in the inner regions in panel (b). This could be a complete artifact of the decomposition pinch, but note that it does not lead to a false crossing. Deprojection assuming a perfectly flat bulge causes the bulge isophotes to stretch into a bar-like feature, but panel (a) shows that no crossing results from that either, presumably because no additional skewness is introduced.

The remaining panels in Figure 7 show the effects of different assumed inclinations (through the disk axis ratio q and major axis position angle pa). We used inclinations and position angles departing from those used by Laurikainen et al. (2004) by $\pm 5^\circ$. The filled circles in Figure 7 show the locations of the adopted CR radii from Table 1. Naturally, changing the orientation parameters moves the CR locations since the skewness of the pattern is either diminished or amplified. When the revised CR locations are plotted on the corresponding deprojected images, however, the CR circle for the bar still lies close to or just beyond the bar ends. We conclude that uncertainties in the assumed bulge shape and in the orientation parameters are not seriously impacting our results.

5.3. High-Luminosity Grand-Design Spirals

We have shown that in four exceptionally strong grand-design spirals, NGC 908, 5054, 5247, 5248, the phase-shift method mostly favors a single CR in the middle of the spiral. This is consistent with the modal theory (Bertin et al. 1989a,b), which demonstrated that spiral modes generally extend to their OLR. Contopoulos & Grosbol (1986) and Patsis and

Kaufmann (1999) argue that the strong part of a spiral mode extends mainly to the inner 4:1 resonance, beyond which it is insufficiently organized. While there might be galaxies where this is the case (e.g., NGC 3627, Zhang et al. 1993), this is not likely to be true in general. The spirals simulated by Zhang (1996, 1998, 1999) all extend to their OLR.

Figure 8 shows how the locations of CR radii for NGC 908, 5054, 5247, 5248, as well as NGC 157 and 7412 which show two CRs in the spiral region, compare with the maximum in relative Fourier amplitudes of the light distribution. These show a tendency for the CR radii to lie near the maxima of the dominant Fourier term. For NGC 157, each main CR is associated with a distinct m=2 maximum, while for NGC 7412 the two CRs share a single m=2 maximum. In NGC 908, 5247, and 5248, the single main CR lies within a broad maximum distribution of m=2 amplitude. For NGC 5054, the same is found but for m=3, which is the dominant term in that case. These findings are also consistent with the modal theory (Bertin et al. 1989a,b; Elmegreen and Elmegreen 1990).

6. Discussion

6.1. Further comments on the Robustness of the Method and Additional Support for the Results

This paper is the first application of the potential-density phase-shift method to a large sample of spiral galaxies covering almost all Hubble types. We have shown a clear relationship between phase-shift crossings and observed morphological features in many galaxies, and highlighted a possibly significant trend of correlation between the ratio $\mathcal{R}$ with the de Vaucouleurs-revised Hubble type, which is similar to what has been found in simulation studies of the same image database by RSL08. Despite the fact that the quantitative value of the trend depends on which crossing we chose to use as the bar CR

radius, the gross qualitative trend appears to be rather robust after we have experimented with the different choices of the bar CR values in cases of potential ambiguity, as shown in Figure 3. We have highlighted counter-intuitive examples where the bulk of a bar's extent may lie outside its CR radius, and such examples may be found across the morphological sequence though they are most concentrated among the intermediate Hubble types.

Figure 9 summarizes the types of bar-spiral combinations we have highlighted in our discussion. In the upper left panels, NGC 7479 and NGC 4314 are presented as cases where the bar and the spiral have the same pattern speed. The bars have positive phase-shifts throughout most of their extent, and the single major P/N crossing almost exactly encircles the bar ends. In these galaxies, the bar extends exactly to its CR, and is a conventional fast bar.

In the upper right panels of Figure 9, NGC 150 and NGC 3507 show fast bars where the spirals are likely independent patterns with their own CR and pattern speed. Again, the bars have positive phase-shifts throughout most of their extent, and appear to end exactly at their CR.

The situation is noticeably different for the two galaxies in the lower left panels of Figure 9. In each case, there is a well-defined N/P crossing almost exactly at the bar ends, indicating a decoupling point. NGC 4902, as we noted in section 5.1.3, shows the expected one positive, followed by one negative zone for an inner mode, and taking this literally we are forced to conclude that the bar CR corresponds to the innermost circle, not the more comforting choice of the intermediate circle. NGC 5643 is similar except for some negative phaseshifts near the center, which may signify an unresolved inner mode. In both cases, the narrowest parts of the bar lie completely outside the inner CR and extend to the N/P crossing, which as we have argued is likely to be close to the location of the bar's OLR. Thus, NGC 4902 and 5643 are more consistently interpreted as "super-fast" bars.

We have also found in our analysis suggestive cases of slow bars, but clearcut examples are actually not strong. In most of the high $\mathcal{R}$ cases based on the asterisked radii in Table 1, there are negative phase-shifts in the bar region. This suggests ongoing decoupling of the bar from the spiral. A possible example of this is seen in NGC 3513 (Figure 2.54), which has a very conspicuous bar and spiral. Only a single P/N crossing is found, yet the bar has negative phase-shifts throughout and a bump in the inner regions suggestive of a decoupling pattern. Thus, although $\mathcal{R} = 2.15$ based on the single P/N crossing, it is not clear this is a genuine slow bar case. The two suggested examples of slow bars in the lower right panels of Figure 9 are also weak because phase-shifts are low or nearly zero along the bar. In NGC 3686, the phase-shifts are almost entirely negative but within the noise of being zero. It could be argued that in both of these galaxies, the bar and spiral are still decoupling. Based on our analysis, we do not find a single absolutely compelling case of a slow bar.

Even though Figure 9 shows that we can identify systematic trends in phase-shift distributions that have specific physical meanings, our experience has also shown that phase-shift distributions can be complicated and difficult to interpret. It would be a fair criticism of the method that we do not yet have a robust rule for deciding in general which phase-shift plots and crossings are to be trusted, and which are not. Our approach, by combining the phase-shift information with what we see in the image, is probably the best in general. The ambiguity and the variety of situations we encounter in these plots might be partly due to the fact that an existing stage of galaxy morphology is a result of both its initial condition at the time of galaxy formation and its subsequent interaction history. No two galaxies will go through exactly the same stages of evolution. The broad categories we use to classify the evolution stages (i.e. galaxy morphological types) reflect only a general trend, but do not exhaust all the real-world possibilities. Except for the best-defined bars and spirals, this complex history of evolution, coupled with the complexity that arises when the pattern is not yet quasi-steady, is why there are no set rules in general for interpreting

what an observed phase-shift trend really means dynamically, apart from giving the signs of the instantaneous torquing action between a wave and the basic state.

RSL08 have argued that the results of the phase-shift method are of questionable validity, owing to the cases where we deduce that $\mathcal{R}$ is considerably less than 1. We have made our arguments in favor of such cases nonetheless, but it is also important to note that the passive orbit analysis that Contopoulos (1980) used to deduce $\mathcal{R} \geq 1$ as a rule is not necessarily valid when collective effects are taken into account. These cases are also supported by several other lines of argument. In the case of a massive bar with little spiral component connecting to it, such as NGC 4665, the bar necessarily extends beyond its CR because for the SWING amplifier (Toomre 1981) to work in generating the bar mode, there needs to be density wave content outside CR to receive the energy transmitted from the over-reflection of the waves inside CR.

Also, as we have argued in Paper I, the N-body bar described by Sparke & Sellwood (1987) showed evidence that at least in certain stages of its evolution the bar can extend beyond its CR, possibly all the way to its OLR. In its earlier phases, this bar, although not well-formed and not yet steady, extends much beyond its CR (their Figure 3, left panel), while at later phases the bar is more developed and has a pattern speed low enough to end near its CR. In the N-body simulations of Sparke and Sellwood, these different stages of bar evolution happen rather fast, which is partly a result of the fact that the initial condition of this N-body simulation (i.e. the basic state) is not entirely compatible with the unstable mode that emerges out of it, so the whole system evolves relatively fast in the course of the simulation to achieve overall global self-consistency and equilibrium. In physical galaxies, the basic state and the mode are always in a co-evolution process during the Hubble-type transformation process in a galaxy's lifetime, so the intermediate stages of the evolution could potentially last much longer than have been demonstrated

in the past N-body simulations. A more robust proof of the long-lasting nature of these intermediate-type super-fast bars will likely emerge from a careful demonstration of the morphological transformation along the Hubble sequence throughout the lifetime of an individual galaxy using a fully-self-consistent 3D N-body simulation, a demanding task that currently still has not yet been achieved.

In addition, as we have already argued, in the nested-pattern formation scenario outlined in this paper, some inner bars decouple from a skewed long bar, which can otherwise be regarded as a spiral. Since the spiral pattern has been in multiple instances shown to extend beyond its CR, these long, skewed bars can as well, i.e., in reality there is no hard dividing line between a bar and a spiral.

Finally, the continuity of the phase-shift curves themselves demands that the positive-humps and negative-humps form in mutual succession, and their relation to the direction of angular momentum exchange (between the wave and the basic state) demands that we interpret the N/P crossings as the locations where the successive modes decouple, and the CRs are positioned in between at the P/N crossings. This condition by itself dictates that a density wave mode in general extends beyond its CR. The CR radius and bar radius can become equal only when there is a spiral component outside the bar (and connecting to it to form the same mode) to receive the transmitted wave.

6.2. Support for the Modal Nature of the Spiral and Bar Patterns in Galaxies

We have shown that more than half of our OSUBGS sample galaxies possess grand-design density wave patterns. Furthermore, the nested patterns organize themselves in a clear sequence of overlapping resonance features, which appear to develop gradually in well-coordinated mode-decoupling processes. These and other evidences found in this

work as well as in previous works by other researchers show that the density wave patterns in most disk galaxies are likely to be self-organized, quasi-stationary modes which undergo slow secular morphological transformation together with the slow evolution of the basic state. This picture is inconsistent with the alternative view of the fast transient nature of density wave patterns in disk galaxies (see, for example, Carlberg & Sellwood 1985, hereafter CS85), which argues that spiral patterns die out and re-emerge on the time scale of the orbital period of the disk stars (see the first paragraph of the Introduction section of CS85. The orbital period of stars for the solar neighborhood is on the order of 250 Myr). Such hypothesized fast change is incompatible, in a statistical sense, with the predominance of well-organized, strong density wave patterns which appear to be the norm among especially the intermediate and early Hubble-type galaxies in this study and in other near-infrared samples of disk galaxies.

Furthermore, our results and the previous results of Zhang (1996,1998,1999) could not be understood in a "broadening of resonances" sense as advocated by some transient spiral supporters. This is because in the resonance-broadening scenario, even though the mass flow directions predicted near the ILR and OLR are consistent with what we found using the phase shift method, these same mass flow directions at the ILR and OLR were found (CS85, p. 88) to be "independent of the winding sense of the spiral (see LBK)". This result of CS85 or LBK is expected since resonant interaction is a local effect, so the winding sense of the pattern does not matter. In contrast, for the collective effect we are dealing with here, the sense of the phase-shift is critically dependent on whether the wave is leading or trailing, since the geometrical phase shift is determined by the Poisson equation, whereas the physical sense of whether the potential is torquing the density forward or backward depends on which direction the pattern is rotating. This fact alone tells us that the collective dissipation effect in spiral galaxies cannot be viewed as a broadening-of-resonance effect. In addition, the resonance-broadening effect is a kind of

top-down-control effect – it is a single-orbit's response to the applied potential (CS85, p. 81, mentioned the equivalence of their current approach with LBK's single-orbit approach, even though one is Eulerian and the other is Lagrangian). In a self-organized instability it is the "sideways" interactions among stars themselves that leads to pattern coherence and collective dissipation. This latter effect cannot be modeled entirely as a top-down-control hierarchy due to an *applied* spiral or bar potential. An additional piece of evidence of the disparity of the two approaches is that, near the CR region, the sense of angular momentum exchange between the basic state and the wave, and thus the sense of mass flow predicted by the broadening-of-resonance approach (see Sellwood & Binney 2002, Figure 4) are exactly opposite to that predicted by the phase shift method (the latter being consistent with that needed to build up the Hubble sequence), and thus the behavior at CR of the resonance-broadening approach could not lead to the secular mass re-distribution needed to build up the Hubble sequence.

Finally, we comment that in many of the past N-body simulations of transient spiral formation (see, e.g. Sellwood 2008 and the references therein), the spiral patterns' transience is a direct result of the choice of basic state, i.e., Sellwood and coworkers had consistently chosen the kind of disks that are *stable* to spiral mode formation. However, in the simulation of barred galaxies (e.g. Sparke & Sellwood 1987), Sellwood and coworkers had consistently chosen basic states that are *unstable* to bar mode formation. Such disparity in the choice of basic state, which reflected partly the authors' bias, appears now to be untenable in accounting for the morphological features of real galaxies: As we have seen amply in this study, the spiral and bar modes intermingle and inter-transform throughout the radial extent of the disk of a galaxy, and throughout the lifetime of a galaxy. It is no longer possible for a simulator to arbitrarily choose one kind of basic state characteristics for spirals and another for bars, since these features are interconnected. Both kinds of density wave patterns appear to have originated as unstable modes in galaxy disks, and the

self-organization and collective dissipation processes go hand in hand to guarantee both the short-term quasisteady nature of the pattern, as well as the long-term slow evolution of the parent galaxy's mass and velocity distribution – and the latter evolution of the basic state of the disk in turn leads to the slow transformation of the density-wave pattern's modal morphology so as to be compatible with the evolving basic-state's characteristics (Zhang 1998, 1999; Bertin et al. 1989a,b).

7. Conclusions

We have used the potential-density phase-shift method to locate corotation radii in 153 OSUBGS galaxies using deprojected H-band images. This is the first application of the method to a large number of galaxies across the full range of spiral sub-types. Our main conclusions are:

1. Most phase-shift distributions do not appear to be simply noise. Most OSUBGS galaxies show well-defined phase-shift crossings which correspond to grand-design density wave resonance features.

2. Multiple corotations are found in many galaxies. For example, NGC 4303 shows five well-defined crossings within $r_o(25)$. Nevertheless, a single-pattern-speed model of RSL08 had also been shown to be able to account for many aspects of this galaxy's morphology.

3. Some phase-shift distributions (and corroborated by galaxy images) show evidence of pattern decoupling, where a change in the phase-shift leads mostly to a near-crossing rather than a full-fledged crossing. This type of resonant pattern evolution and successive decoupling favors a continuously-present and evolving density wave pattern, not a recurrent one as is advocated in the case of bar formation by Bournaud & Combes (2002). It also contradicts the rapidly-changing recurrent spiral scenario of Carlberg & Sellwood (1985).

4. For grand-design spirals, the phase-shift method places corotation in the middle of the spiral, suggesting that these spirals actually extend to near their OLR and not the inner 4:1 resonance as suggested by some earlier theoretical studies. We also find that the CR radii of several grand-design spirals lie near the maximum of their dominant Fourier term, as expected from the modal theory of spiral structure.

5. A comparison between phase-shift bar CR radii and numerical simulation CR radii (RSL08) shows that the phase-shift method generally gives smaller values. Some of this disagreement is due to the tendency for the numerical simulation method to latch on to the pattern speed of the spiral rather than the pattern speed of the bar, as also acknowledged by RSL08. When more outer phase-shift CR radii are compared with RSL08 values, much better agreement is found.

6. We confirm a likely type-dependence in the ratio $\mathcal{R} = r(CR)/r(bar)$ if we generally select the P/N crossings that lie near or just outside the ends of the bar as the bar CR radius. The average $\mathcal{R}$ ranges from 1.03±0.37 for types Sbc and earlier, to 1.50±0.63 for types Sc and later. This is similar to what was found by RSL08 in spite of the use of different CR radii. Nevertheless, we have shown that if we follow our rule of one positive and one negative portion of the phase-shift distribution for a single mode, then many of the bars we observe are actually "super-fast" and the type dependence in $\mathcal{R}$ is considerably weakened, reducing to average values of 0.94±0.40 for types Sbc and earlier and 1.15±0.70 for types Sc and later. Super-fast bars still appear to favor the intermediate to late types. Such cases of super-fast bars are *not* predicted by passive-orbit theory of galaxy model construction, which clearly favors no bar extending beyond its CR radius (Contopoulos 1980).

7. We find compelling evidence of normal fast bars having $\mathcal{R} \approx 1$ and either a coupled spiral having the same pattern speed (e.g., NGC 4314, 7479), or a decoupled one having a different pattern speed (e.g., NGC 150, 3507). We do not find as much compelling evidence

for genuine slow bars in our sample. Many of those having $\mathcal{R} > 1.4$ based on our Table 1, asterisked CR selections have near-zero or negative phase-shifts in the bar region, suggesting ongoing pattern decoupling. An example of this is NGC 3513 which has only a single P/N crossing at more than twice the bar radius and yet the phase-shift distribution is negative throughout the bar's extent. Our two best slow bar cases are NGC 1493 and 3686 and even these are not clearcut.

8. Our confirmation of the presence of quasi-steady *nested wave modes* and their close correspondence with the phase-shift distribution is in direct contradiction with Lynden-Bell and Kalnajs (1972)'s and Binney & Tremaine (2008)'s conclusion of a constant angular momentum flux throughout the galactic disk: such a flux pattern does not deposit angular momentum locally onto the disk *en route* of the outward angular momentum transport by the wave, and thus does not promote the growth of the nested resonance patterns that we have found in real galaxies.

We thank E. Laurikainen and H. Salo for the deprojected OSUBGS images used for this study. RB acknowledges the support of NSF grant AST-0507140 to the University of Alabama. Funding for the OSUBGS was provided by grants from the NSF (grants AST 92-17716 and AST 96-17006), with additional funding from the Ohio State University. NED is operated by the Jet Propulsion Laboratory, California Institute of Technology, under contract with NASA. Funding for the creation and distribution of the SDSS Archive has been provided by the Alfred P. Sloan Foundation, the Participating Institutions, NASA, NSF, the U.S. Department of Energy, the Japanese Monbukagakusho, and Max Planck Society.

References

Bertin, G., Lin, C.C., Lowe, S.A., & Thurstans, R.P. 1989a, ApJ, 338, 78

Bertin, G., Lin, C.C., Lowe, S.A., & Thurstans, R.P. 1989b, ApJ, 338, 104

Binney, J., & Tremaine, S. 2008, Galactic Dynamics (Princeton:Princeton Univ. Press)

Bournaud, F. & Combes, F. 2002, A&A, 392, 83

Buta, R. & Crocker, D. A. 1993, AJ, 106, 1344

Buta, R., Laurikainen, E., & Salo, H. 2004, AJ, 127, 279

Buta, R., van Driel, W., Braine, J., Combes, F., Wakamatsu, K., Sofue, Y., & Tomita, A. 1995, ApJ, 450, 593

Buta, R., Vasylyev, S., Salo, H., and Laurikainen, E. 2005, AJ, 130, 506

Buta, R. J., Corwin, H. G., & Odewahn, S. C. 2007, The de Vaucouleurs Atlas of Galaxies, Cambridge: Cambridge U. Press

Carlberg, R.G., & Sellwood, J.A., 1985, ApJ, 292, 79

Contopoulos, G. 1980, A&A, 31, 198

Contopoulos, G. & Grosbol, P. 1986, A&A, 155, 11

Debattista, V.P., & Sellwood, J.A. 2000, ApJ, 543, 704

de Vaucouleurs, G., de Vaucouleurs, A., Corwin, H. G., Buta, R. J., Paturel, G., & Fouque, P. 1991, Third Reference Catalog of Bright Galaxies (New York: Springer) (RC3)

Elmegreen, B. G. & Elmegreen, D. M. 1985, ApJ, 288, 438

Elmegreen, B. G. & Elmegreen, D. M. 1990, ApJ, 355, 52

Elmegreen, D. M. & Elmegreen, B. G. 1982, MNRAS, 201, 1021

Elmegreen, D. M. & Elmegreen, B. G. 1987, ApJ, 314, 3

Eskridge, P. B., Frogel, J. A., Pogge, R. W., et al. 2002, ApJS, 143, 73

Garcia-Burillo, S., Fernandez-Garcia, S., Combes, F., Hunt, L. K., Haan, S., Schinnerer, E., Boone, F., Krips, M., & Marquez, I. 2008, astro-ph 0810.4892

Gnedin, O.Y., Goodman, J., & Frei, Z. 1995, AJ, 110, 1105

Kalnajs, A. 1971, ApJ, 166, 275

Knapen, J. Whyte, L. F., De Blok, W. J. G., & van der Hulst, J. M. 2004, A&A, 423, 481

Kormendy, J. and Kennicutt, R. 2004, ARAA, 42, 603

Laurikainen, E., Salo, H., Buta, R., & Vasylyev, S. 2004, MNRAS, 355, 1251

Laurikainen, E., Salo, H., Buta, R., & Knapen, J. H. 2007, MNRAS, 381, 401

Lynden-Bell, D., & Kalnajs, A.J., 1972, MNRAS, 157, 1

Masset, F. & Tagger, M. 1997, A&A, 322, 442

Mazzuca, L. M., Knapen, J. H., Veilleux, S., & Regan, M. W. 2008, ApJS, 174, 337

Mihos, C. & Bothun, G. 1997, ApJ, 481, 781

Patsis, P. A. & Kaufmann, D. E. 1999, A&A, 352, 469

Quillen, A. C., Frogel, J. A., & González, R. A. 1994, ApJ, 437, 162

Rautiainen, P. & Salo, H. 1999, A&A. 348, 737

Rautiainen, P., Salo, H., & Laurikainen, E. 2005, ApJ, 631, L129

Rautiainen, P., Salo, H., & Laurikainen, E. 2008, MNRAS, 388, 1803

Sellwood, J.A. 2008, in Formation and Evolution of Galaxy Disks, Eds. J.G. Funes, S.J., and E.M. Corsini (SFO: ASP), 241

Sellwood, J.A., & Binney, J.J. 2002, MNRAS, 336, 785

Sempere, M. J. & Rozas, M. 1997, A&A, 317, 405

Snow, C. 1952, Hypergeometric and Legendre Functions with Applications to Integral Equations of Potential Theory (NBS/AMS 19; Washington, DC: National Bureau of Standards)

Sparke, L.S., & Sellwood, J.A. 1987, MNRAS, 225, 653

Thornley, M. D. 1996, ApJ, 469, L45

Toomre, A. 1981, in Structure and Dynamics of Normal Galaxies, ed. S. M. Fall & D. Lynden-Bell (Cambridge: Cambridge Univ. Press), 111

Zhang, X. 1996, ApJ, 457, 125

Zhang, X. 1998, ApJ, 499, 93

Zhang, X. 1999, ApJ, 518, 613

Zhang, X. 2003, JKAS, 36, 223

Zhang, X. & Buta, R. 2007, AJ, 133, 2584

Zhang, X., Wright, M., & Alexander, P. 1993, ApJ, 418, 100

Table 1. Summary of Corotation Radii in OSUBGS Galaxies[a]

Galaxy	CR_1	err	code	CR_2	err	code	CR_3	err	code	CR_4	err	code
1	2	3	4	5	6	7	8	9	10	11	12	13
NGC 150	38.0*	...	3	72.2	...	1	...	...	.	...	...	.
NGC 157	6.4	...	3	40.0	...	3	72.9	...	3	...	...	.
NGC 210	36.7*	3.8	3	80.8	...	3	....	...	.	...	...	.
NGC 278	25.3	...	3	...	...	.	...	...	.	...	...	.
NGC 289	3.9	0.3	1	21.3*	...	3	66.2	...	3	133.2	...	1
NGC 428	54.8*	...	3	...	...	.	...	...	.	...	...	.
NGC 488	13.6	0.8	1	34.5	...	1	70.3	...	3	...	...	.
NGC 578	19.1*	...	3	38.8	...	3	79.9	...	1	...	...	.
NGC 613	5.0	...	3	**55.1**	...	3	88.0*	...	3	...	...	.
NGC 685	19.3*	...	3	92.5	...	1	...	...	.	...	...	.
NGC 864	**6.5**	...	3	33.0*	...	3	57.3	...	1	...	...	.
NGC 908	7.9	0.6	3	21.0	...	1	78.6	...	3	...	...	.
NGC 1042	3.3	...	3	34.7	...	3	84.4	...	3	...	...	.
NGC 1058	30.5	...	3	...	...	.	...	...	.	...	...	.
NGC 1073	38.0*	...	3	89.3	...	3	...	...	.	...	...	.
NGC 1084	22.4	...	3	44.9	1.6	1	...	...	.	...	...	.
NGC 1087	2.1	...	3	35.3*	...	3	...	...	.	...	...	.
NGC 1187	**13.0**	1.9	3	55.0*	...	3	113.1	...	1	...	...	.
NGC 1241	12.4*	1.1	3	...	...	.	...	...	.	...	...	.
NGC 1300	54.8*	1.4	3	142.3	...	3	...	...	.	...	...	.

Table 1—Continued

Galaxy	CR_1	err	code	CR_2	err	code	CR_3	err	code	CR_4	err	code
1	2	3	4	5	6	7	8	9	10	11	12	13
NGC 1302	31.0*	...	3	55.0	...	1	83.6	...	1	...	...	.
NGC 1309	7.8	...	1	15.3	...	3	34.2	1.9	3	...	...	.
NGC 1317	18.8	...	3	43.3*	...	3	105.4	...	1	...	...	.
NGC 1350	**11.8**	1.1	3	135.0*	...	3	...	...	.	...	...	.
NGC 1371	19.5	...	3	63.0	...	1	81.5	...	1	...	...	.
NGC 1385	31.9*	...	3	...	...	.	...	...	.	...	...	.
NGC 1493	37.5*	...	3	...	...	.	...	...	.	...	...	.
NGC 1559	18.6*	...	3	...	...	.	...	...	.	...	...	.
NGC 1617	14.2	...	3	38.0*	...	3	...	...	.	...	...	.
NGC 1637	3.2	...	1	23.3*	1.2	3	50.5	...	3	...	...	.
NGC 1703	25.5*	...	3	59.2	...	1	...	...	.	...	...	.
NGC 1792	37.0	...	1	55.8	...	1	...	...	.	...	...	.
NGC 1808	7.0	0.2	3	74.4*	...	3	106.0	...	1	...	...	.
NGC 1832	22.6*	...	3	38.6	...	1	...	...	.	...	...	.
NGC 2090	25.1	...	3	78.8	...	1	...	...	.	...	...	.
NGC 2139	21.7*	...	3	...	...	.	...	...	.	...	...	.
NGC 2196	12.8	1.8	3	64.8	...	1	...	...	.	...	...	.
NGC 2442	11.4	2.6	1	86.6*	...	3	...	...	.	...	...	.
NGC 2559	38.5*	...	3	...	...	.	...	...	.	...	...	.
NGC 2566	56.2*	...	1	98.6	...	3	...	...	.	...	...	.

Table 1—Continued

Galaxy	CR_1	err	code	CR_2	err	code	CR_3	err	code	CR_4	err	code
1	2	3	4	5	6	7	8	9	10	11	12	13
NGC 2775	64.0	...	1	104.0	...	1	...	...	.	...	...	.
NGC 2964	3.0	...	1	36.7*	...	3	...	...	.	...	...	.
NGC 3059	25.9*	2.0	3	...	...	.	...	...	.	...	...	.
NGC 3166	54.6*	4.8	3	...	...	.	...	...	.	...	...	.
NGC 3223	23.2	...	3	62.0	...	3	...	...	.	...	...	.
NGC 3227	47.0*	4.7	3	108.7	...	3	...	...	.	...	...	.
NGC 3261	28.6*	...	3	37.7	...	1	52.3	...	1	...	...	.
NGC 3275	6.1	0.2	3	25.7*	1.3	3	...	...	.	...	...	.
NGC 3319	9.5	...	3	37.7*	...	3	126.4	...	3	...	...	.
NGC 3338	18.1*	1.4	3	50.3	...	3	163.3	...	3	...	...	.
NGC 3423	17.9	1.3	3	...	...	.	...	...	.	...	...	.
NGC 3504	24.3	...	3	41.9*	...	1	...	...	.	...	...	.
NGC 3507	26.3*	...	3	52.1	1.7	3	...	...	.	...	...	.
NGC 3513	2.0	...	3	59.6*	...	3	...	...	.	...	...	.
NGC 3583	3.3	...	1	30.5*	...	3	64.6	...	1	...	...	.
NGC 3593	8.8	0.7	1	29.5	...	1	51.6	...	1	...	...	.
NGC 3596	12.3	...	3	32.2	...	3	49.8	...	1	71.1	...	1
NGC 3646	15.4	...	3	74.4	...	3	...	...	.	...	...	.
NGC 3675	6.7	...	3	27.4*	...	1	83.9	...	3	...	...	.
NGC 3681	20.4*	...	3	...	...	.	...	...	.	...	...	.

Table 1—Continued

Galaxy	CR_1	err	code	CR_2	err	code	CR_3	err	code	CR_4	err	code
1	2	3	4	5	6	7	8	9	10	11	12	13
NGC 3684	27.7	...	3	60.8	...	3	...	...	.	...	...	.
NGC 3686	41.8*	...	3	...	...	.	...	...	.	...	...	.
NGC 3726	21.9*	1.0	3	65.2	2.1	3	114.1	...	1	...	...	.
NGC 3810	14.2	...	3	64.3	...	1	83.8	...	1	...	...	.
NGC 3887	28.0*	...	3	57.1	...	3	...	...	.	...	...	.
NGC 3893	20.8	...	3	61.0	...	3	...	...	.	...	...	.
NGC 3938	25.0	...	3	61.7	...	3	...	...	.	...	...	.
NGC 3949	7.8	...	1	37.5	...	1	...	...	.	...	...	.
NGC 4027	24.0*	...	3	53.2	...	1	...	...	.	...	...	.
NGC 4030	10.4	...	3	29.7	...	3	55.7	...	3	91.5	...	1
NGC 4051	3.3	...	3	70.4*	...	3	...	...	.	...	...	.
NGC 4123	18.0	...	3	55.4*	...	3	108.9	...	1	...	...	.
NGC 4136	6.8	...	3	24.7*	1.9	3	34.2	0.6	3	60.8	...	1
NGC 4145	46.6*	...	3	122.4	...	3	...	...	.	...	...	.
NGC 4151	5.7	...	3	69.8	...	3	99.4*	...	3	...	...	.
NGC 4212	35.6	...	3	...	...	.	...	...	.	...	...	.
NGC 4242	30.4	...	3	...	...	.	...	...	.	...	...	.
NGC 4254	7.5	...	3	20.8	...	3	55.8	...	3	90.7	...	3
NGC 4293	15.0	1.5	1	79.3*	...	3	142.3	...	1	...	...	.
NGC 4303[b]	20.8*	...	3	48.8	...	3	69.6	...	1	84.9	...	1

Table 1—Continued

Galaxy	CR_1	err	code	CR_2	err	code	CR_3	err	code	CR_4	err	code
1	2	3	4	5	6	7	8	9	10	11	12	13
NGC 4314	3.3	...	3	76.9*	...	3	...	...	.	...	...	.
NGC 4394	**16.7**	...	3	42.4*	...	3	89.6	...	1	...	...	.
NGC 4414	20.7	...	3	49.3	...	3	76.2	...	3	...	...	.
NGC 4450	4.5	...	1	30.5*	...	3	59.4	...	3	156.5	...	1
NGC 4457	44.2*	...	3	...	...	.	...	...	.	...	...	.
NGC 4487	20.5*	0.6	3	42.8	1.6	1	...	...	.	...	...	.
NGC 4496	9.1	...	3	60.0*	...	3	102.5	...	1	...	...	.
NGC 4504	10.3	1.2	1	26.6	...	3	...	...	.	...	...	.
NGC 4527	65.2*	...	3	...	...	.	...	...	.	...	...	.
NGC 4548	19.0	...	3	74.8*	...	3	...	...	.	...	...	.
NGC 4571	5.3	...	1	50.5	2.6	3	...	...	.	...	...	.
NGC 4579	8.7	...	1	**24.7**	...	3	48.0*	...	1	81.3	...	3
NGC 4580	15.4	...	3	38.7	0.8	3	...	...	.	...	...	.
NGC 4593	12.3	...	3	65.8*	...	3	97.4	...	3	...	...	.
NGC 4618	83.0*	...	3	...	...	.	...	...	.	...	...	.
NGC 4643	6.2	...	1	50.2*	...	1	...	...	.	...	...	.
NGC 4647	**6.1**	...	3	17.0*	...	3	50.5	...	1	...	...	.
NGC 4651	6.1	0.5	3	36.5*	...	3	51.8	...	3	88.9	2.5	3
NGC 4654	4.3	0.3	3	20.1*	0.7	3	78.6	1.9	3	...	...	.
NGC 4665	16.8	...	3	47.2*	...	3	...	...	.	...	...	.

Table 1—Continued

Galaxy	CR_1	err	code	CR_2	err	code	CR_3	err	code	CR_4	err	code
1	2	3	4	5	6	7	8	9	10	11	12	13
NGC 4689	34.1	0.8	3	66.5	1.4	3	103.0	...	3	...	...	.
NGC 4691	34.1*	...	3	...	...	.	...	...	.	...	...	.
NGC 4699	2.5	...	1	14.9*	...	3	...	...	.	...	...	.
NGC 4772	52.5	...	1	...	...	.	...	...	.	...	...	.
NGC 4775	38.0	...	3	...	...	.	...	...	.	...	...	.
NGC 4781	2.4	...	1	**15.2**	...	3	42.4*	...	3	61.3	...	3
NGC 4900	**9.2**	...	3	34.6*	...	3	...	...	.	...	...	.
NGC 4902	**9.0**	...	3	38.6*	...	3	59.5	...	1	86.6	...	1
NGC 4930	4.5	...	3	46.2*	...	3	96.8	7.3	3	...	...	.
NGC 4939	17.3*	...	3	37.6	...	3	69.3	...	3	120.3	4.6	3
NGC 4941	57.1	...	1	...	...	.	...	...	.	...	...	.
NGC 4995	21.6*	0.8	3	37.7	0.8	3	64.5	...	3	...	...	.
NGC 5005	29.4	0.6	3	51.6*	...	3	...	...	.	...	...	.
NGC 5054	74.0	...	3	...	...	.	...	...	.	...	...	.
NGC 5085	7.5	...	3	21.6	0.3	3	47.2	...	3	97.3	...	1
NGC 5101	10.3	3.0	3	54.3*	...	3	93.5	...	3	...	...	.
NGC 5121	37.1	...	3	...	...	.	...	...	.	...	...	.
NGC 5247	14.0	1.0	3	87.2	...	3	...	...	.	...	...	.
NGC 5248	12.5	...	3	69.6	...	3	...	...	.	...	...	.
NGC 5334	**6.0**	...	3	42.5*	...	3	81.8	...	3	...	...	.

Table 1—Continued

Galaxy	CR_1	err	code	CR_2	err	code	CR_3	err	code	CR_4	err	code
1	2	3	4	5	6	7	8	9	10	11	12	13
NGC 5427	7.3	0.2	3	38.0	...	3	63.3	...	1	...	...	.
NGC 5483	2.6	...	3	18.0*	...	3	25.6	...	3	72.7	...	1
NGC 5643	**23.6**	...	3	66.9*	...	3	104.7	...	3	...	...	.
NGC 5676	23.2	...	3	38.2	...	3	61.2	...	1	...	...	.
NGC 5701	15.4	...	3	52.5*	...	3	86.9	...	3	...	...	.
NGC 5713	**5.0**	...	3	29.3*	...	3	71.3	...	3	...	...	.
NGC 5850	**29.9**	...	3	80.7*	...	3	...	...	.	...	...	.
NGC 5921	20.6	...	3	57.8*	...	3	137.5	...	3	...	...	.
NGC 5962	27.3*	...	3	...	...	.	...	...	.	...	...	.
NGC 6215	27.3	4.3	3	57.0	...	3	72.5	...	3	...	...	.
NGC 6221	14.5	...	3	41.9*	...	3	93.0	...	3	...	...	.
NGC 6300	9.4	...	3	39.1*	...	3	68.5	...	3	106.4	...	1
NGC 6384	20.4*	...	3	68.7	...	3	131.7	...	3	...	...	.
NGC 6753	10.9	...	3	19.4	...	3	37.3	...	3	58.9	...	3
NGC 6782	12.2	...	3	27.6*	...	3	...	...	.	...	...	.
NGC 6902	22.0*	...	3	92.1	1.5	3	...	...	.	...	...	.
NGC 6907	5.7	0.1	3	37.5	2.3	3	...	...	.	...	...	.
NGC 7083	3.7	...	3	18.1	...	3	49.7	...	3	...	...	.
NGC 7205	74.1	...	3	...	...	.	...	...	.	...	...	.
NGC 7213	22.0	...	1	64.9	3.0	1	...	...	.	...	...	.

Table 1—Continued

Galaxy	CR_1	err	code	CR_2	err	code	CR_3	err	code	CR_4	err	code
1	2	3	4	5	6	7	8	9	10	11	12	13
NGC 7217	14.5	1.6	3	43.1	...	3	...	...	.	...	...	.
NGC 7412	13.9	...	3	52.7	...	3	71.0	...	3	...	...	.
NGC 7418	**4.0**	...	3	38.1*	1.8	3	81.3	2.0	3	...	...	.
NGC 7479	6.3	...	3	57.7*	...	3	...	...	.	...	...	.
NGC 7552	4.7	...	3	15.6	...	3	59.0*	...	3	...	...	.
NGC 7582	43.6	...	3	74.3*	...	3	...	...	.	...	...	.
NGC 7713	55.7	...	3	67.9	...	3	...	...	.	...	...	.
NGC 7723	9.3	...	3	20.7*	...	3	40.1	...	3	...	...	.
NGC 7727	29.1*	...	3	114.5	...	1	...	...	.	...	...	.
NGC 7741	51.9*	6.8	3	...	...	.	...	...	.	...	...	.
IC 4444	9.7*	0.4	3	41.4	...	3	...	...	.	...	...	.
IC 5325	15.1*	...	3	25.5	...	3	40.4	1.7	3	...	...	.
ESO 138−10	16.8	0.6	3	79.9	...	3	137.4	...	3	...	...	.

[a]Col. 1: galaxy name; cols. 2,5,8,11: radii of inferred corotations from positive-to-negative potential-density phase-shift crossings, in arcseconds; cols. 3,6,9,12: a number is given in these columns only if the phase-shift crossing is noisy. Then, the value is a standard deviation about an average crossing radius; cols. 4,7,10,13: a code indicating how significant we think a crossing is. Code 3 crossings are considered

more reliable than code 1 crossings.

[b]CR_5=134.″0, code=3

Table 2. Summary of Features[a]

Galaxy	n_{CR}	bar?	oval?	AC	PS-plot	Galaxy	n_{CR}	bar?	oval?	AC	PS-plot
1	2	3	4	5	6	7	8	9	10	11	12
NGC 150	2	y	n	12	well-def	NGC 3227	2:	n	y	7	noisy
NGC 157	3	n	n	12	well-def	NGC 3261	3:	y	n	9B	noisy
NGC 210	2:	n	y	6	noisy	NGC 3275	2	y	n	4	noisy
NGC 278	1:	n	y?	3B	noisy	NGC 3319	3	y	n	5	well-def
NGC 289	4	n	y	12	well-def	NGC 3338	3	n	y?	9	well-def
NGC 428	1+	n	y	1	well-def	NGC 3423	1:	n	y:	2	noisy
NGC 488	3:	n	y	3	noisy	NGC 3504	2	y	y	8	well-def
NGC 578	3	y	n	9	well-def	NGC 3507	2	y	n	9	well-def
NGC 613	3	y	n	9	well-def	NGC 3513	2	y	n	12	well-def
NGC 685	2	y	n	2B	well-def	NGC 3583	3	y	n	12	well-def
NGC 864	3	y	n	5	well-def	NGC 3593	3:	n	y	..	noisy/uns
NGC 908	3	n	n	9	well-def	NGC 3596	4:	n	y	5	noisy
NGC 1042	3	n	n	9	well-def	NGC 3646	2	n	y?	2	well-def
NGC 1058	1	n	y	3	peculiar	NGC 3675	3:	n	y	3	noisy
NGC 1073	2+	y	n	5	well-def	NGC 3681	1:	n	y	5	noisy
NGC 1084	2	n	y	5	well-def	NGC 3684	2	n	y	5	noisy
NGC 1087	2:	y	n	2	noisy	NGC 3686	1	y	n	5	well-def
NGC 1187	3:	y	n	9	well-def	NGC 3726	3	n	y	5	well-def
NGC 1241	1	y	n	4	well-def	NGC 3810	3:	n	y	2	noisy
NGC 1300	2	y	n	12	well-def	NGC 3887	2	n	y	2	well-def

Table 2—Continued

Galaxy	n_{CR}	bar?	oval?	AC	PS-plot	Galaxy	n_{CR}	bar?	oval?	AC	PS-plo
1	2	3	4	5	6	7	8	9	10	11	12
NGC 1302	3	n	y	8	noisy	NGC 3893	2	n	y	12	well-def
NGC 1309	3:	n	y	3	noisy/unst	NGC 3938	2:	n	n	9	noisy
NGC 1317	2+	y	y	..	noisy	NGC 3949	2:	n	y	1	noisy/u
NGC 1350	2	y	n	12B	well-def	NGC 4027	2	y	n	4	well-def
NGC 1371	3+	n	y	4	noisy	NGC 4030	4	n	y:	9	well-def
NGC 1385	1	y	n	4	well-def	NGC 4051	2	n	y	5	well-def
NGC 1493	1:	y	n	5	well-def:	NGC 4123	3:	y	y	9	noisy
NGC 1559	1	y	n	5B	well-def	NGC 4136	4:	y	n	9	noisy
NGC 1617	2:	n	y	3	noisy	NGC 4145	2	y	n	4	well-def
NGC 1637	3	y	n	5	well-def	NGC 4151	3	y	y	5	well-def
NGC 1703	2	n	y	9B	well-def	NGC 4212	1	n	y	3	noisy
NGC 1792	2	n	n	3	noisy	NGC 4242	1:	n	y	1	noisy
NGC 1808	3	y	n	7B	well-def	NGC 4254	4:	n	y	9	noisy
NGC 1832	2	y	n	5	well-def	NGC 4293	3	y	n	..	well-def
NGC 2090	2	n	y	3B	noisy	NGC 4303	5	n	y	9	well-def
NGC 2139	1:	y	n	2	noisy	NGC 4314	2	y	n	12	well-def
NGC 2196	2	n	y	6	noisy	NGC 4394	3:	y	n	6	noisy
NGC 2442	2	y	n	7	well-def	NGC 4414	3:	n	y	3	noisy
NGC 2559	1	y	n	9B	well-def	NGC 4450	4	n	y	12	well-def
NGC 2566	2	y	n	8B	well-def	NGC 4457	1:	n	y	4	noisy

Table 2—Continued

Galaxy	n_{CR}	bar?	oval?	AC	PS-plot	Galaxy	n_{CR}	bar?	oval?	AC	PS-plo
1	2	3	4	5	6	7	8	9	10	11	12
NGC 2775	2?	n	y	3	noisy/unst	NGC 4487	2:	n	y	5	noisy
NGC 2964	2	y	n	12	well-def	NGC 4496	3:	y	n	2	noisy
NGC 3059	1	y	n	5	noisy	NGC 4504	2:	n	y	5	noisy/u
NGC 3166	1	n	y	..	noisy	NGC 4527	1	n	y	5B	noisy
NGC 3223	2:	n	y?	9B	noisy	NGC 4548	2	y	n	5	well-def

Table 2. Summary of Features (cont.)[a]

Galaxy	n_{CR}	bar?	oval?	AC	PS-plot	Galaxy	n_{CR}	bar?	oval?	AC	PS-plo
NGC 4571	2:	n	n:	3	noisy	NGC 5643	3	y	n	8B	well-def
NGC 4579	4	y	n	9	well=def	NGC 5676	3:	n	y	3	noisy
NGC 4580	2	n	y	12	noisy	NGC 5701	3	y	n	..	noisy
NGC 4593	3	y	n	5	well-def	NGC 5713	3	y	n	4	well-def
NGC 4618	1	y	n	4	well-def	NGC 5850	2	y	n	8	well-def
NGC 4643	2:	y	n	..	noisy	NGC 5921	3	y	n	8	well-def
NGC 4647	3	n	y	3	noisy	NGC 5962	1:	n	y	2	noisy
NGC 4651	4:	n	y	9	noisy	NGC 6215	3	n	n	12	well-def
NGC 4654	3	n	y	4	well-def	NGC 6221	3	y	n	9B	well-def
NGC 4665	2	y	n	..	well-def	NGC 6300	4	y	n	6	well-def
NGC 4689	3	n	n	3	well-def	NGC 6384	3:	n	y	9	noisy
NGC 4691	1:	y	n	..	noisy	NGC 6753	4	n	n	8	noisy
NGC 4699	2	n	y	3	noisy	NGC 6782	2:	y	n	..	noisy
NGC 4772	1:	n	y	8	noisy/unst	NGC 6902	2:	n	y	8B	noisy
NGC 4775	1	n	y:	9	well-def	NGC 6907	2	y	n	12	well-def
NGC 4781	4:	y:	y	4B	noisy	NGC 7083	3	n	y:	9B	noisy
NGC 4900	2	y	n	3	noisy	NGC 7205	1	n	y	5	well-def
NGC 4902	4	y	n	9	well-def	NGC 7213	2:	n	n	..	noisy/u
NGC 4930	3:	y	n	8B	noisy	NGC 7217	2	n	y?	3	noisy
NGC 4939	4	n	y	12	well-def	NGC 7412	3	n	y	9B	well-def

Table 2—Continued

Galaxy	n_{CR}	bar?	oval?	AC	PS-plot	Galaxy	n_{CR}	bar?	oval?	AC	PS-pl
NGC 4941	1:	n	y:	3	noisy/unst	NGC 7418	3	y	n	5B	noisy
NGC 4995	3	y	n	6	well-def	NGC 7479	2	y	n	9	well-d
NGC 5005	2:	n	y	3	noisy	NGC 7552	3	y	n	12B	well-d
NGC 5054	1	n	y	5	well-def	NGC 7582	2:	y	n	12B	well-d
NGC 5085	4:	n	n	2	well-def	NGC 7713	2	n	y	1B	noisy
NGC 5101	3	y	n	..	noisy	NGC 7723	3:	y	n	5	noisy
NGC 5121	1:	n	y:	..	noisy/unst	NGC 7727	2:	n	y	1	noisy
NGC 5247	2	n	n	9	well-def	NGC 7741	1	y	n	5	noisy
NGC 5248	2	n	y	12	well-def	IC 4444	2	n	y	6B	well-d
NGC 5334	3:	y	n	2	noisy	IC 5325	3:	n	y	6B	noisy
NGC 5427	3	n	n	9	well-def	ESO 138- 10	3	n	y	..	noisy
NGC 5483	4:	n	y	5B	noisy	.....	..	..	..	...	.....

[a]Col. 1: galaxy name; col. 2: number of significant or possibly significant corotations (: or ? me uncertain, + means there could be more); col. 3: indicates if a bar is present in the near-IR image: 'y' = 'n' = no; col. 4: indicates if an oval (bar-like) feature is present in the near-IR image; col. 5: Elmegreen class, mostly from Elmegreen & Elmegreen (1987) or estimated by R. Buta from images in the *de Vaucoul Atlas of Galaxies* or other available images; if estimated by Buta, a 'B' follows the arm class; col. 6:

assessment of how coherent the phase-shift plot appears; ‘well-def’ = well-defined and ‘unst’ unsteady; c

7-12: same as columns 1-6.

Table 3. Ratio of Corotation to Selected Bar Radii for 101 Galaxies[a]

Galaxy	$\mathcal{R}$	Galaxy	$\mathcal{R}$	Galaxy	$\mathcal{R}$	Galaxy	$\mathcal{R}$
NGC 150	1.31	NGC 2559	1.15	NGC 4303	0.69	NGC 5101	0.78
NGC 210	0.80	NGC 2566	0.78	NGC 4314	1.03	NGC 5334	2.36
NGC 289	1.08	NGC 2964	1.22	NGC 4394	0.94,0.37	NGC 5483	1.35
NGC 428	1.22	NGC 3059	1.29	NGC 4450	1.02	NGC 5643	1.44,0.51
NGC 578	0.97	NGC 3166	1.21	NGC 4457	0.98	NGC 5701	1.05
NGC 613	0.84,0.53	NGC 3227	0.63	NGC 4487	0.92	NGC 5713	0.98,0.17
NGC 685	0.92	NGC 3261	1.03	NGC 4496	2.35,0.36	NGC 5850	0.90,0.33
NGC 864	1.29,0.25	NGC 3275	0.62	NGC 4527	0.79	NGC 5921	1.10
NGC 1073	1.01	NGC 3319	1.00	NGC 4548	1.11	NGC 5962	1.82
NGC 1087	1.96	NGC 3338	0.81	NGC 4579	1.07,0.55	NGC 6221	1.03
NGC 1187	1.90,0.45	NGC 3504	0.70	NGC 4593	1.08	NGC 6300	0.84
NGC 1241	0.41	NGC 3507	1.17	NGC 4618	2.52	NGC 6384	0.62
NGC 1300	0.63	NGC 3513	2.15	NGC 4643	0.74	NGC 6782	0.59
NGC 1302	1.22	NGC 3583	1.35	NGC 4647	1.48,0.53	NGC 6902	1.26
NGC 1317	0.75	NGC 3675	0.91	NGC 4651	1.62	NGC 7418	2.52,0.26
NGC 1350	1.66,0.15	NGC 3681	1.36	NGC 4654	1.03	NGC 7479	0.96
NGC 1385	3.43	NGC 3686	2.32	NGC 4665	0.79	NGC 7552	0.85
NGC 1493	1.61	NGC 3726	0.73	NGC 4691	0.76	NGC 7582	0.80
NGC 1559	1.07	NGC 3887	0.69	NGC 4699	1.04	NGC 7723	0.86
NGC 1617	1.71	NGC 4027	1.20	NGC 4781	1.09,0.39	NGC 7727	1.08
NGC 1637	1.03	NGC 4051	1.56	NGC 4900	1.92,0.51	NGC 7741	0.99

Table 3—Continued

Galaxy	$\mathcal{R}$	Galaxy	$\mathcal{R}$	Galaxy	$\mathcal{R}$	Galaxy	$\mathcal{R}$
NGC 1703	2.29	NGC 4123	1.06	NGC 4902	1.74,0.41	IC 4444	0.44
NGC 1808	0.86	NGC 4136	1.65	NGC 4930	1.04	IC 5325	0.65
NGC 1832	1.36	NGC 4145	2.39	NGC 4939	0.99	.....	....
NGC 2139	1.31	NGC 4151	1.02	NGC 4995	0.96	.....	....
NGC 2442	0.93	NGC 4293	1.18	NGC 5005	1.15	.....	....

[a]$\mathcal{R}$=$r(CR)/r(bar)$. Proposed CR radii for the bar are indicated by asterisks in Table 1. If two values are listed, the second is for an alternative proposed bar CR radius (indicated by bold-face) in Table 1. Bar radii are from Table 3 of Laurikainen et al. (2004).

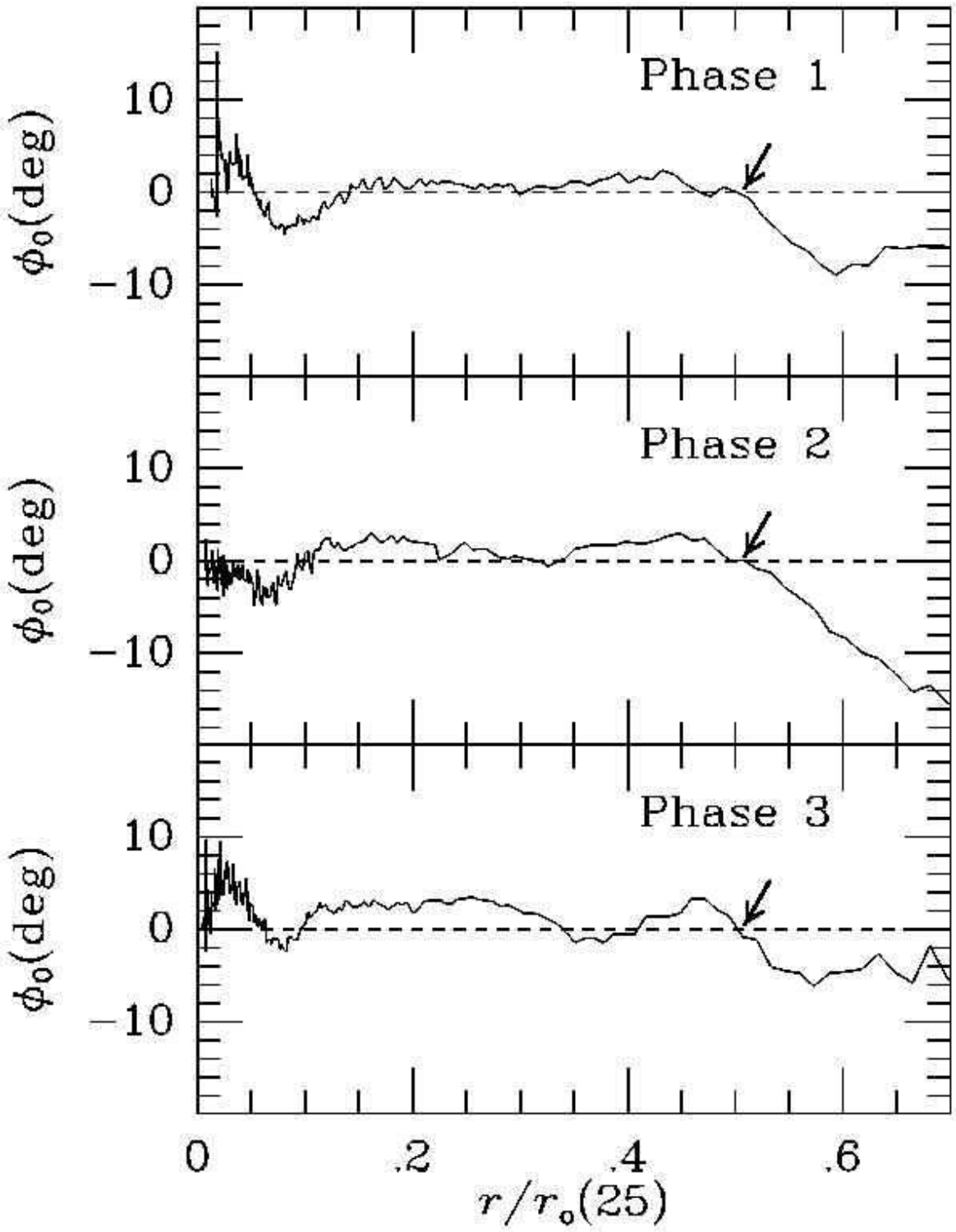

Fig. 1.—

Fig. 1 (cont.) Schematics of the possible evolution of a phase-shift distribution. In phase 1, the bar and the spiral share a single pattern speed and there is one major P/N crossing. In phase 2, there is a weak P/N crossing in the intermediate region of the bar, indicating decoupling of patterns. In phase 3, this decoupling has been largely completed, and there are now separate crossings for the bar and the spiral. The "model" for phase 1 is NGC 7479, that for phase 2 is NGC 613, and that for phase 3 is NGC 4593. In each case, the radii have been scaled to place the main CR (arrows) in the same relative position.

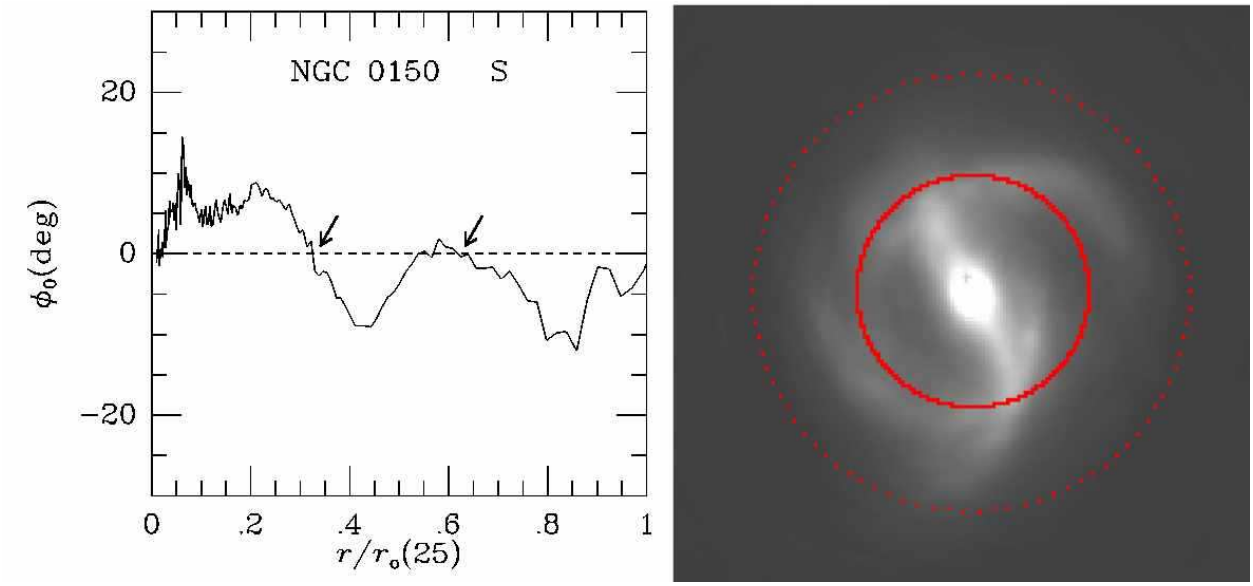

Fig. 2.1.— (left) Phase-shift distribution and (right) 21-term Fourier-smoothed H-band image with overlays at CR positions (red circles) for NGC 150. In the phase-shift plot, the radius is normalized to the "face-on," extinction-corrected isophotal radius, $r_o(25) = D_o/2$, at μ_B=25.00 mag arcsec^{-2}, from RC3. The arrows indicate corotation radii from major positive-to-negative crossings. These radii are listed in arcseconds in Table 1. In the image, the overlaid circles show the arrowed radii. Solid red circles indicate likely more reliable crossings than dotted circles.

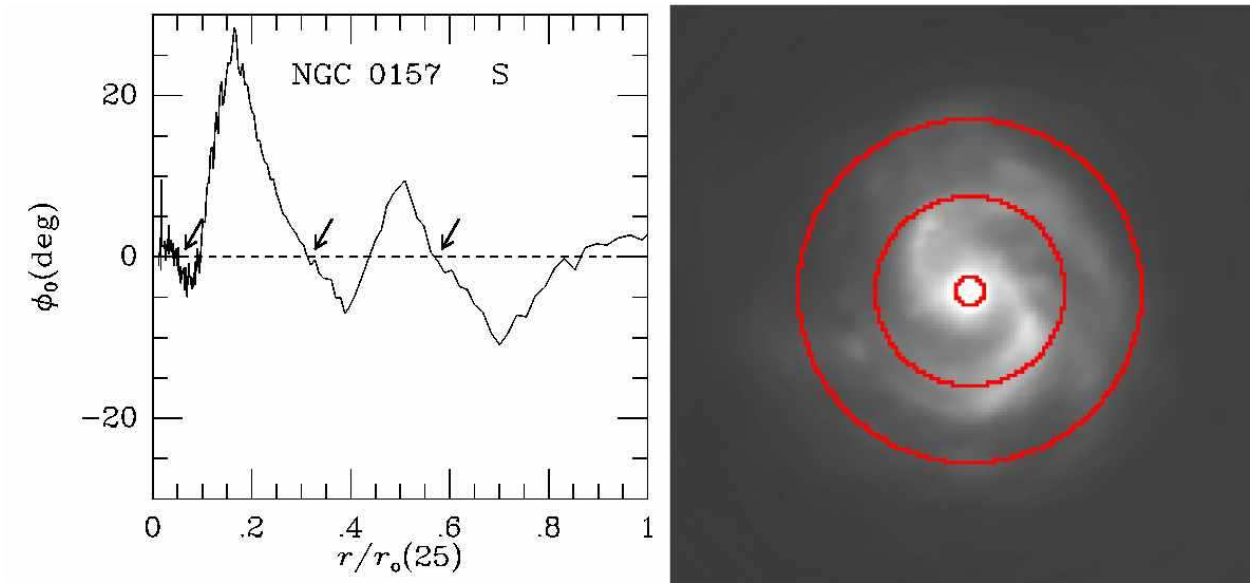

Fig. 2.2.— Same as Figure 2.1 for NGC 157.

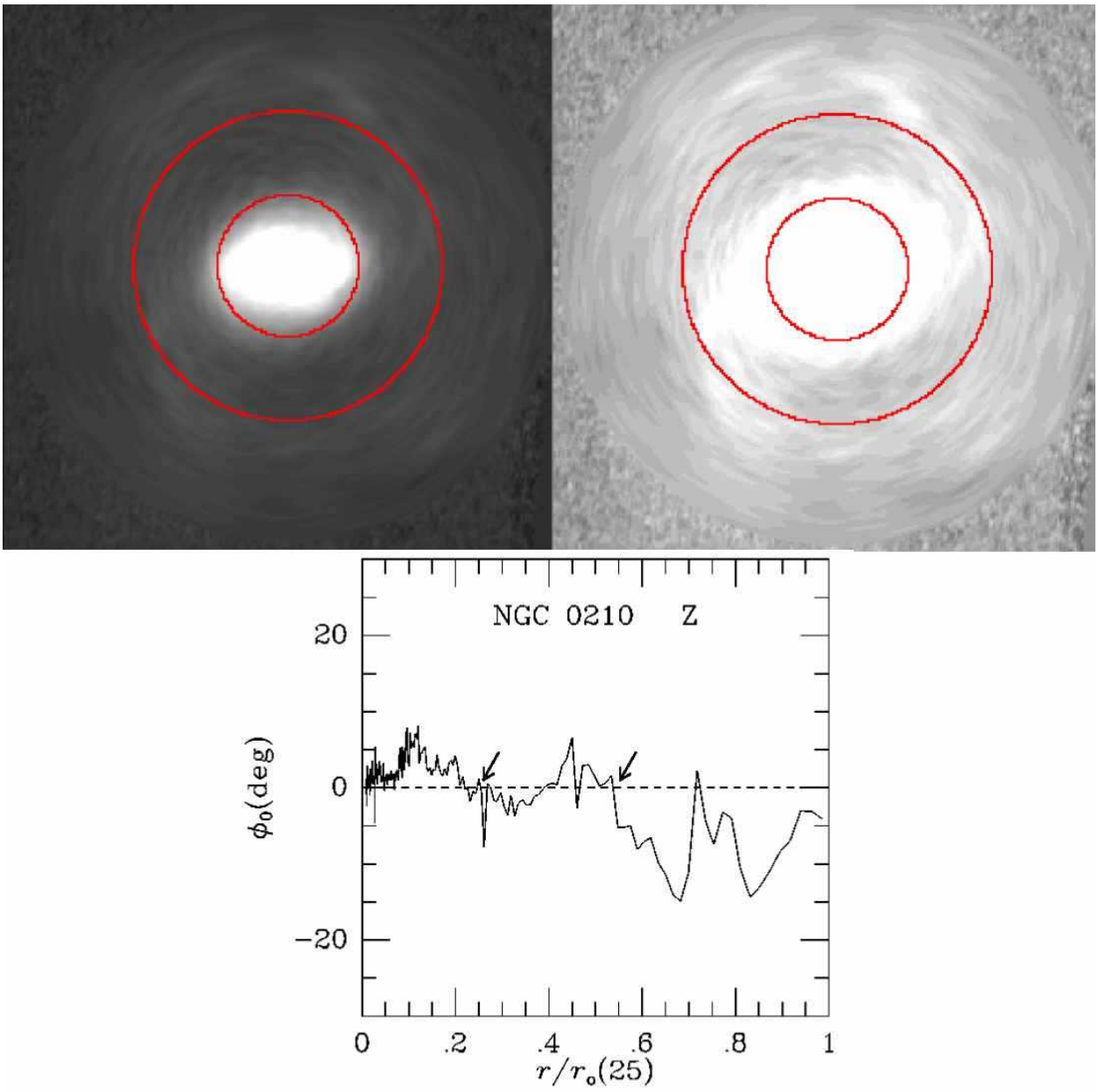

Fig. 2.3.— Same as Figure 2.1 for NGC 210.

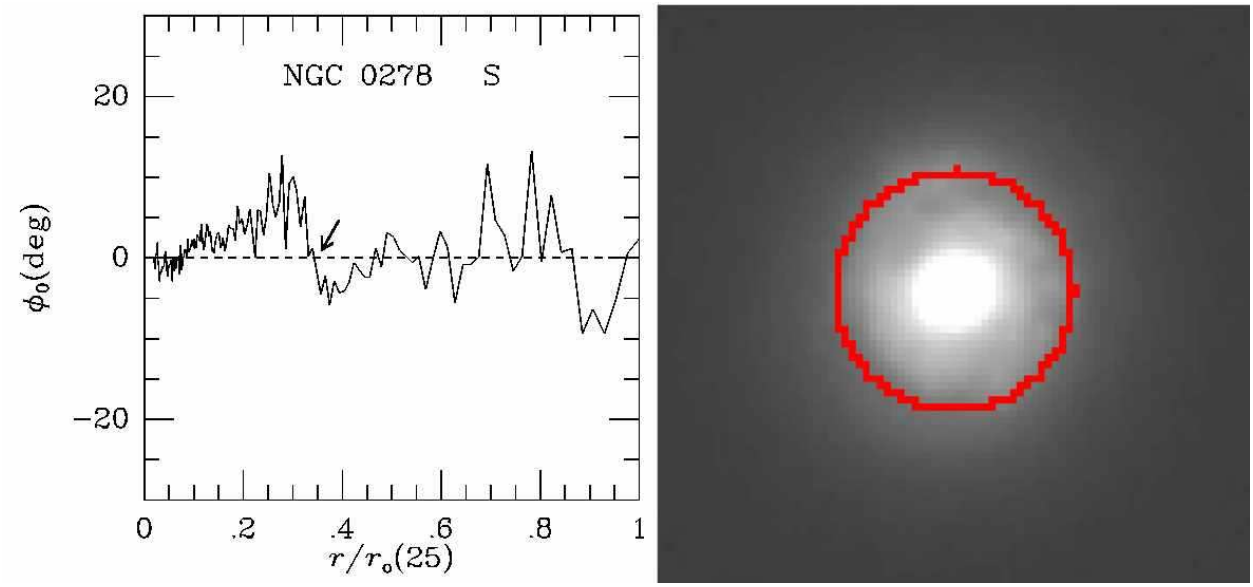

Fig. 2.4.— Same as Figure 2.1 for NGC 0278

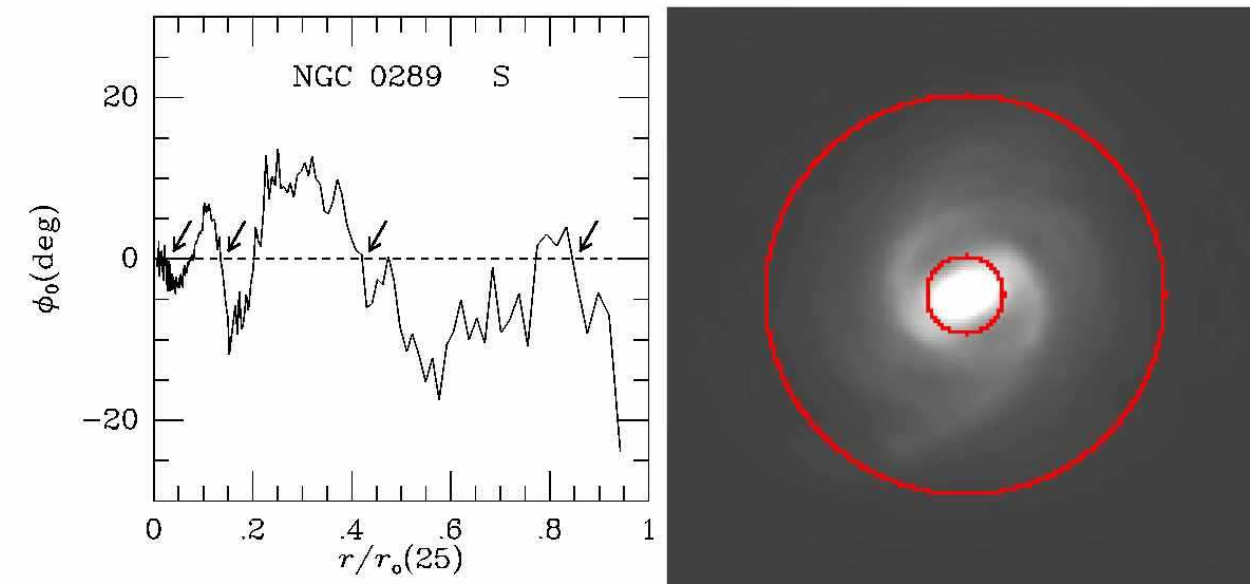

Fig. 2.5.— Same as Figure 2.1 for NGC 289. Only CR_2 and CR_3 from Table 1 are are shown overlaid on the image.

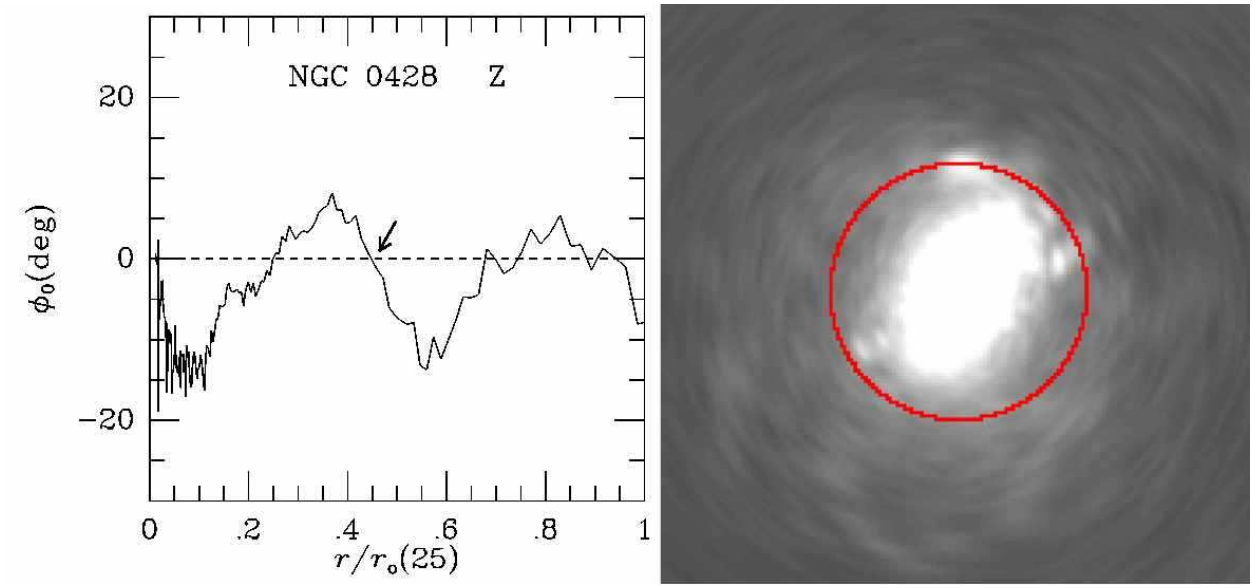

Fig. 2.6.— Same as Figure 2.1 for NGC 428.

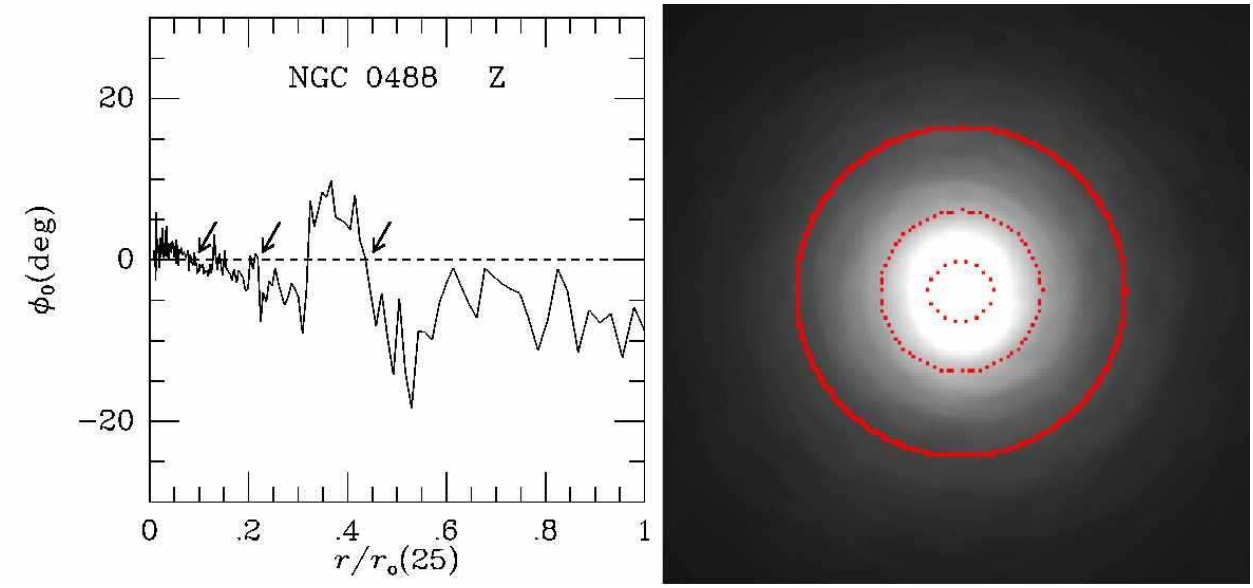

Fig. 2.7.— Same as Figure 2.1 for NGC 488.

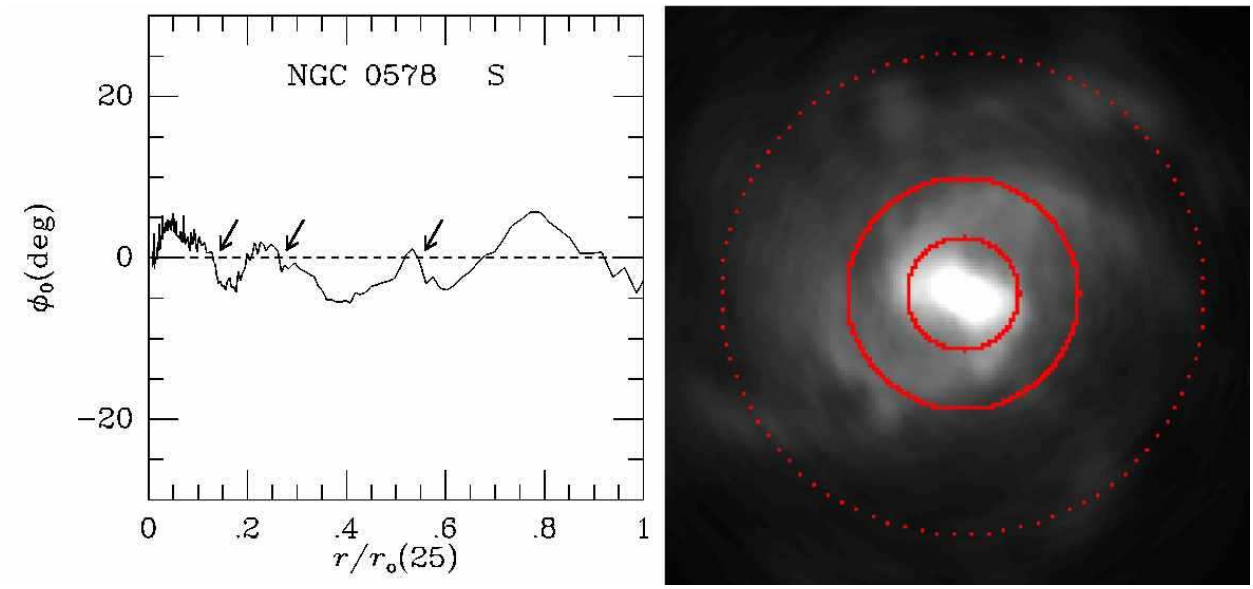

Fig. 2.8.— Same as Figure 2.1 for NGC 578.

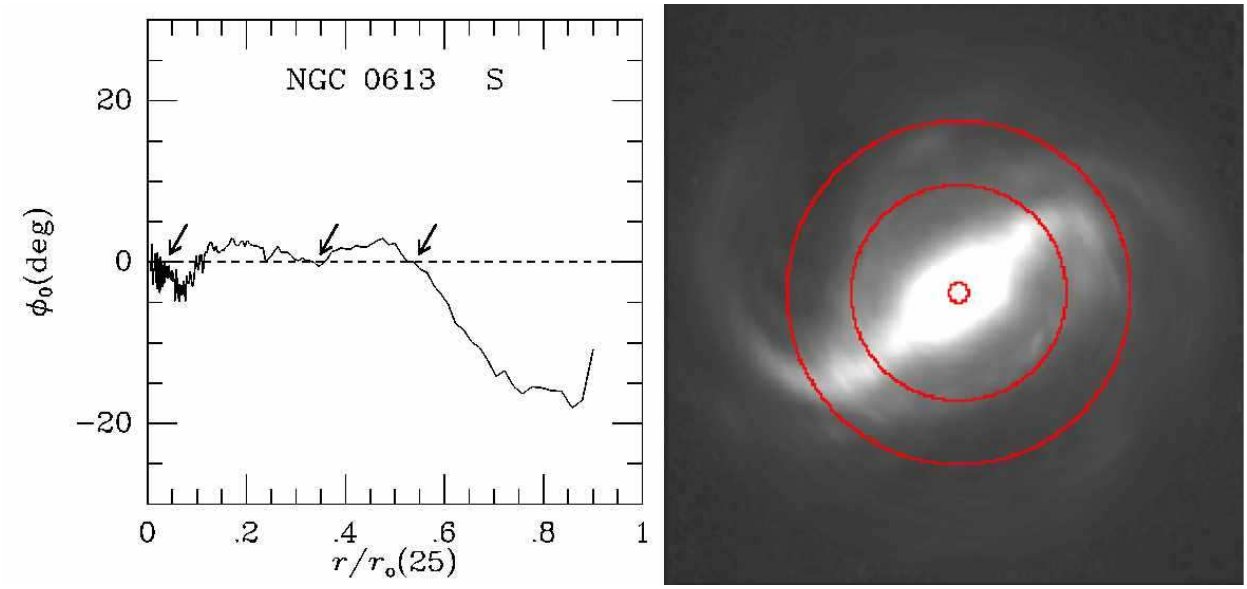

Fig. 2.9.— Same as Figure 2.1 for NGC 613.

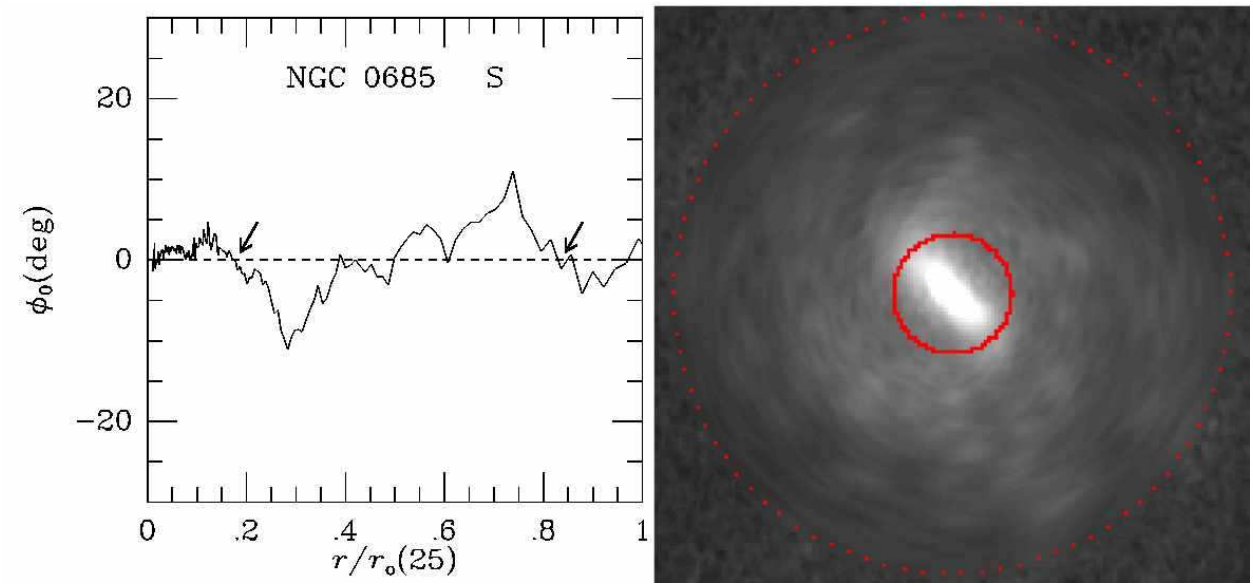

Fig. 2.10.— Same as Figure 2.1 for NGC 685.

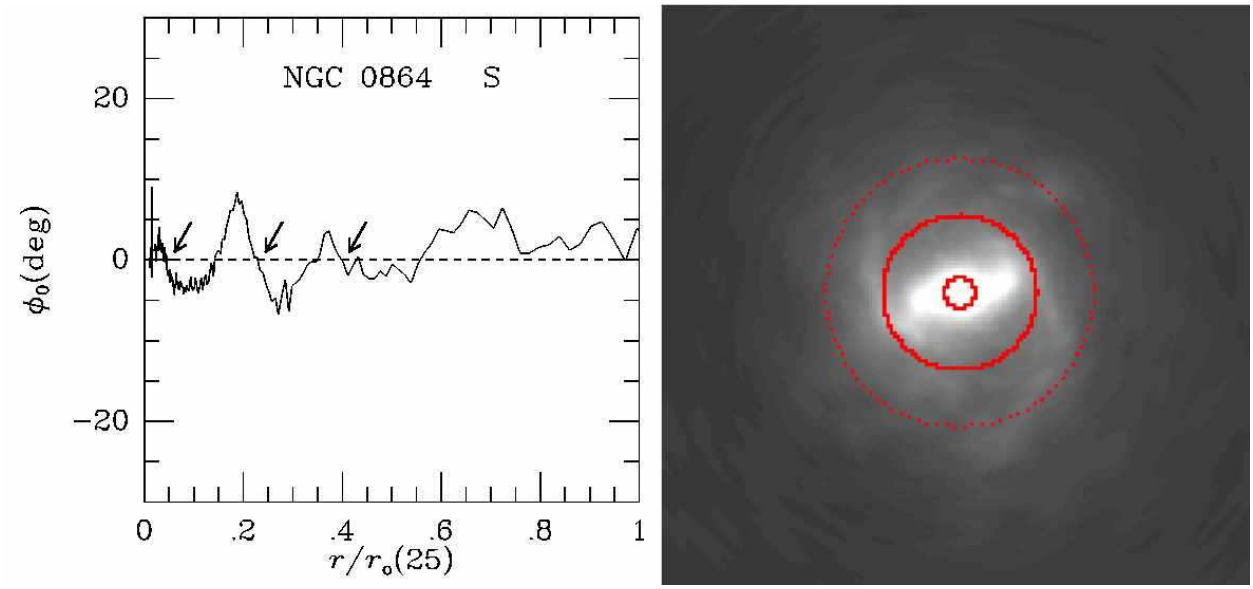

Fig. 2.11.— Same as Figure 2.1 for NGC 864.

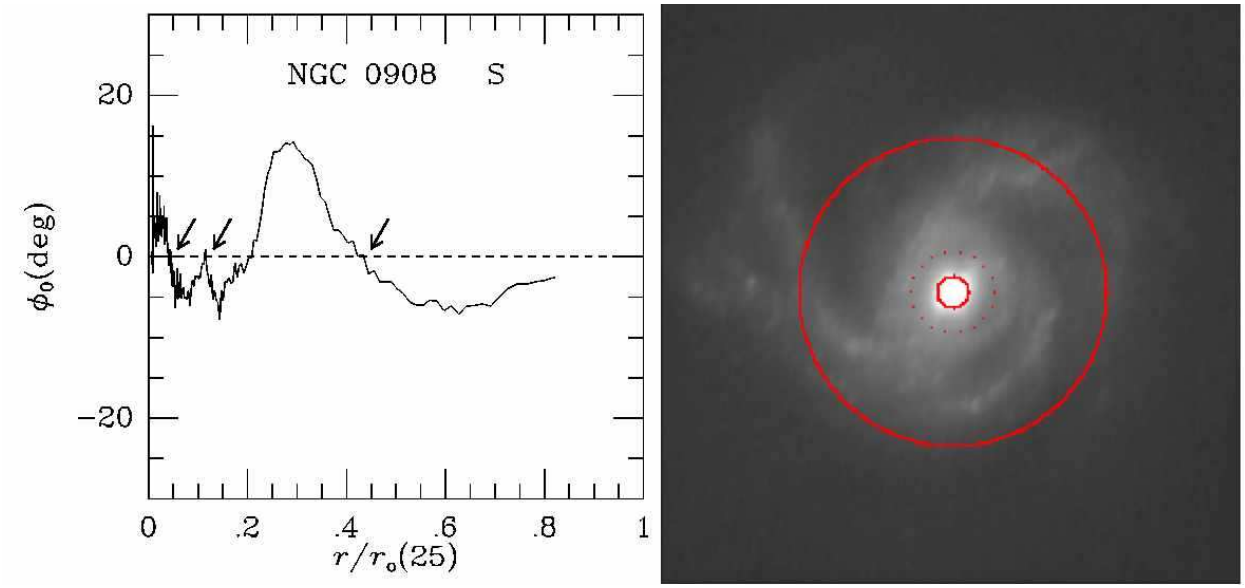

Fig. 2.12.— Same as Figure 2.1 for NGC 908

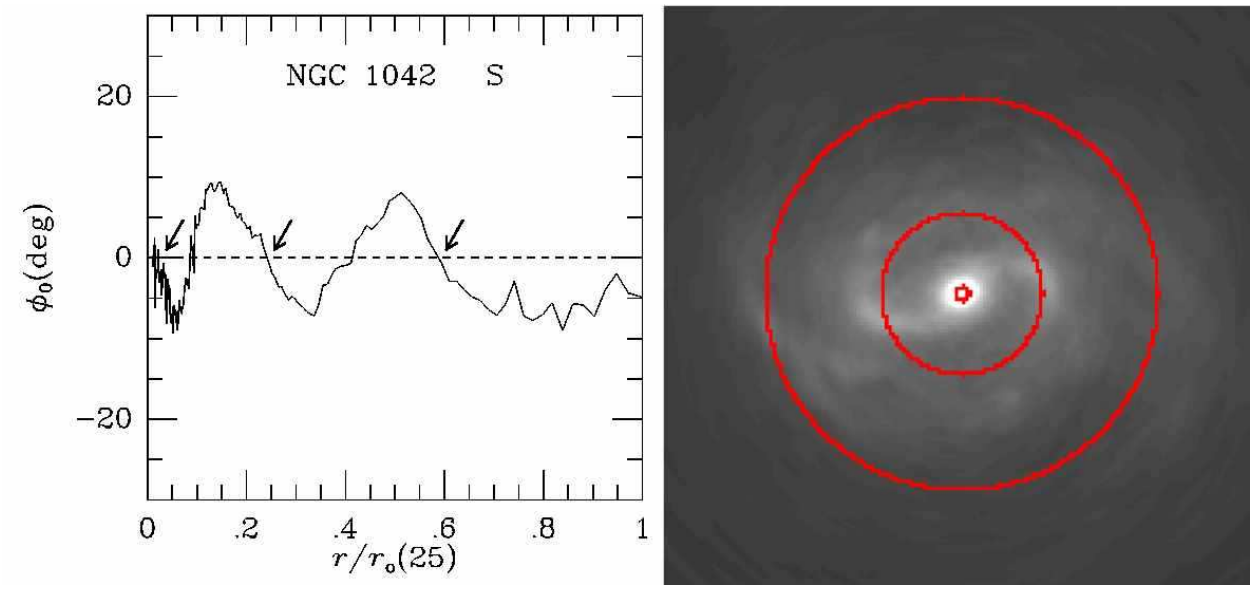

Fig. 2.13.— Same as Figure 2.1 for NGC 1042.

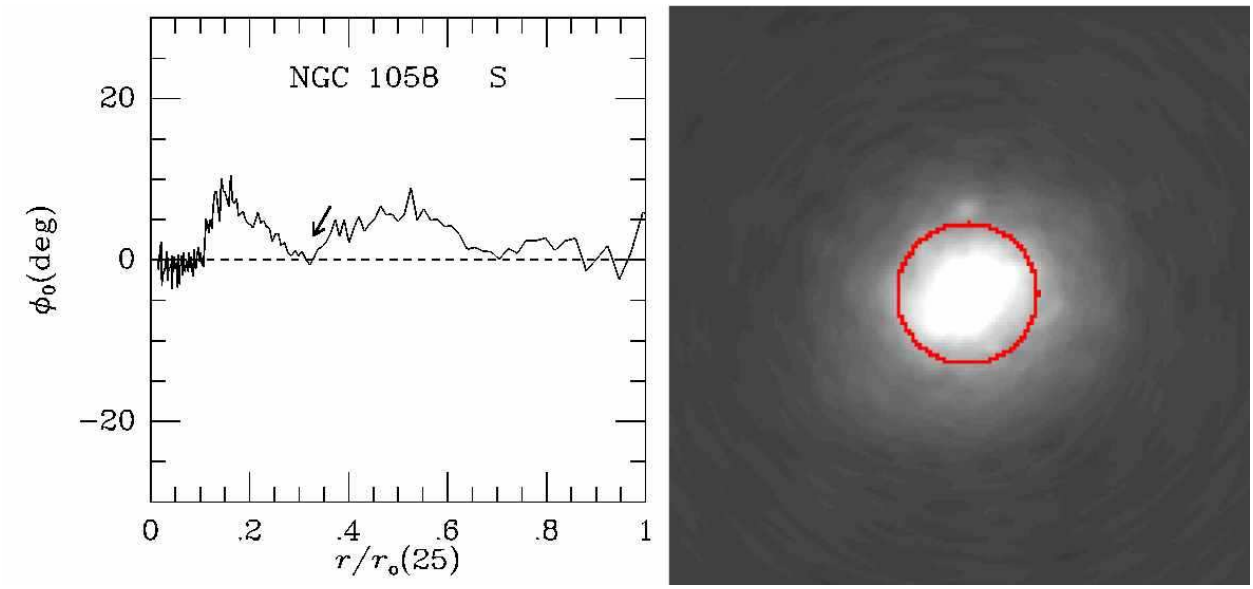

Fig. 2.14.— Same as Figure 2.1 for NGC 1058.

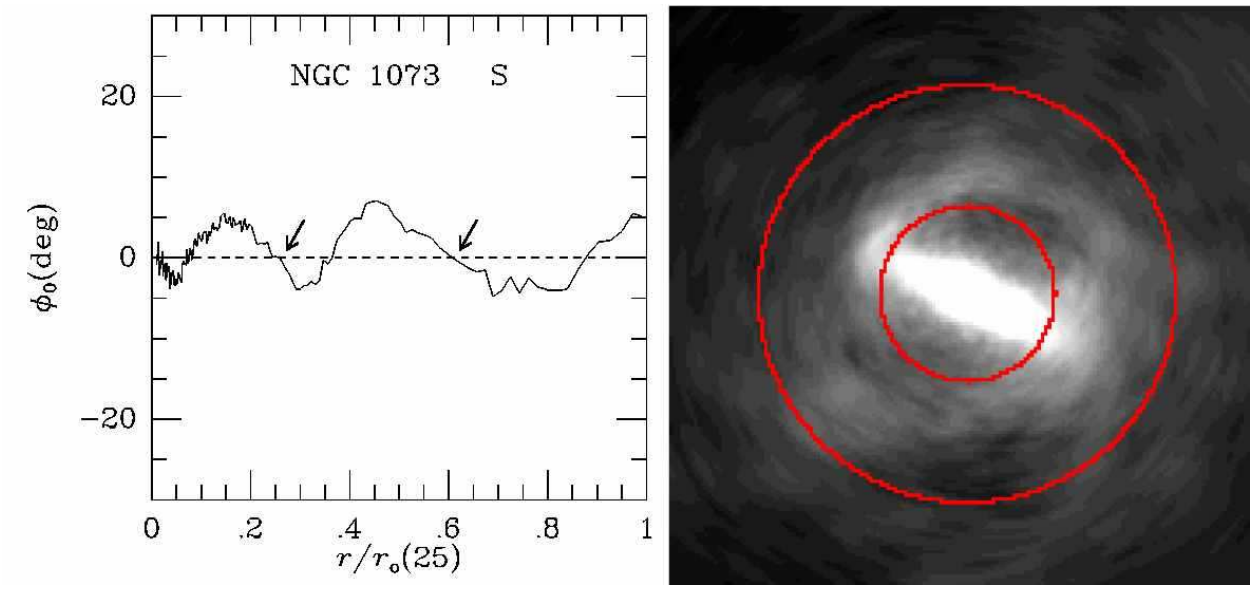

Fig. 2.15.— Same as Figure 2.1 for NGC 1073.

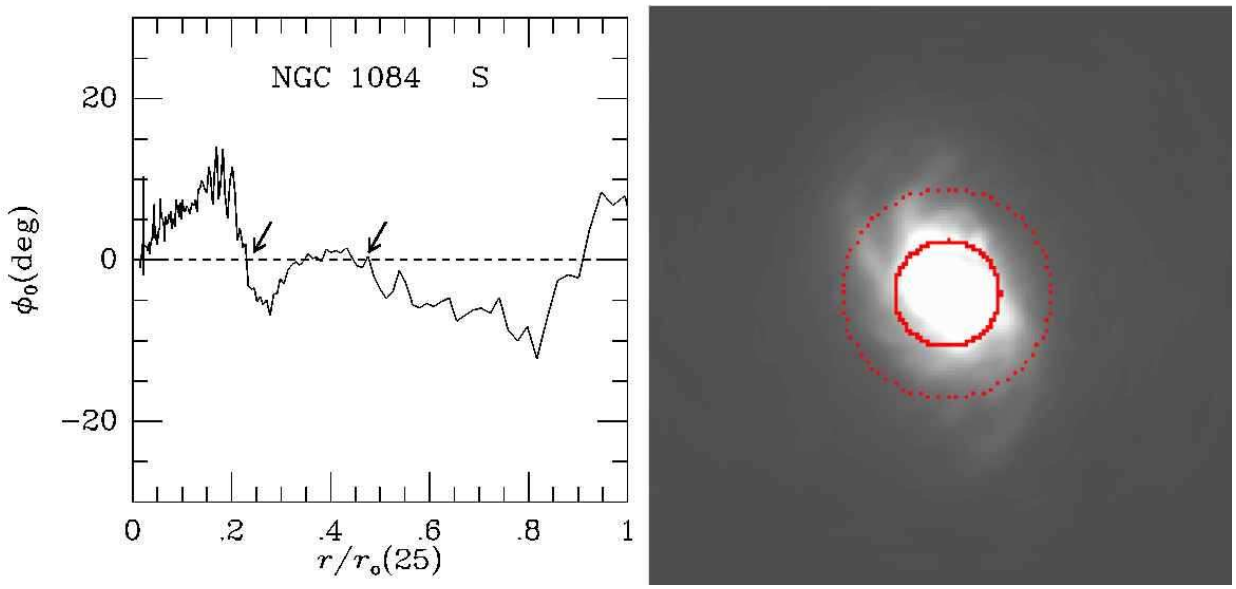

Fig. 2.16.— Same as Figure 2.1 for NGC 1084.

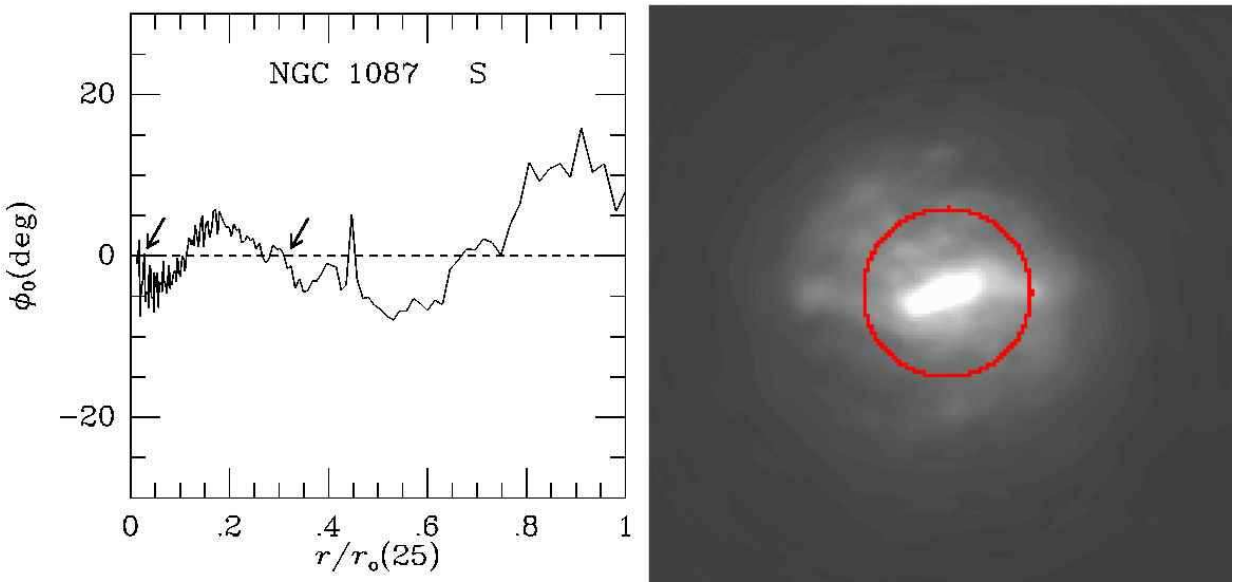

Fig. 2.17.— Same as Figure 2.1 for NGC 1087. Only CR_2 from Table 1 is shown overlaid on the image.

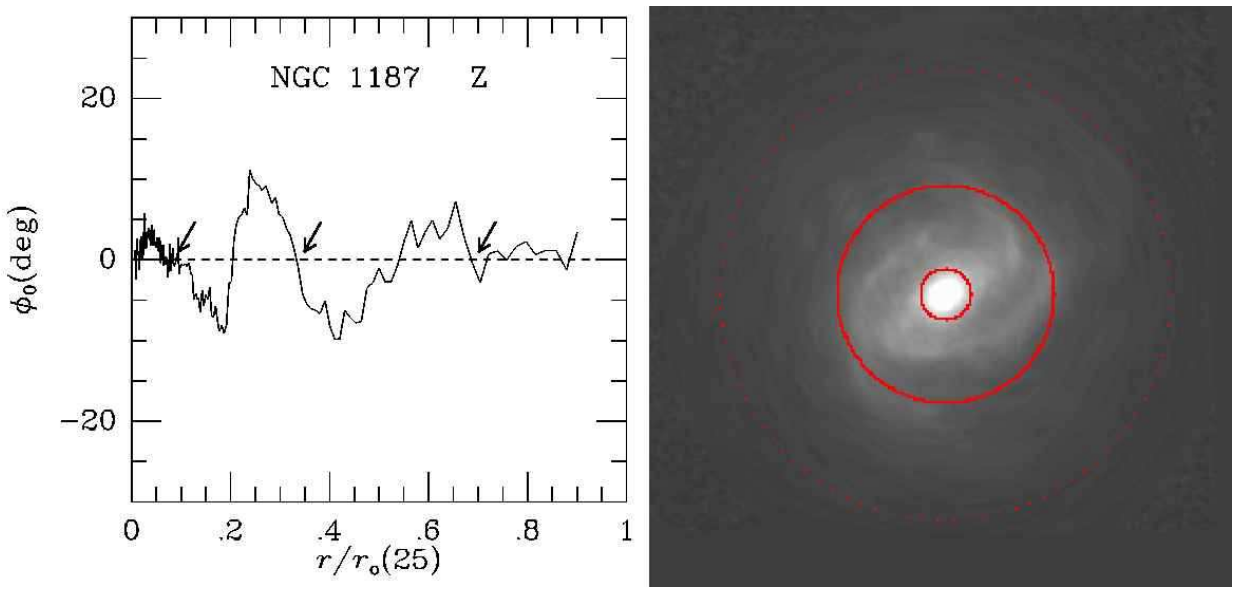

Fig. 2.18.— Same as Figure 2.1 for NGC 1187.

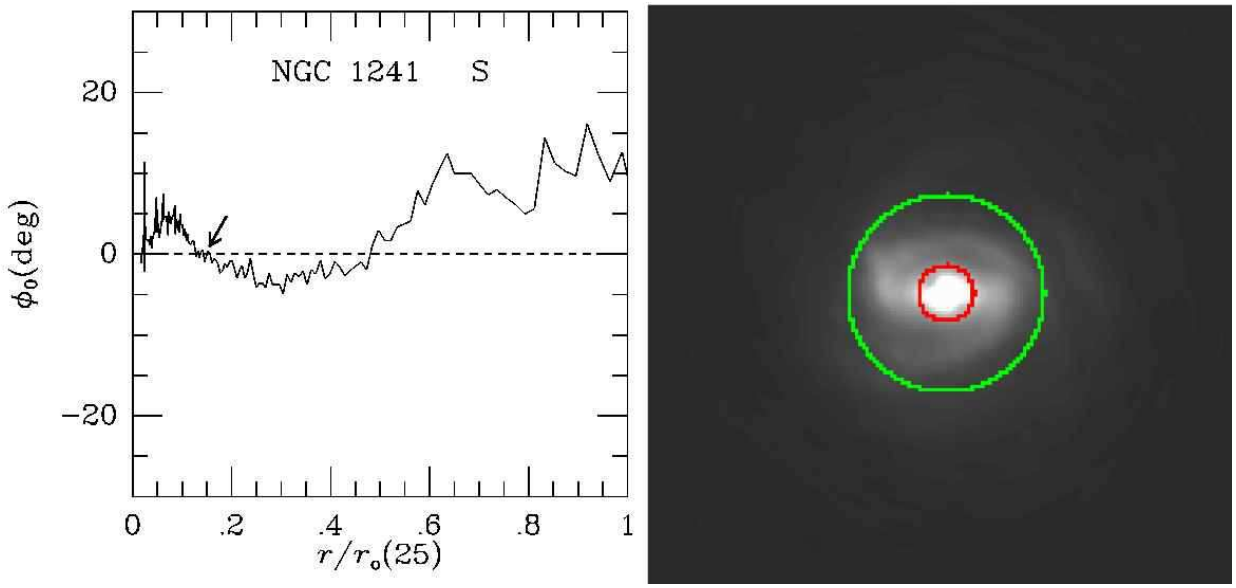

Fig. 2.19.— Same as Figure 2.1 for NGC 1241. The green circle shows the well-defined N/P crossing near $r/r_o(25)\approx 0.5$.

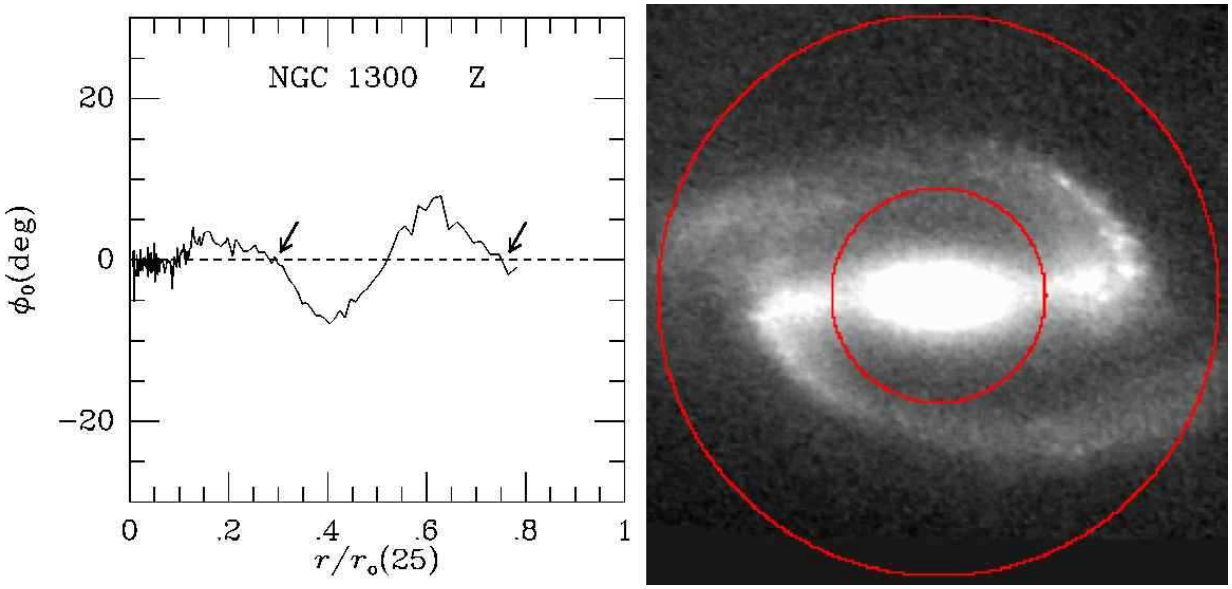

Fig. 2.20.— Same as Figure 2.1 for NGC 1300.

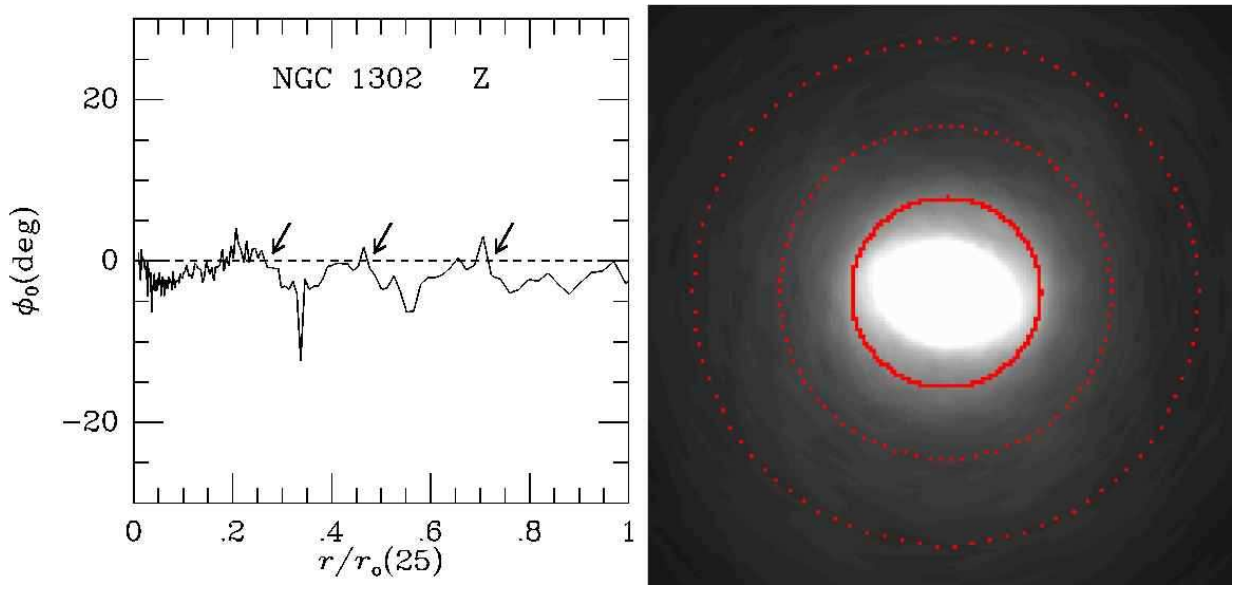

Fig. 2.21.— Same as Figure 2.1 for NGC 1302.

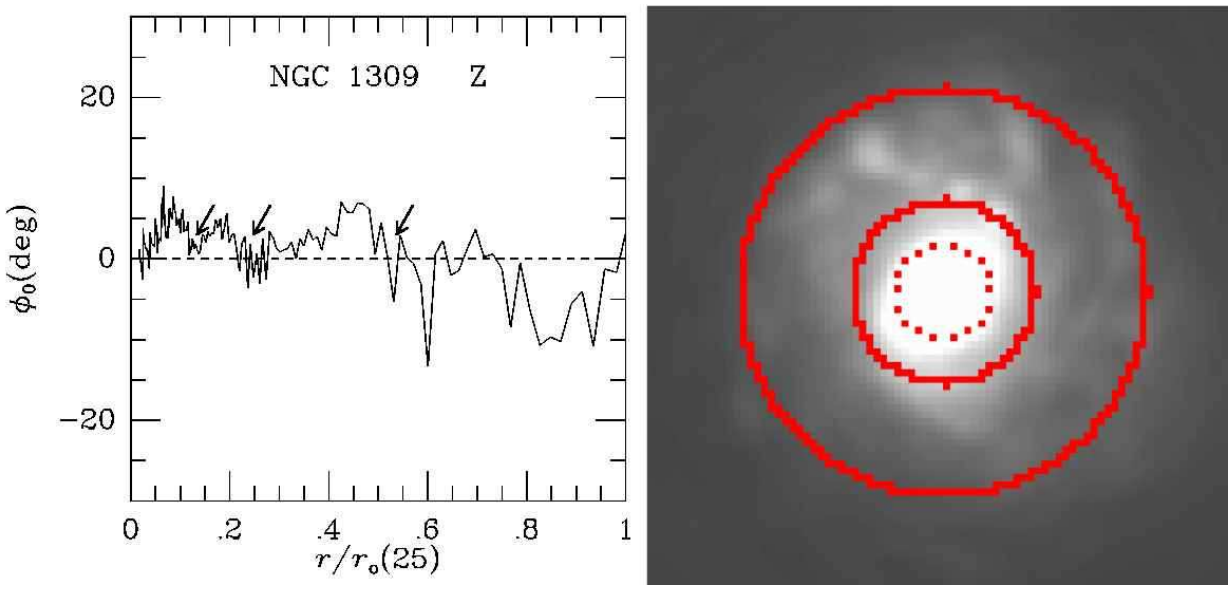

Fig. 2.22.— Same as Figure 2.1 for NGC 1309.

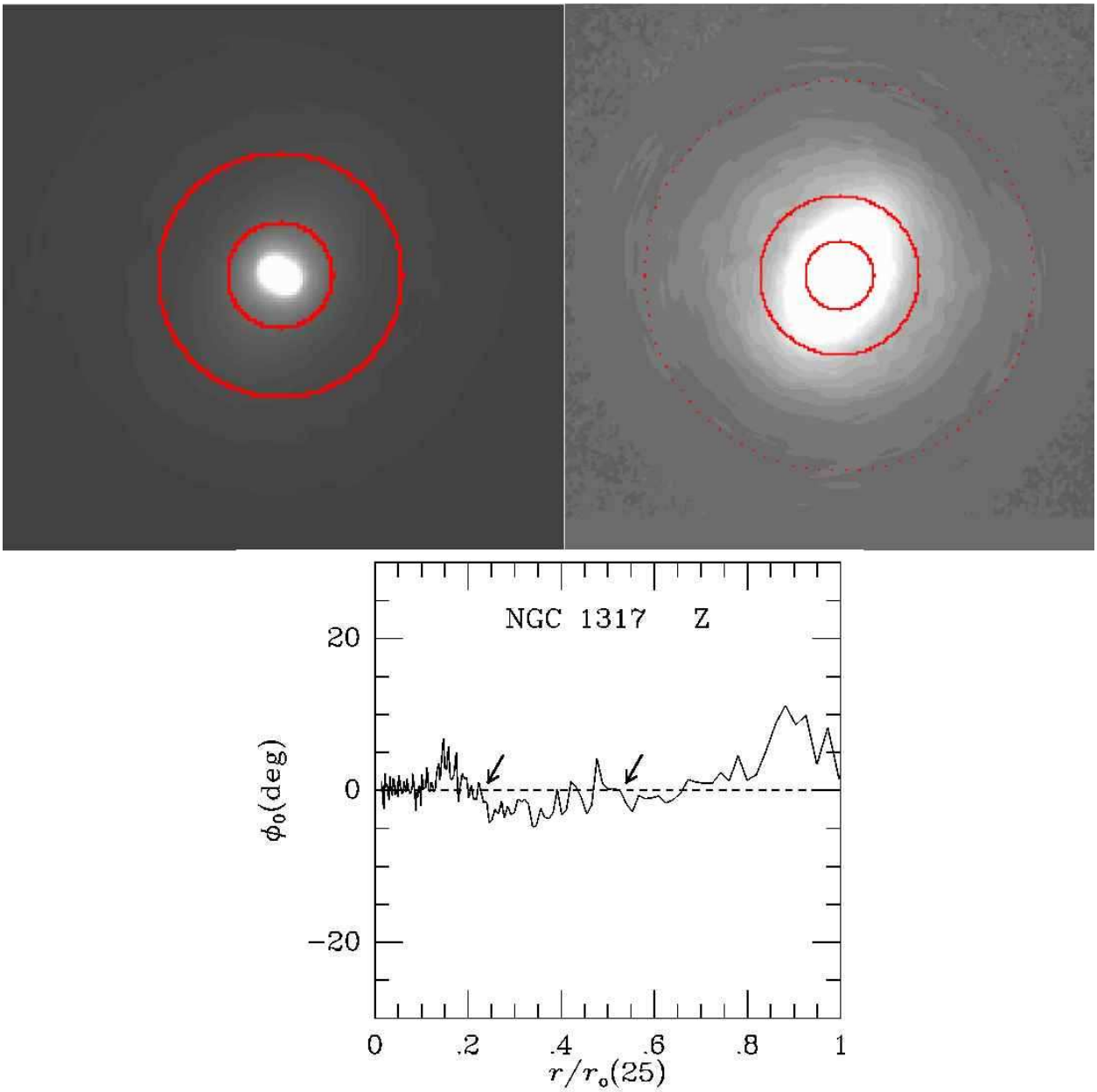

Fig. 2.23.— Same as Figure 2.1 for NGC 1317. The upper left image has CR_1 and CR_2 from Table 1 overlaid as solid circles. These are also shown at upper right, where CR_3 is included as a dotted circle.

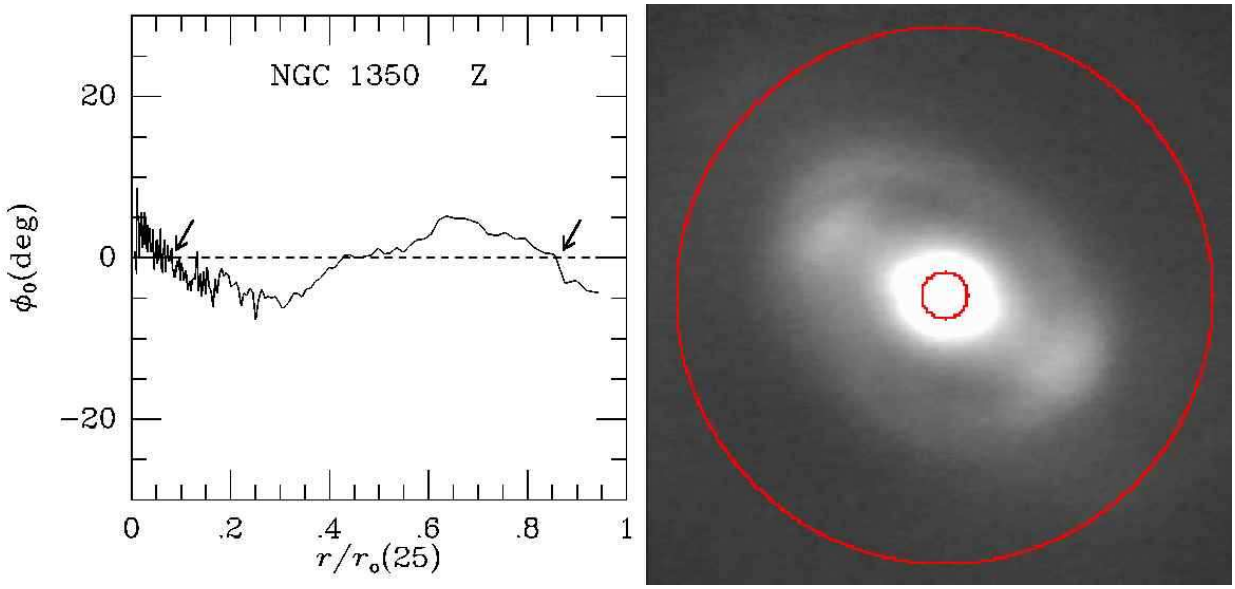

Fig. 2.24.— Same as Figure 2.1 for NGC 1350

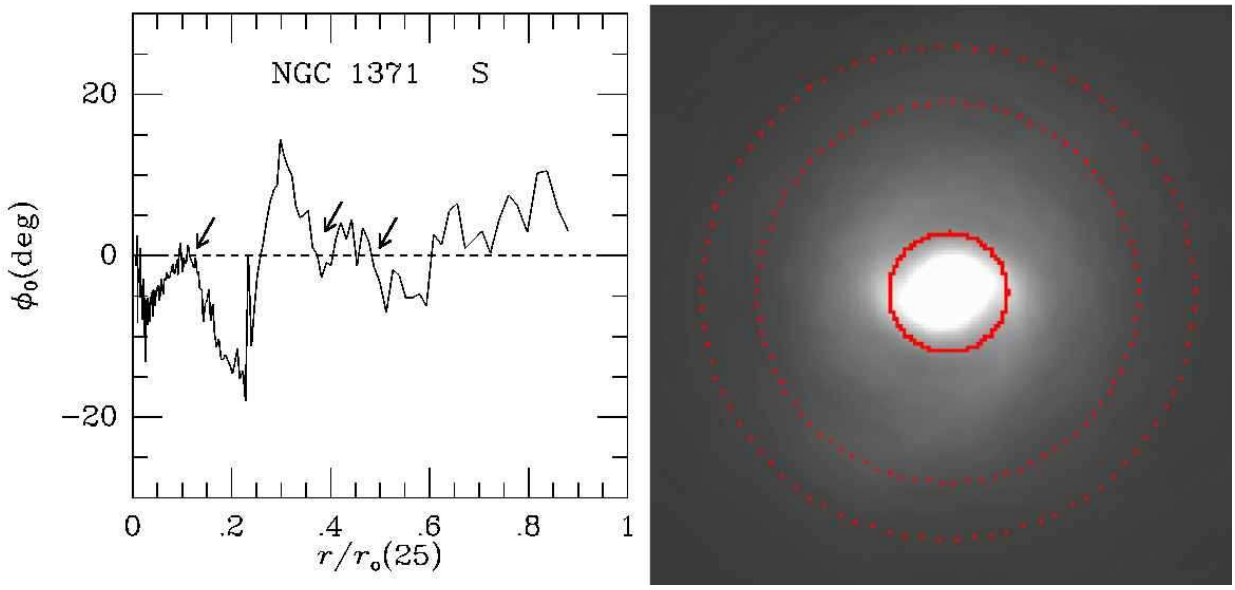

Fig. 2.25.— Same as Figure 2.1 for NGC 1371.

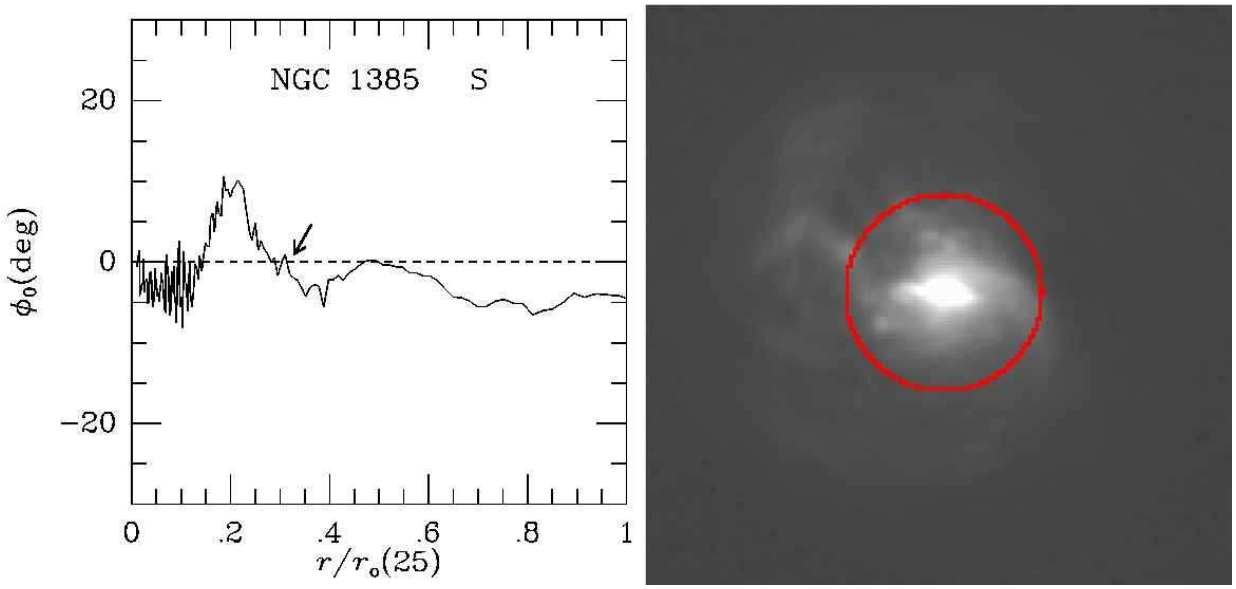

Fig. 2.26.— Same as Figure 2.1 for NGC 1385.

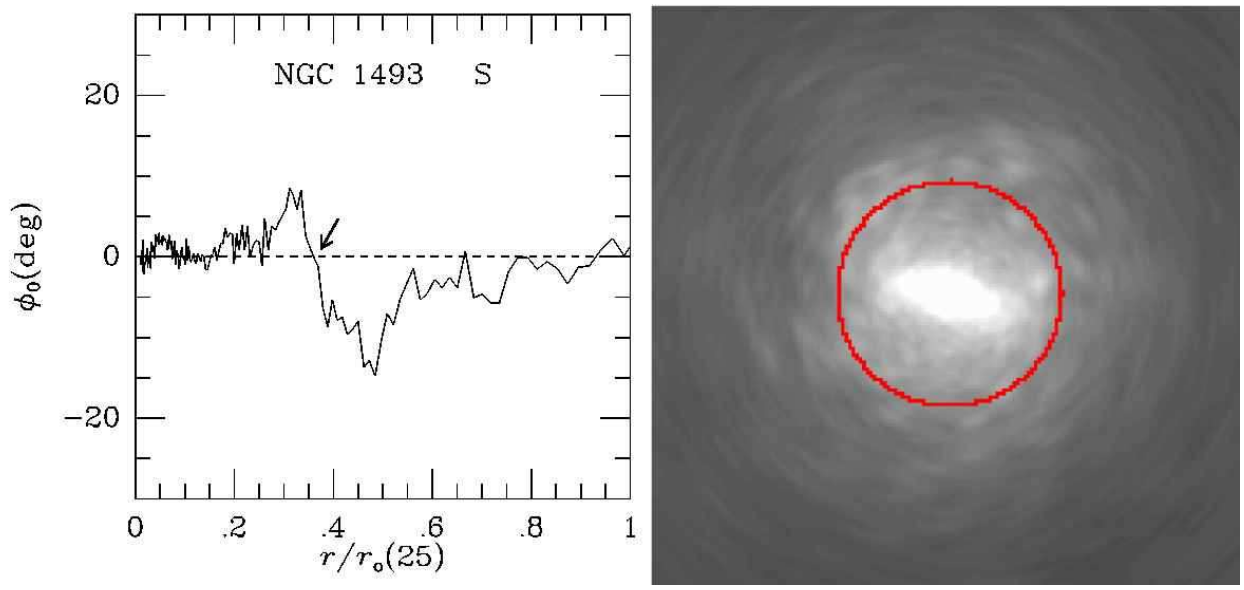

Fig. 2.27.— Same as Figure 2.1 for NGC 1493.

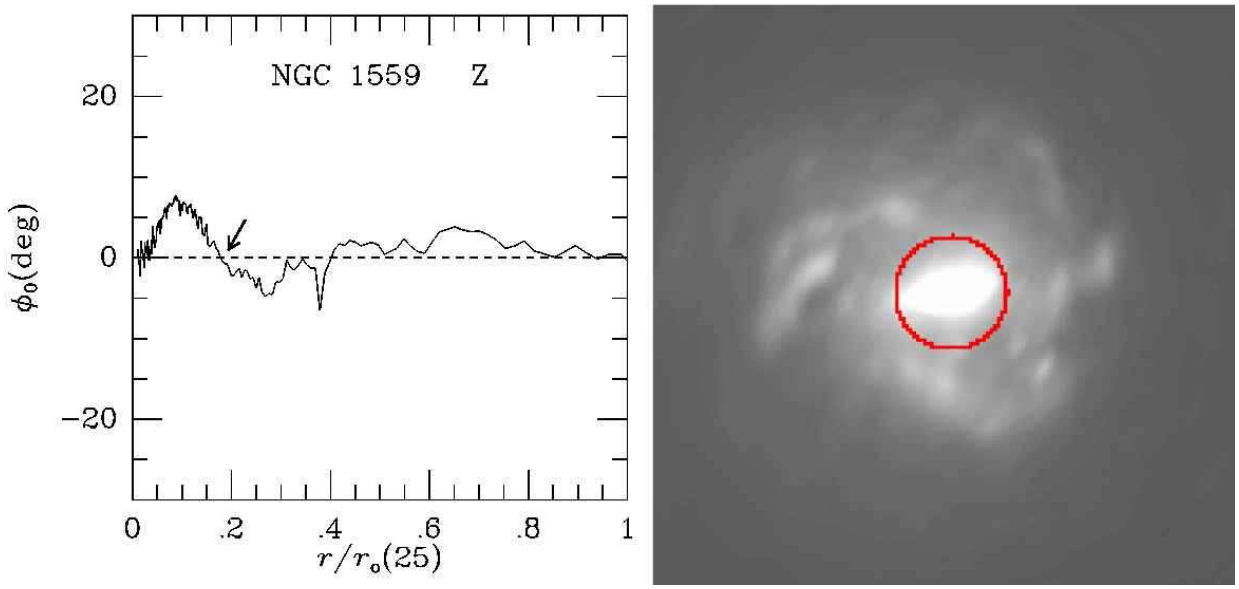

Fig. 2.28.— Same as Figure 2.1 for NGC 1559.

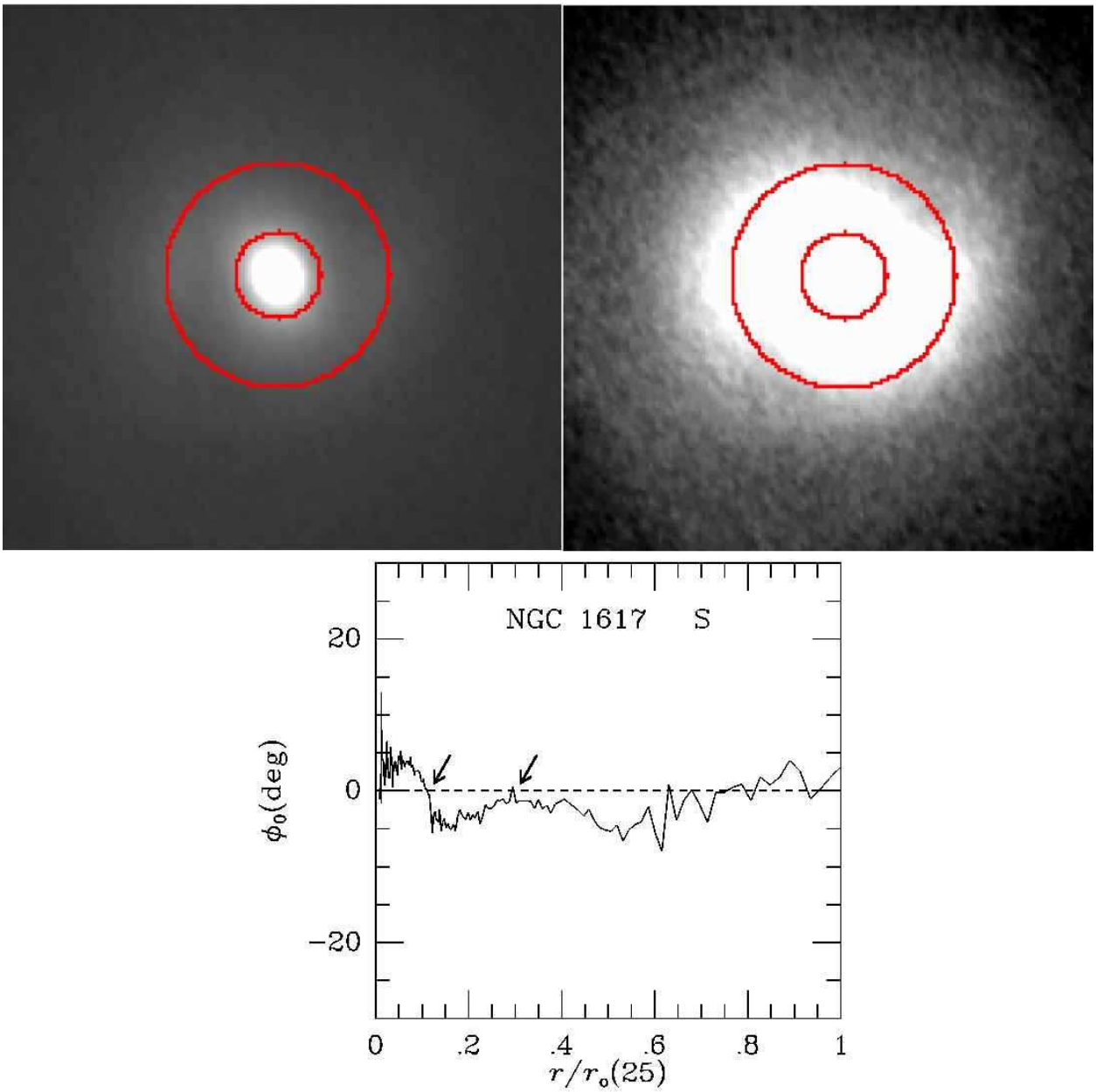

Fig. 2.29.— Same as Figure 2.1 for NGC 1617.

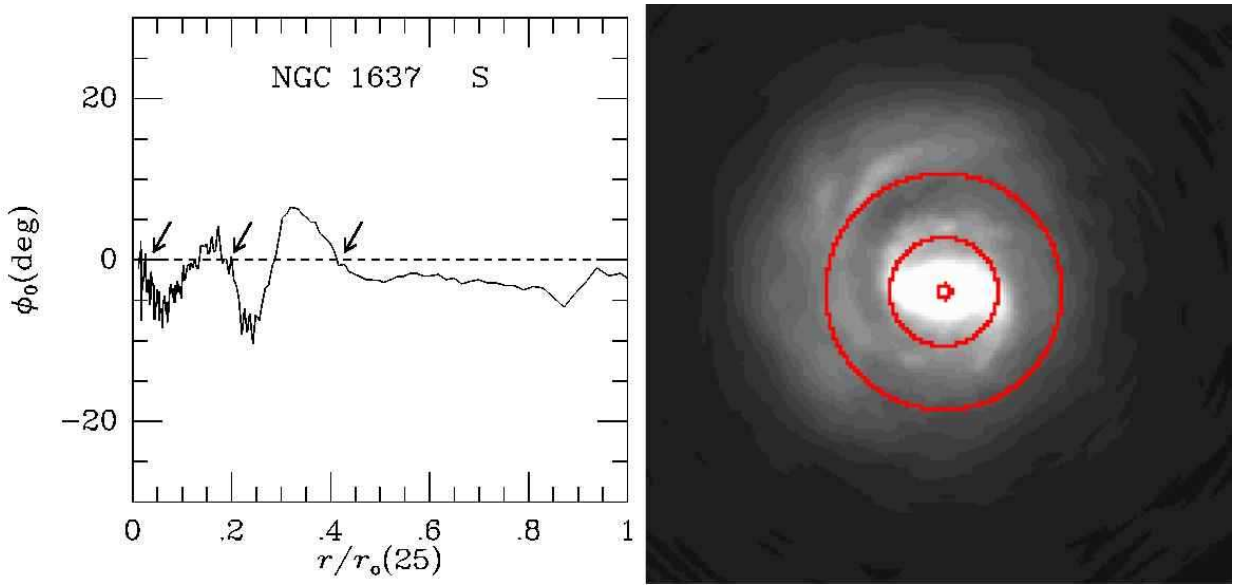

Fig. 2.30.— Same as Figure 2.1 for NGC 1637.

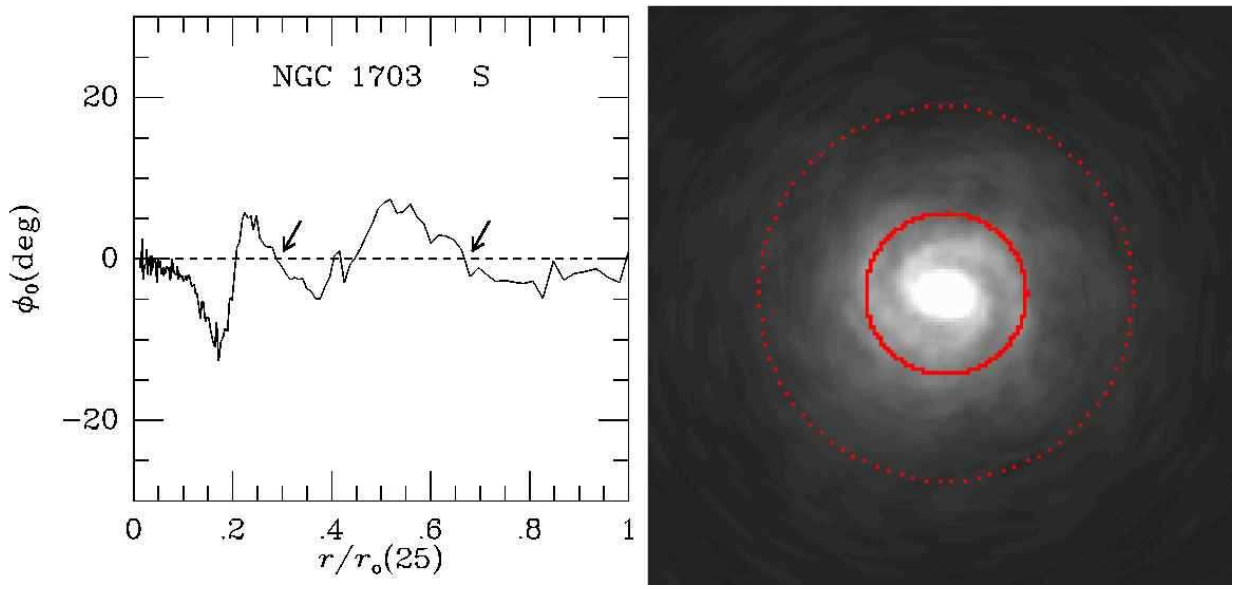

Fig. 2.31.— Same as Figure 2.1 for NGC 1703.

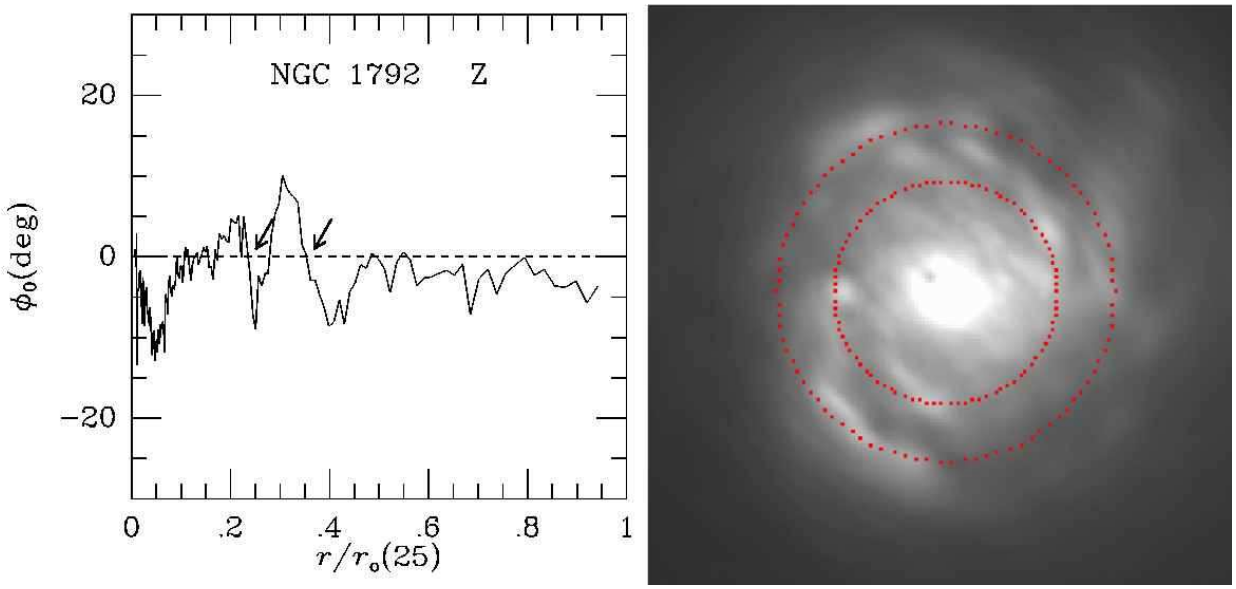

Fig. 2.32.— Same as Figure 2.1 for NGC 1792.

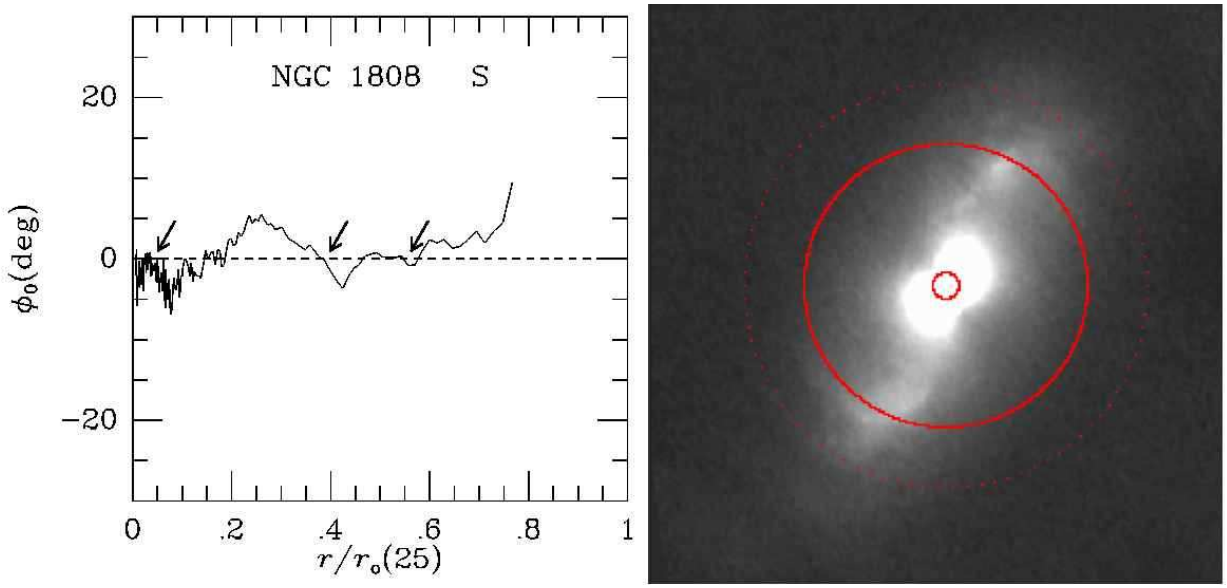

Fig. 2.33.— Same as Figure 2.1 for NGC 1808

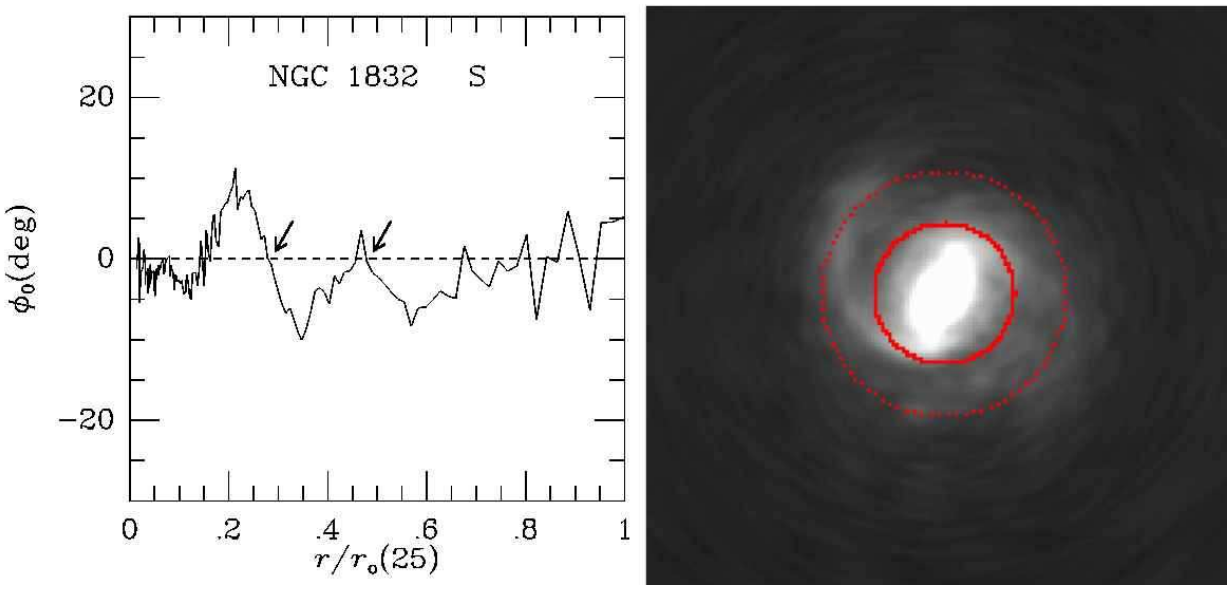

Fig. 2.34.— Same as Figure 2.1 for NGC 1832.

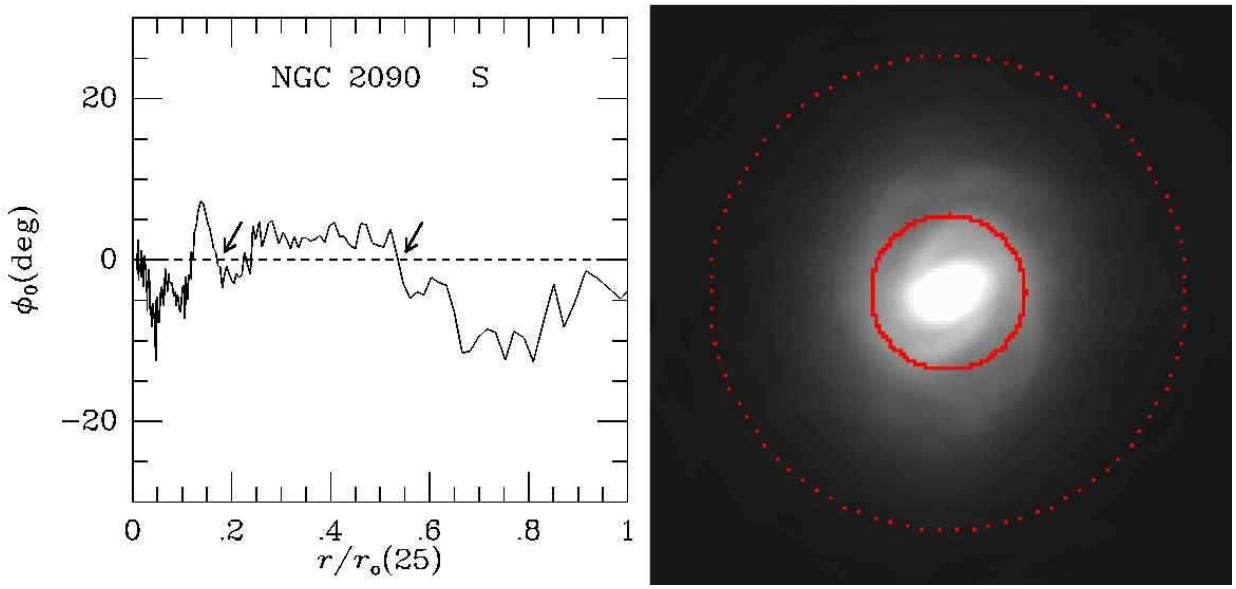

Fig. 2.35.— Same as Figure 2.1 for NGC 2090.

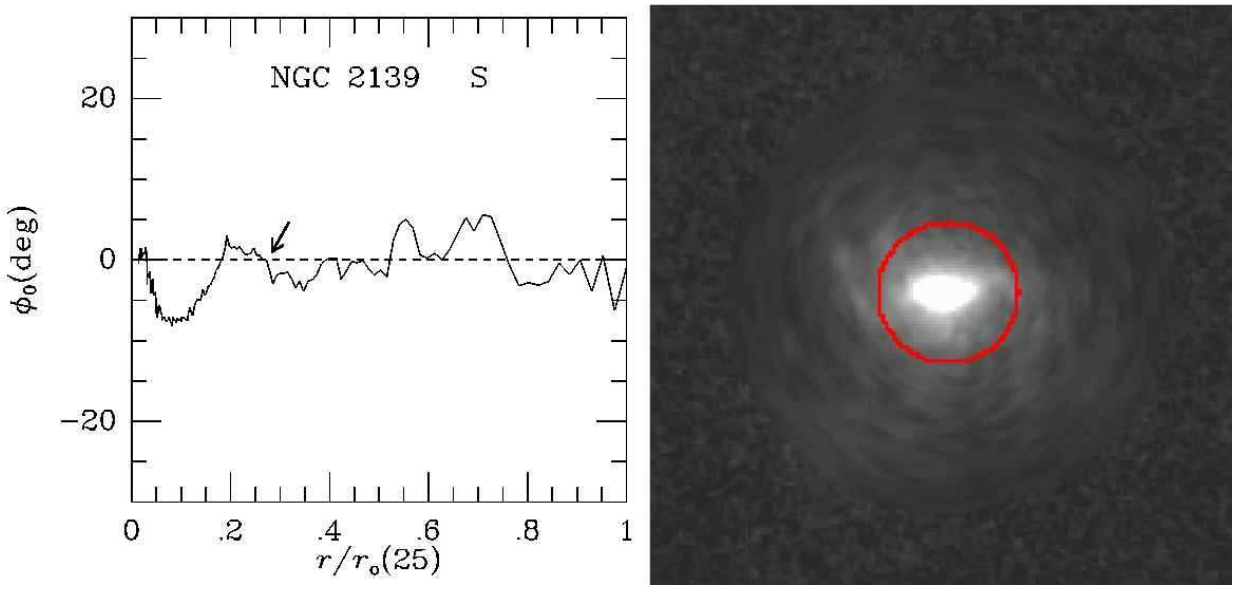

Fig. 2.36.— Same as Figure 2.1 for NGC 2139.

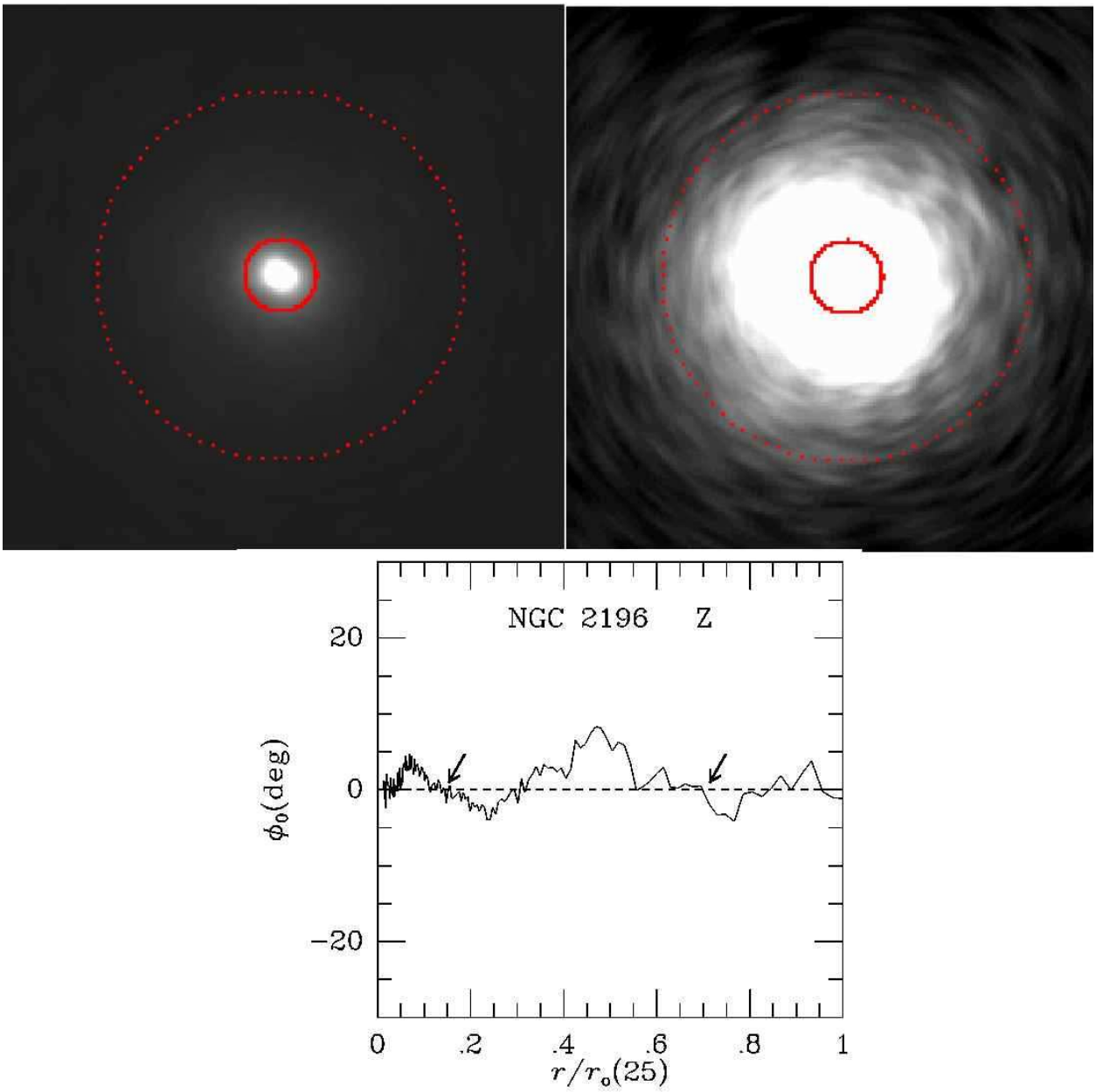

Fig. 2.37.— Same as Figure 2.1 for NGC 2196.

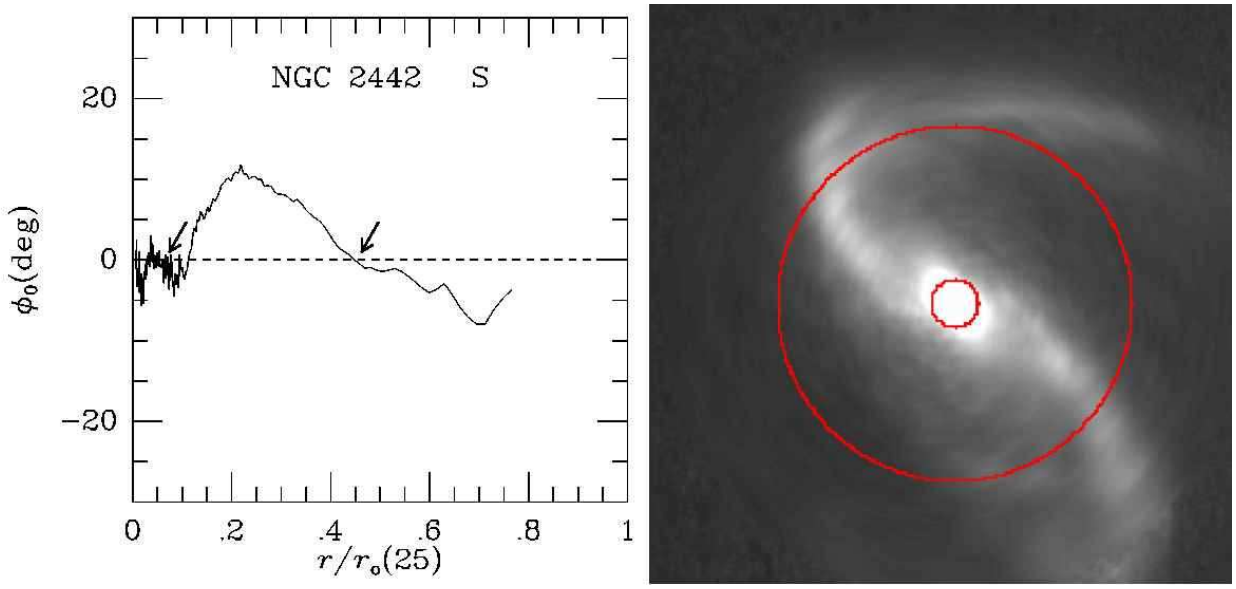

Fig. 2.38.— Same as Figure 2.1 for NGC 2442.

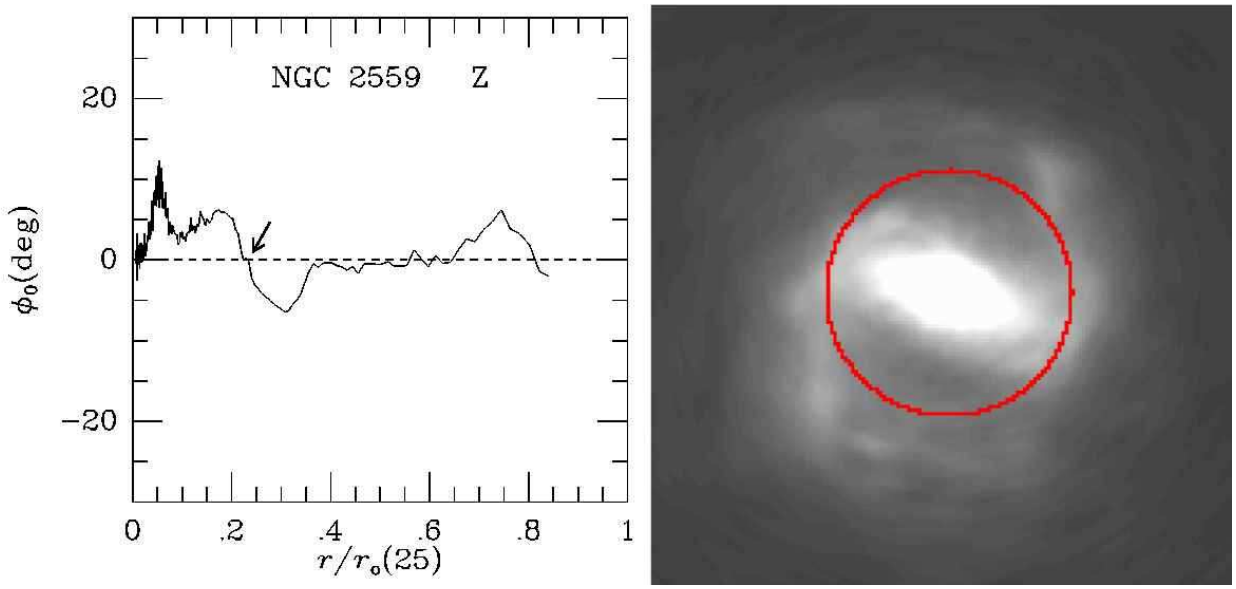

Fig. 2.39.— Same as Figure 2.1 for NGC 2559

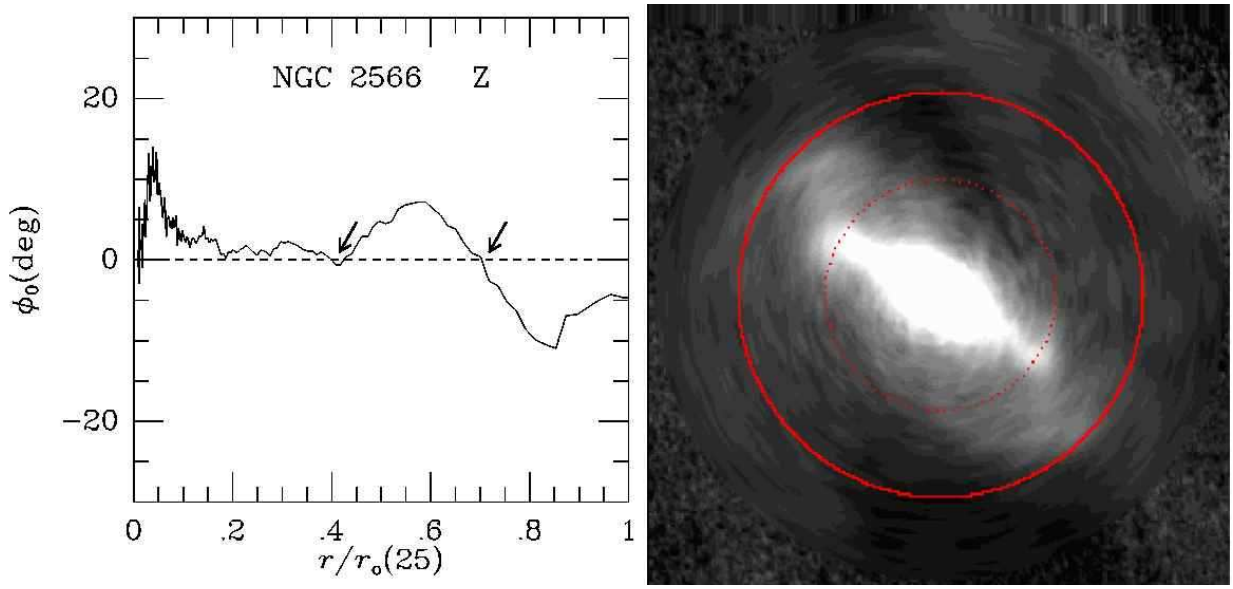

Fig. 2.40.— Same as Figure 2.1 for NGC 2566

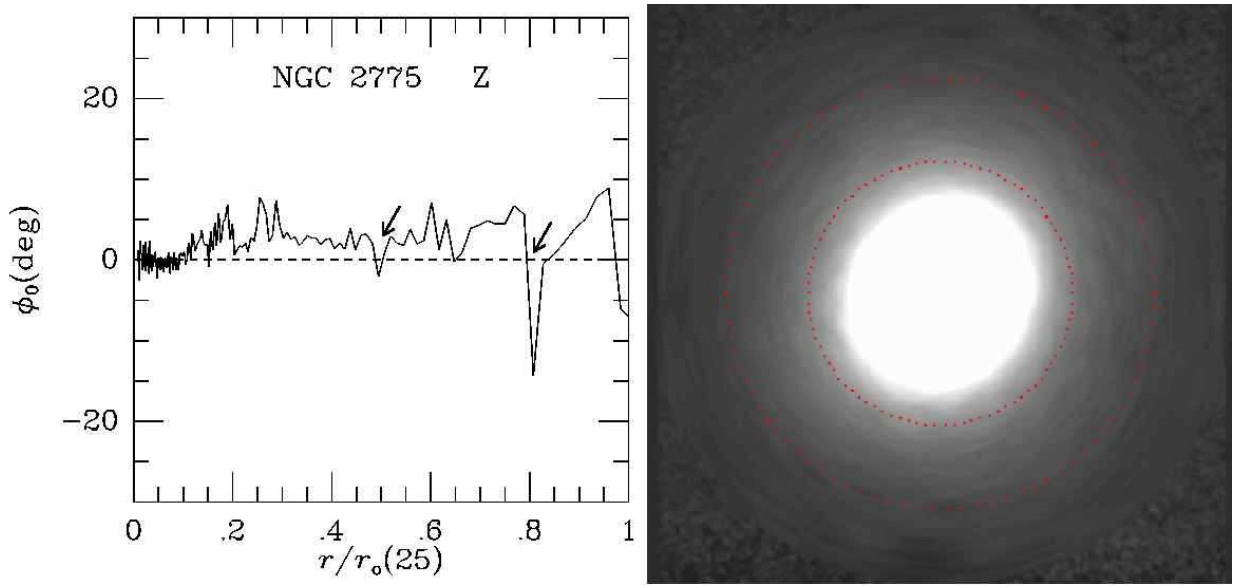

Fig. 2.41.— Same as Figure 2.1 for NGC 2775

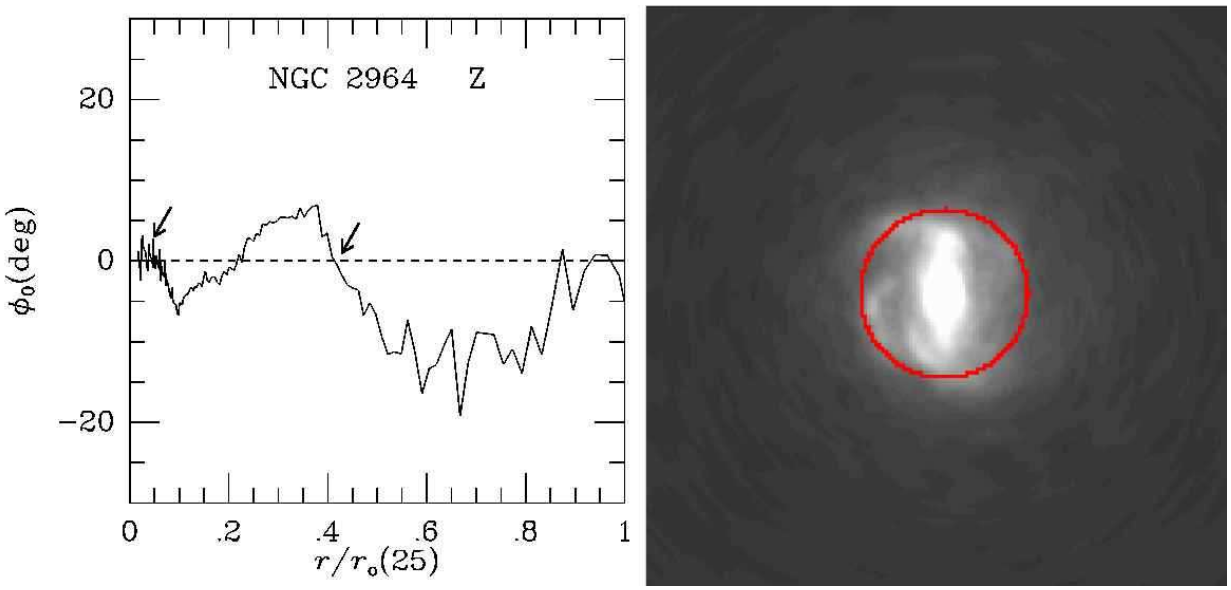

Fig. 2.42.— Same as Figure 2.1 for NGC 2964. Only CR_2 from Table 1 is shown overlaid on the image.

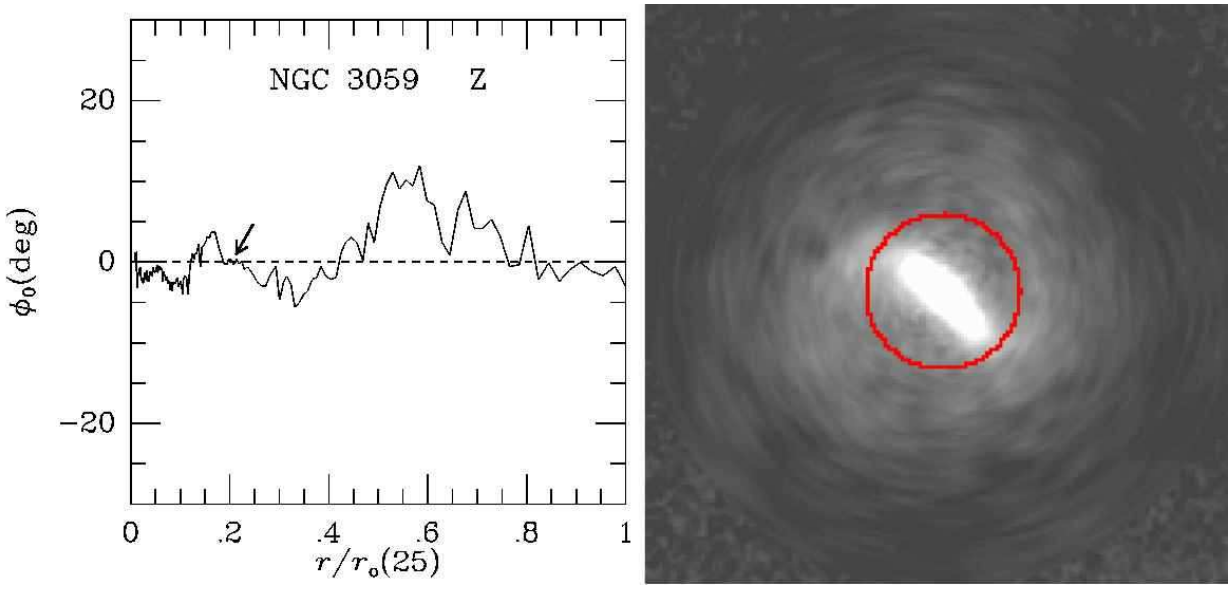

Fig. 2.43.— Same as Figure 2.1 for NGC 3059

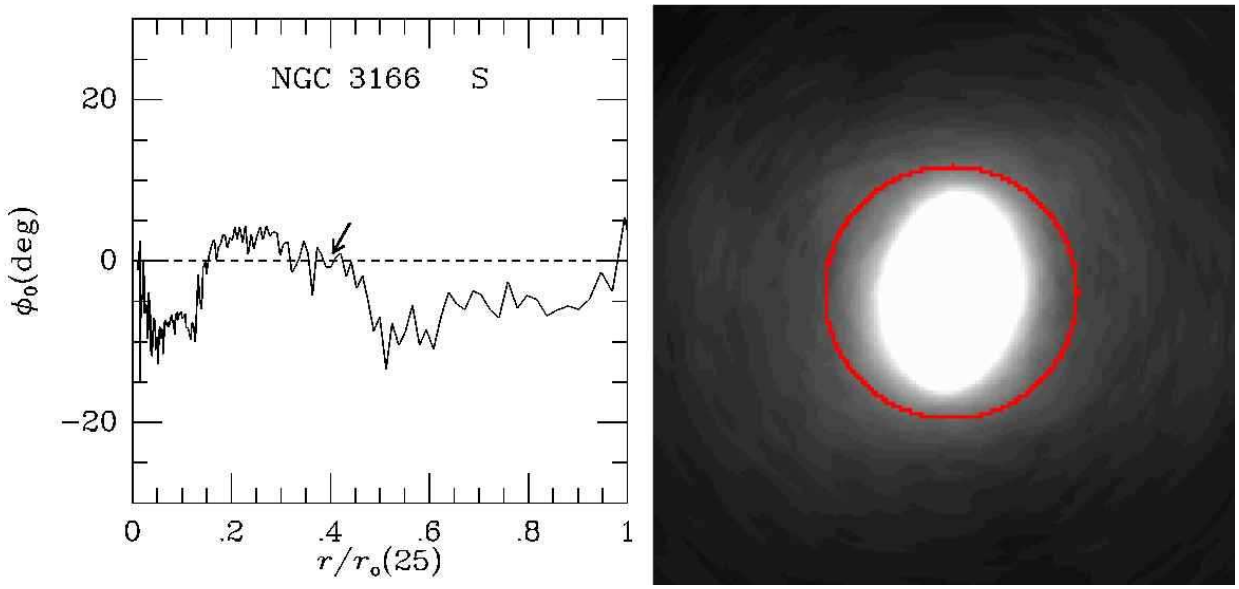

Fig. 2.44.— Same as Figure 2.1 for NGC 3166

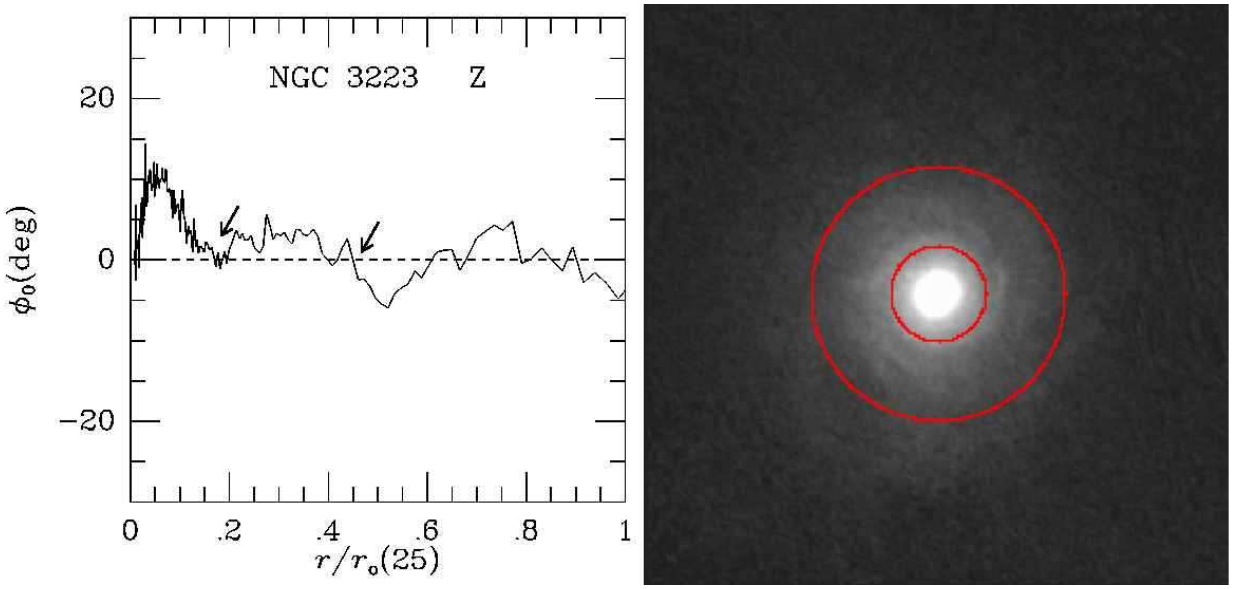

Fig. 2.45.— Same as Figure 2.1 for NGC 3223

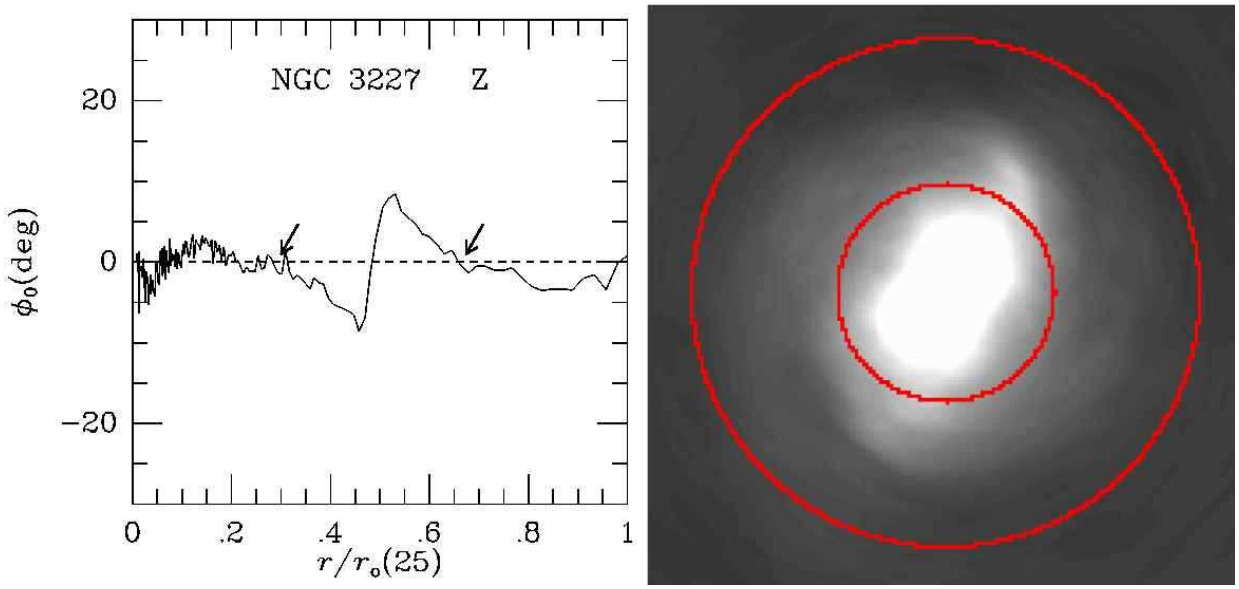

Fig. 2.46.— Same as Figure 2.1 for NGC 3227

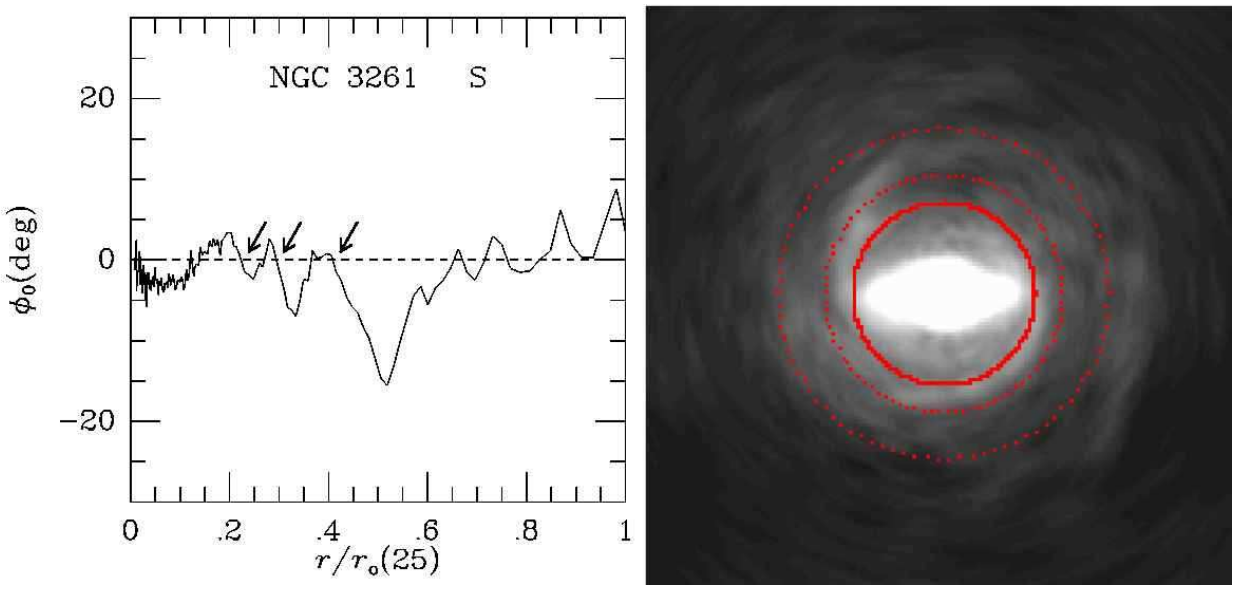

Fig. 2.47.— Same as Figure 2.1 for NGC 3261

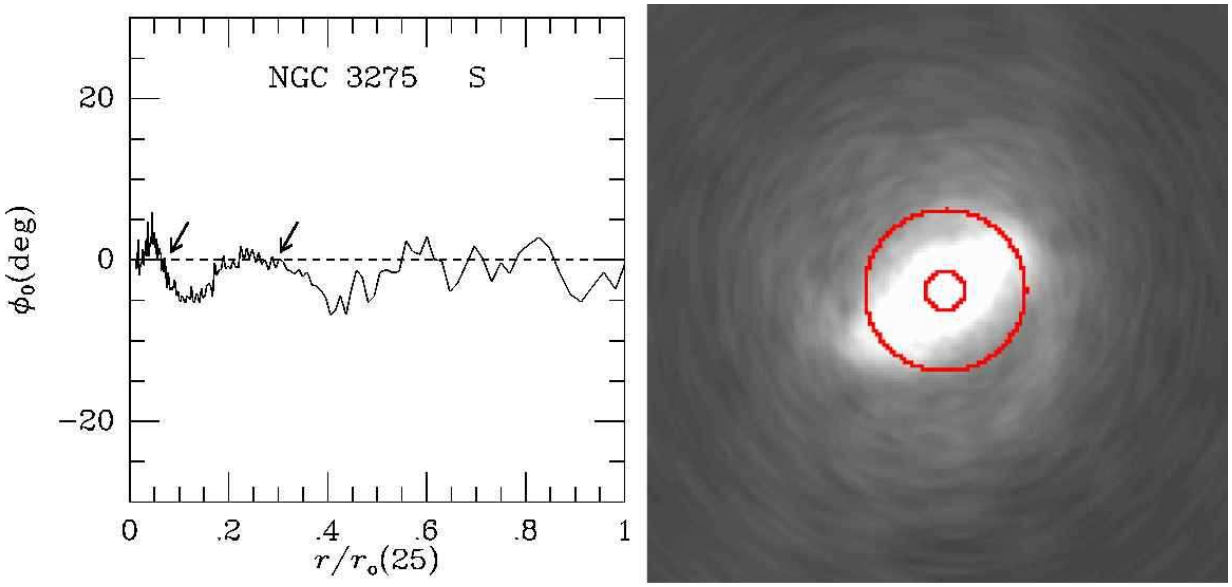

Fig. 2.48.— Same as Figure 2.1 for NGC 3275

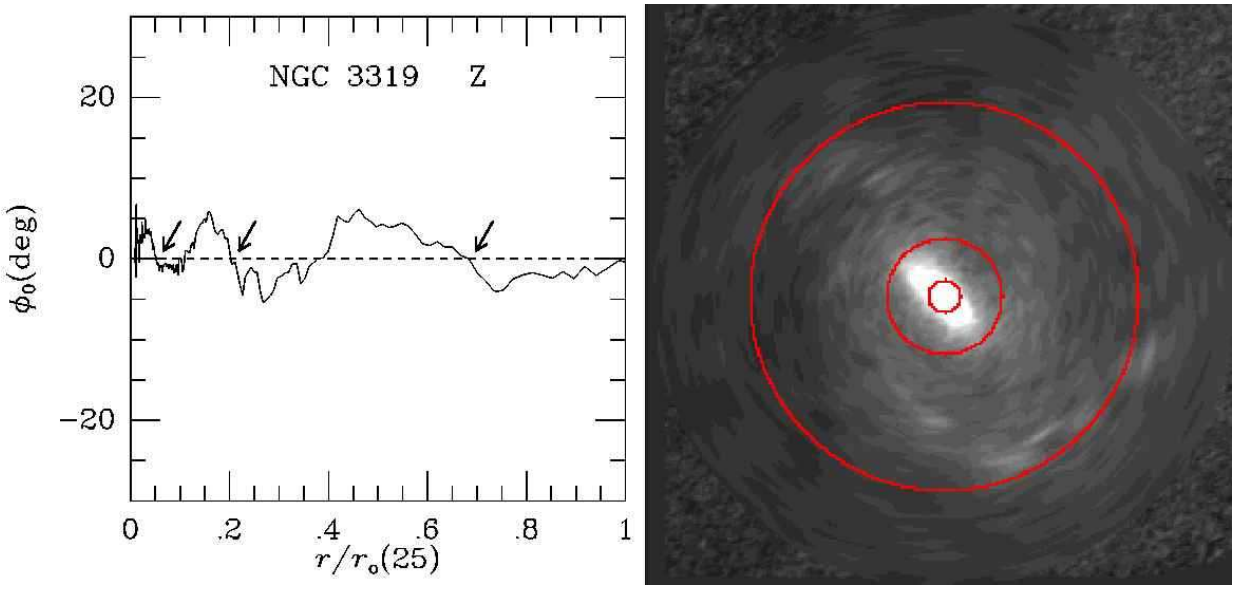

Fig. 2.49.— Same as Figure 2.1 for NGC 3319

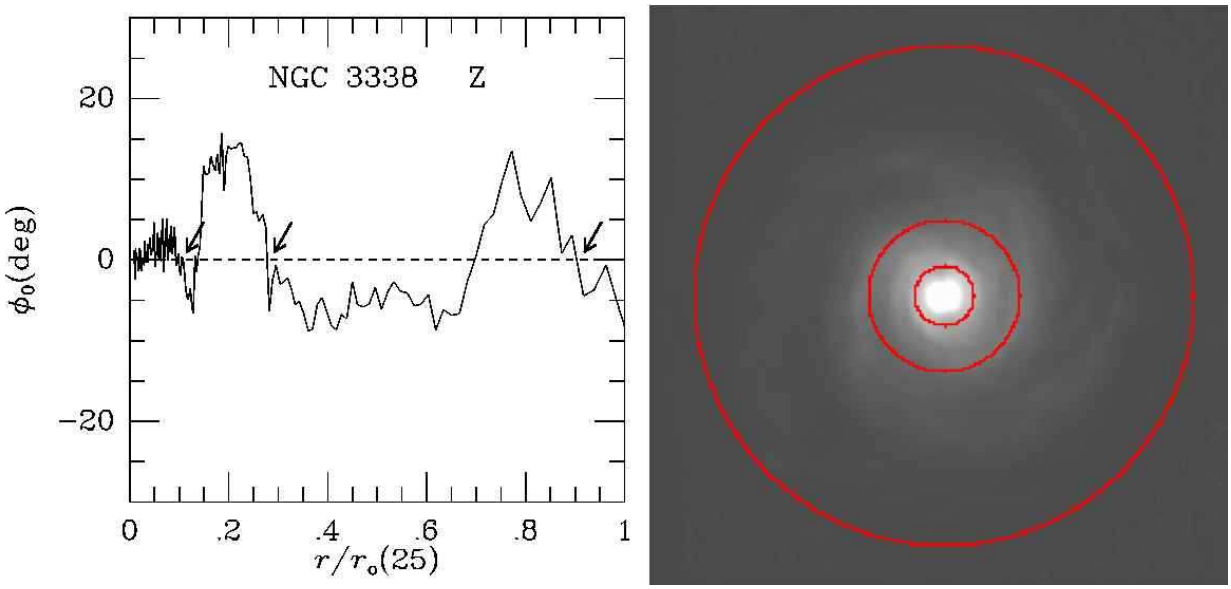

Fig. 2.50.— Same as Figure 2.1 for NGC 3338

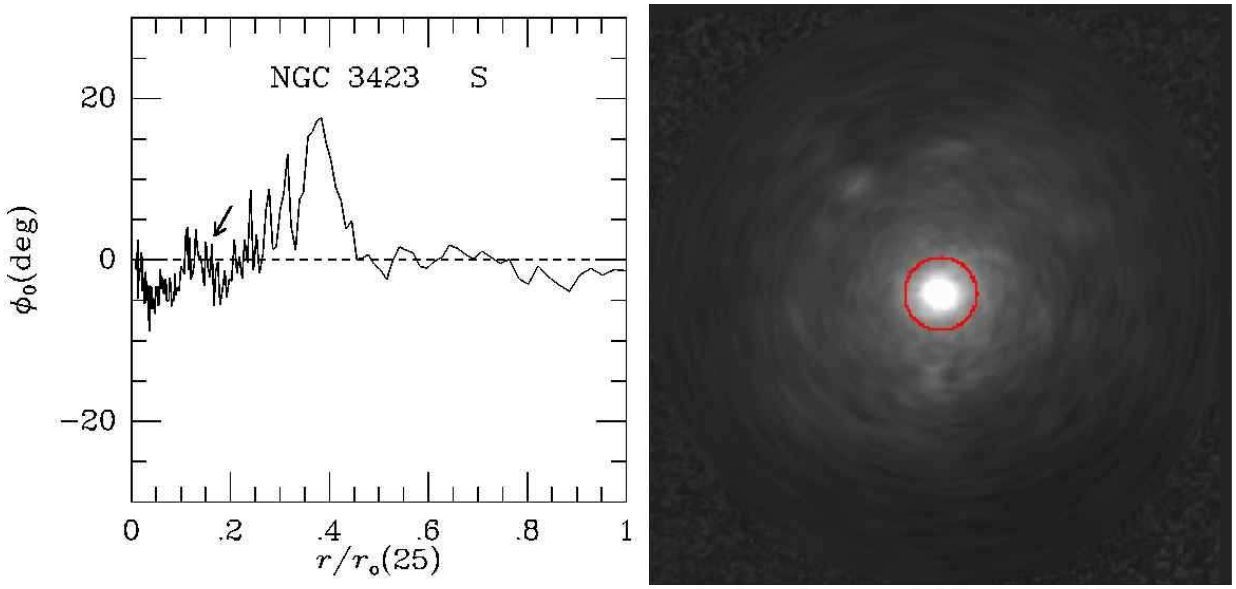

Fig. 2.51.— Same as Figure 2.1 for NGC 3423

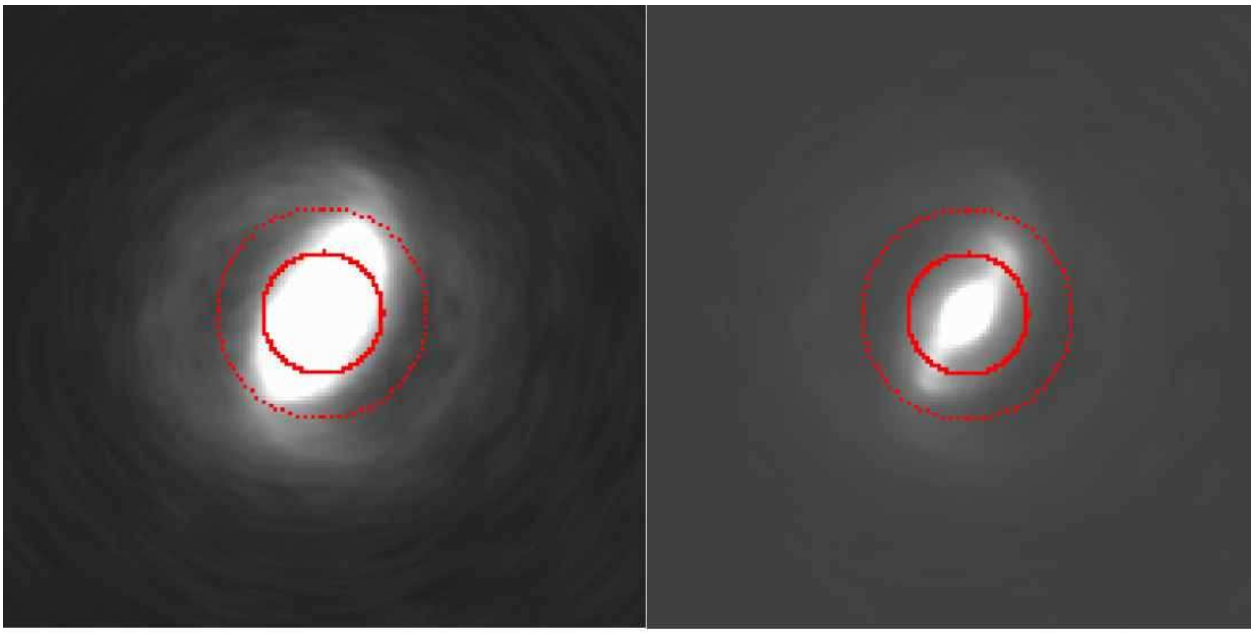

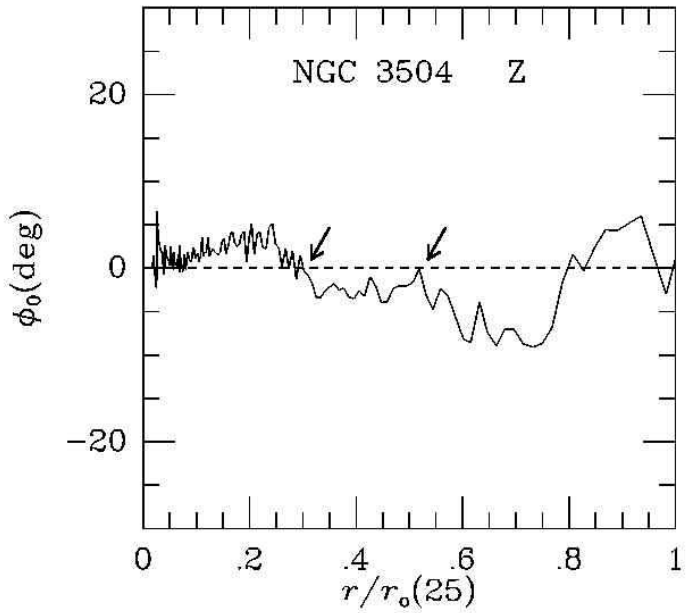

Fig. 2.52.— Same as Figure 2.1 for NGC 3504

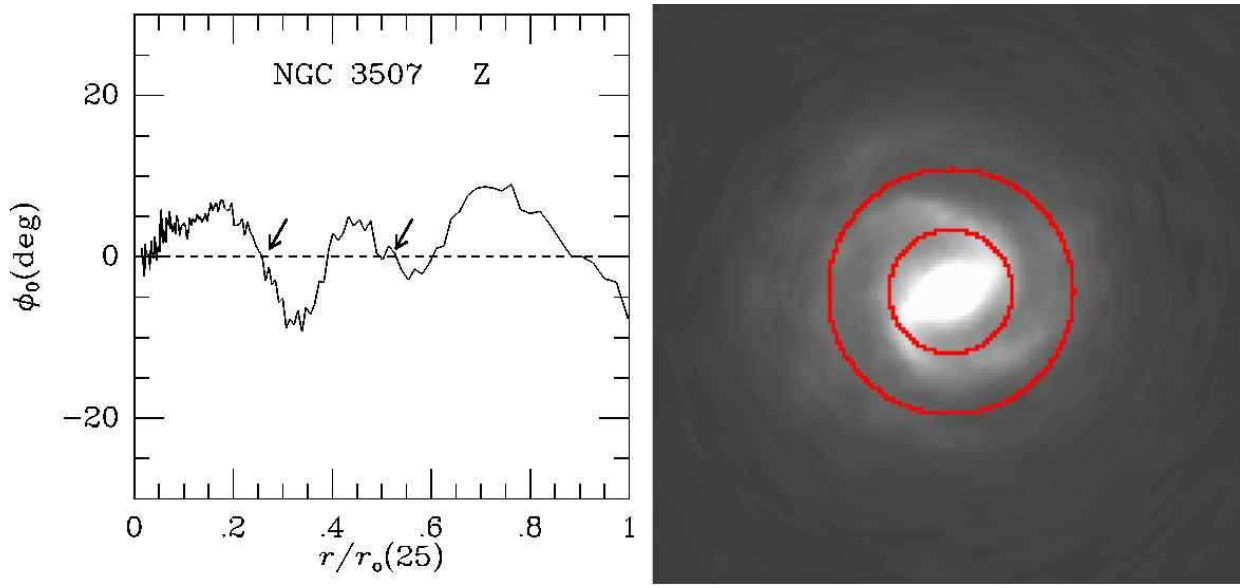

Fig. 2.53.— Same as Figure 2.1 for NGC 3507

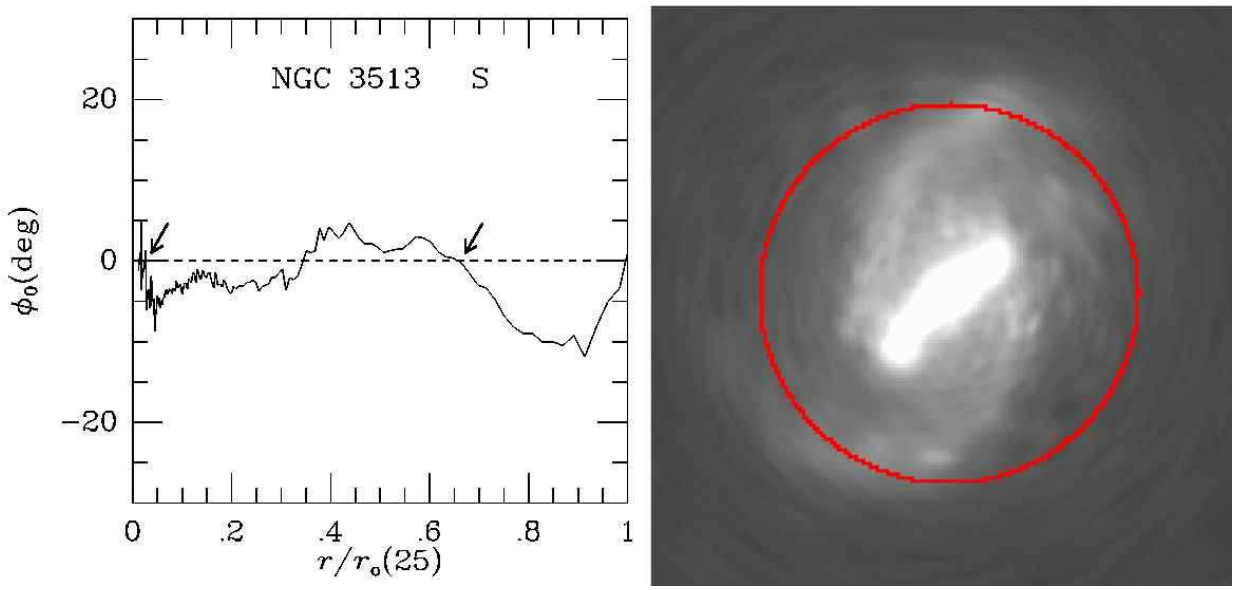

Fig. 2.54.— Same as Figure 2.1 for NGC 3513. Only CR_2 from Table 1 is shown overlaid on the image.

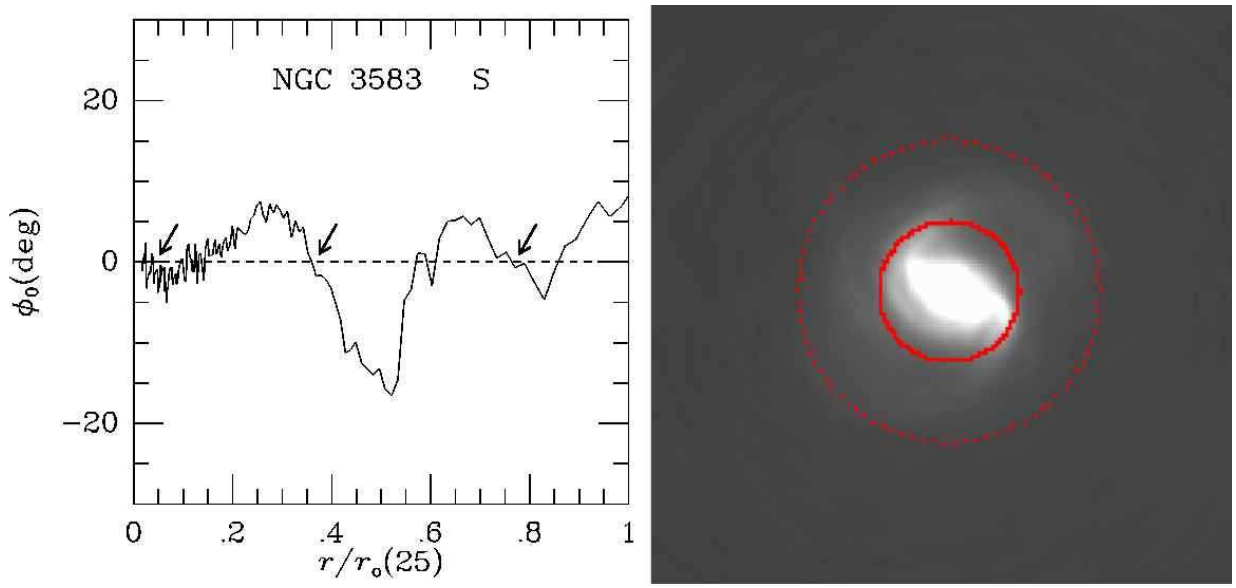

Fig. 2.55.— Same as Figure 2.1 for NGC 3583. Only CR_2 and CR_3 from Table 1 are shown overlaid on the image.

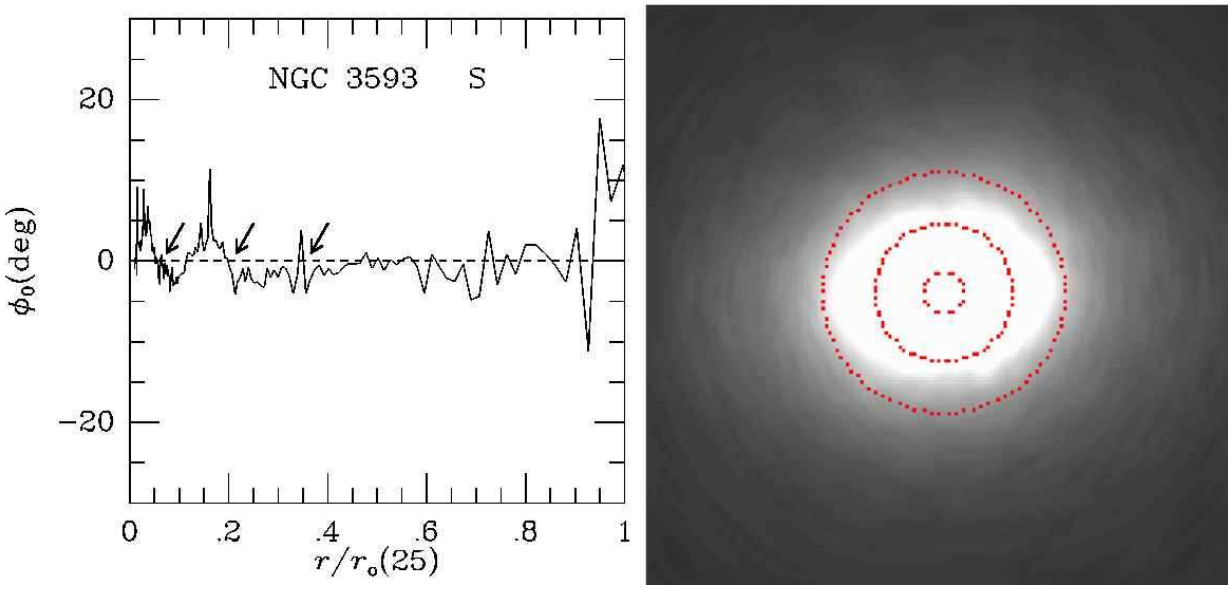

Fig. 2.56.— Same as Figure 2.1 for NGC 3593

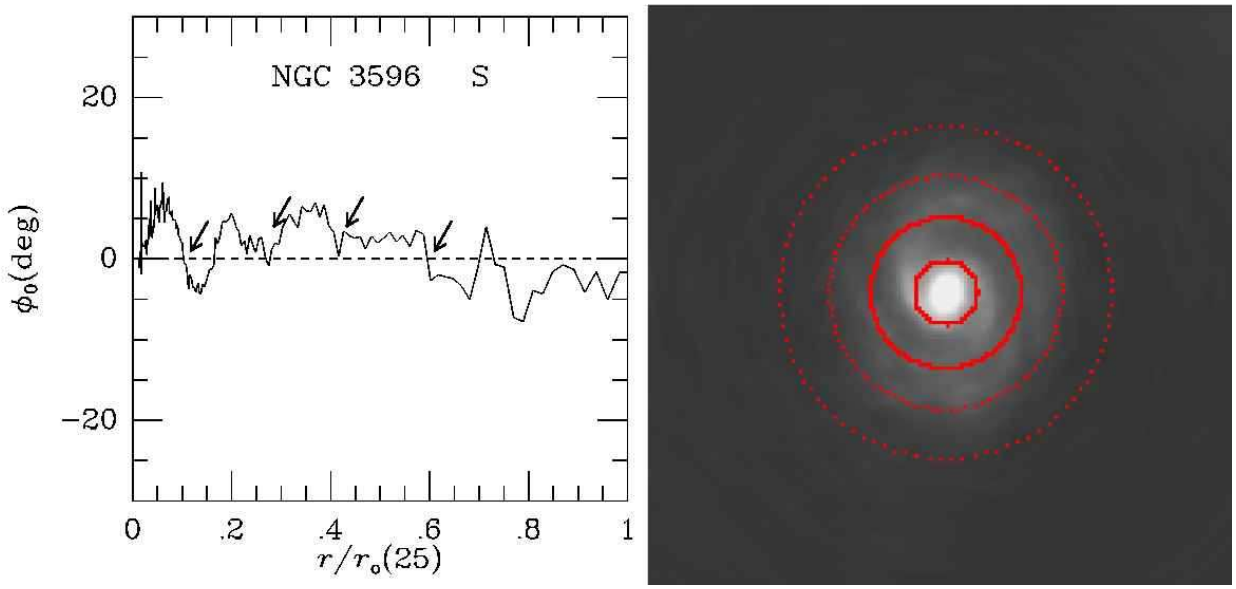

Fig. 2.57.— Same as Figure 2.1 for NGC 3596

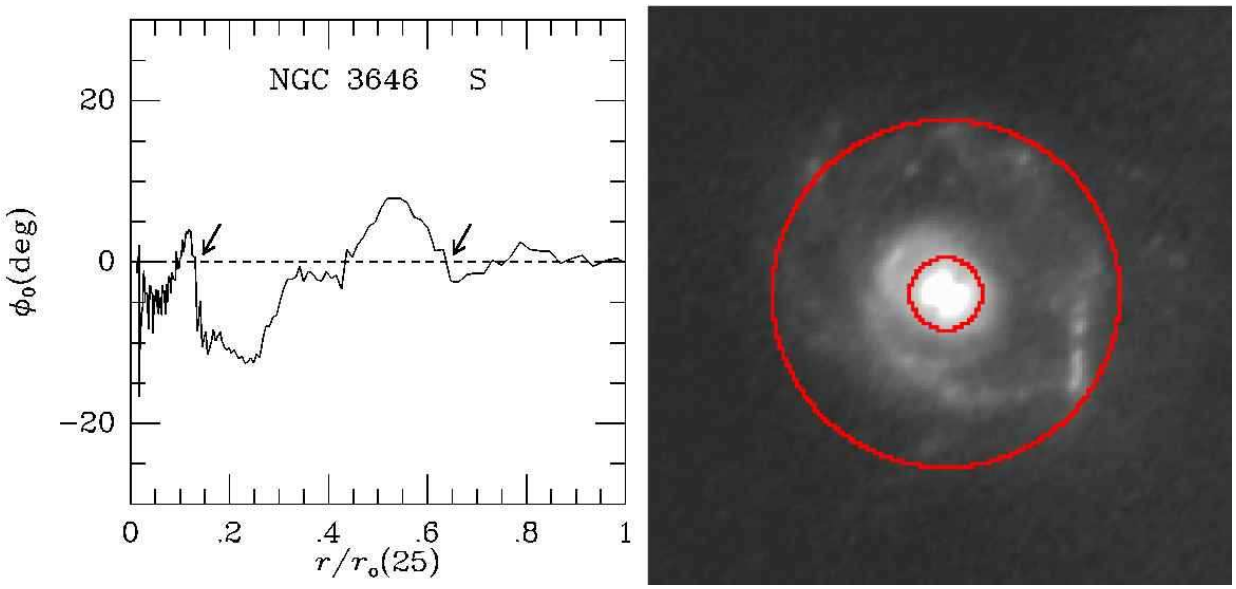

Fig. 2.58.— Same as Figure 2.1 for NGC 3646

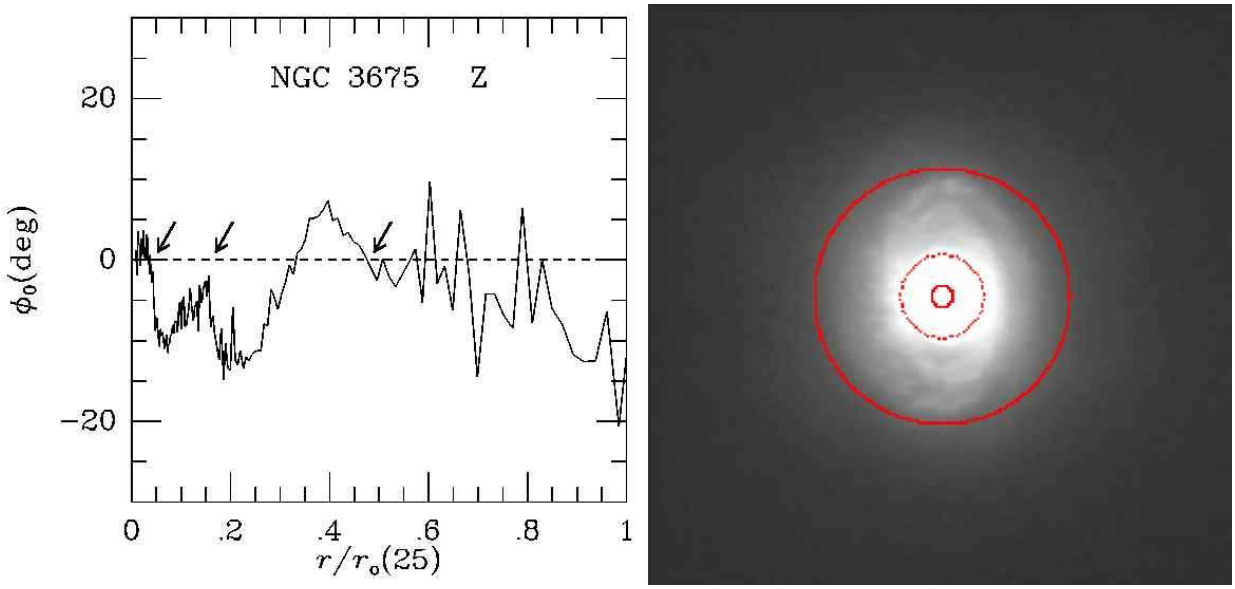

Fig. 2.59.— Same as Figure 2.1 for NGC 3675. The dotted circle, CR_2, is a "near" crossing.

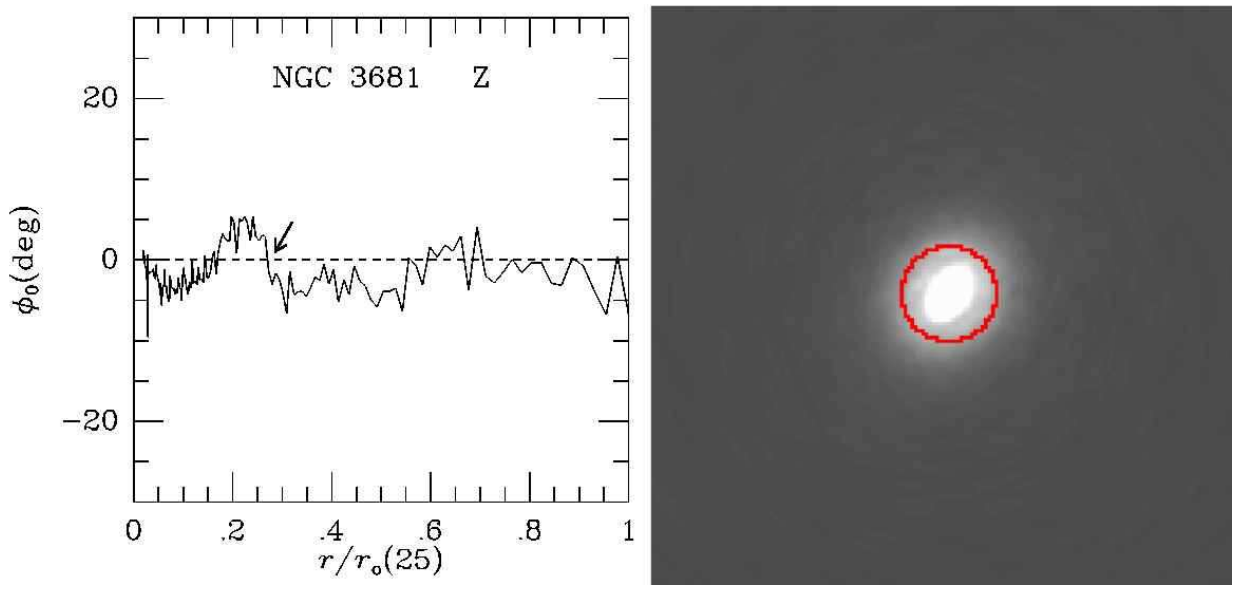

Fig. 2.60.— Same as Figure 2.1 for NGC 3681

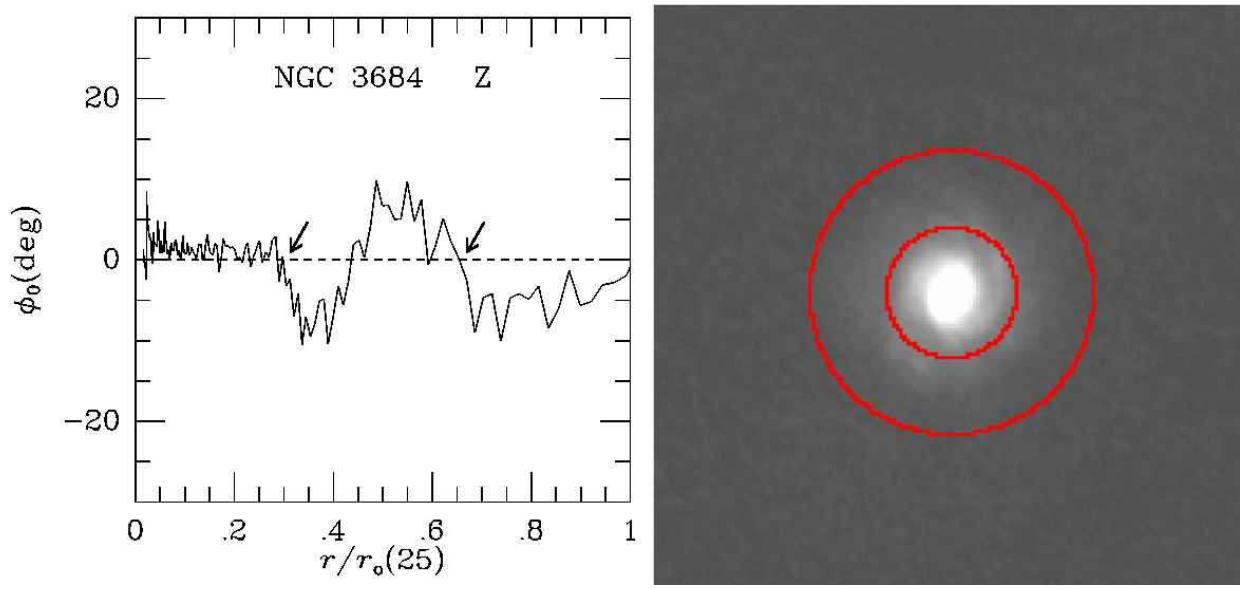

Fig. 2.61.— Same as Figure 2.1 for NGC 3684

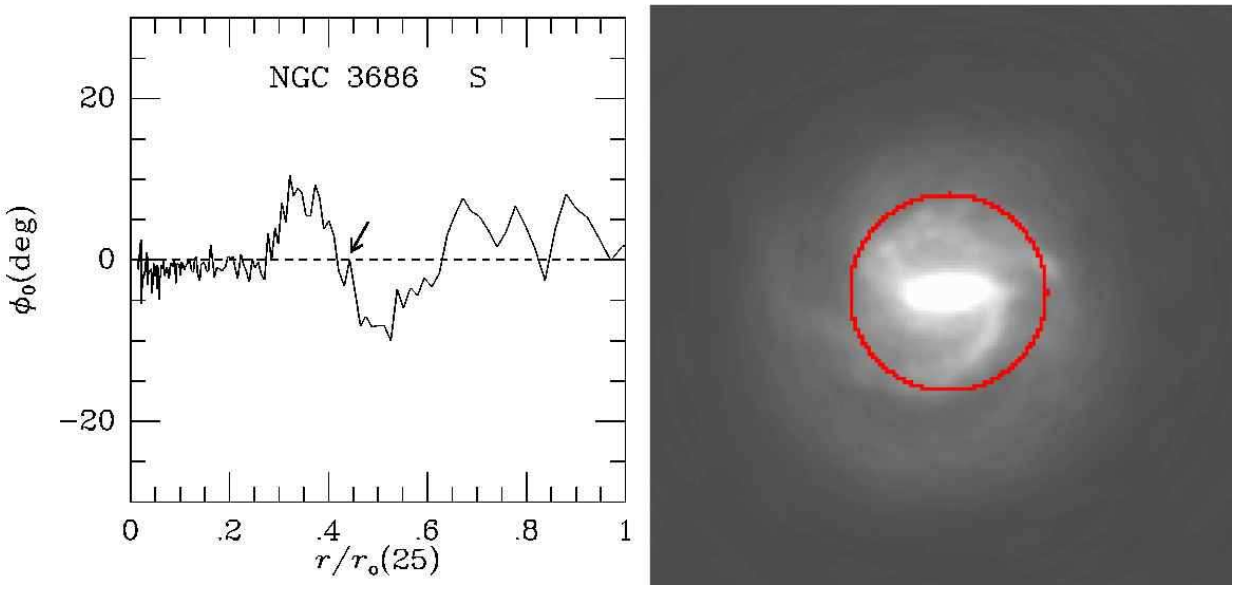

Fig. 2.62.— Same as Figure 2.1 for NGC 3686

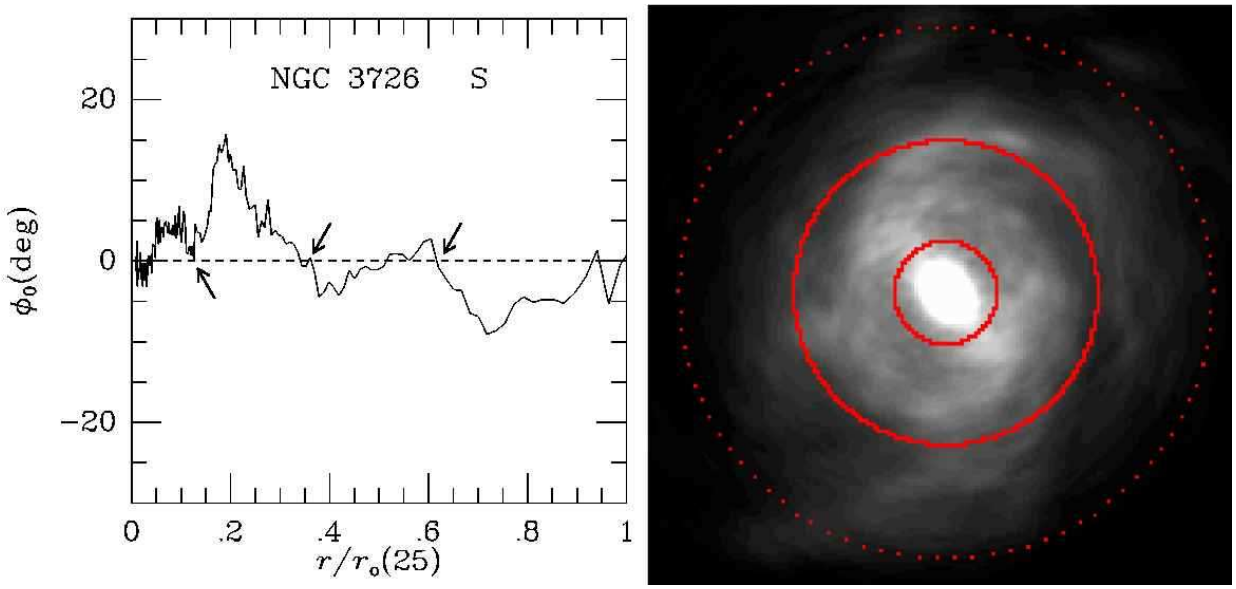

Fig. 2.63.— Same as Figure 2.1 for NGC 3726

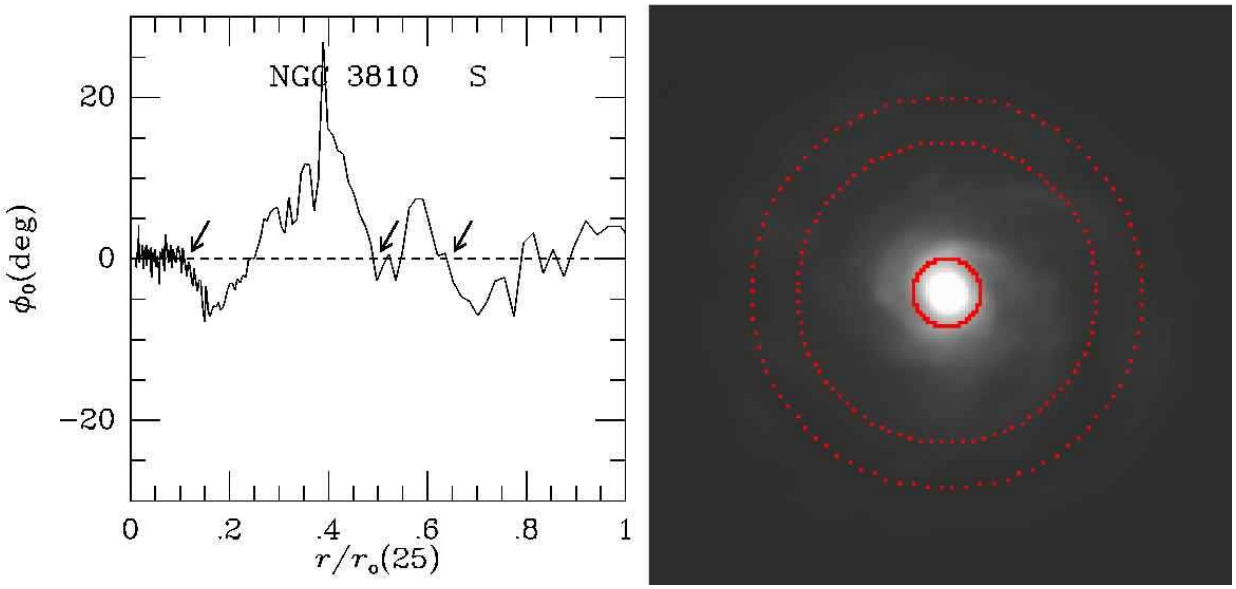

Fig. 2.64.— Same as Figure 2.1 for NGC 3810

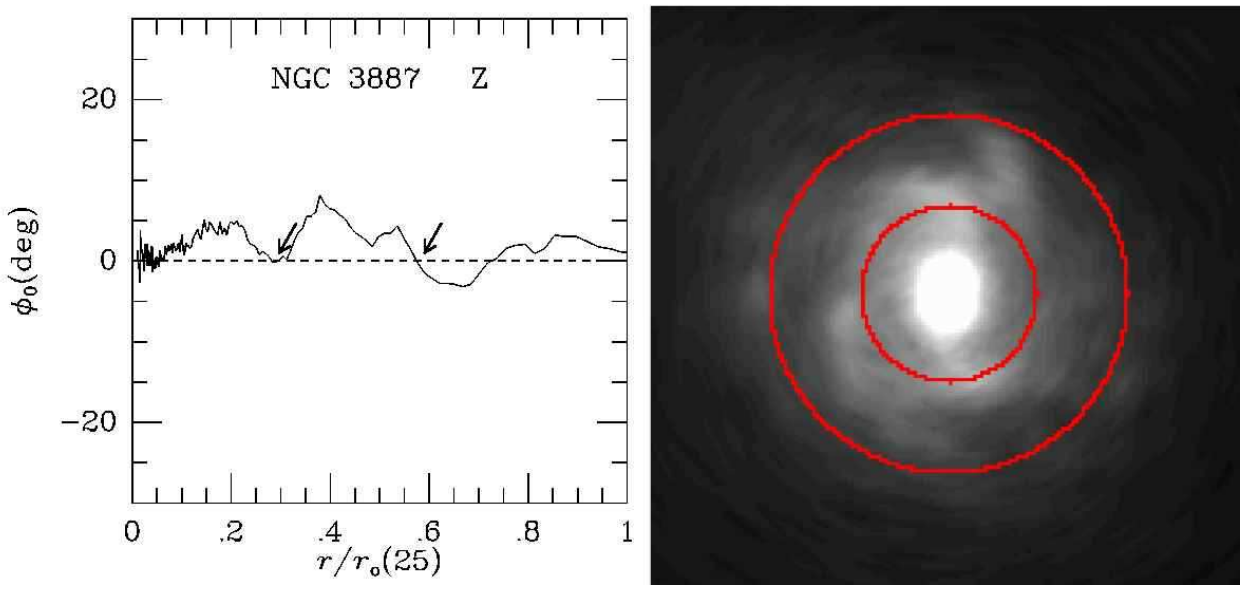

Fig. 2.65.— Same as Figure 2.1 for NGC 3887

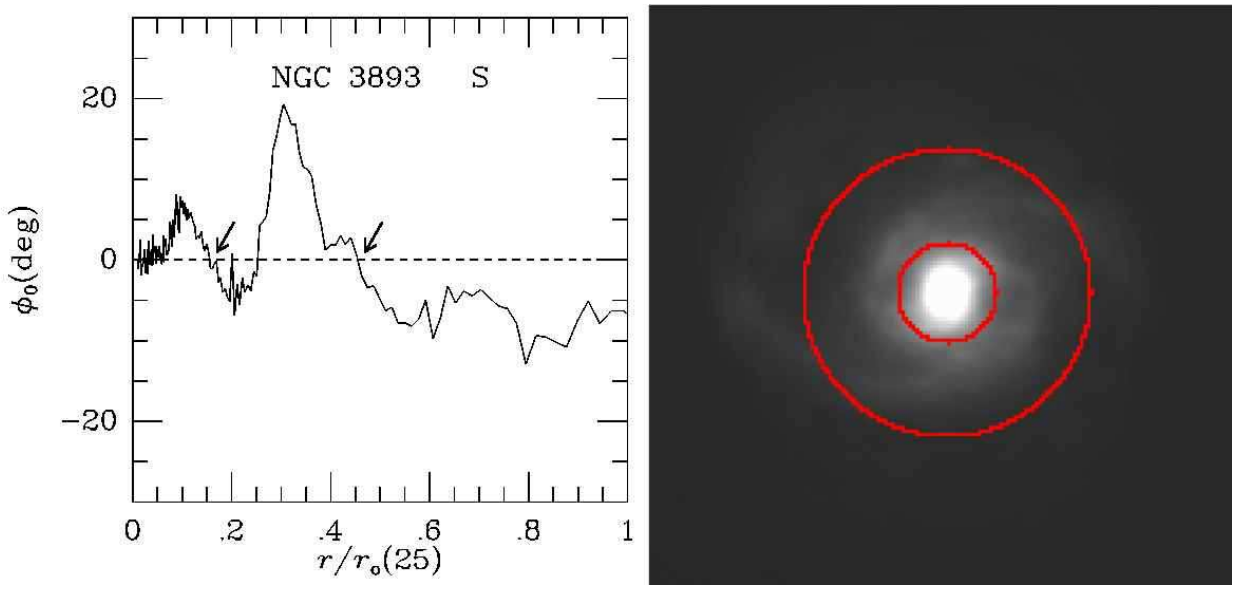

Fig. 2.66.— Same as Figure 2.1 for NGC 3893

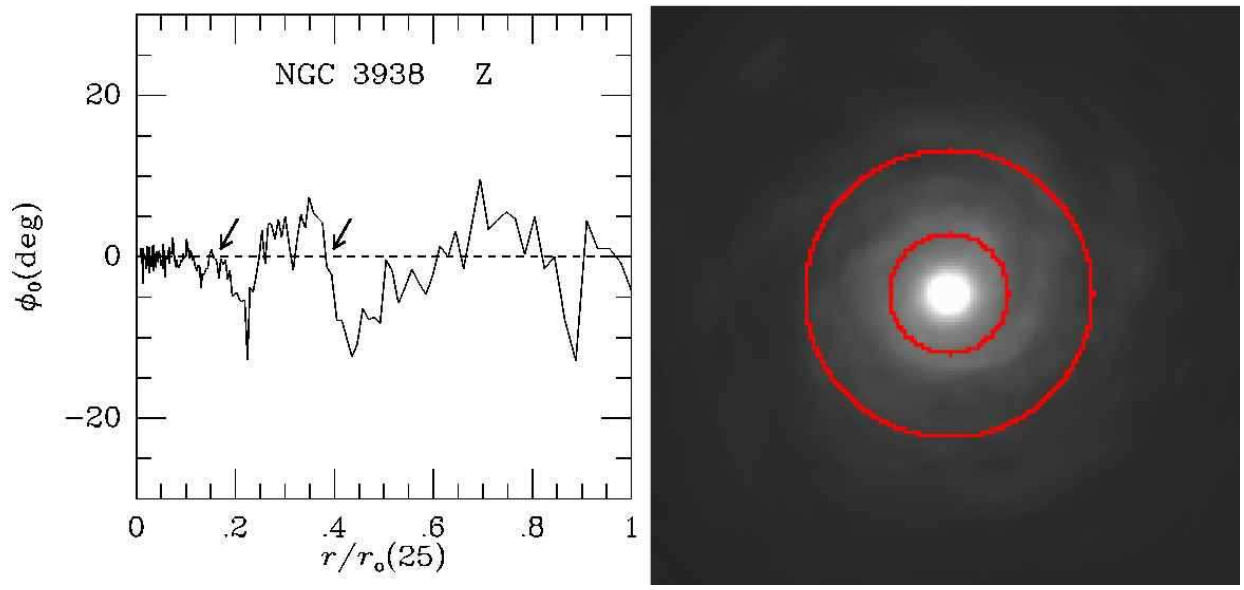

Fig. 2.67.— Same as Figure 2.1 for NGC 3938

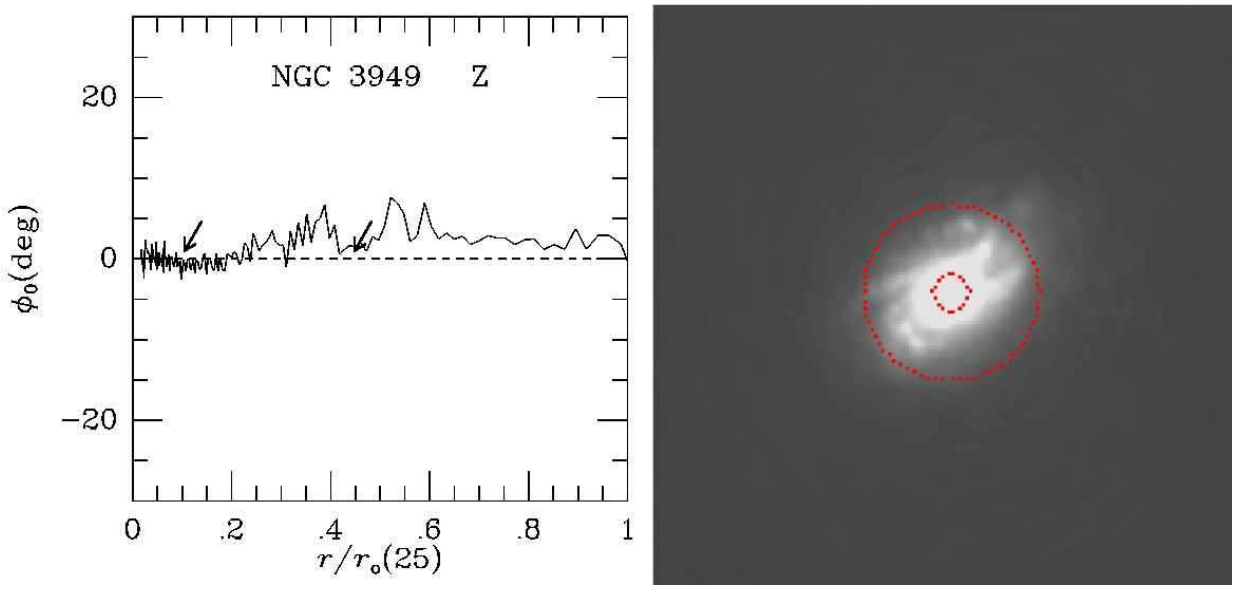

Fig. 2.68.— Same as Figure 2.1 for NGC 3949

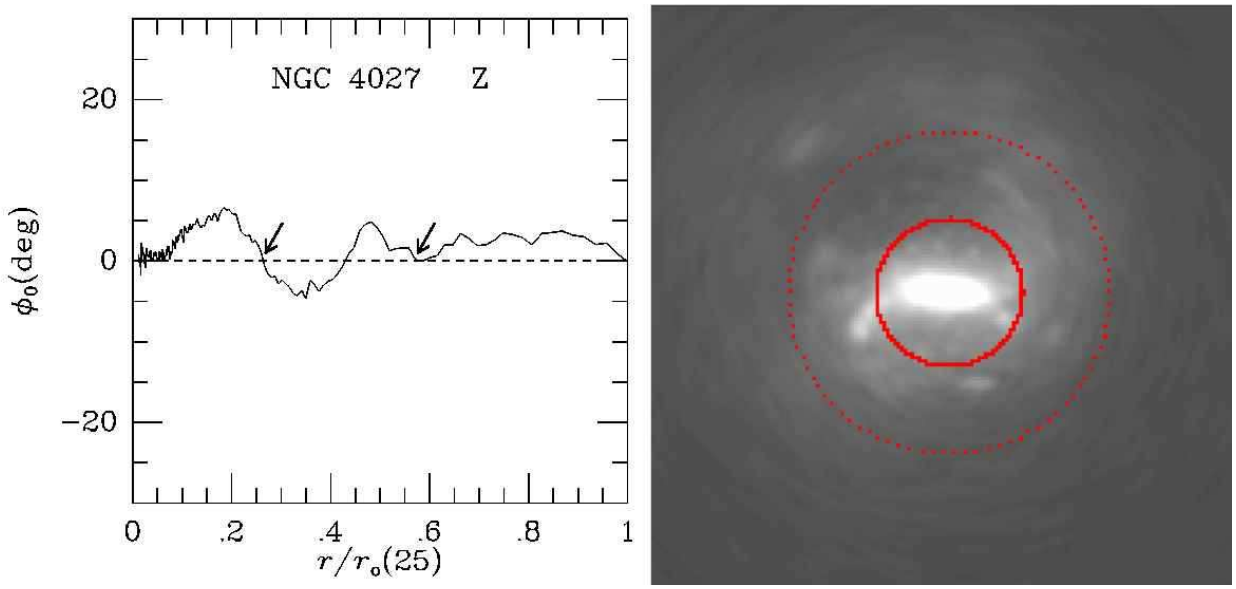

Fig. 2.69.— Same as Figure 2.1 for NGC 4027

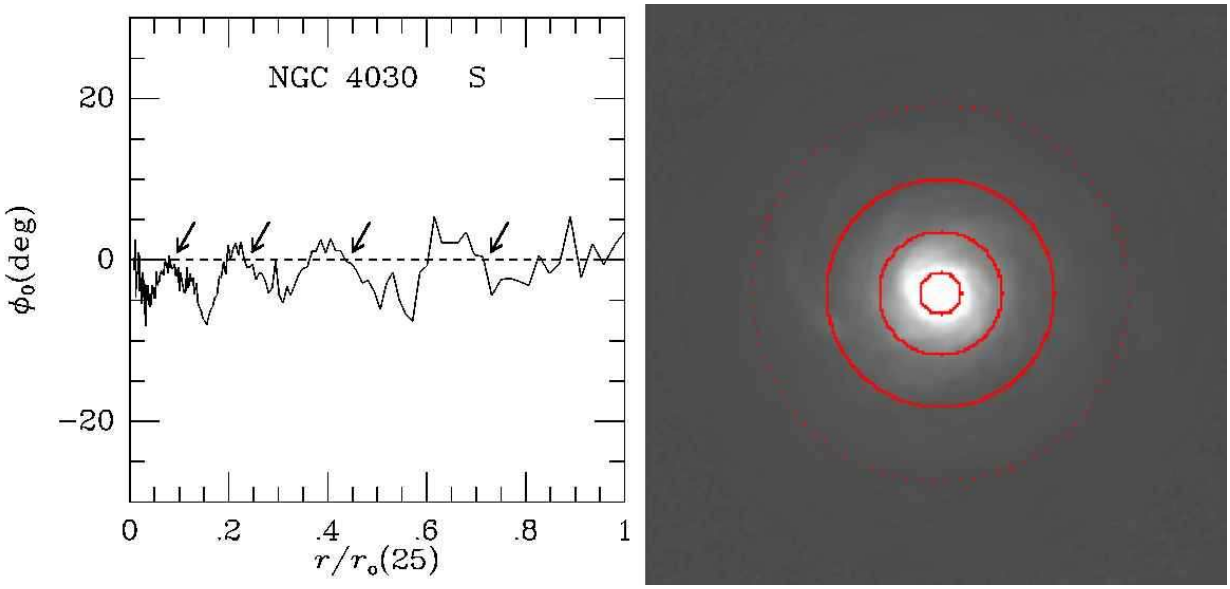

Fig. 2.70.— Same as Figure 2.1 for NGC 4030

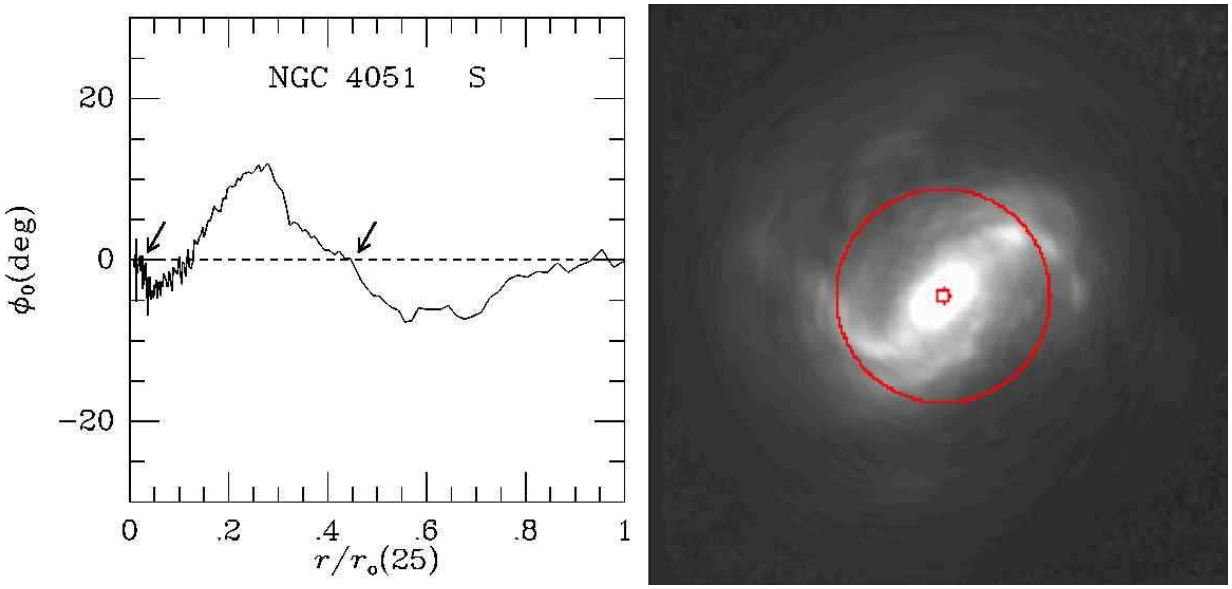

Fig. 2.71.— Same as Figure 2.1 for NGC 4051

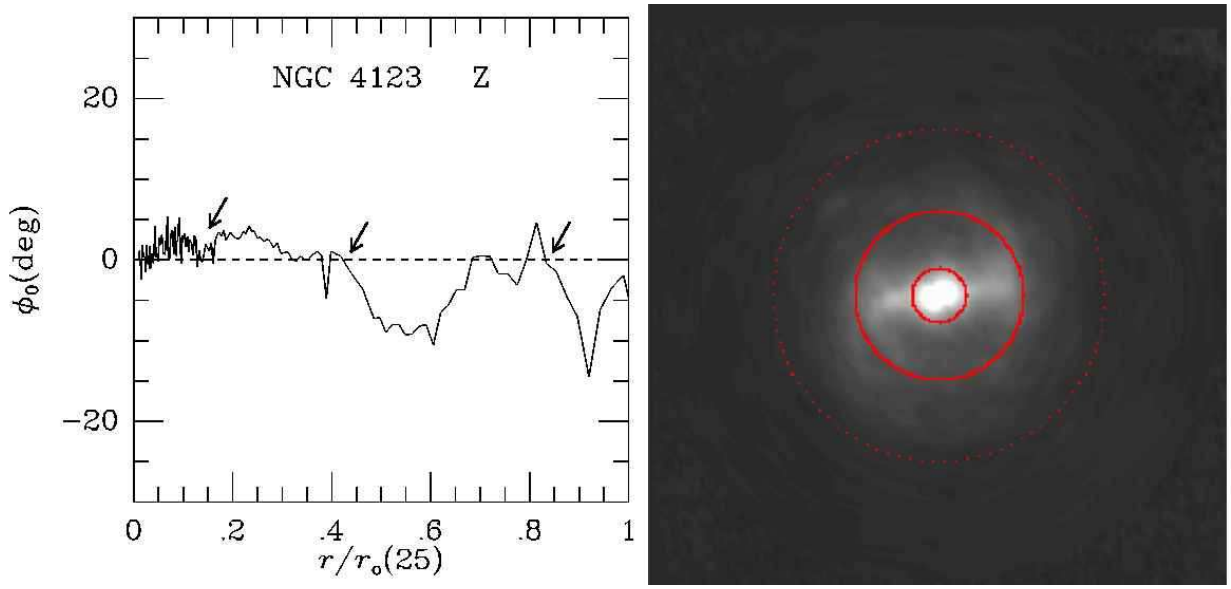

Fig. 2.72.— Same as Figure 2.1 for NGC 4123

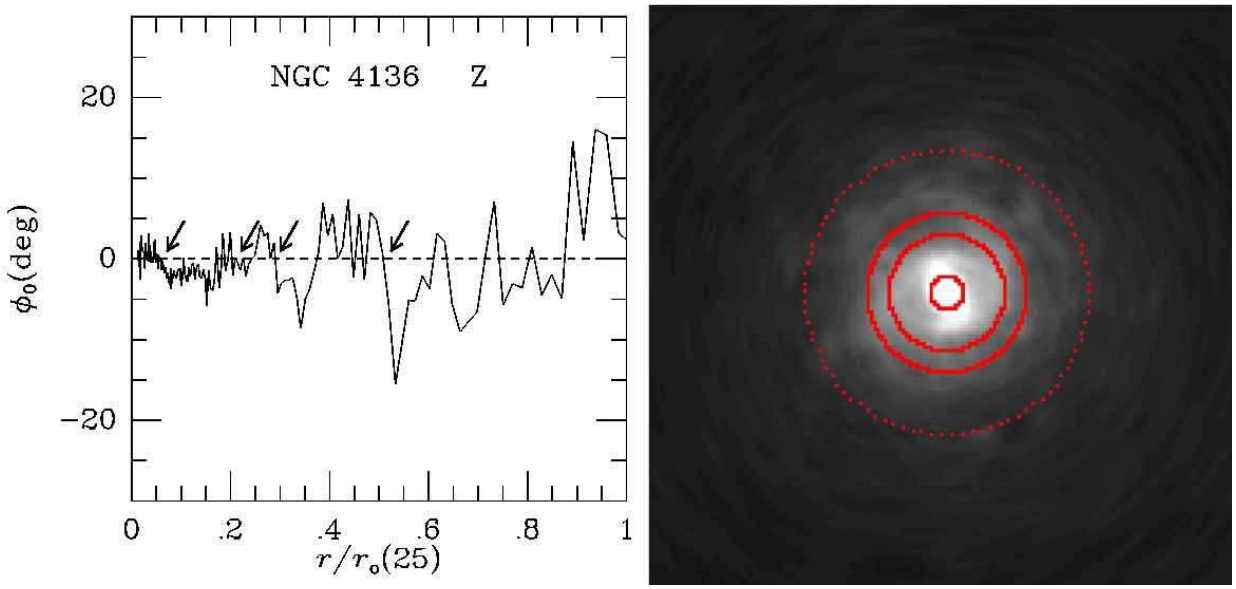

Fig. 2.73.— Same as Figure 2.1 for NGC 4136

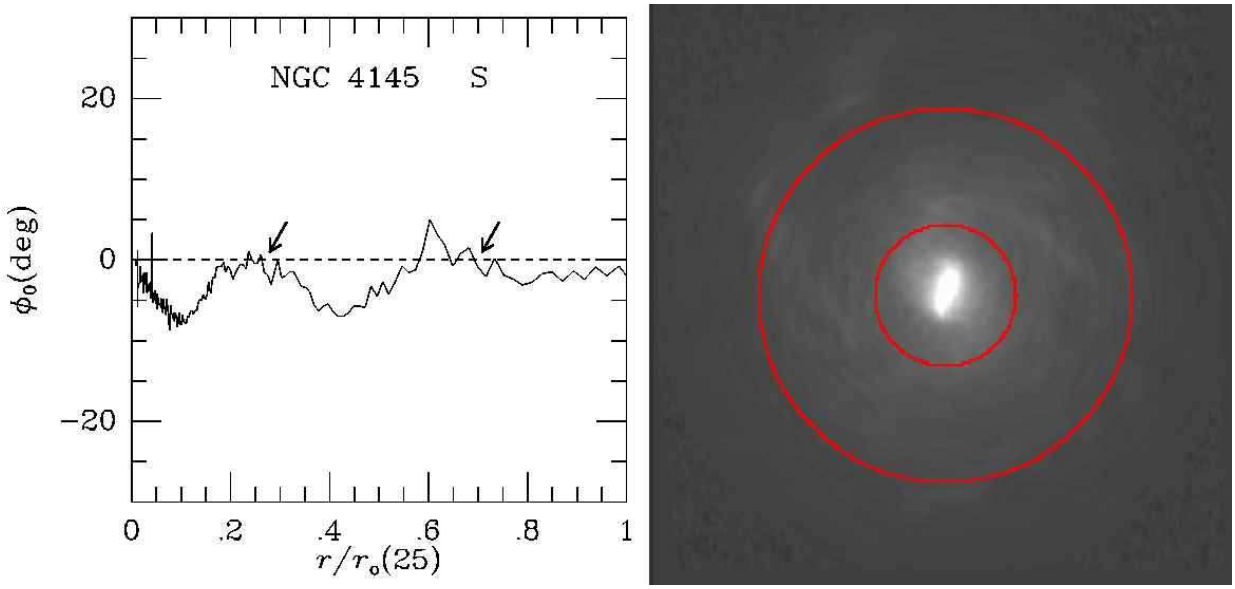

Fig. 2.74.— Same as Figure 2.1 for NGC 4145

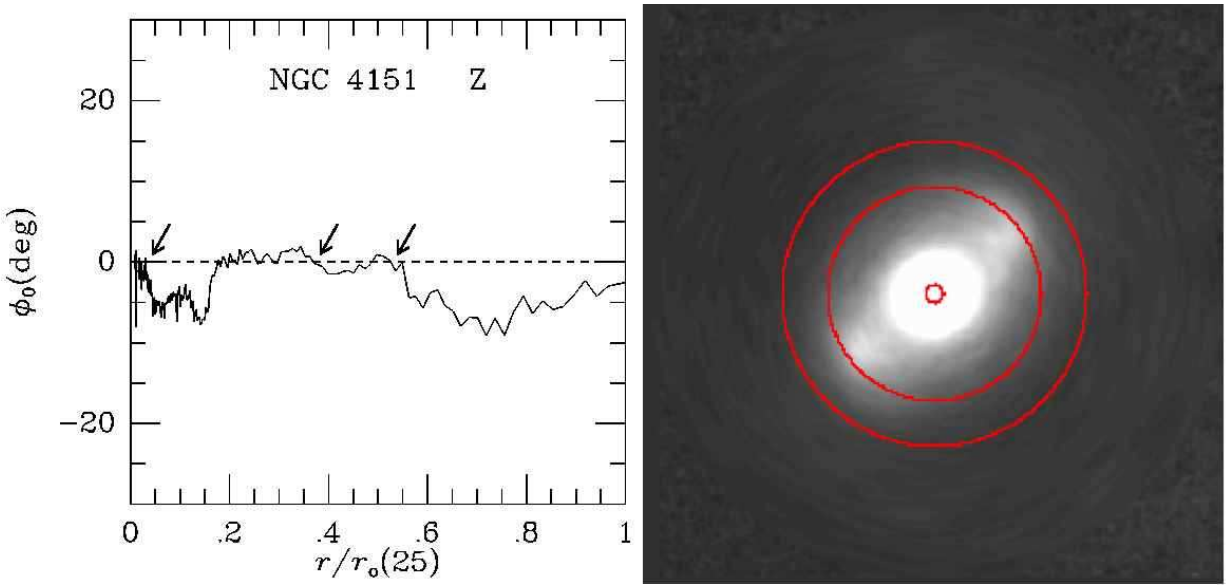

Fig. 2.75.— Same as Figure 2.1 for NGC 4151

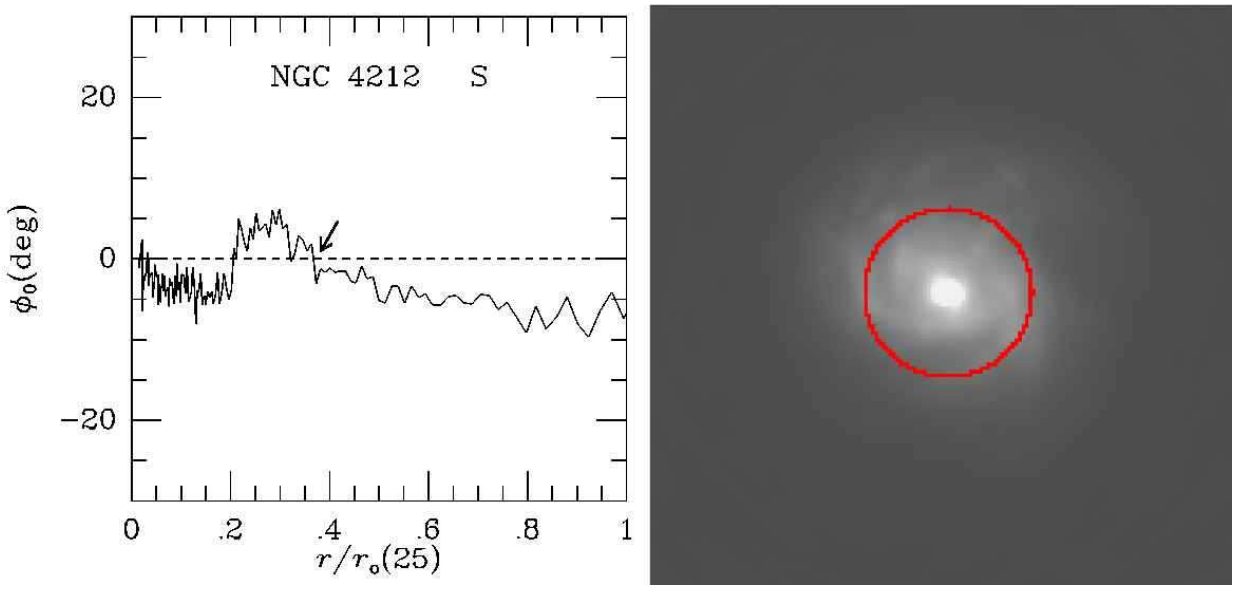

Fig. 2.76.— Same as Figure 2.1 for NGC 4212

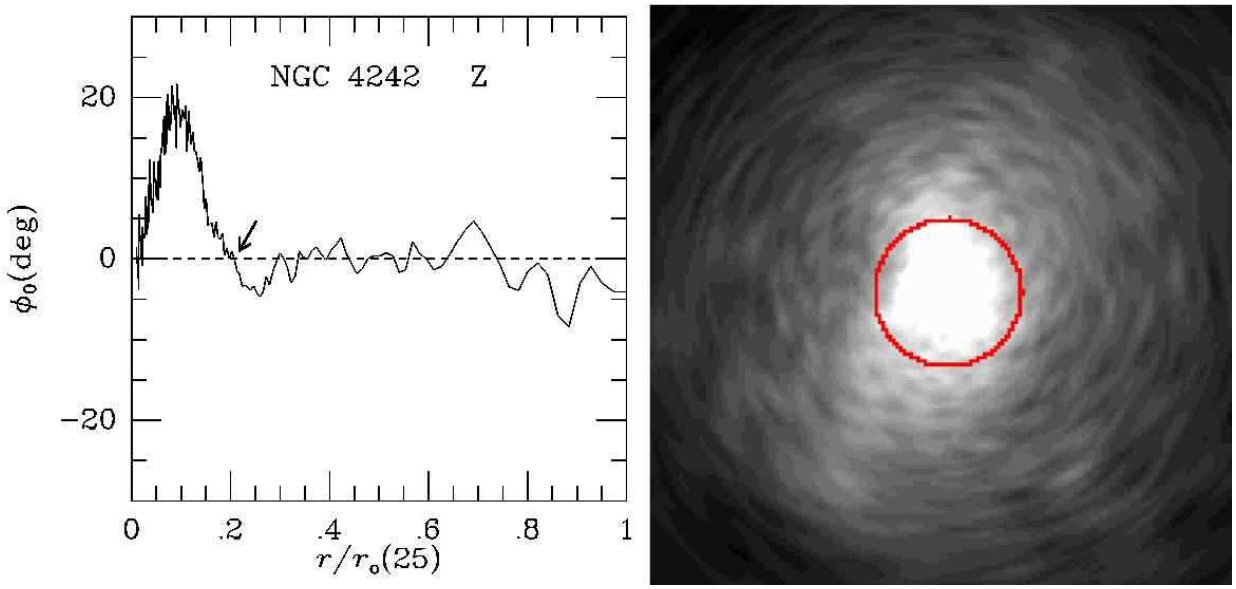

Fig. 2.77.— Same as Figure 2.1 for NGC 4242

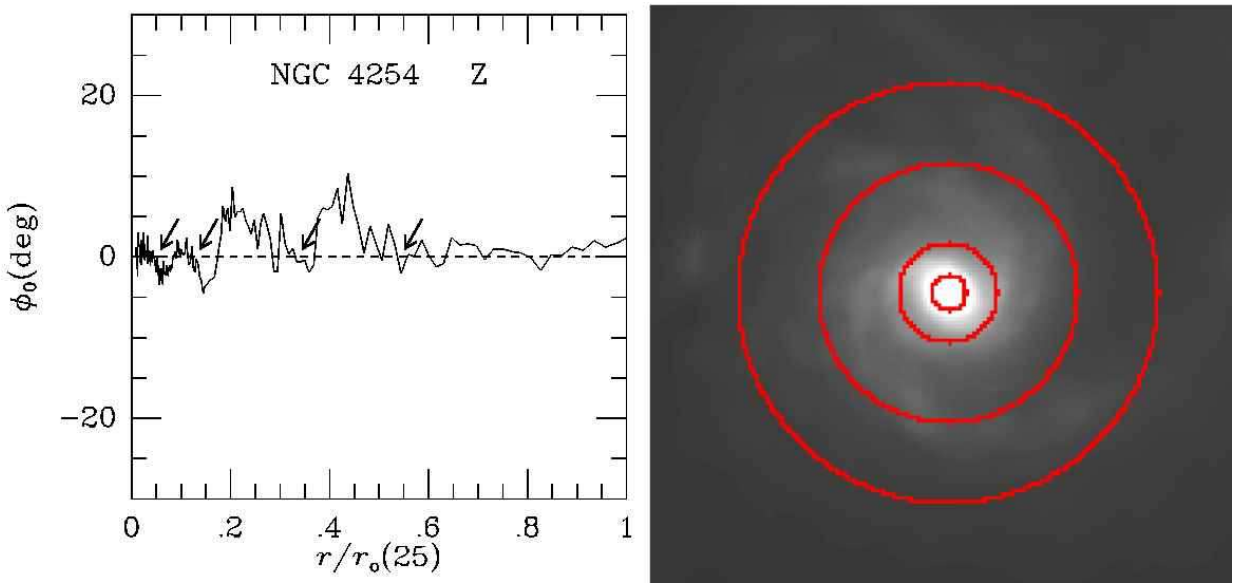

Fig. 2.78.— Same as Figure 2.1 for NGC 4254

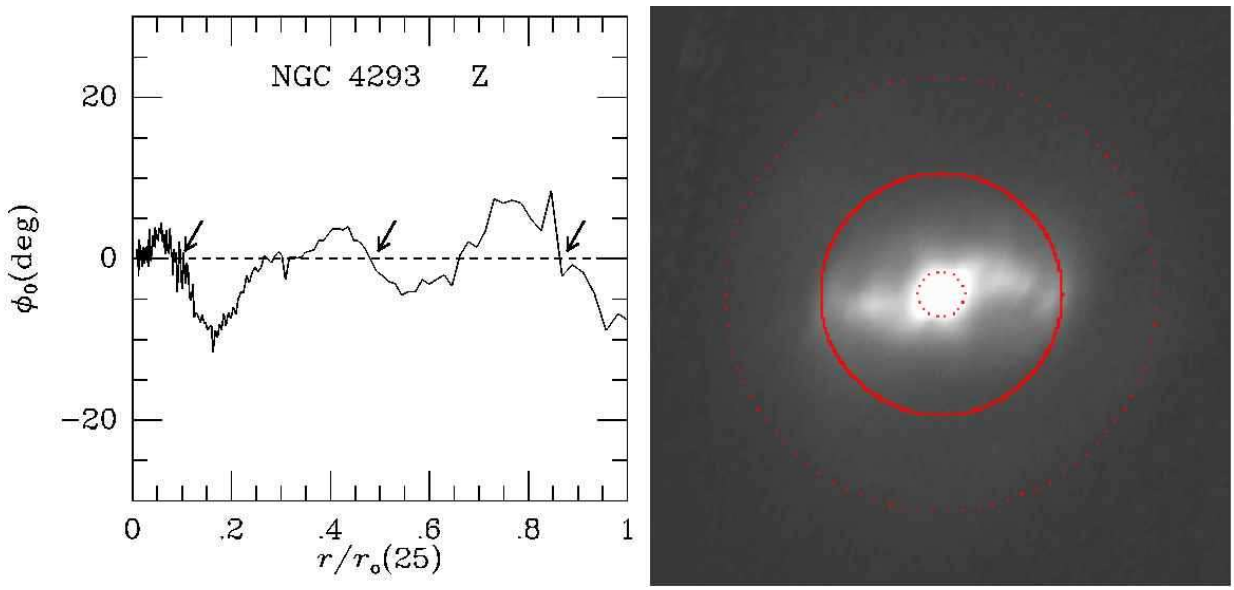

Fig. 2.79.— Same as Figure 2.1 for NGC 4293

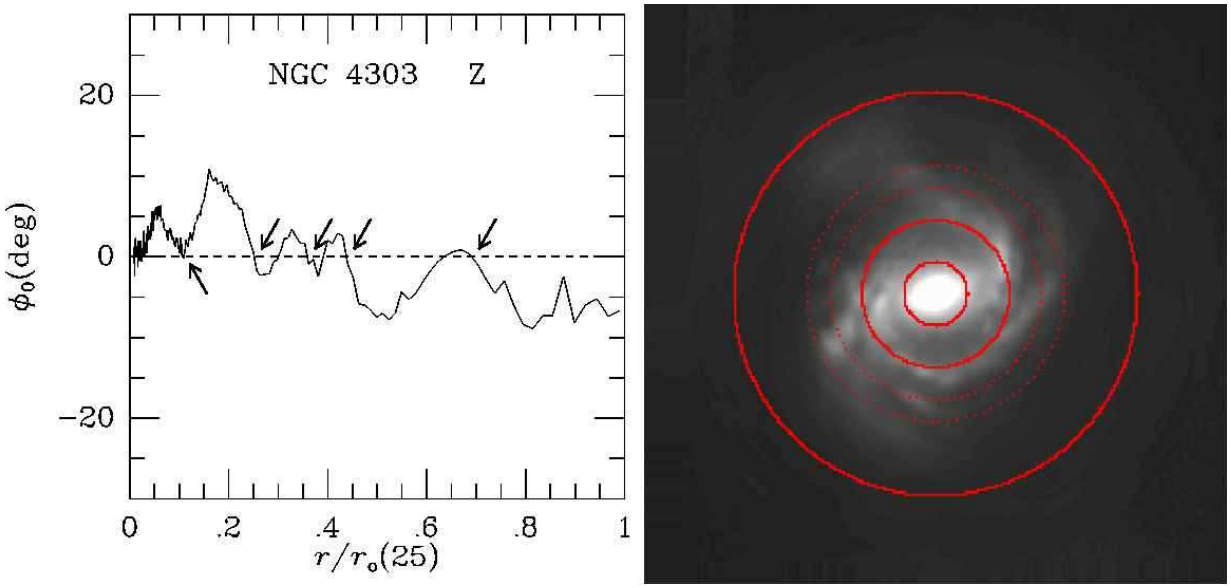

Fig. 2.80.— Same as Figure 2.1 for NGC 4303

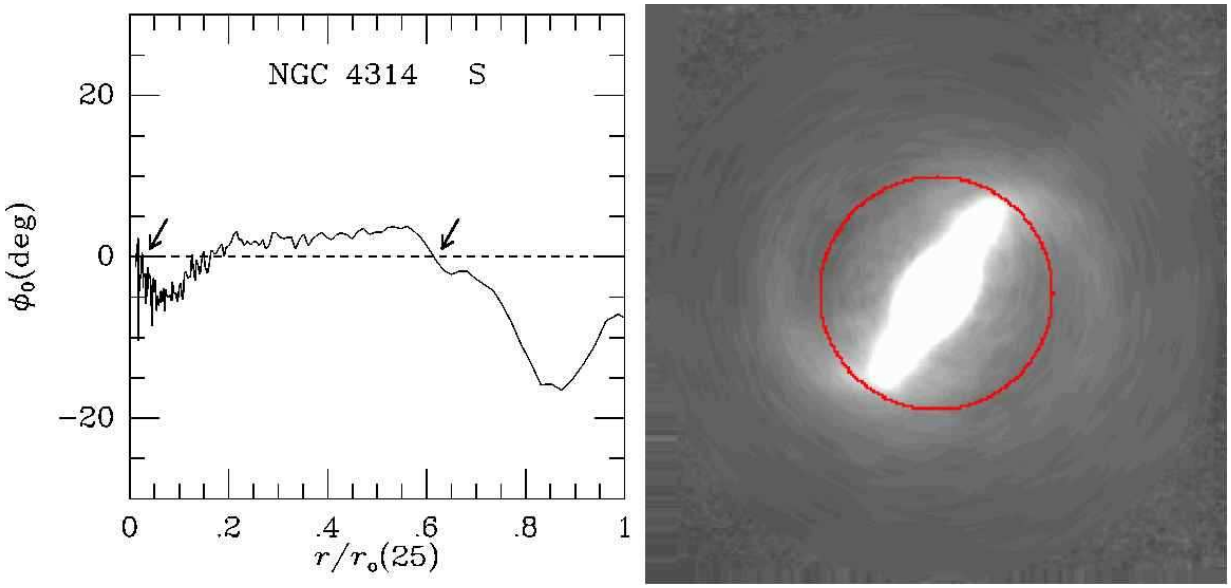

Fig. 2.81.— Same as Figure 2.1 for NGC 4314. Only CR_2 is shown overlaid on the image.

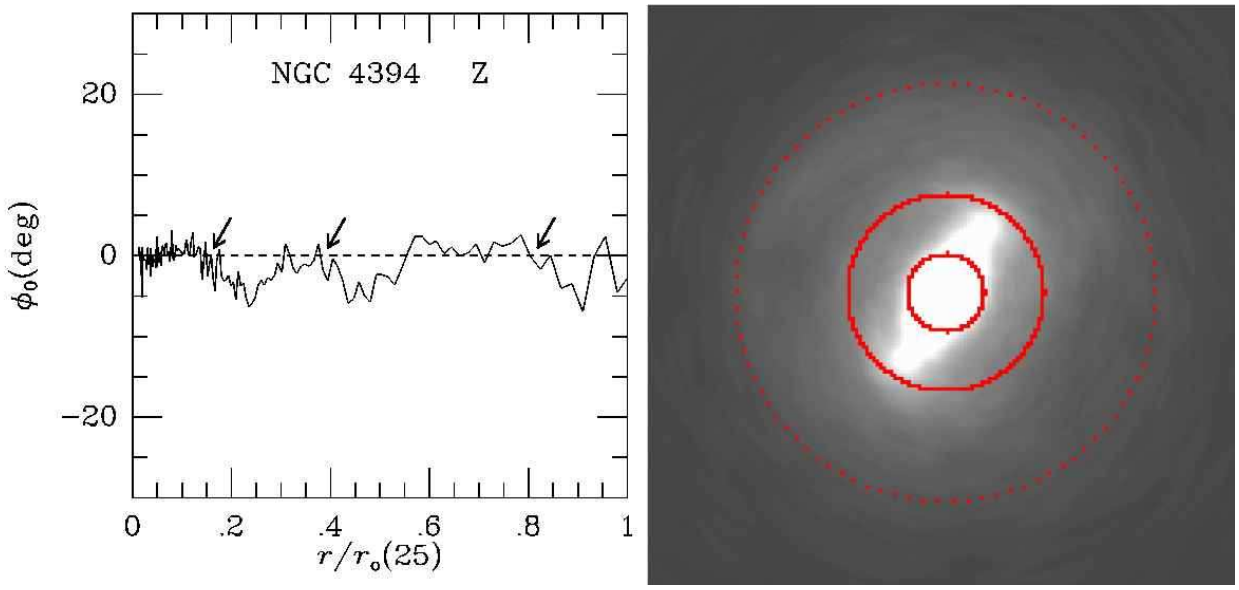

Fig. 2.82.— Same as Figure 2.1 for NGC 4394

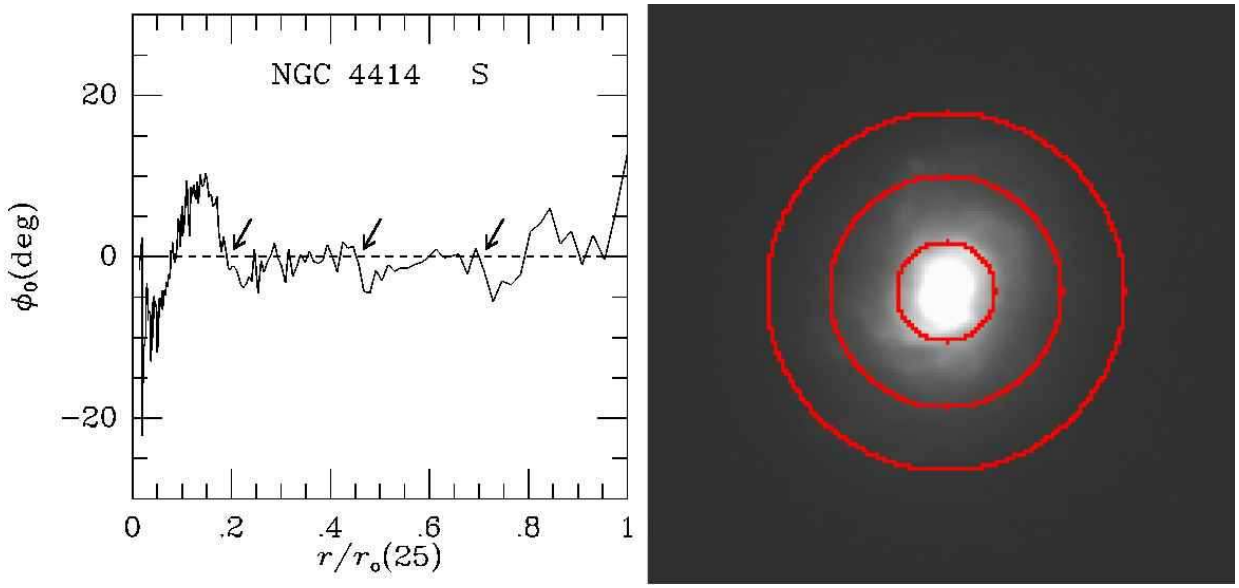

Fig. 2.83.— Same as Figure 2.1 for NGC 4414

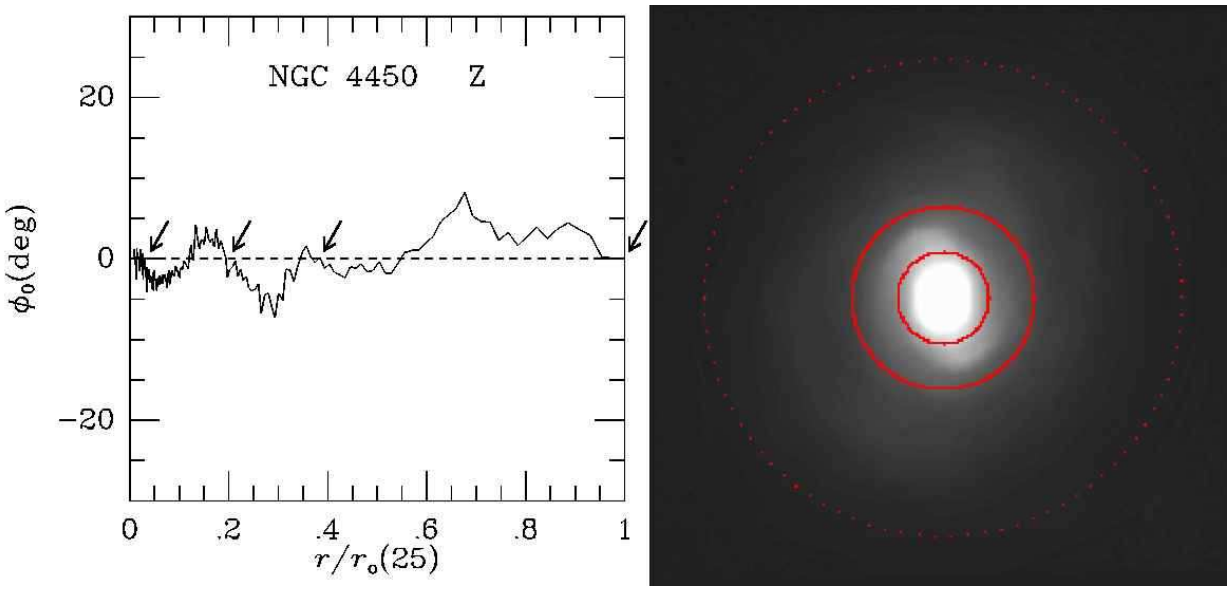

Fig. 2.84.— Same as Figure 2.1 for NGC 4450. Only CR_2, CR_3, and CR_4 in Table 1 are overlaid on the image.

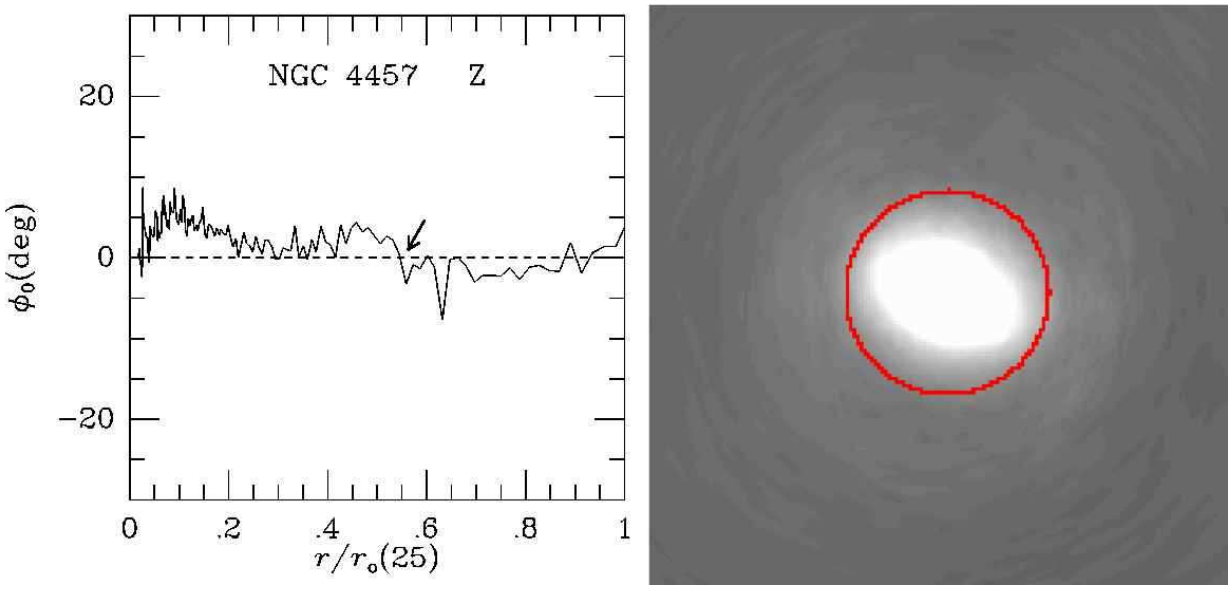

Fig. 2.85.— Same as Figure 2.1 for NGC 4457

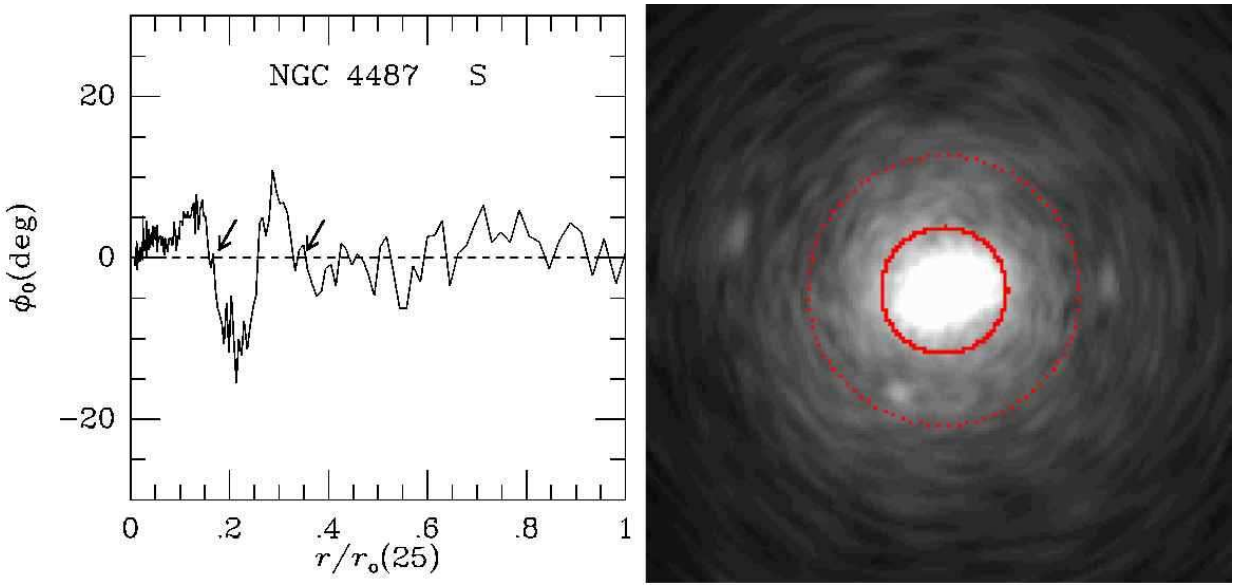

Fig. 2.86.— Same as Figure 2.1 for NGC 4487

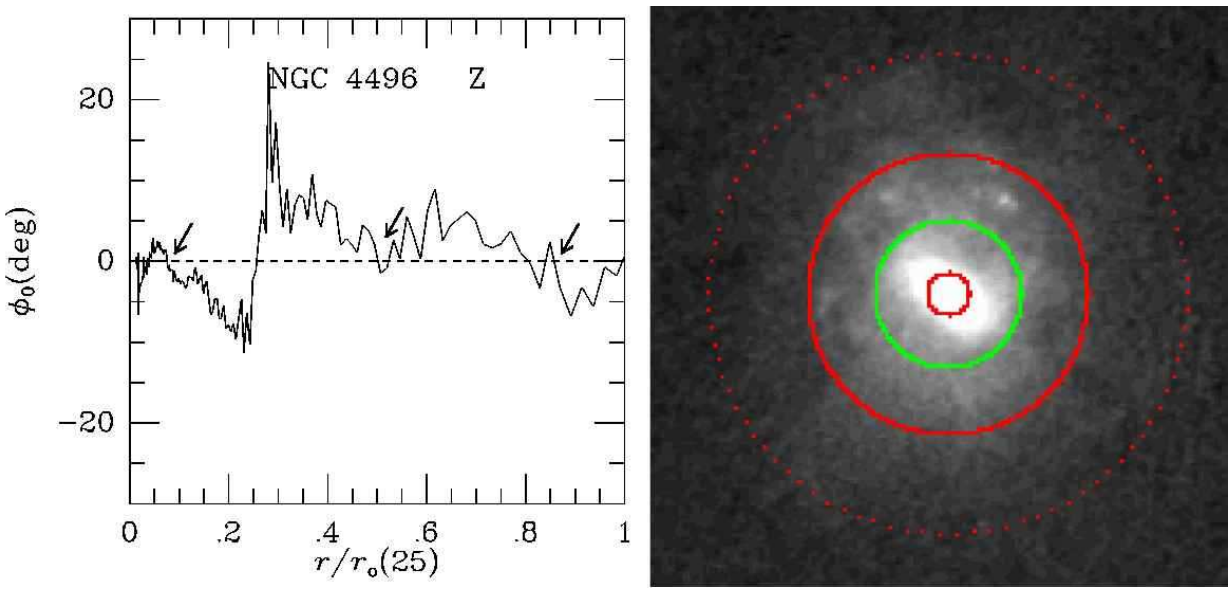

Fig. 2.87.— Same as Figure 2.1 for NGC 4496. The green circle indicates the major N/P crossing at $r/r_o(25)\approx 0.25$.

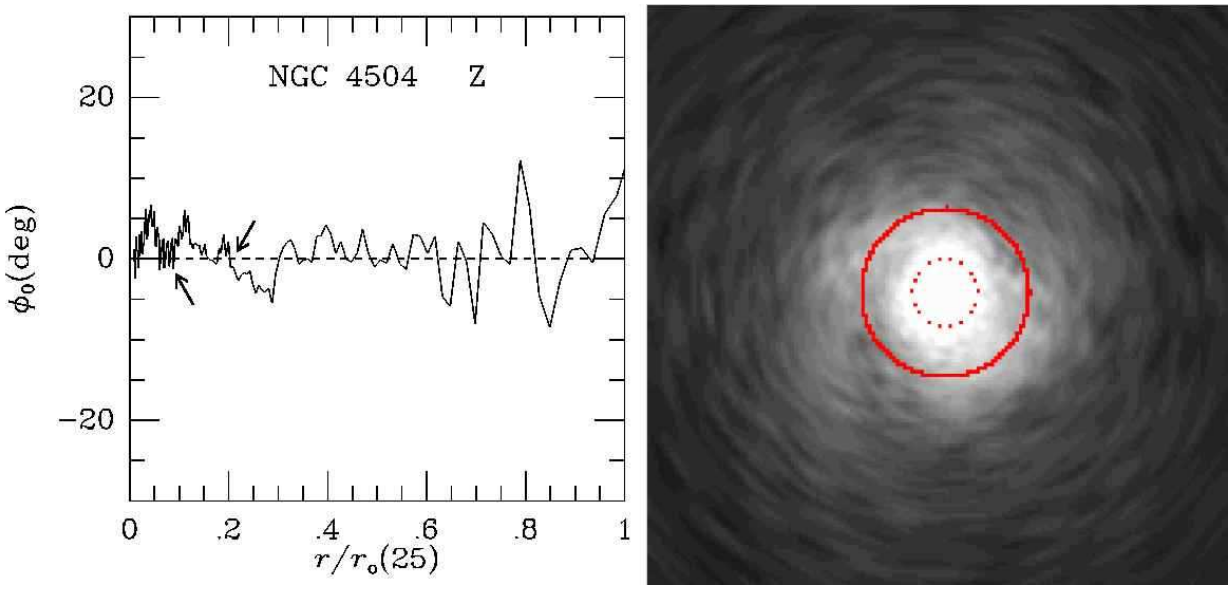

Fig. 2.88.— Same as Figure 2.1 for NGC 4504

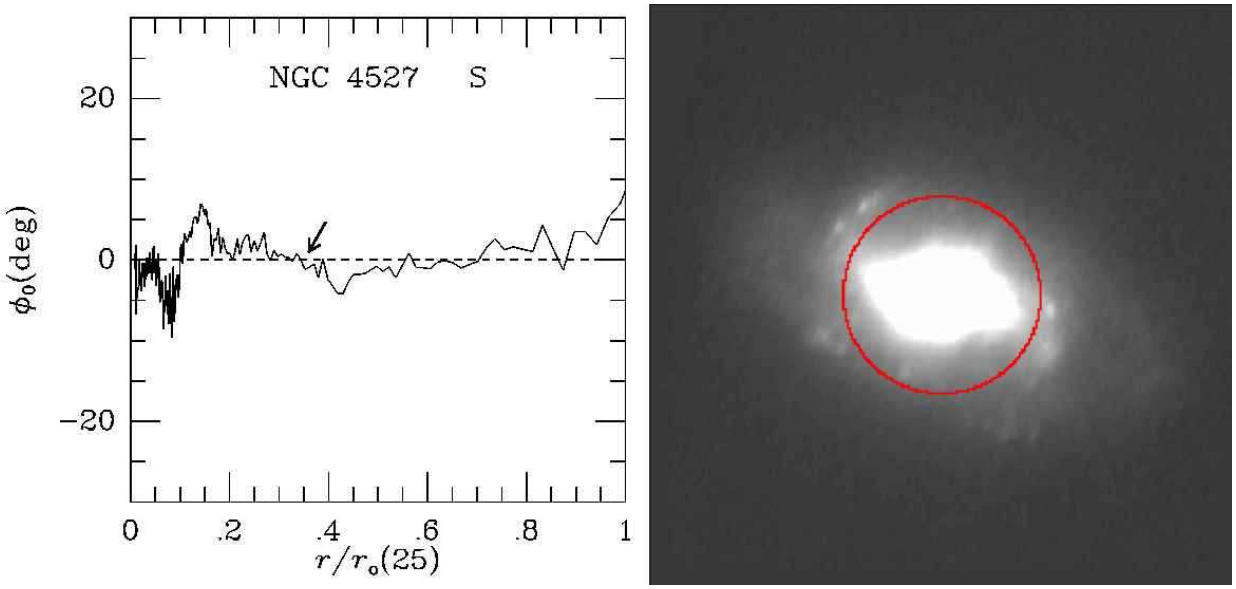

Fig. 2.89.— Same as Figure 2.1 for NGC 4527

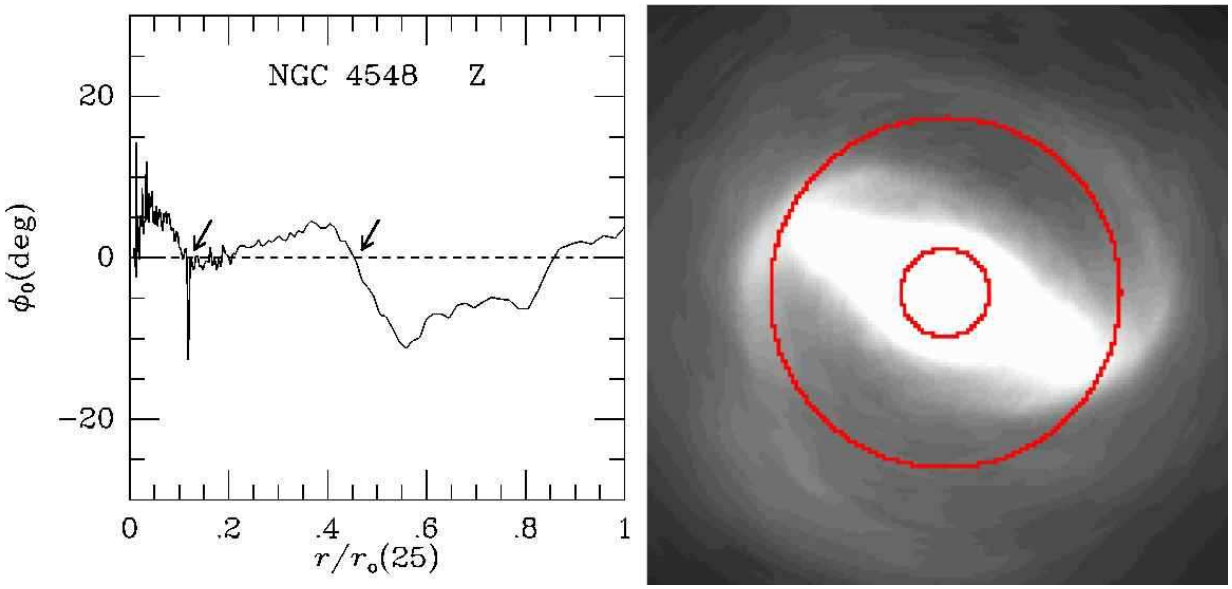

Fig. 2.90.— Same as Figure 2.1 for NGC 4548

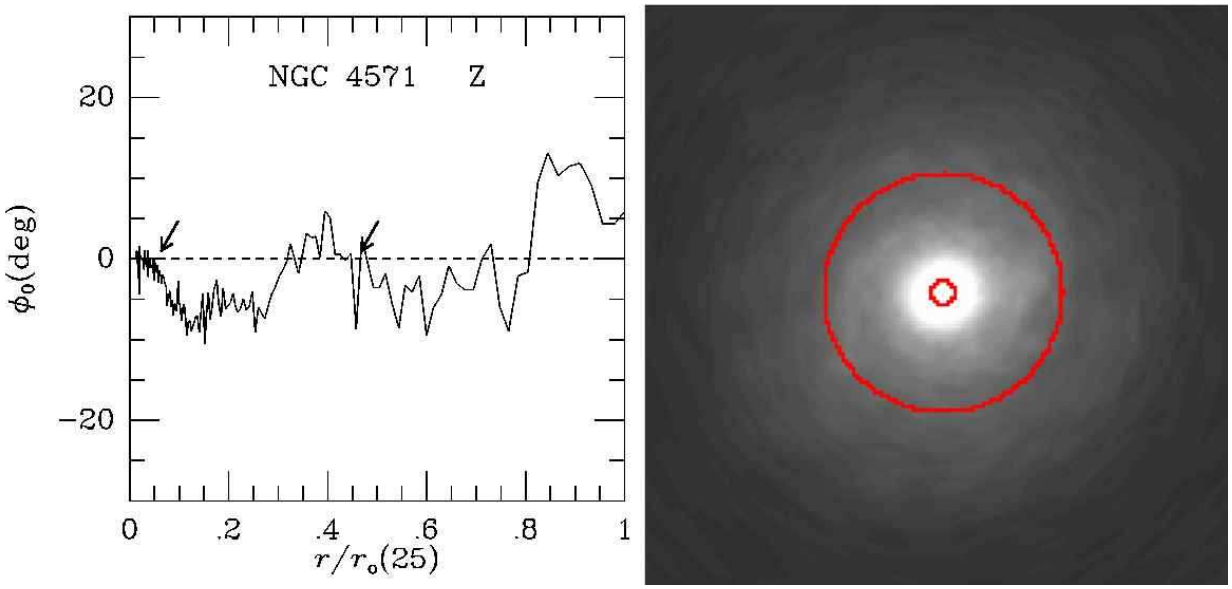

Fig. 2.91.— Same as Figure 2.1 for NGC 4571

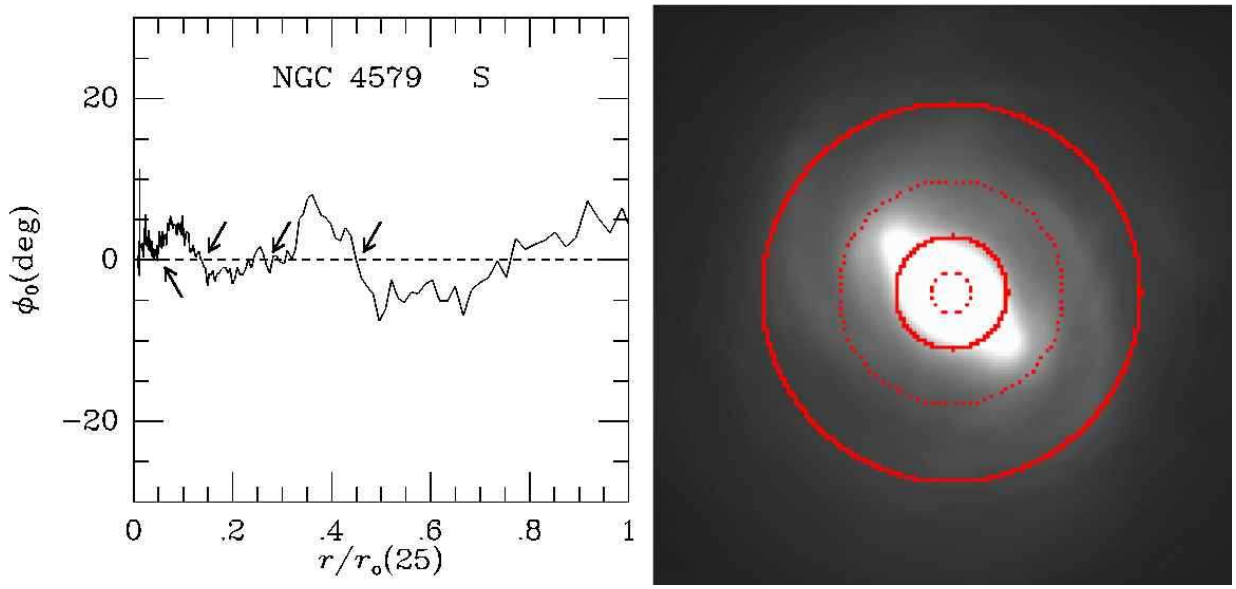

Fig. 2.92.— Same as Figure 2.1 for NGC 4579

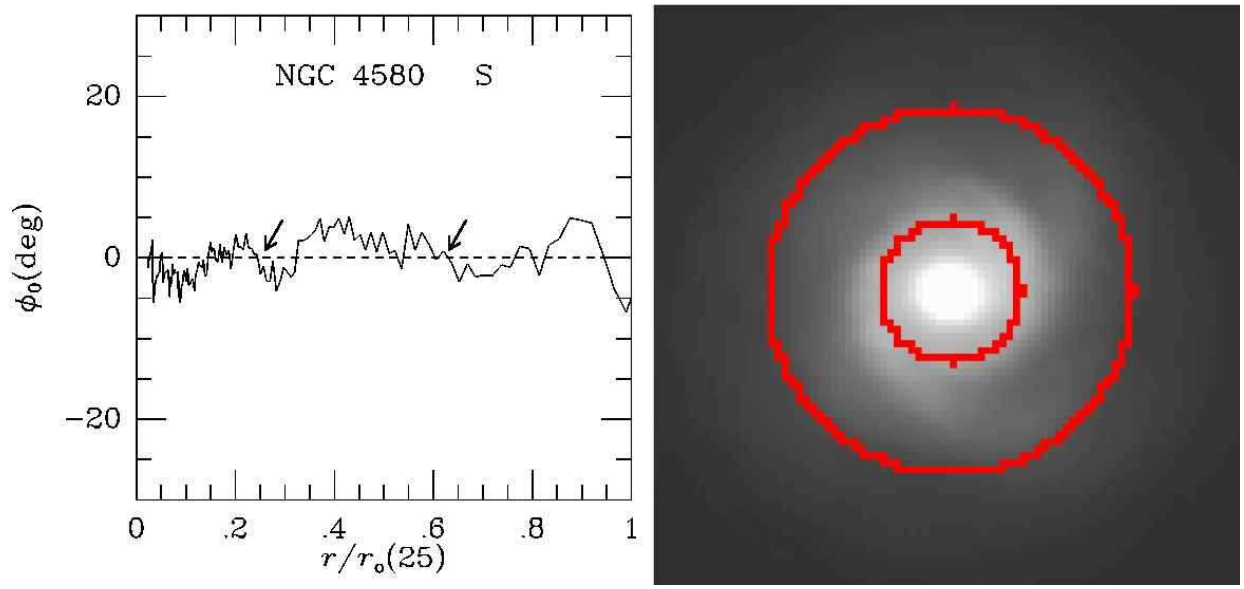

Fig. 2.93.— Same as Figure 2.1 for NGC 4580

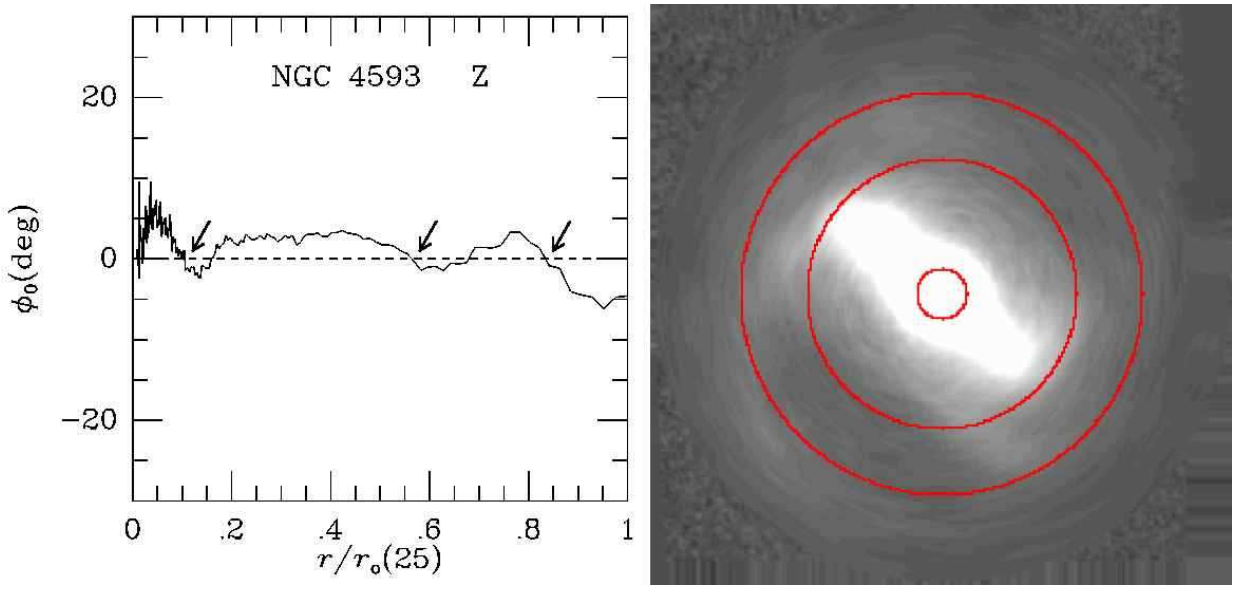

Fig. 2.94.— Same as Figure 2.1 for NGC 4593

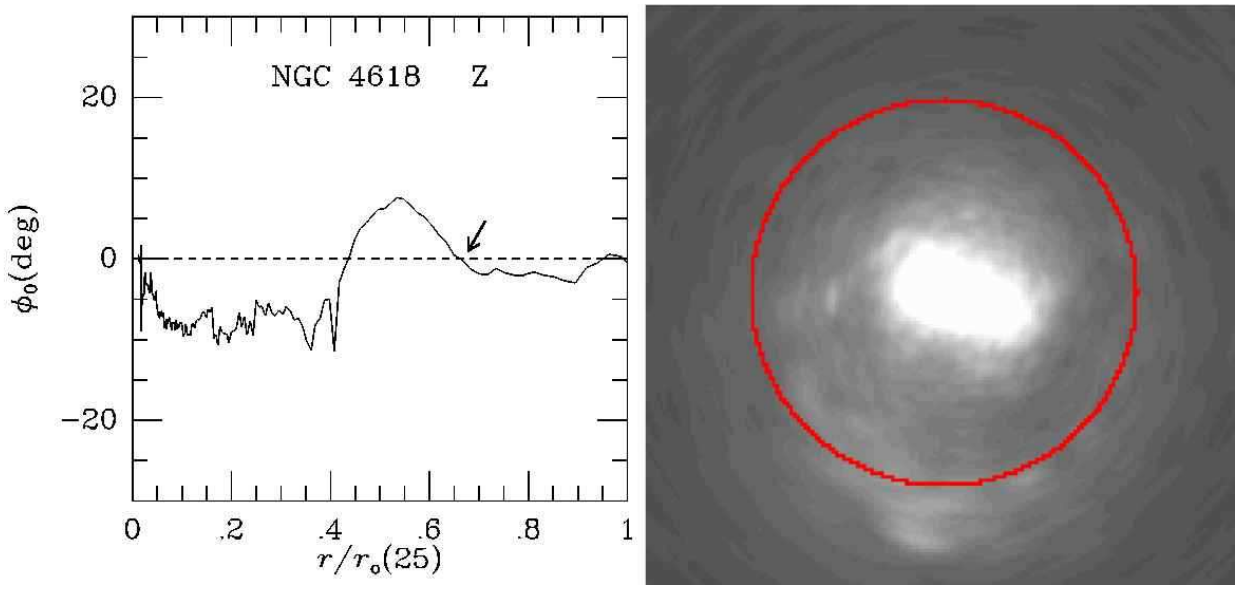

Fig. 2.95.— Same as Figure 2.1 for NGC 4618

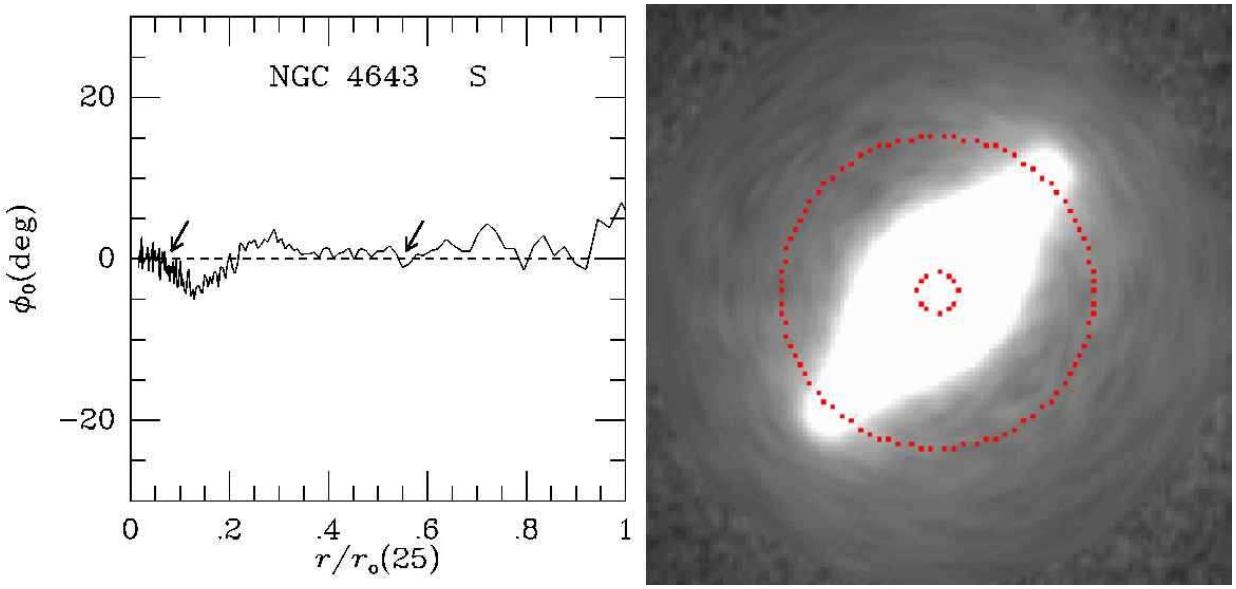

Fig. 2.96.— Same as Figure 2.1 for NGC 4643

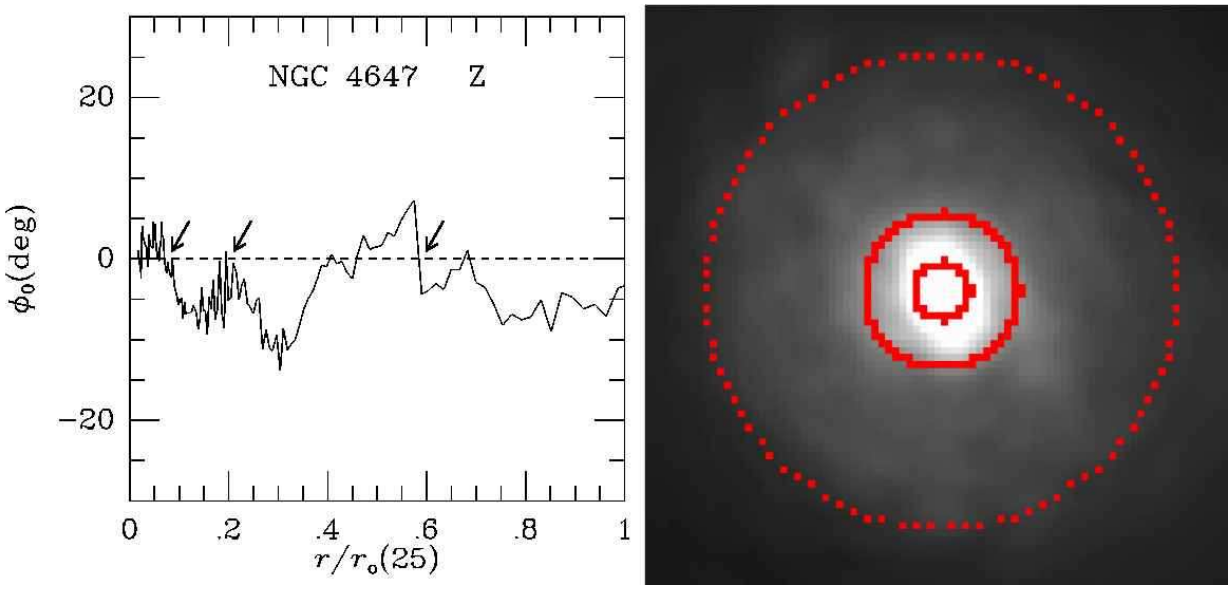

Fig. 2.97.— Same as Figure 2.1 for NGC 4647

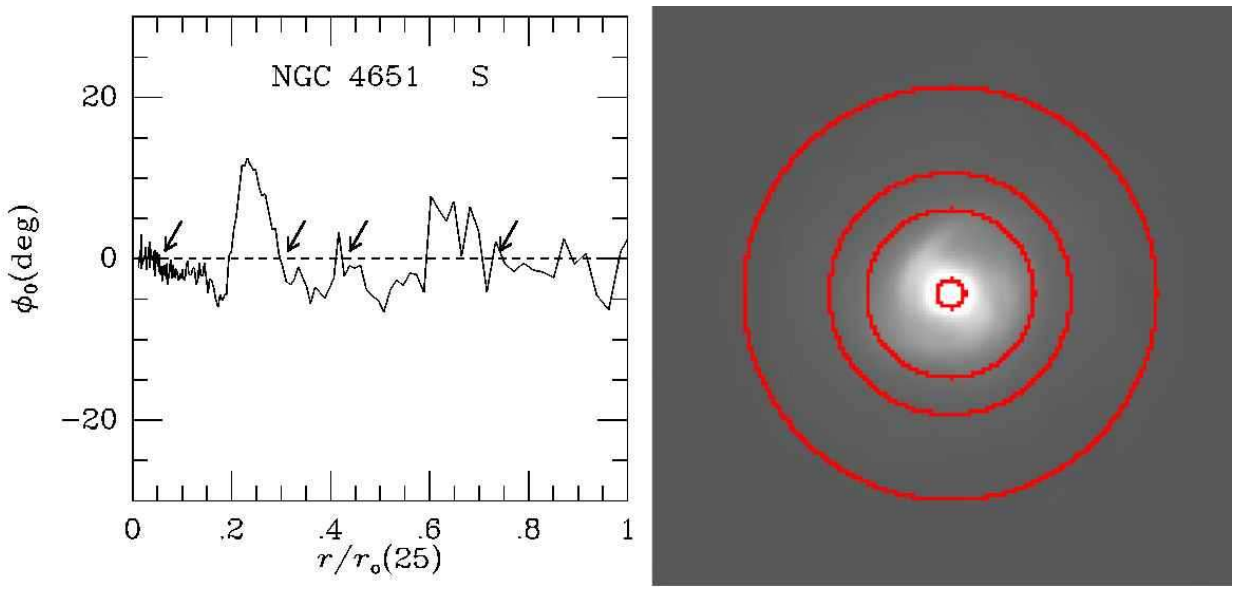

Fig. 2.98.— Same as Figure 2.1 for NGC 4651

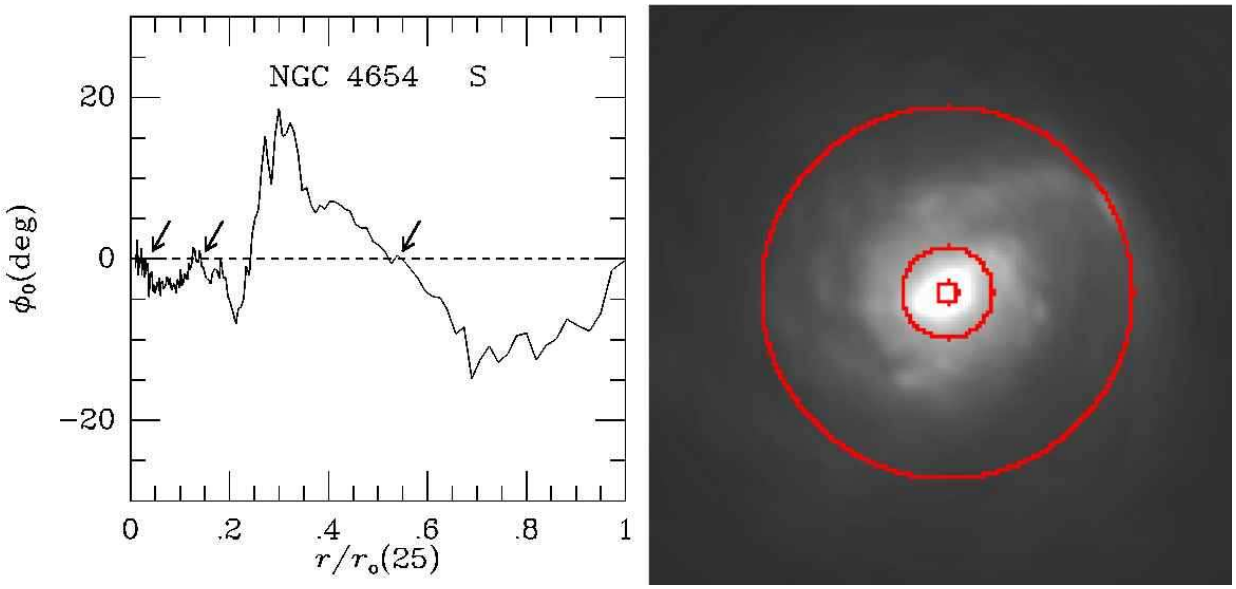

Fig. 2.99.— Same as Figure 2.1 for NGC 4654

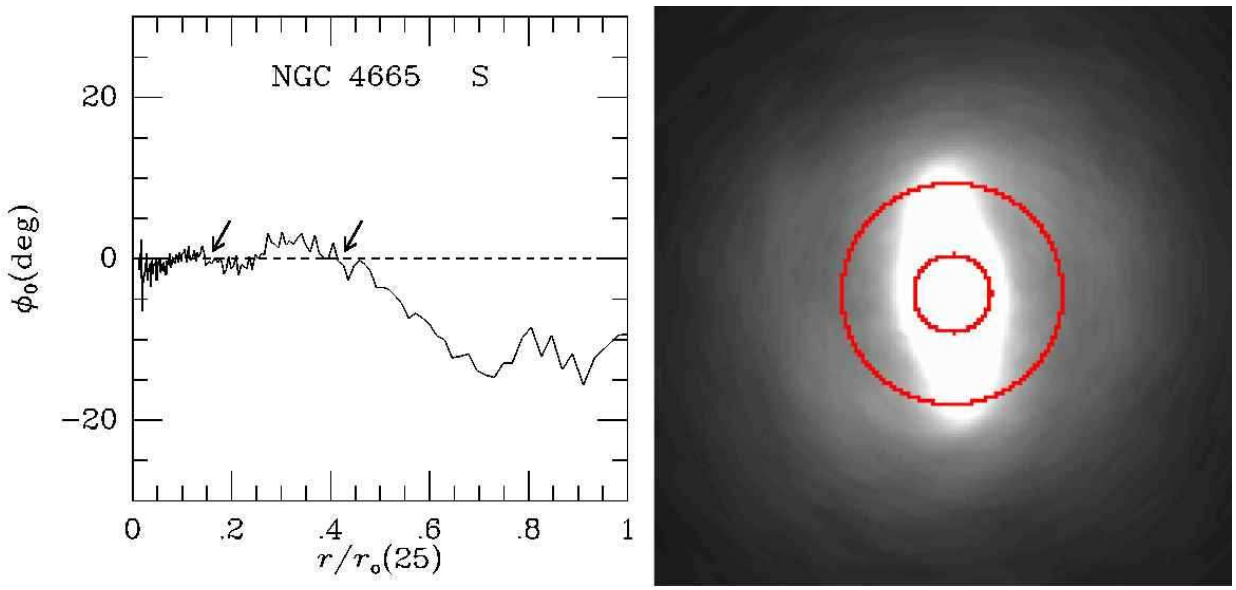

Fig. 2.100.— Same as Figure 2.1 for NGC 4665

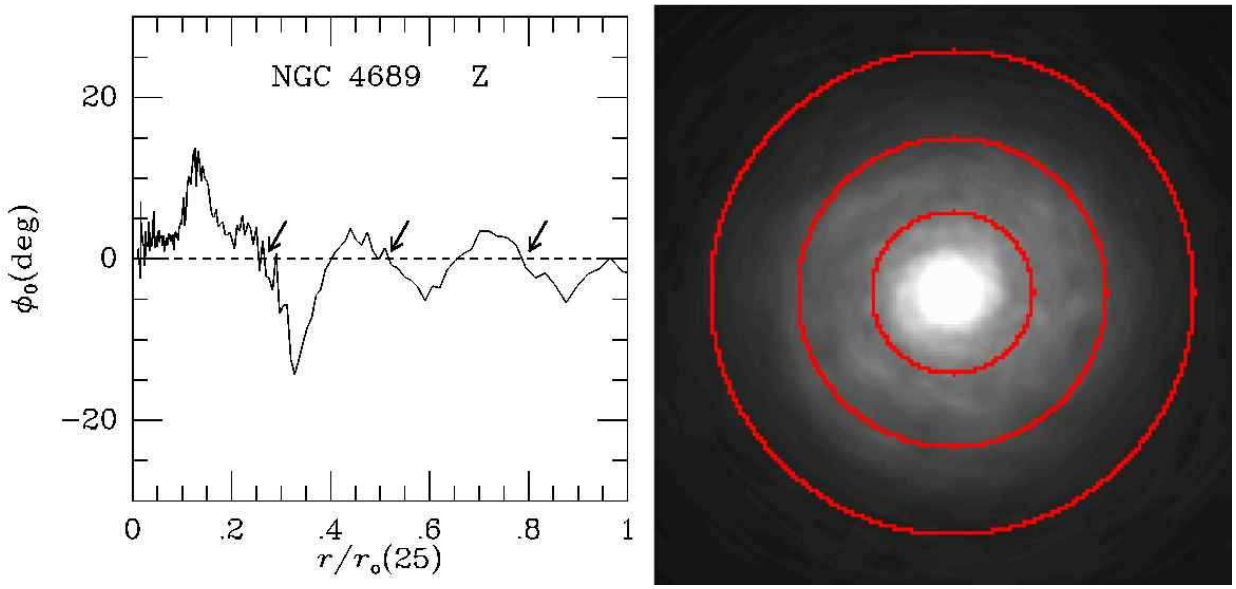

Fig. 2.101.— Same as Figure 2.1 for NGC 4689

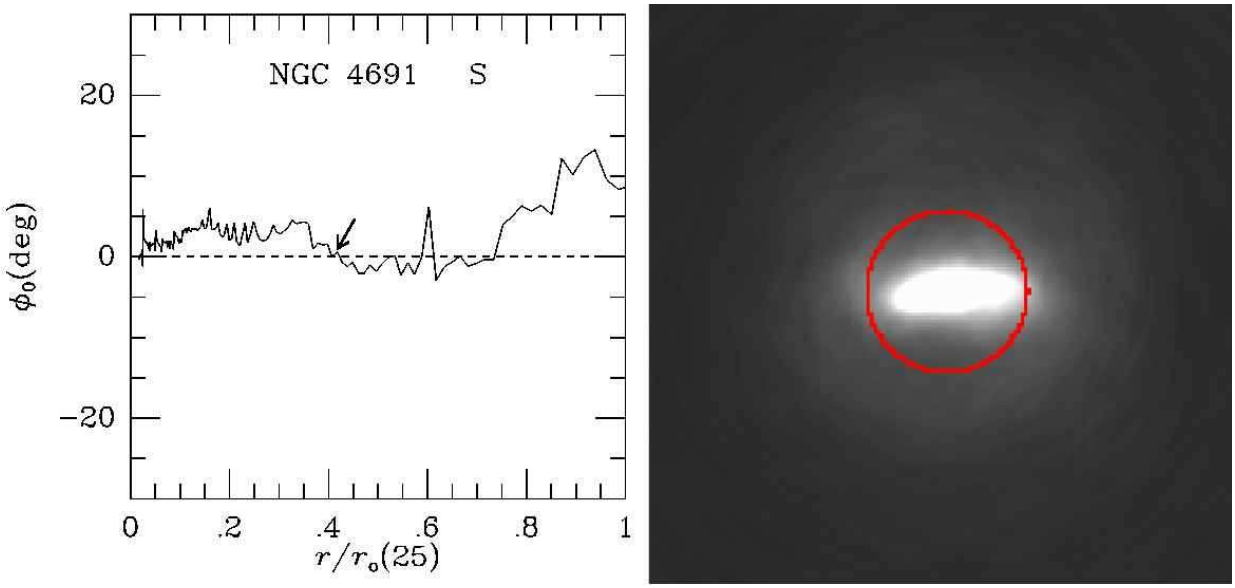

Fig. 2.102.— Same as Figure 2.1 for NGC 4691

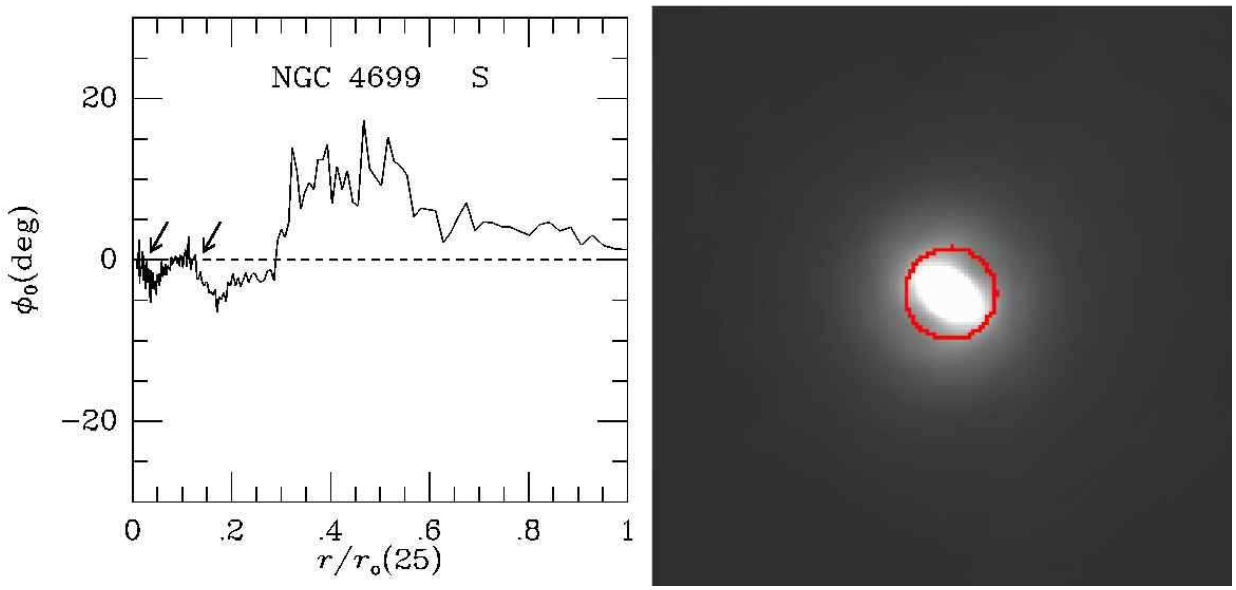

Fig. 2.103.— Same as Figure 2.1 for NGC 4699. Only CR_2 from Table 1 is overlaid on the image.

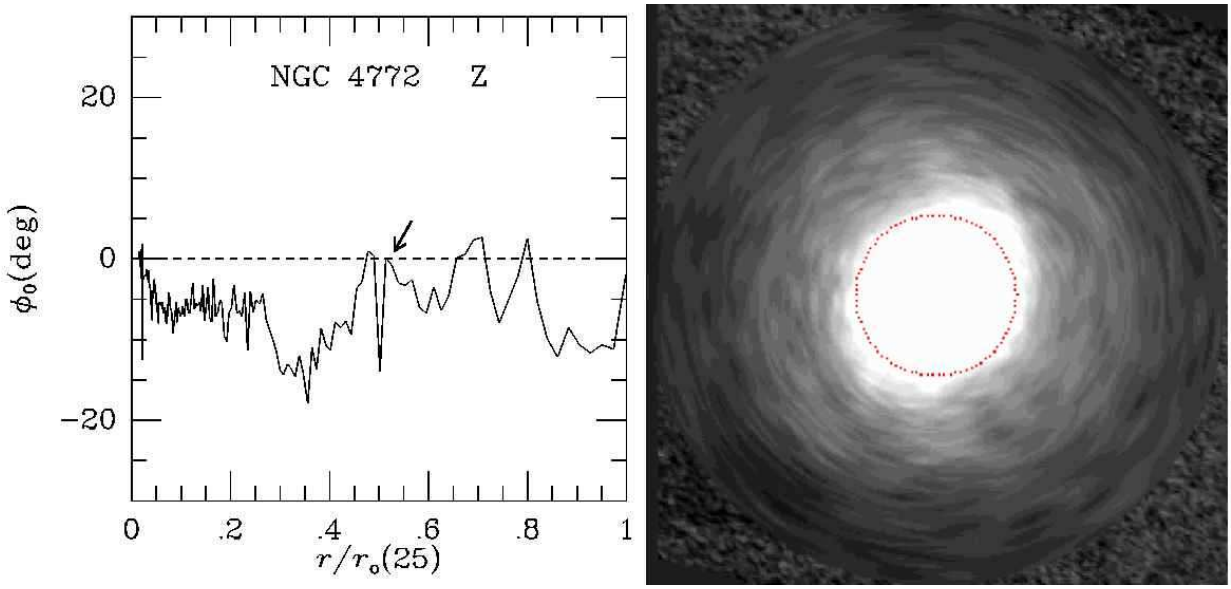

Fig. 2.104.— Same as Figure 2.1 for NGC 4772

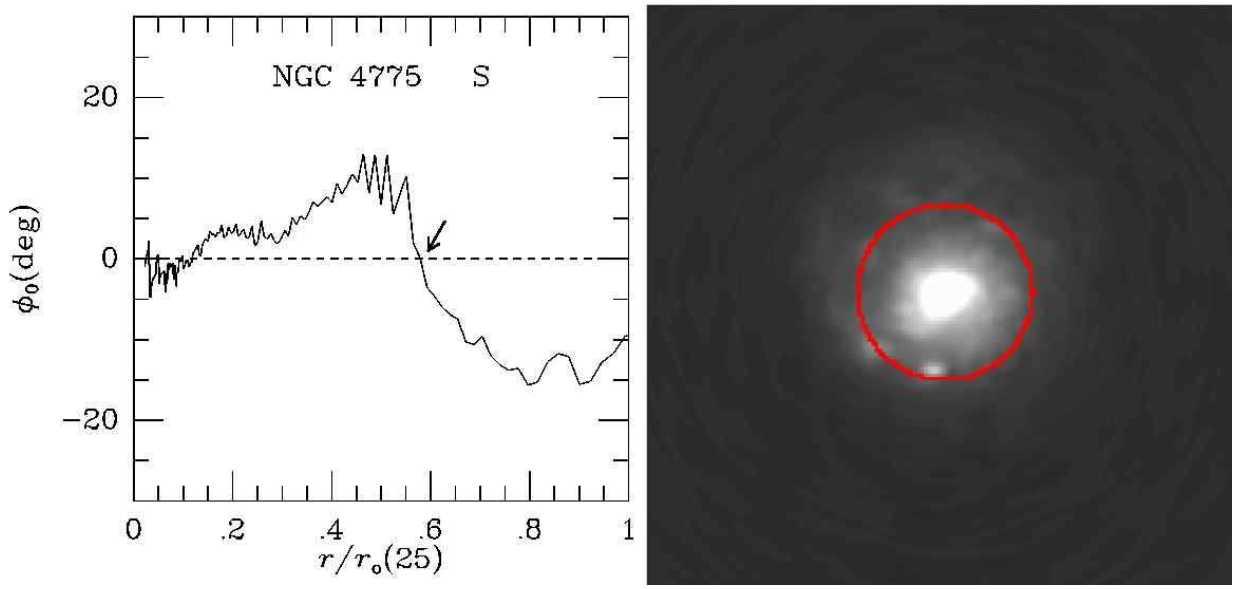

Fig. 2.105.— Same as Figure 2.1 for NGC 4775

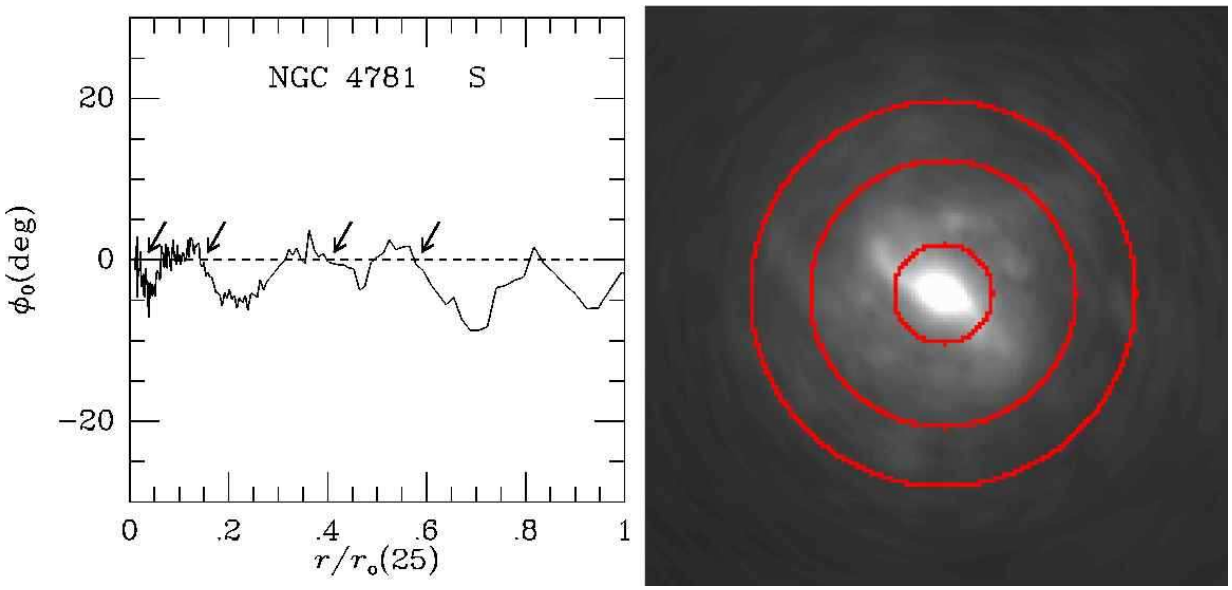

Fig. 2.106.— Same as Figure 2.1 for NGC 4781. Only CR_2, CR_3, and CR_4 in Table 1 are overlaid on the image.

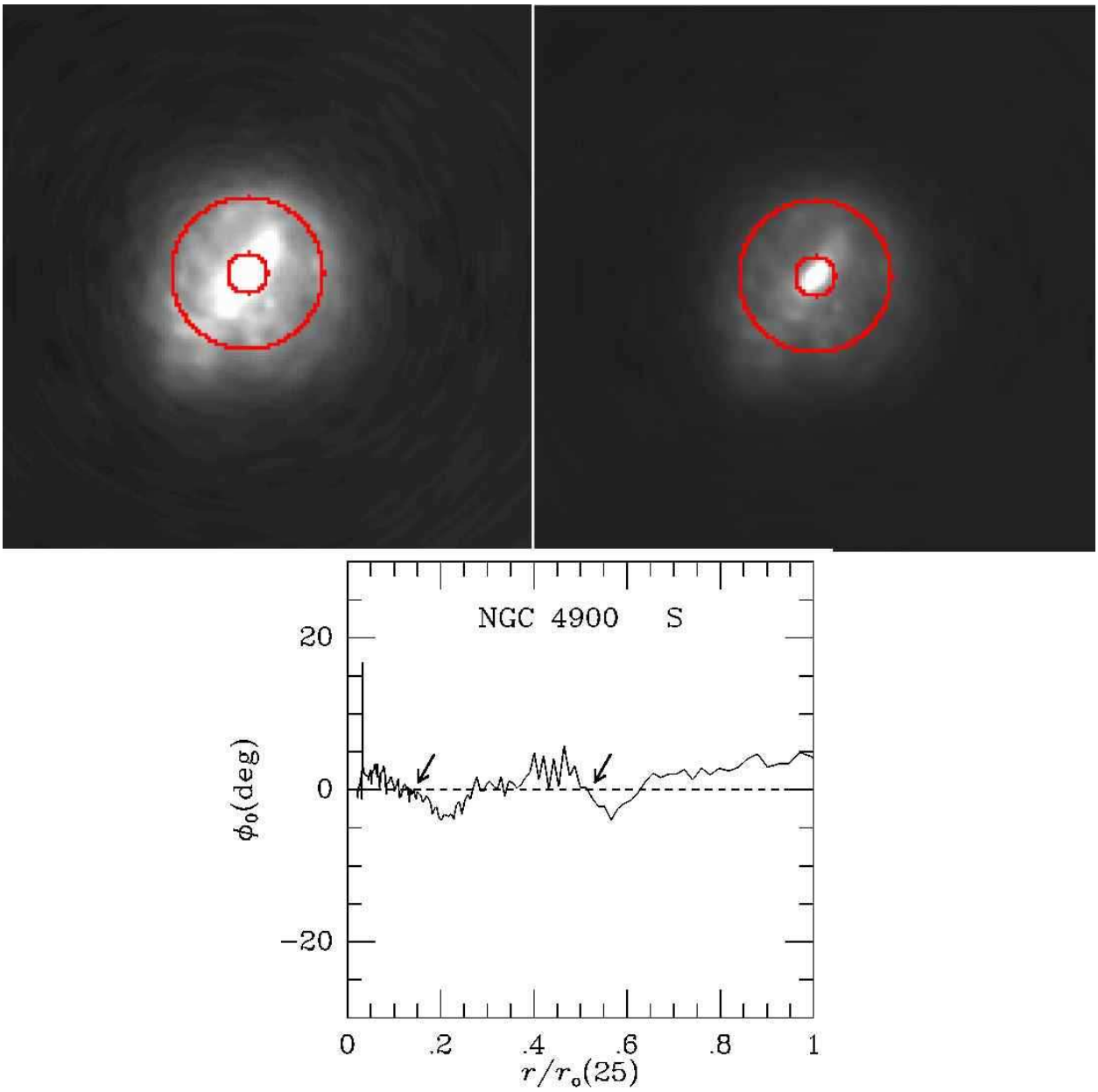

Fig. 2.107.— Same as Figure 2.1 for NGC 4900

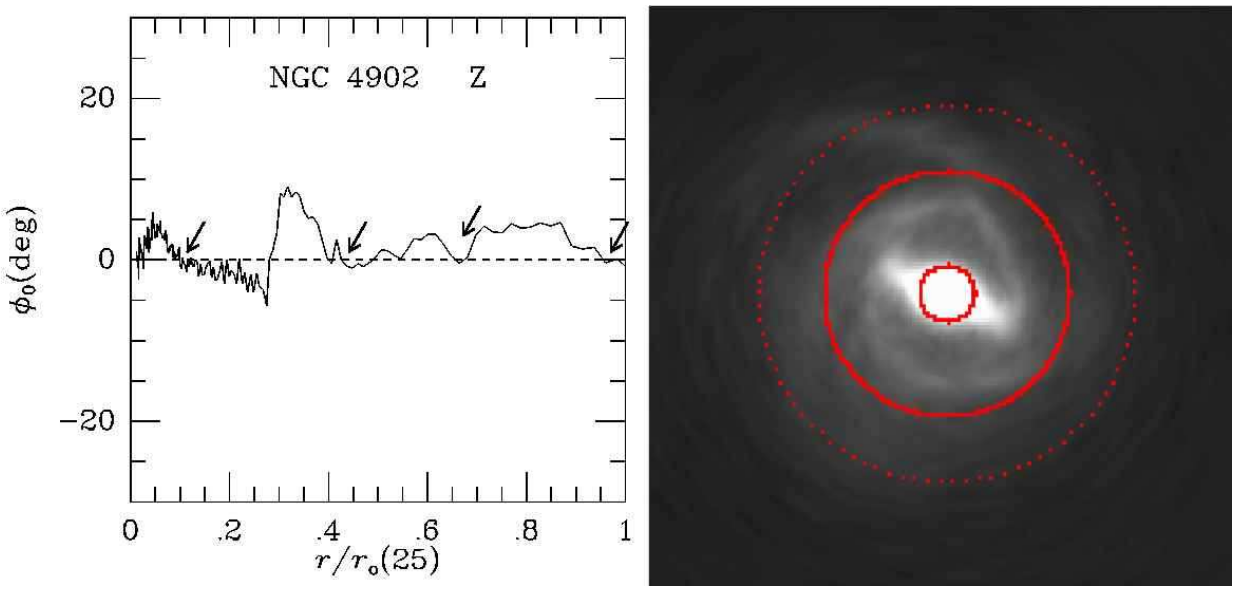

Fig. 2.108.— Same as Figure 2.1 for NGC 4902. CR_4 from Table 1 is not overlaid on the image.

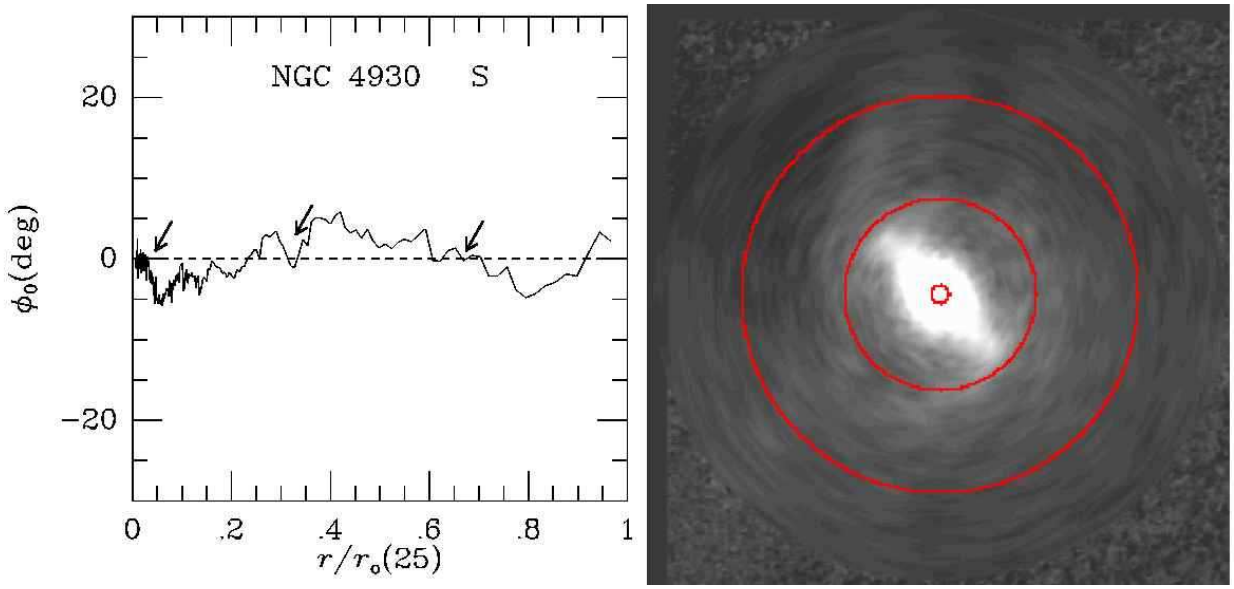

Fig. 2.109.— Same as Figure 2.1 for NGC 4930

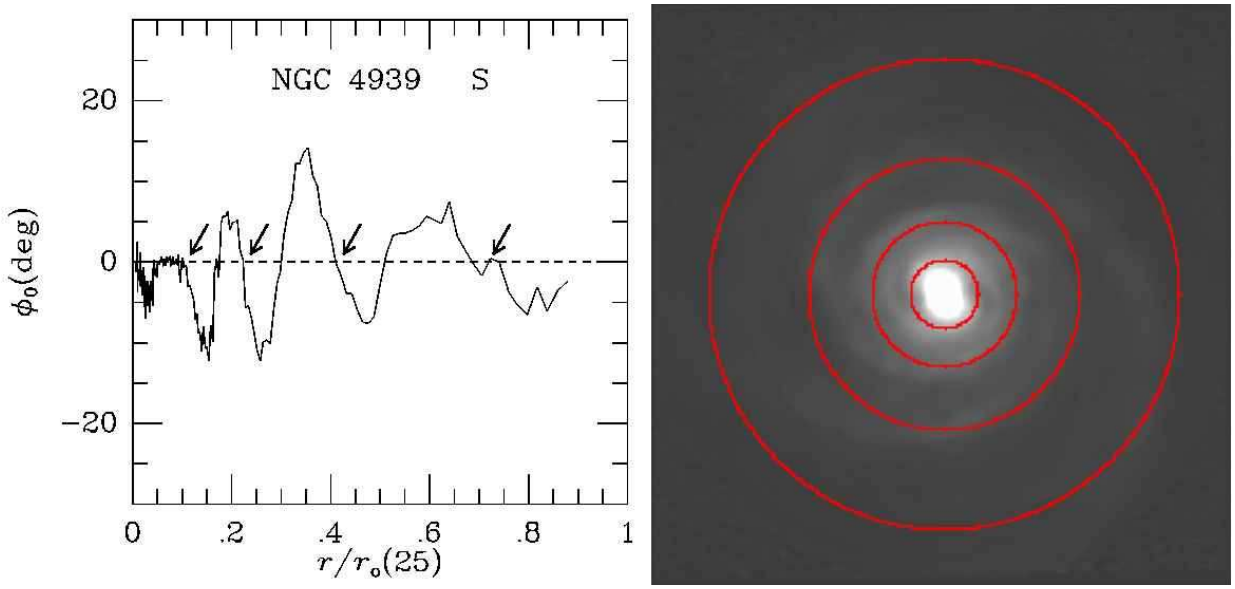

Fig. 2.110.— Same as Figure 2.1 for NGC 4939

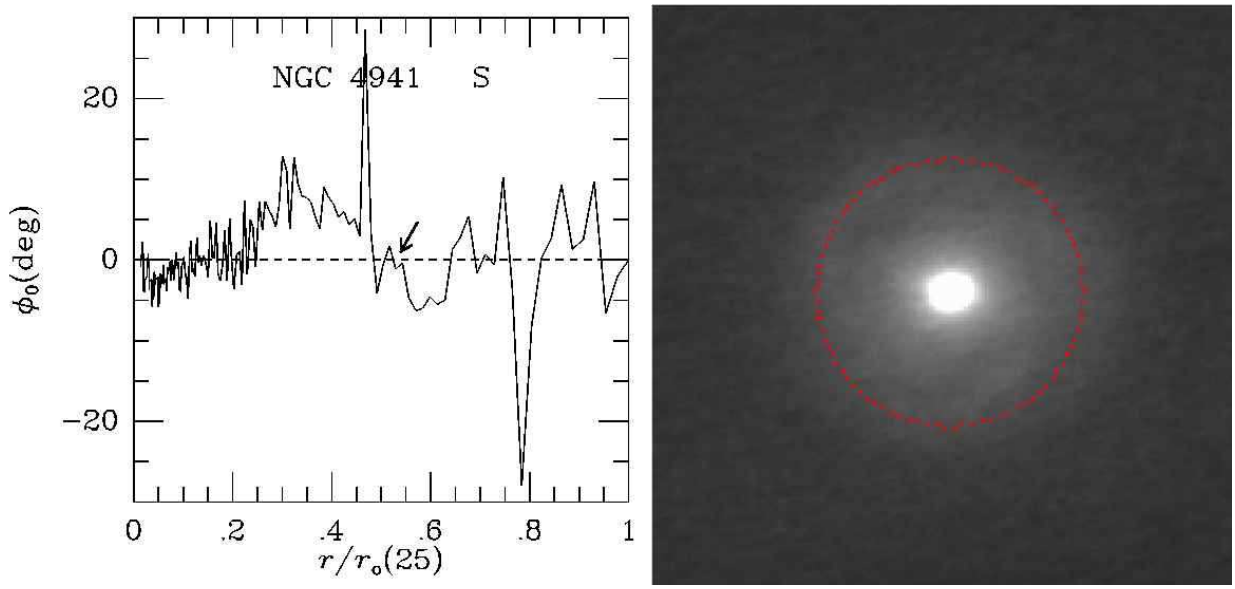

Fig. 2.111.— Same as Figure 2.1 for NGC 4941

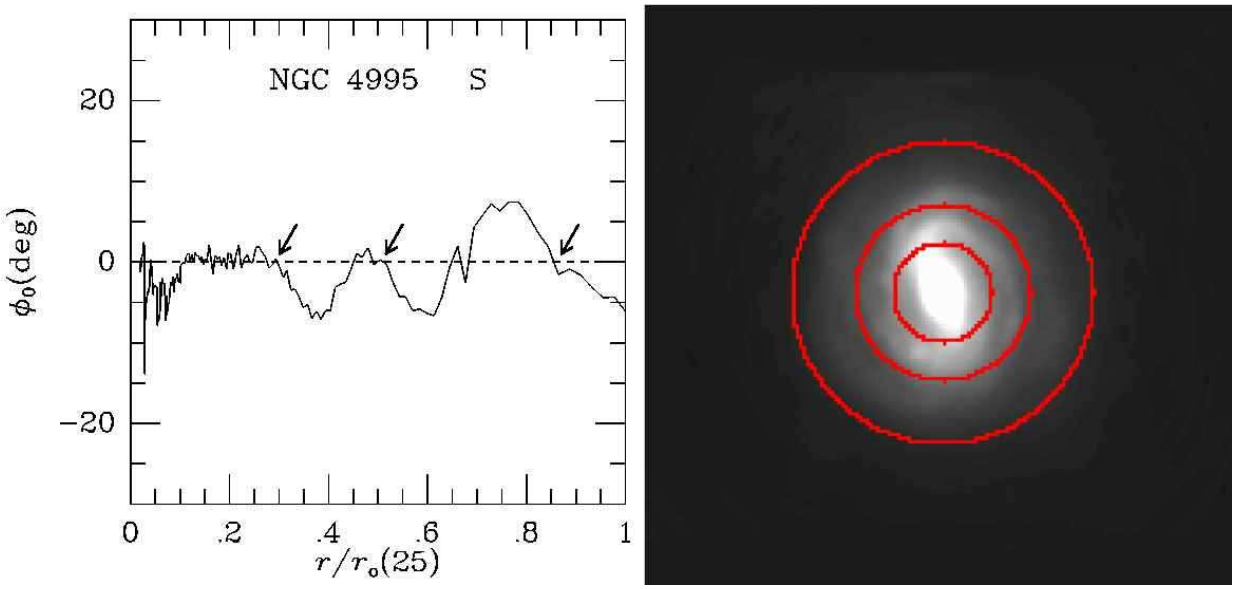

Fig. 2.112.— Same as Figure 2.1 for NGC 4995

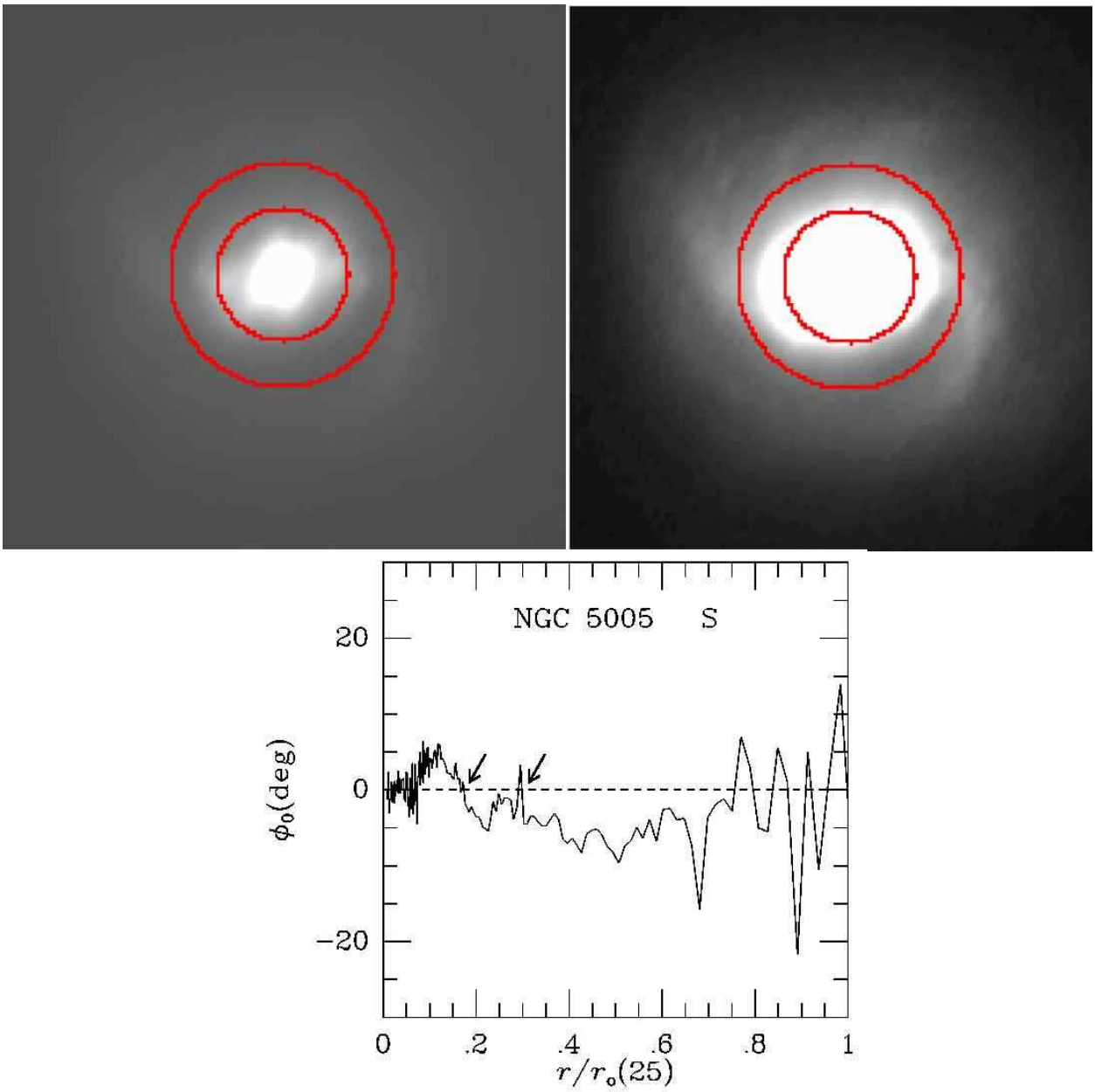

Fig. 2.113.— Same as Figure 2.1 for NGC 5005

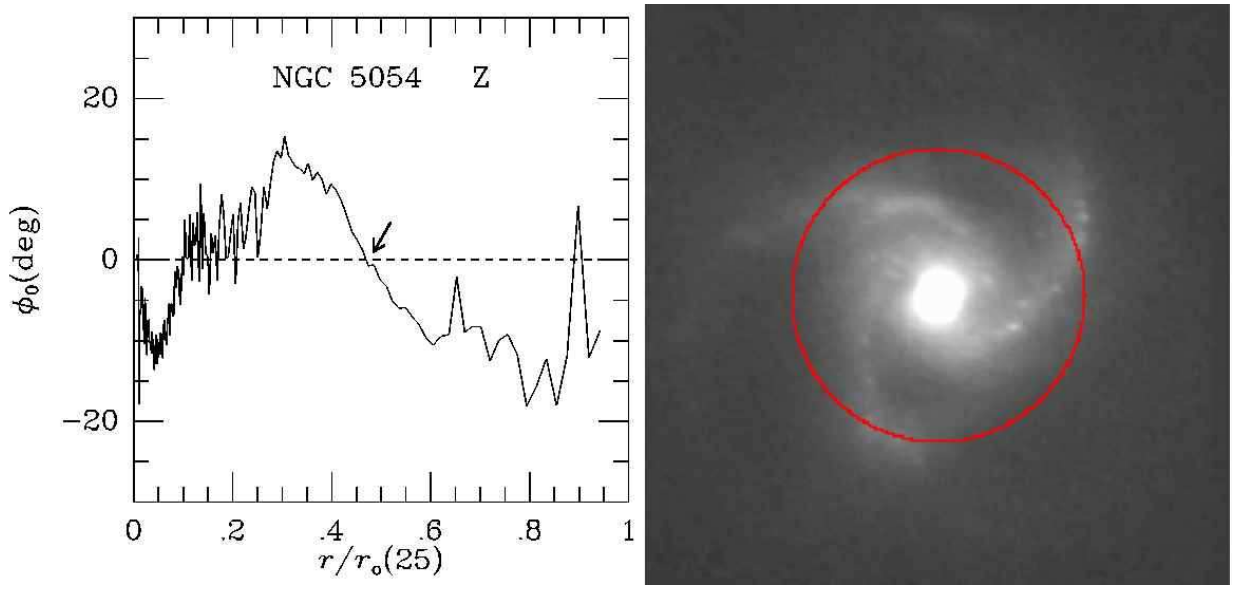

Fig. 2.114.— Same as Figure 2.1 for NGC 5054

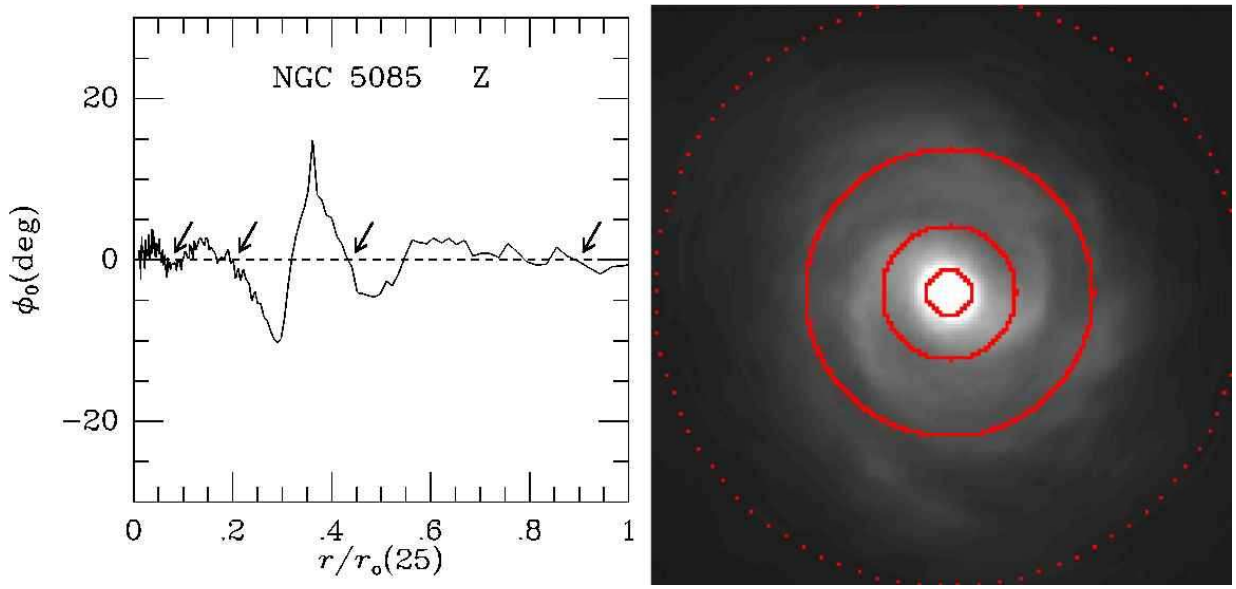

Fig. 2.115.— Same as Figure 2.1 for NGC 5085

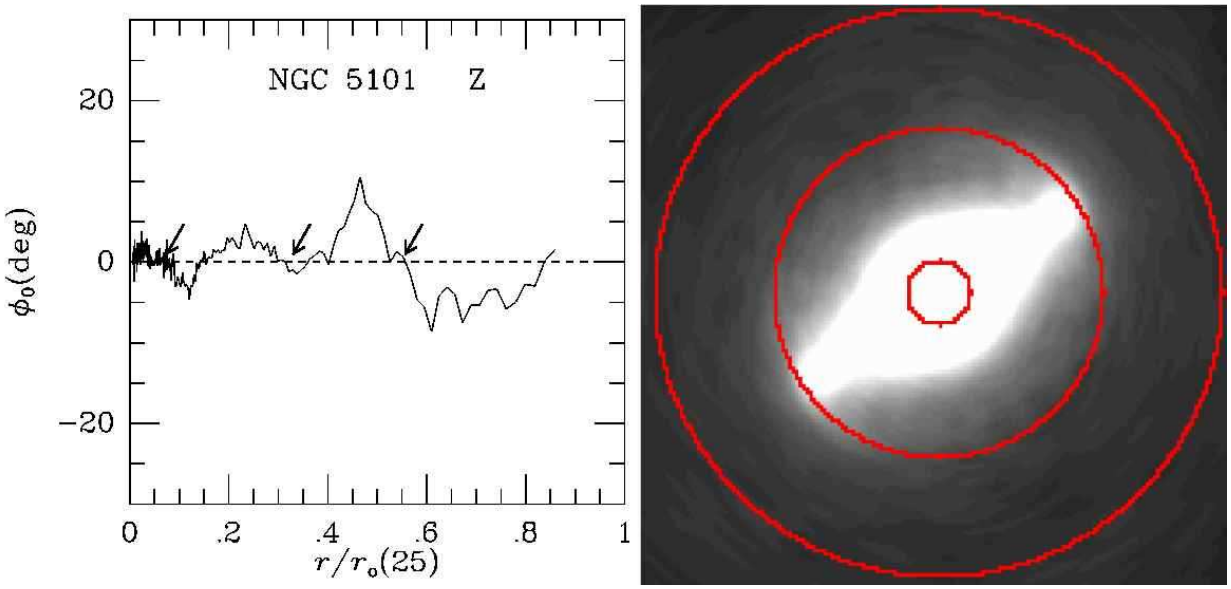

Fig. 2.116.— Same as Figure 2.1 for NGC 5101

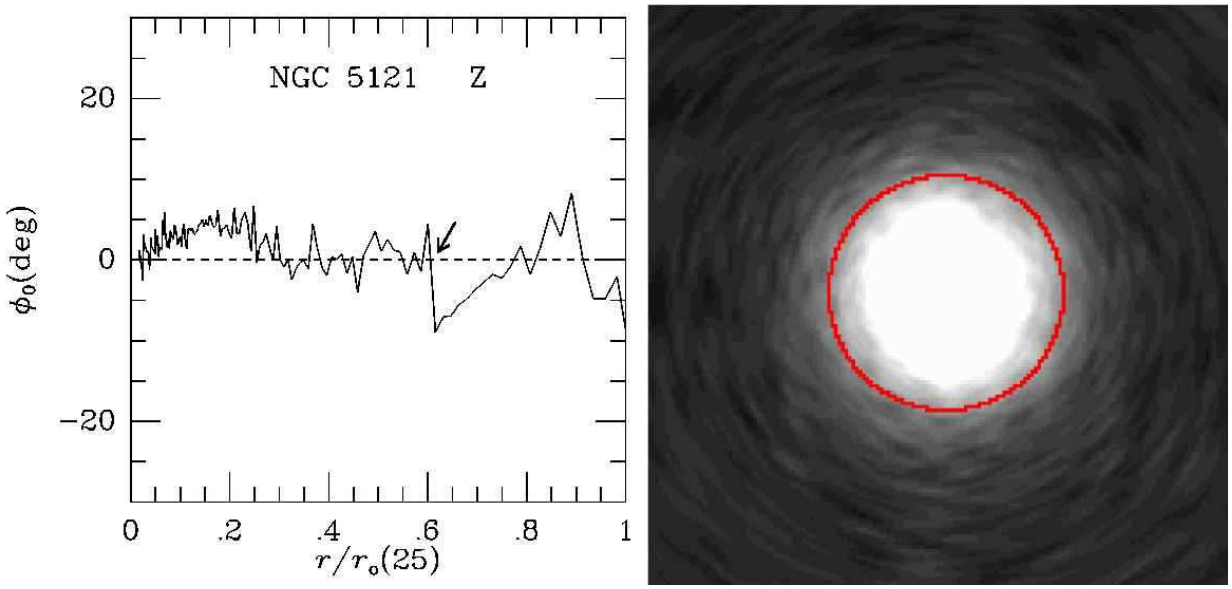

Fig. 2.117.— Same as Figure 2.1 for NGC 5121

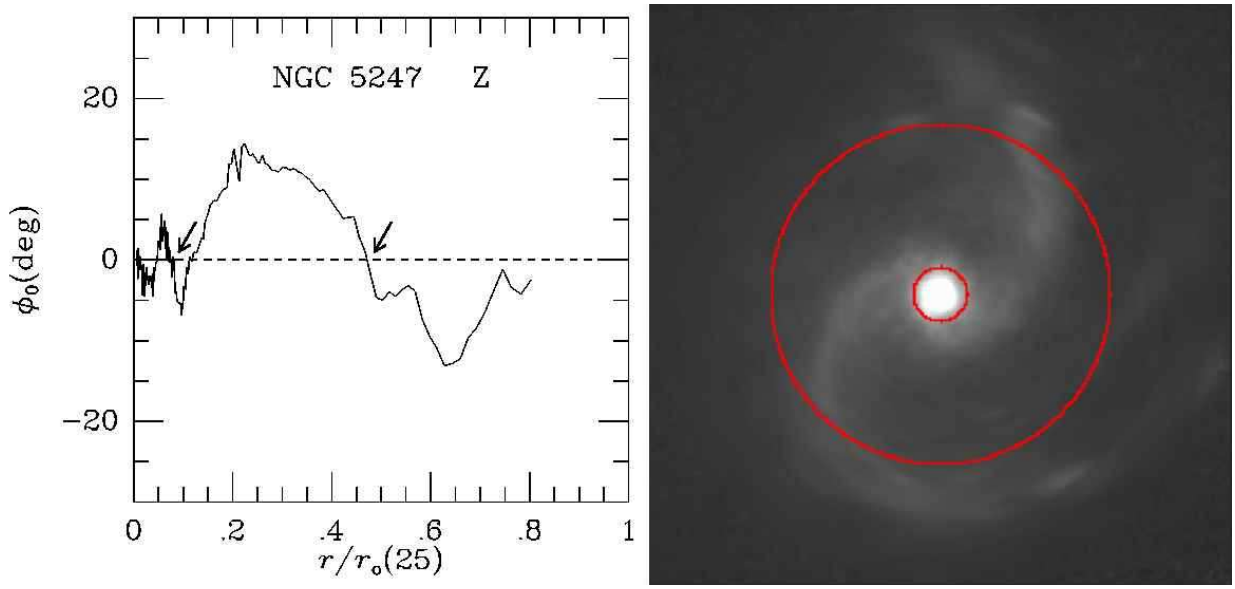

Fig. 2.118.— Same as Figure 2.1 for NGC 5247

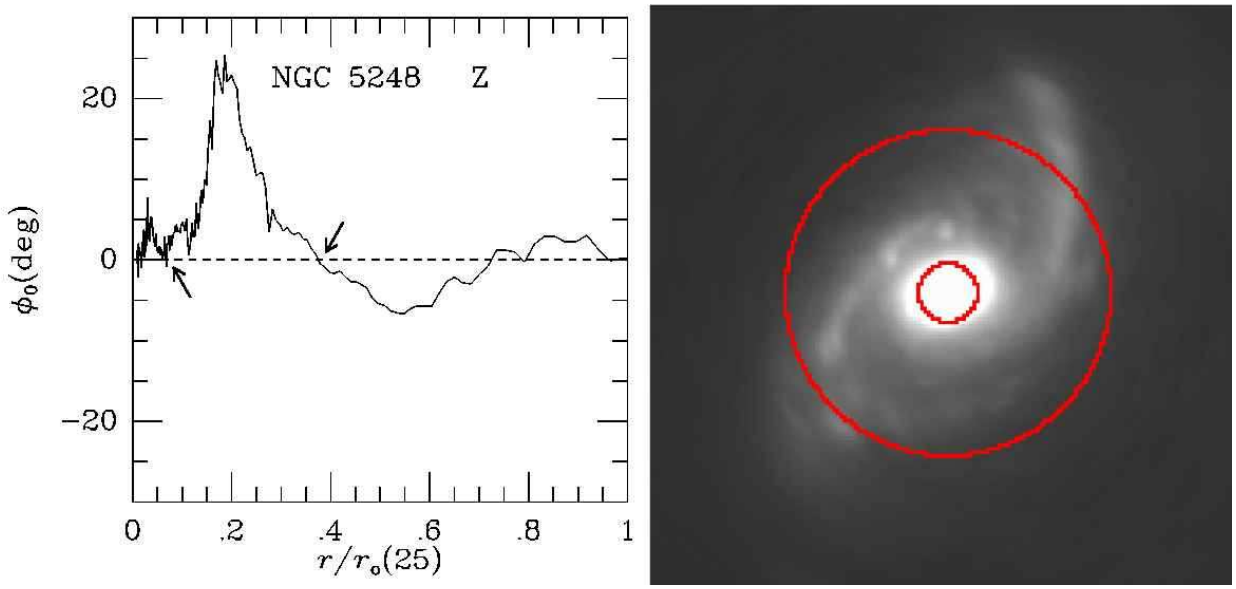

Fig. 2.119.— Same as Figure 2.1 for NGC 5248

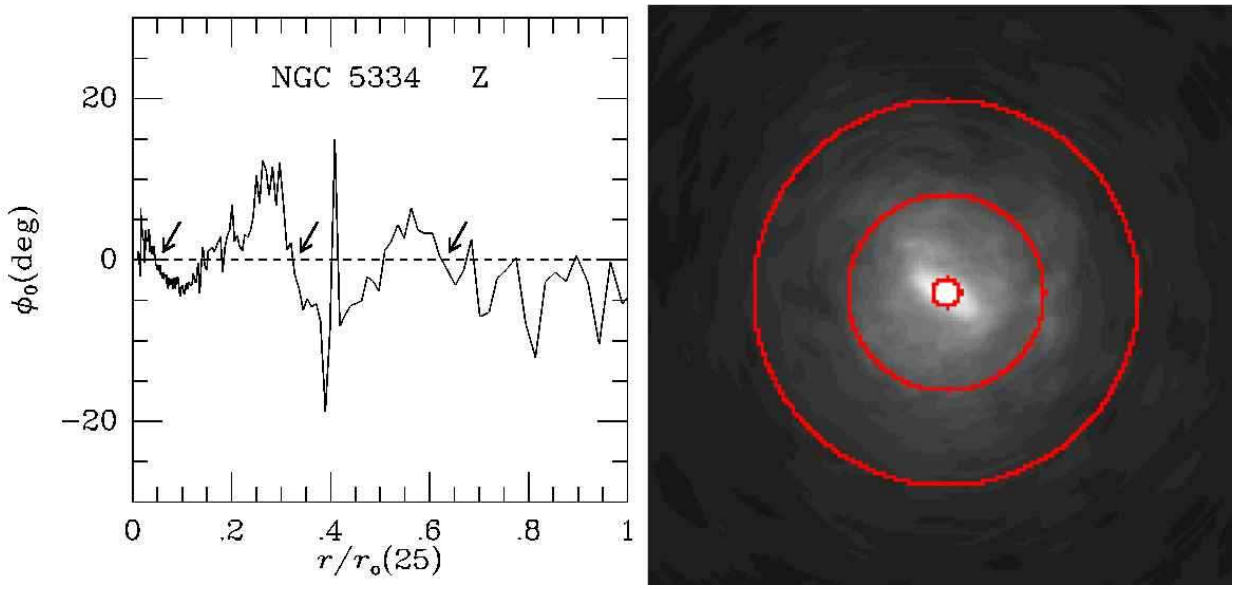

Fig. 2.120.— Same as Figure 2.1 for NGC 5334

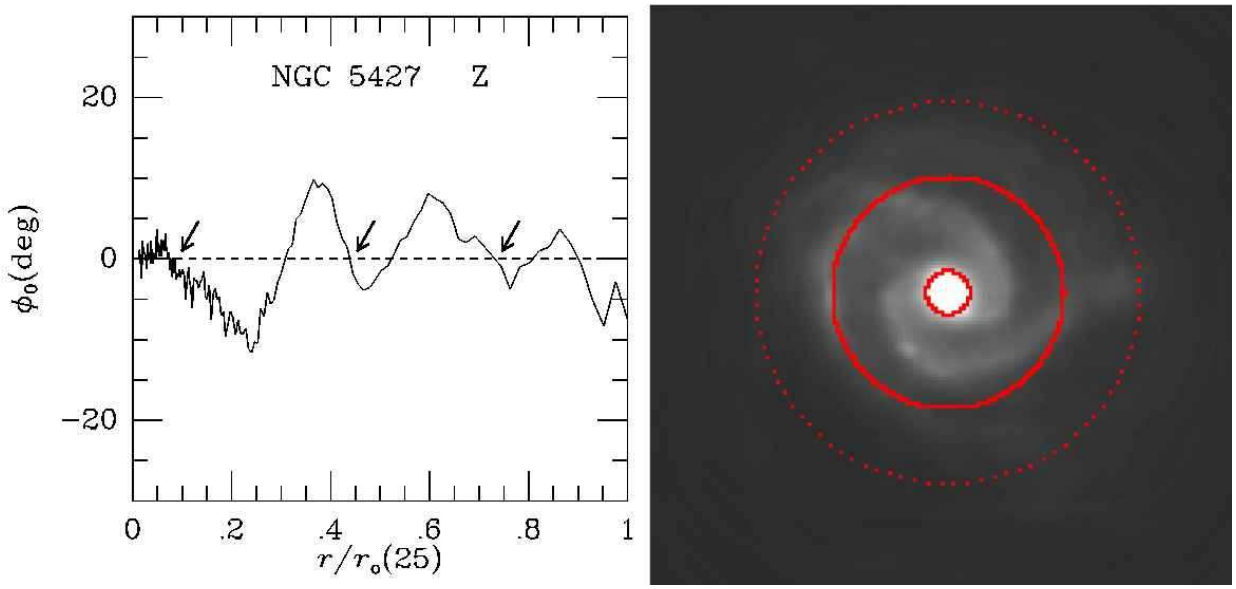

Fig. 2.121.— Same as Figure 2.1 for NGC 5427

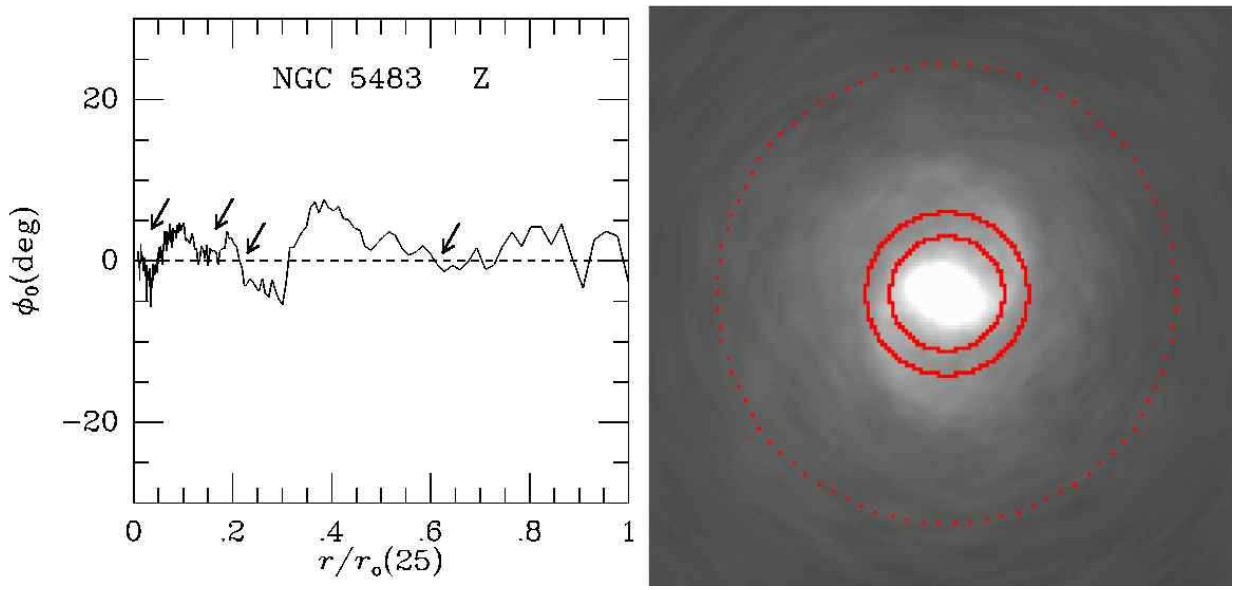

Fig. 2.122.— Same as Figure 2.1 for NGC 5483. CR_1 from Table 1 is not overlaid on the image.

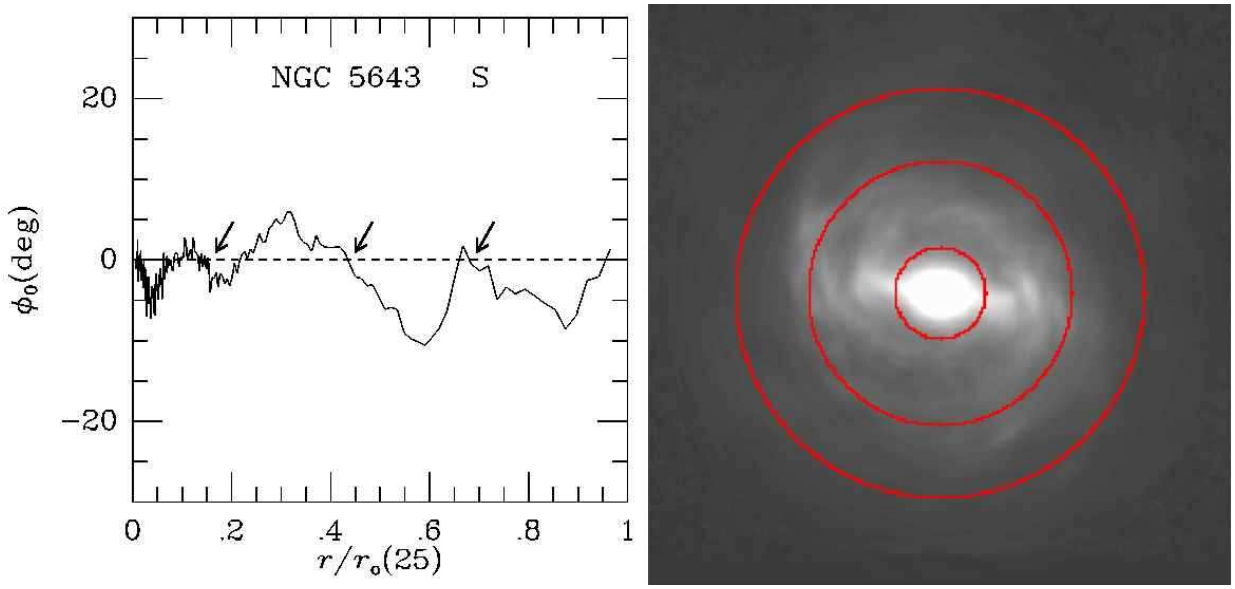

Fig. 2.123.— Same as Figure 2.1 for NGC 5643

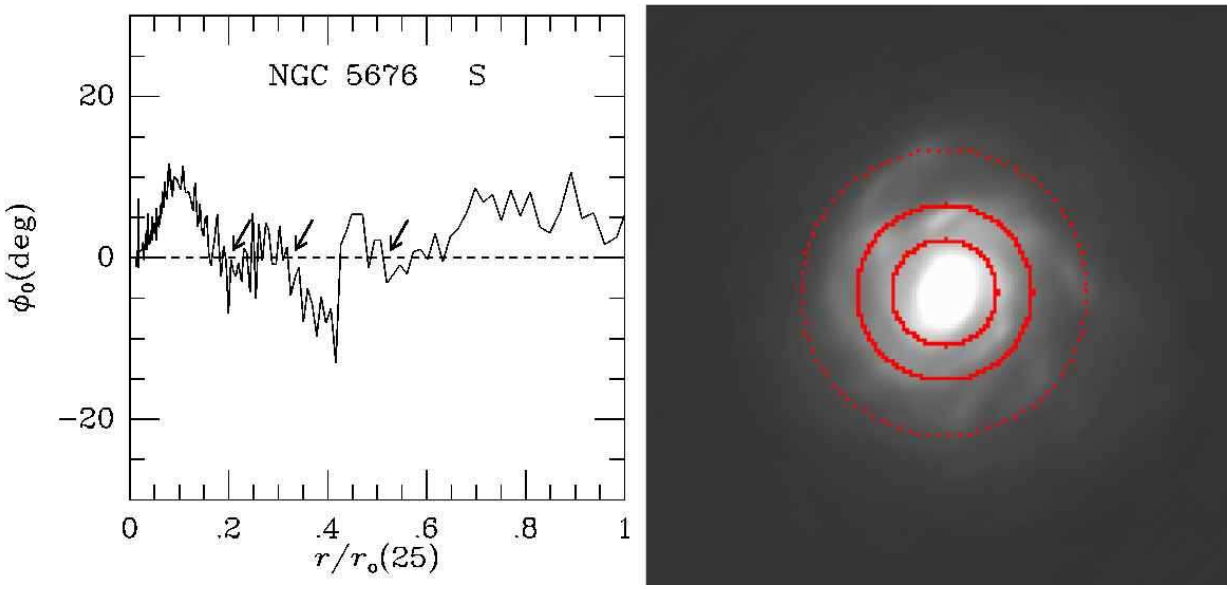

Fig. 2.124.— Same as Figure 2.1 for NGC 5676

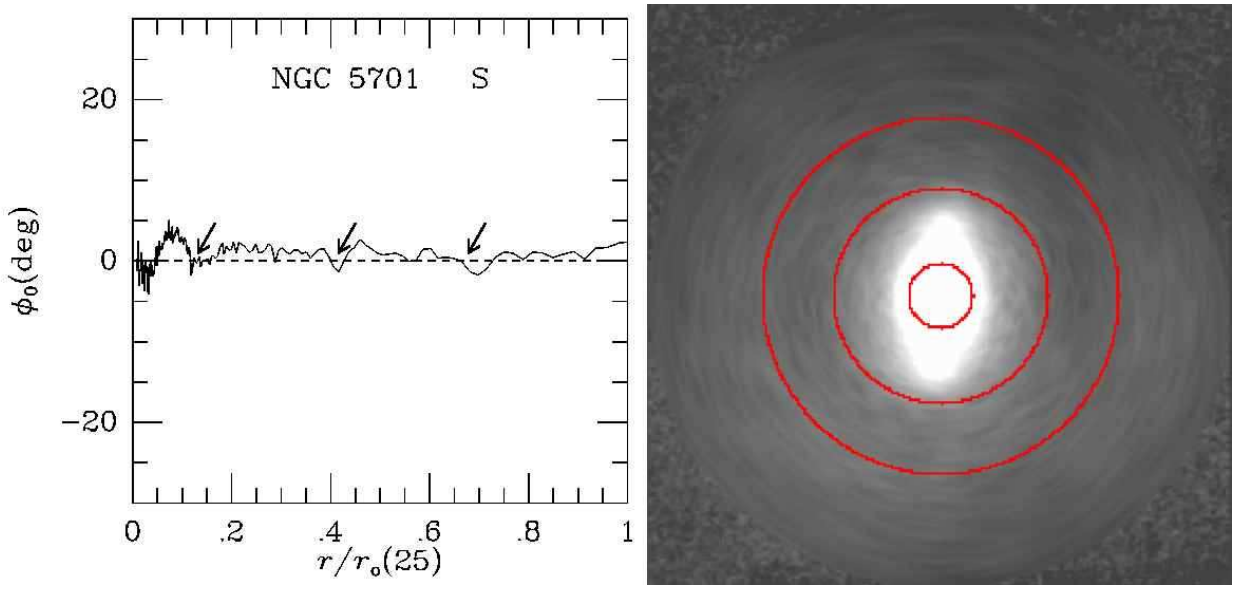

Fig. 2.125.— Same as Figure 2.1 for NGC 5701

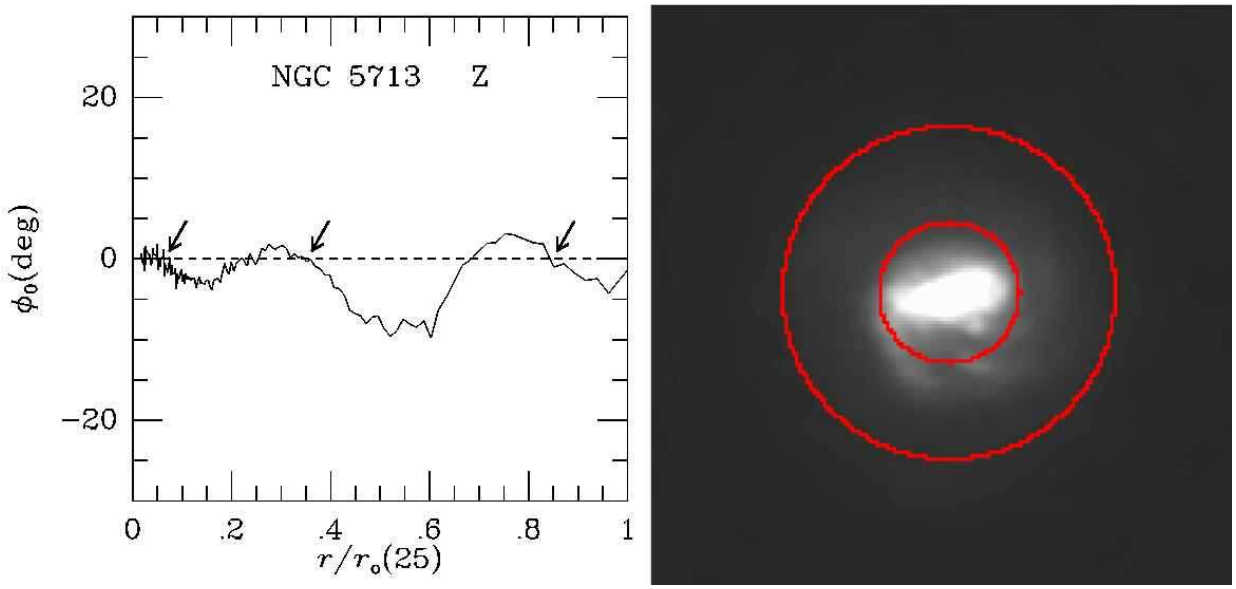

Fig. 2.126.— Same as Figure 2.1 for NGC 5713

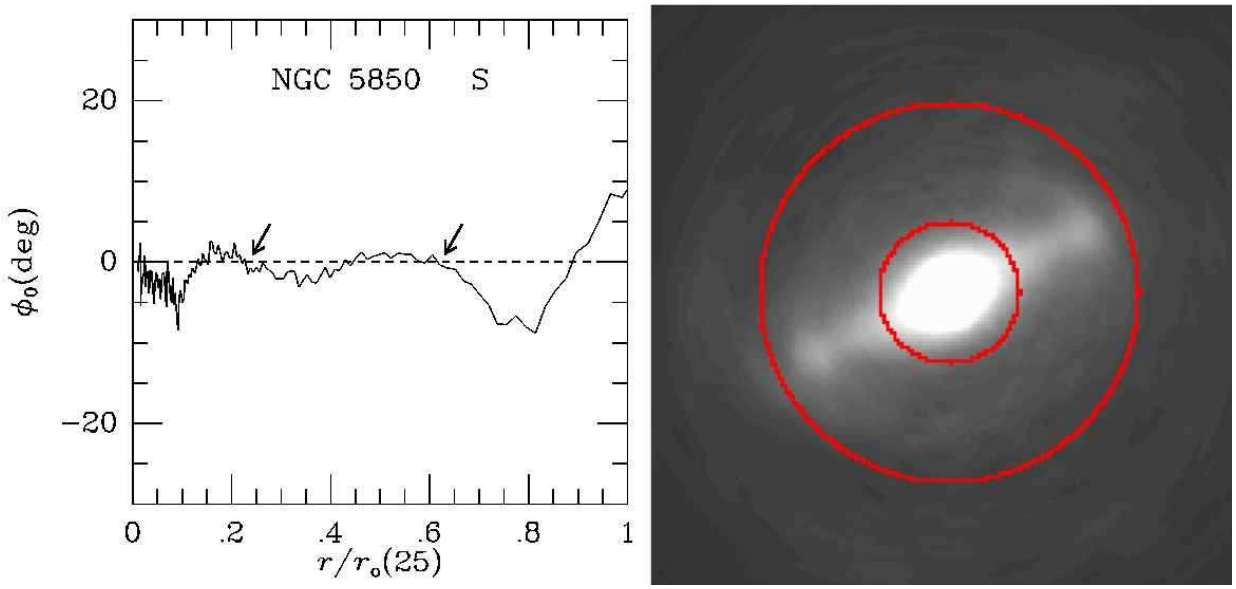

Fig. 2.127.— Same as Figure 2.1 for NGC 5850

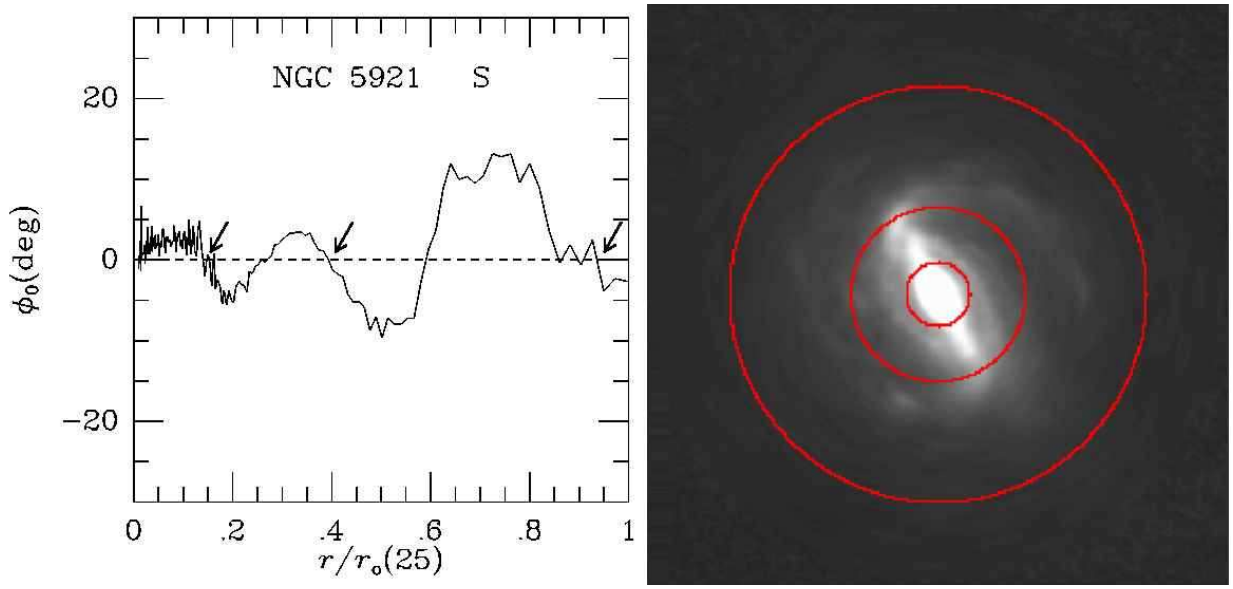

Fig. 2.128.— Same as Figure 2.1 for NGC 5921

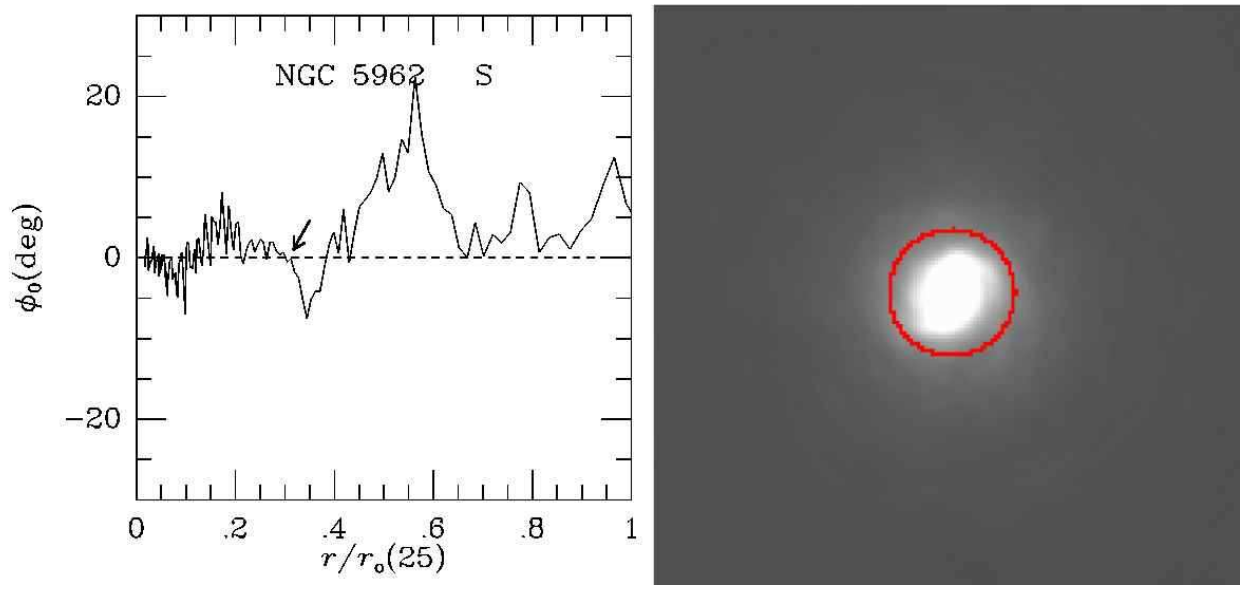

Fig. 2.129.— Same as Figure 2.1 for NGC 5962

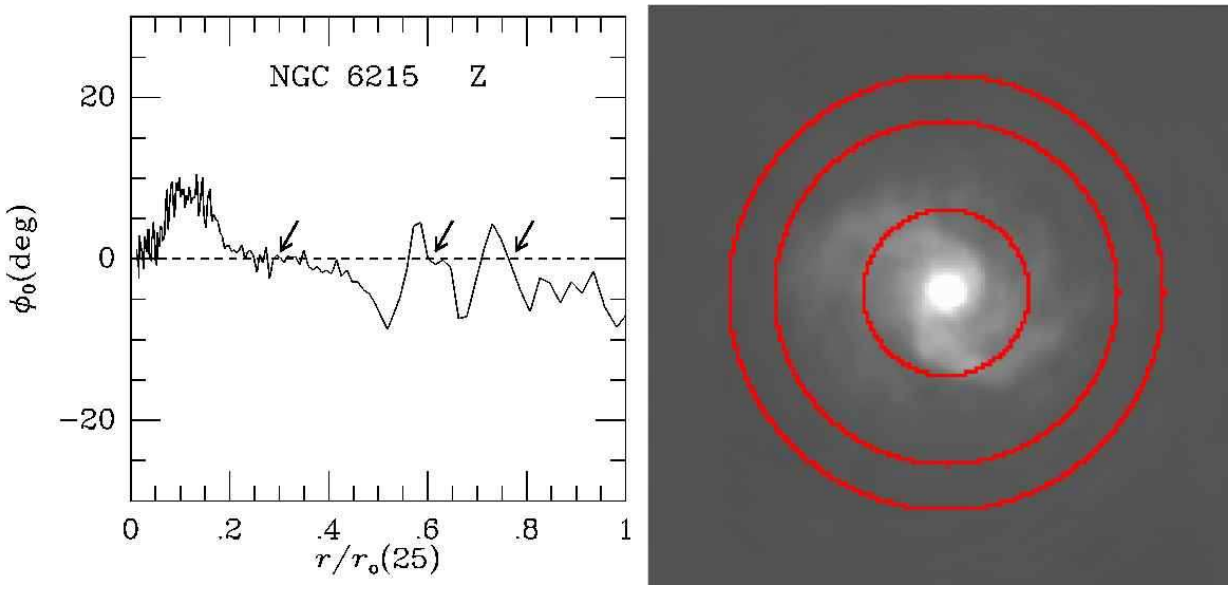

Fig. 2.130.— Same as Figure 2.1 for NGC 6215

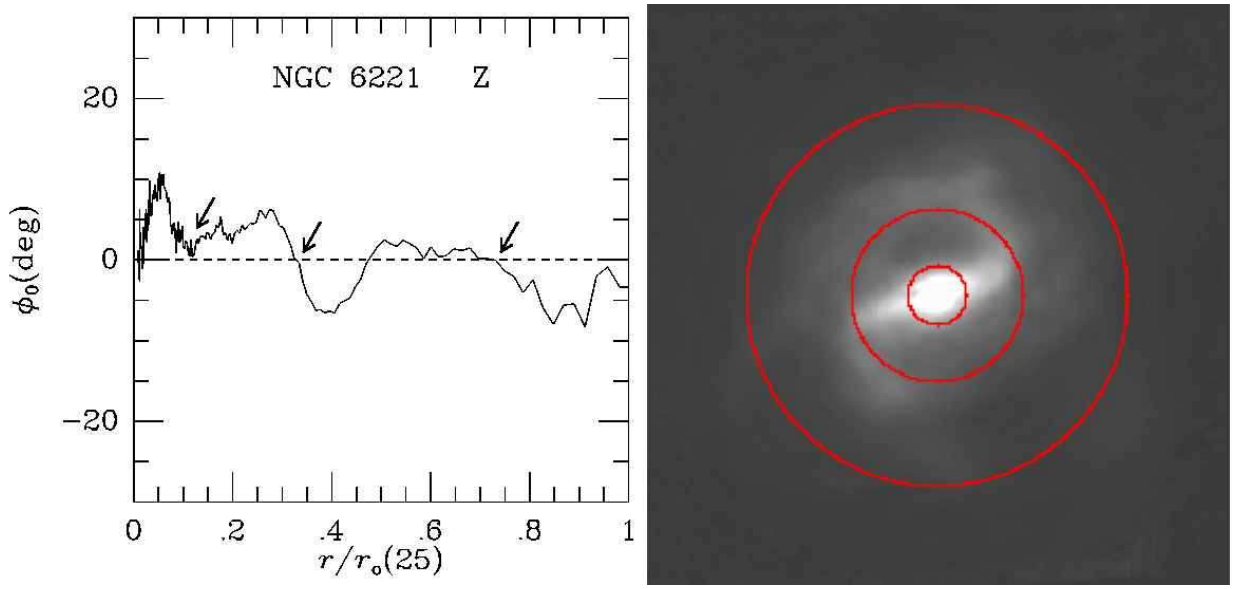

Fig. 2.131.— Same as Figure 2.1 for NGC 6221

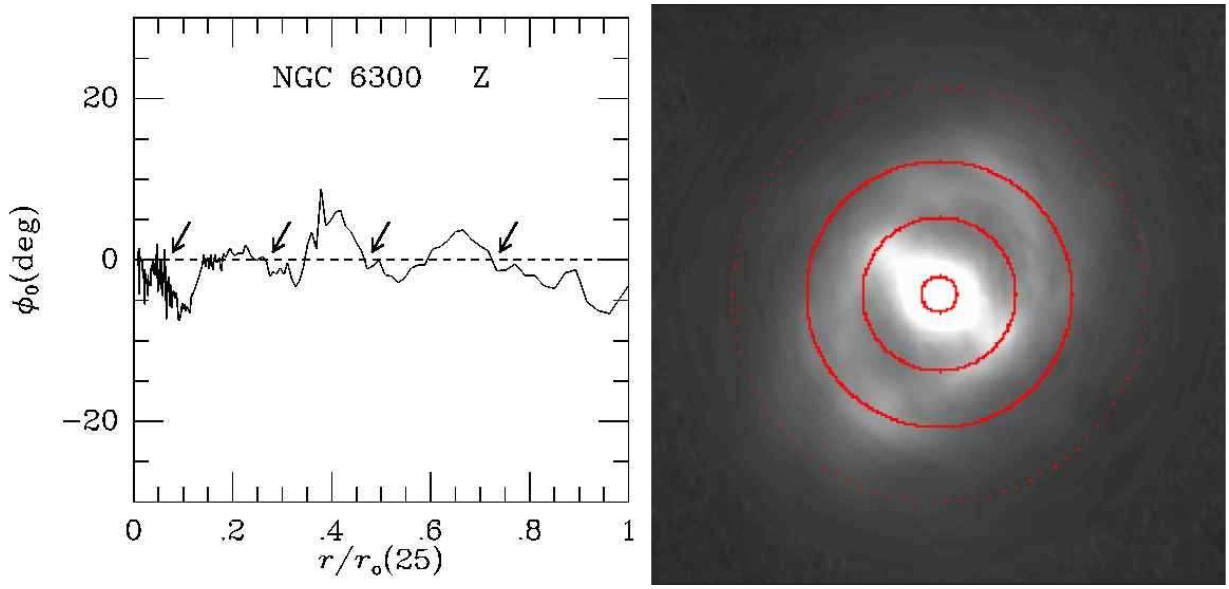

Fig. 2.132.— Same as Figure 2.1 for NGC 6300

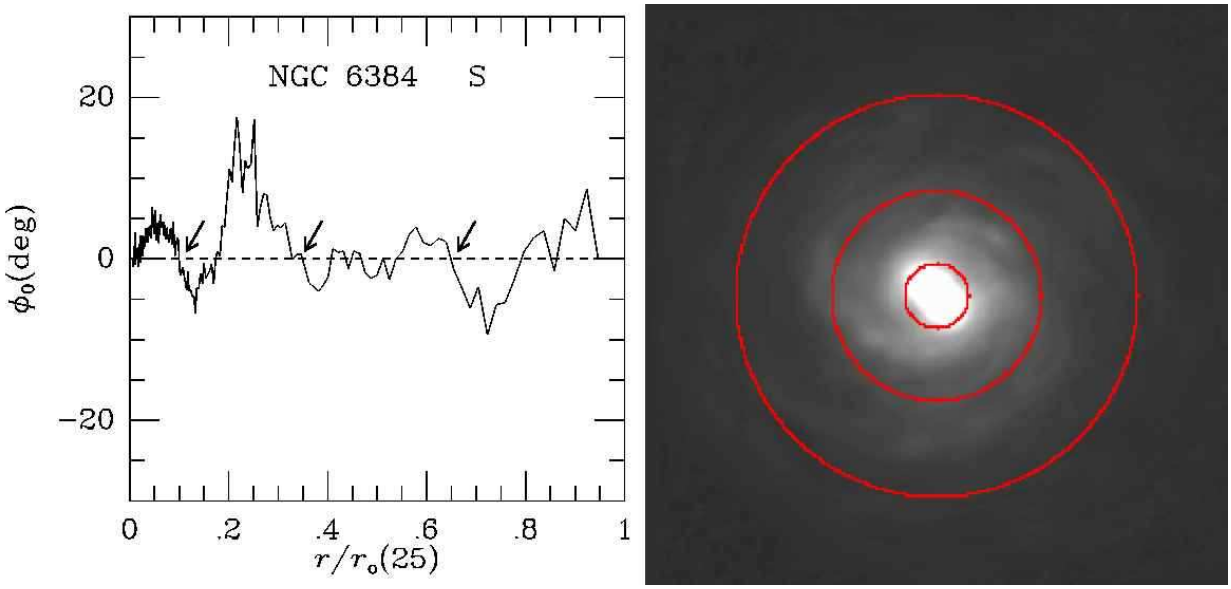

Fig. 2.133.— Same as Figure 2.1 for NGC 6384

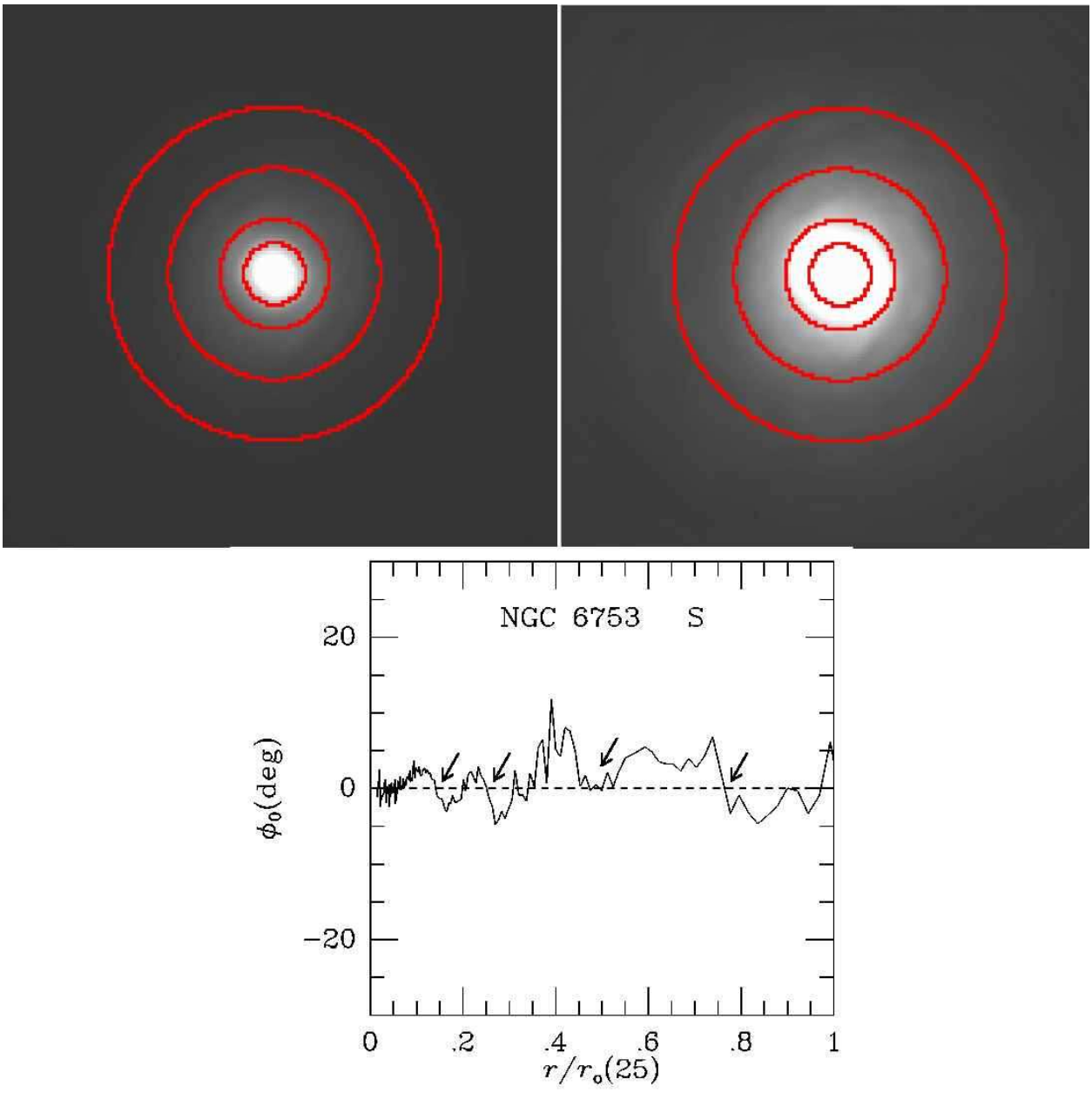

Fig. 2.134.— Same as Figure 2.1 for NGC 6753

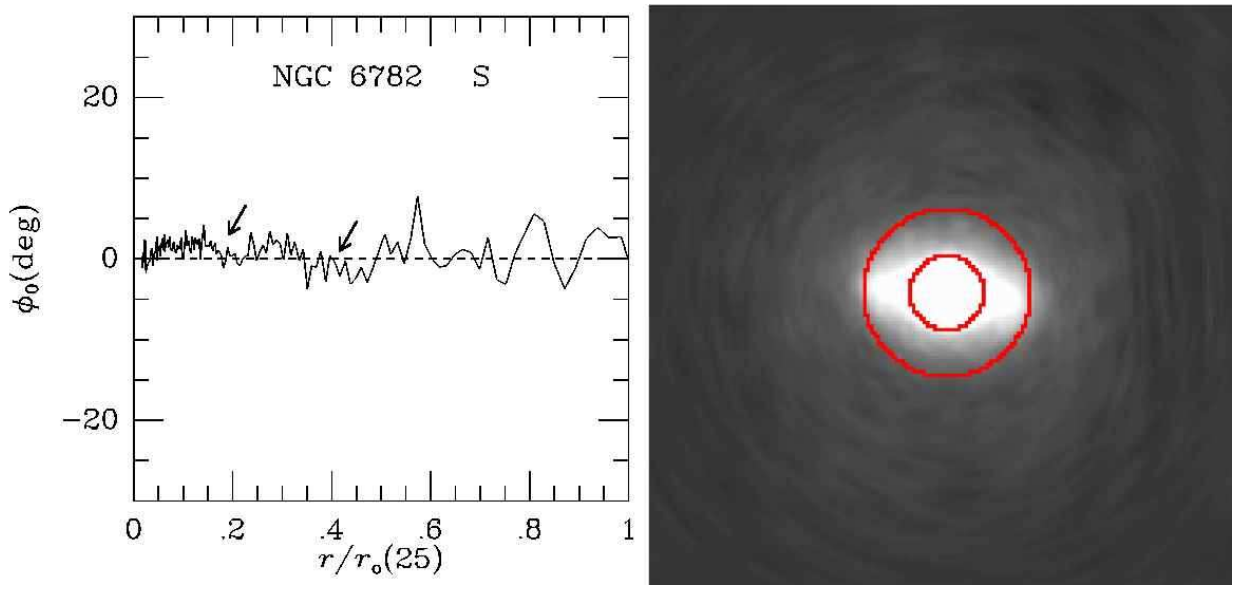

Fig. 2.135.— Same as Figure 2.1 for NGC 6782

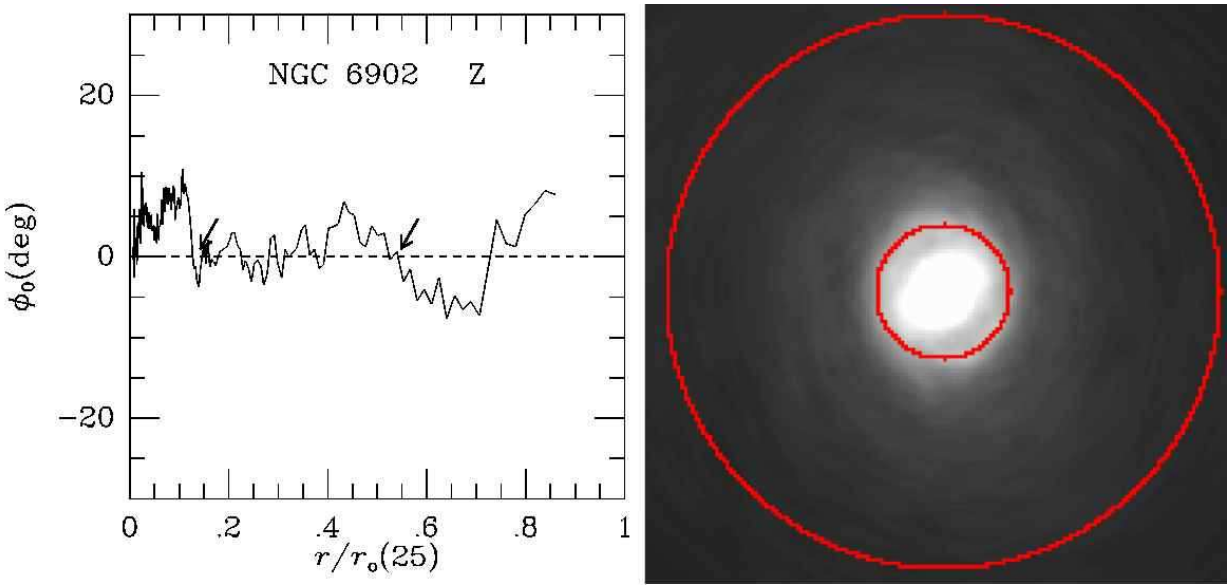

Fig. 2.136.— Same as Figure 2.1 for NGC 6902

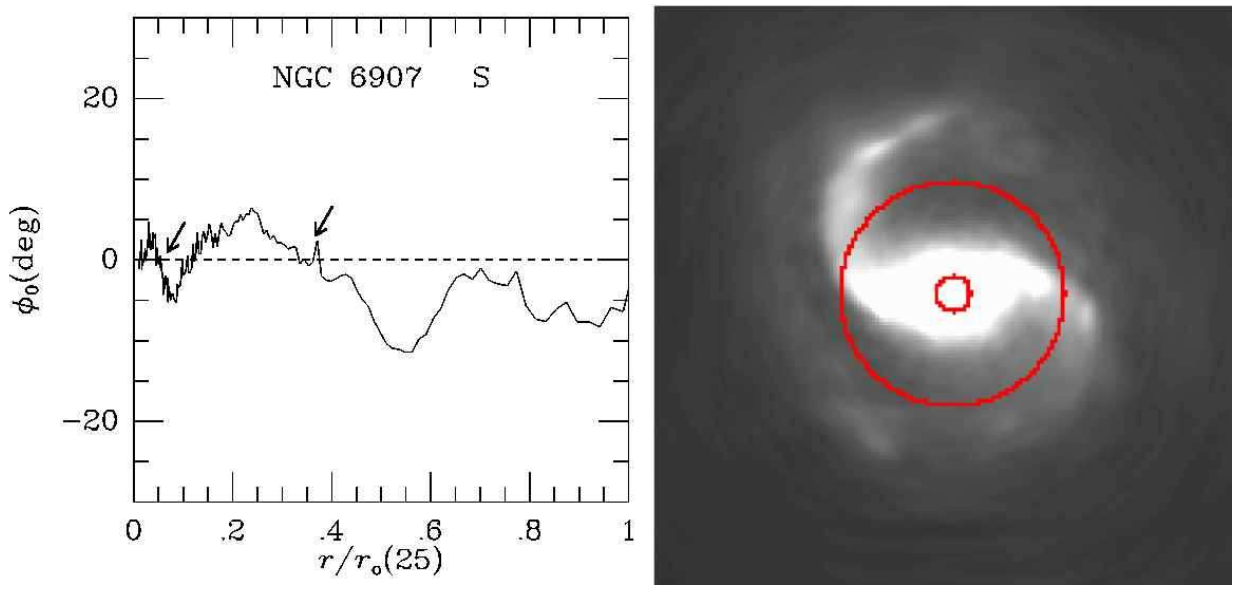

Fig. 2.137.— Same as Figure 2.1 for NGC 6907

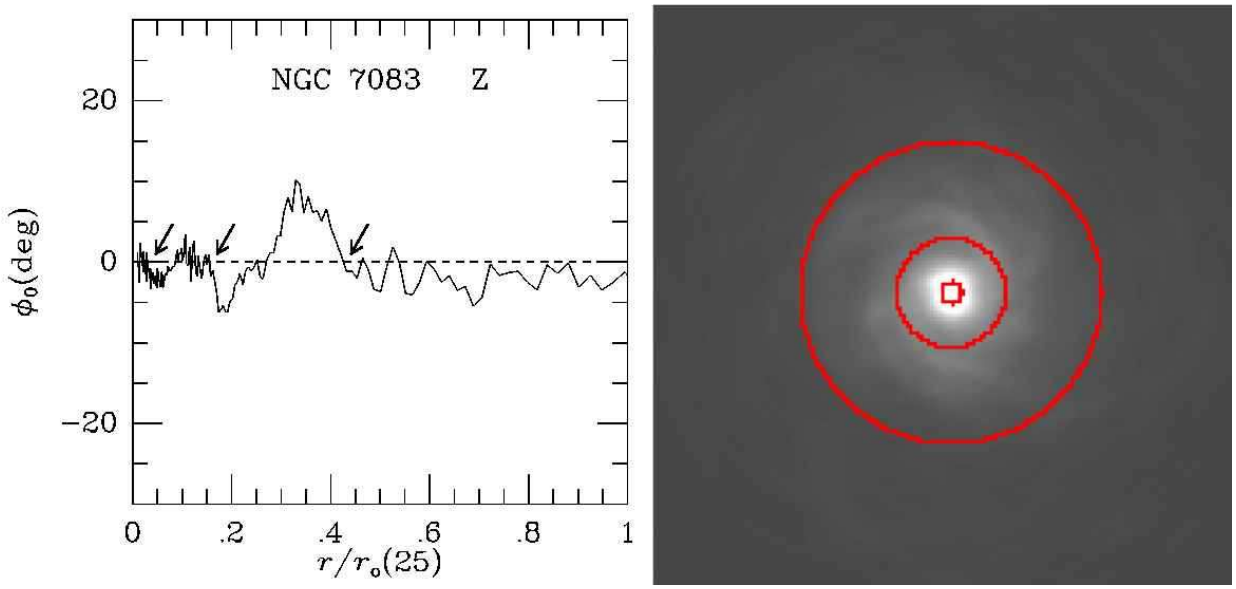

Fig. 2.138.— Same as Figure 2.1 for NGC 7083

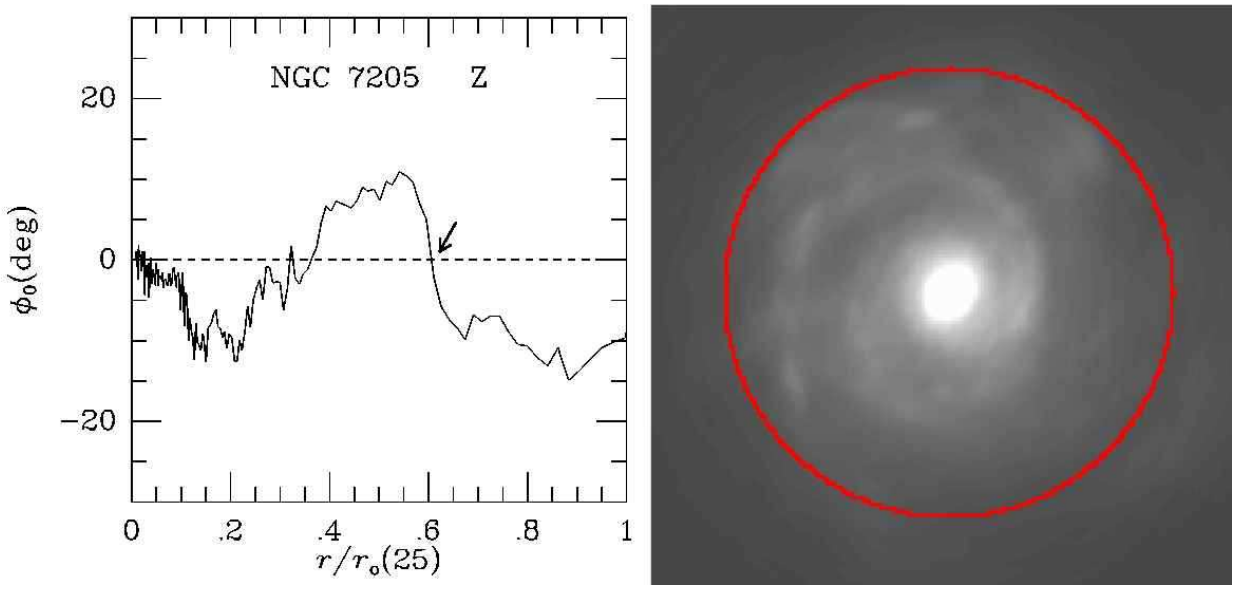

Fig. 2.139.— Same as Figure 2.1 for NGC 7205

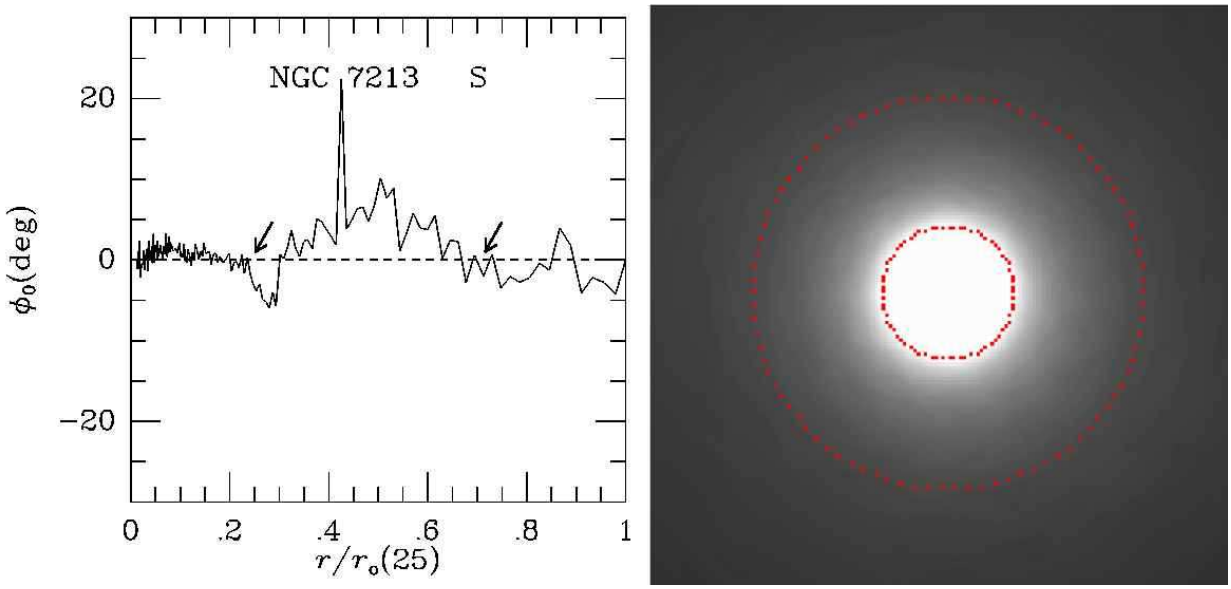

Fig. 2.140.— Same as Figure 2.1 for NGC 7213

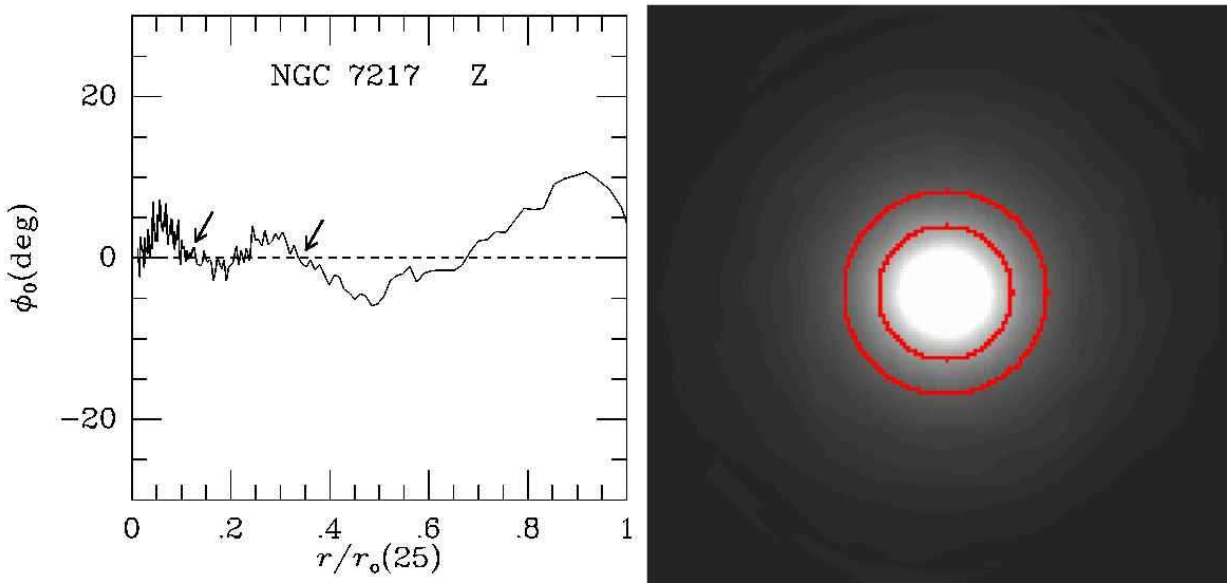

Fig. 2.141.— Same as Figure 2.1 for NGC 7217

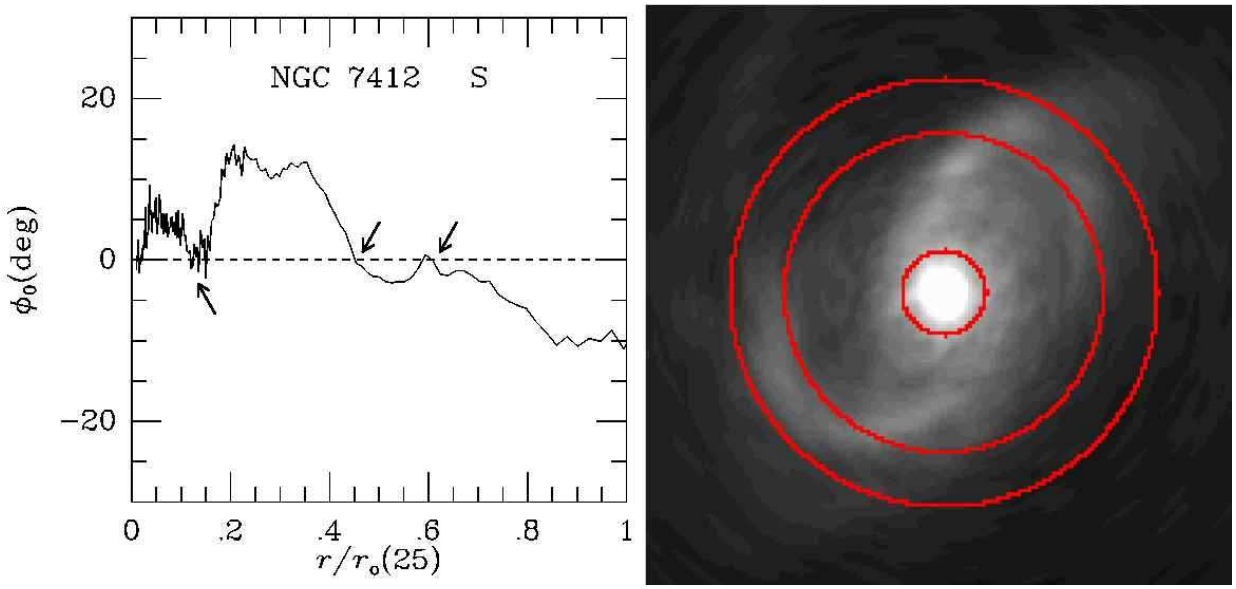

Fig. 2.142.— Same as Figure 2.1 for NGC 7412

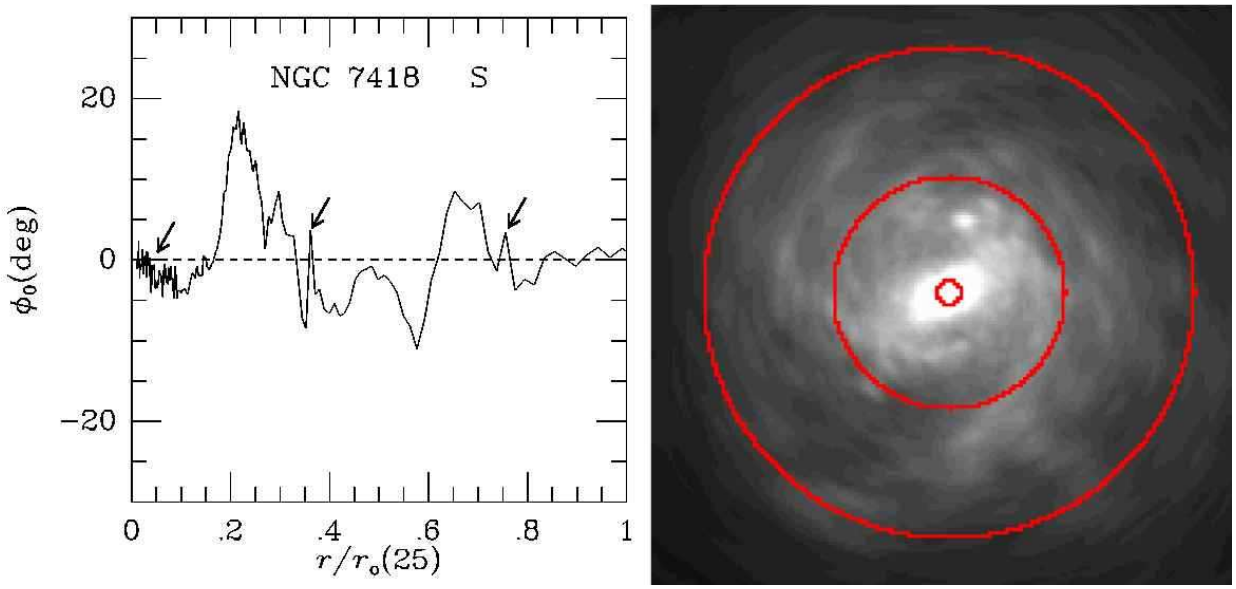

Fig. 2.143.— Same as Figure 2.1 for NGC 7418

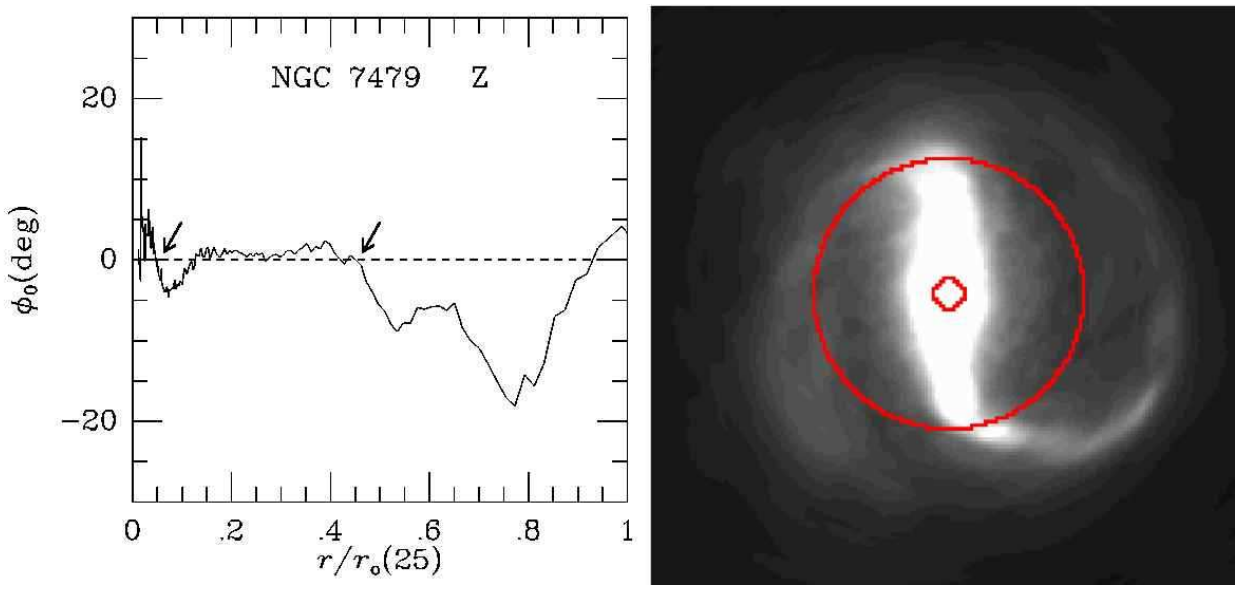

Fig. 2.144.— Same as Figure 2.1 for NGC 7479

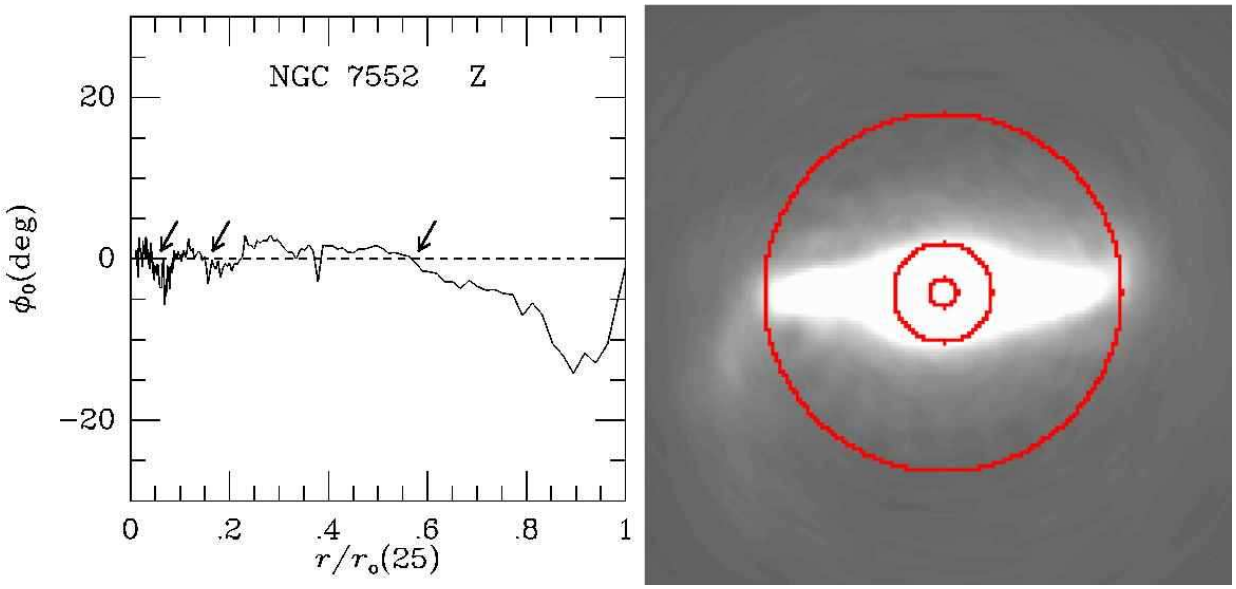

Fig. 2.145.— Same as Figure 2.1 for NGC 7552

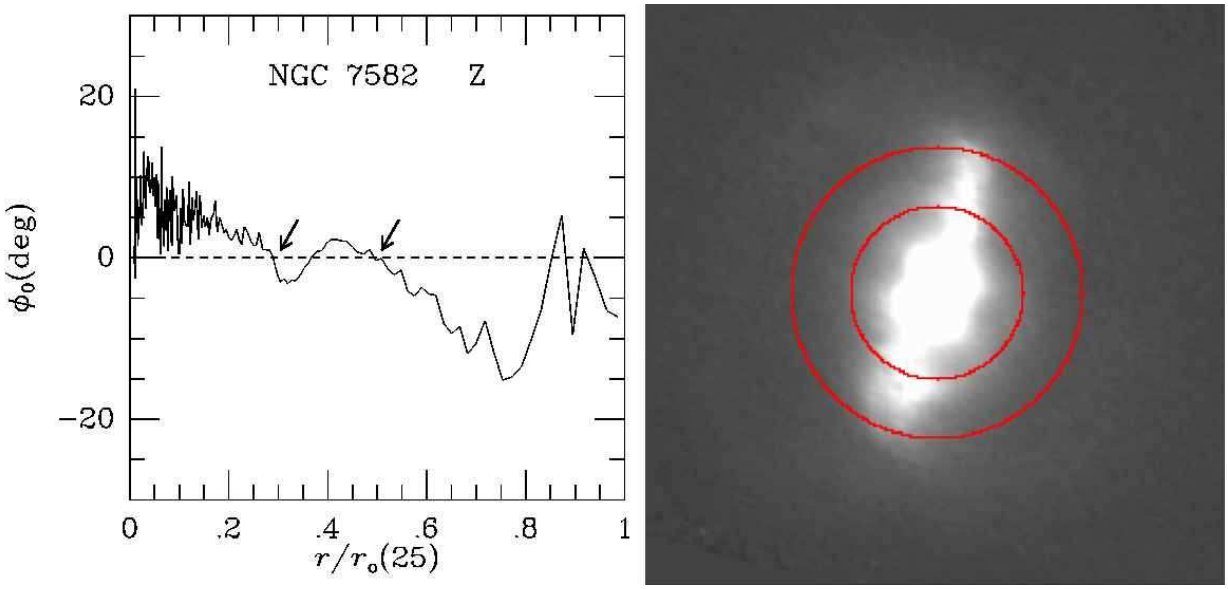

Fig. 2.146.— Same as Figure 2.1 for NGC 7582

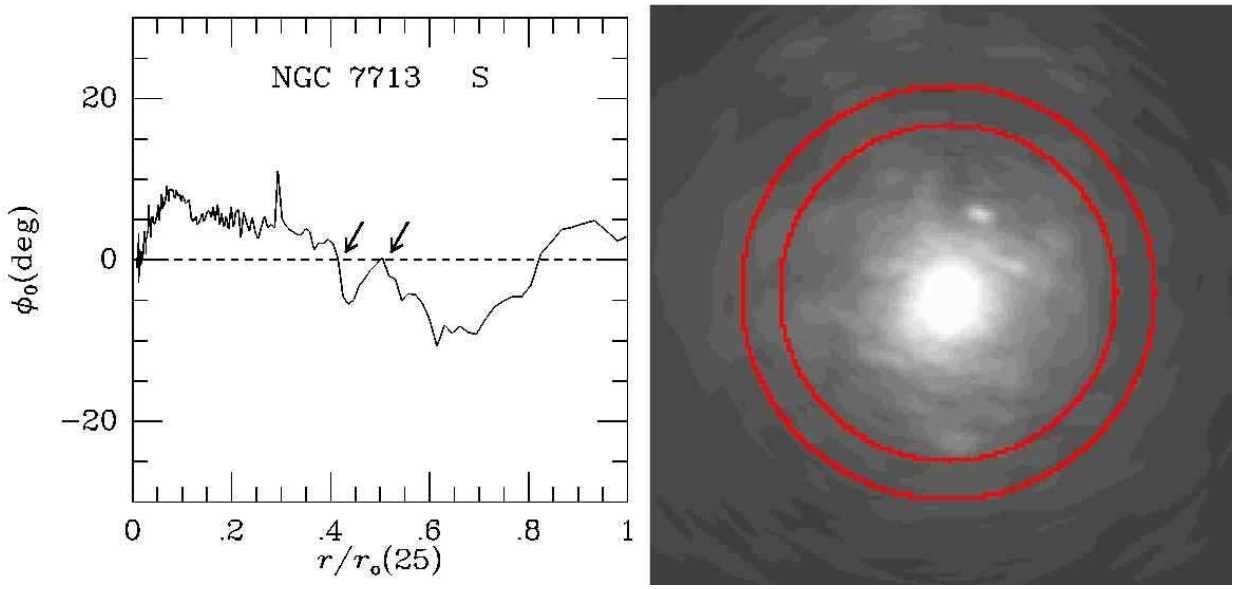

Fig. 2.147.— Same as Figure 2.1 for NGC 7713

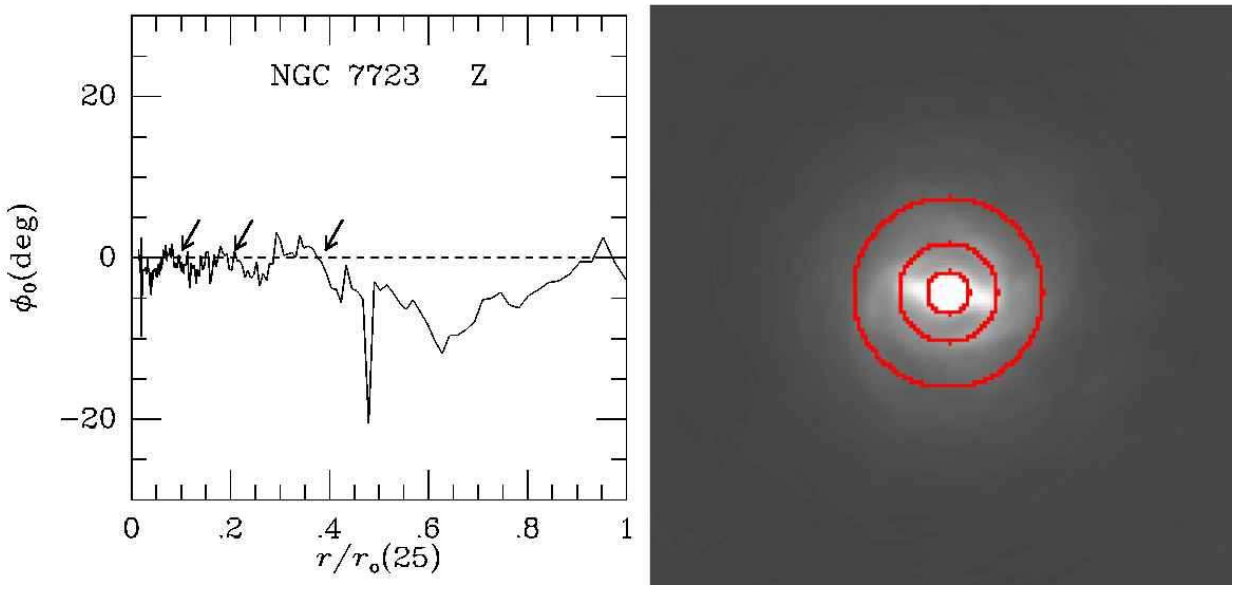

Fig. 2.148.— Same as Figure 2.1 for NGC 7723

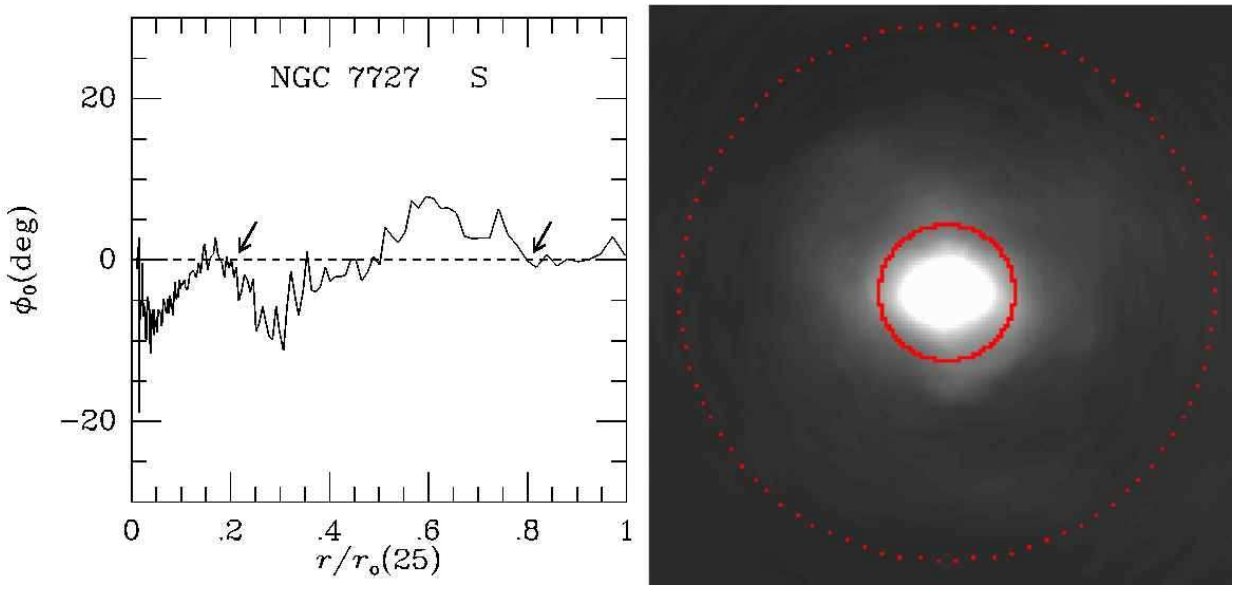

Fig. 2.149.— Same as Figure 2.1 for NGC 7727

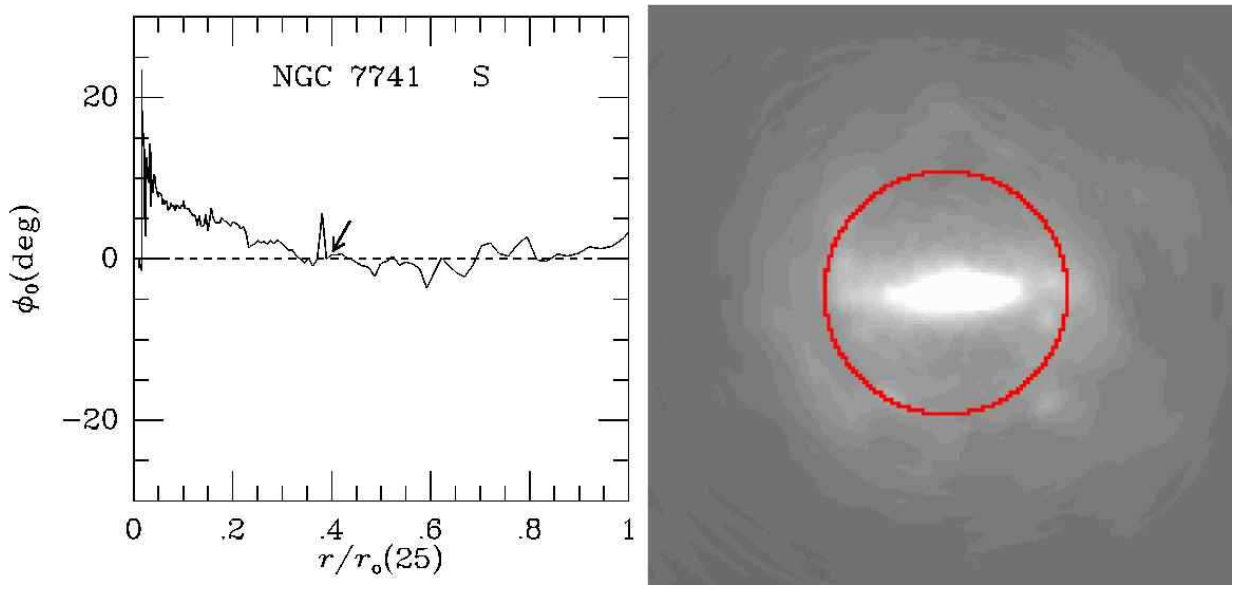

Fig. 2.150.— Same as Figure 2.1 for NGC 7741

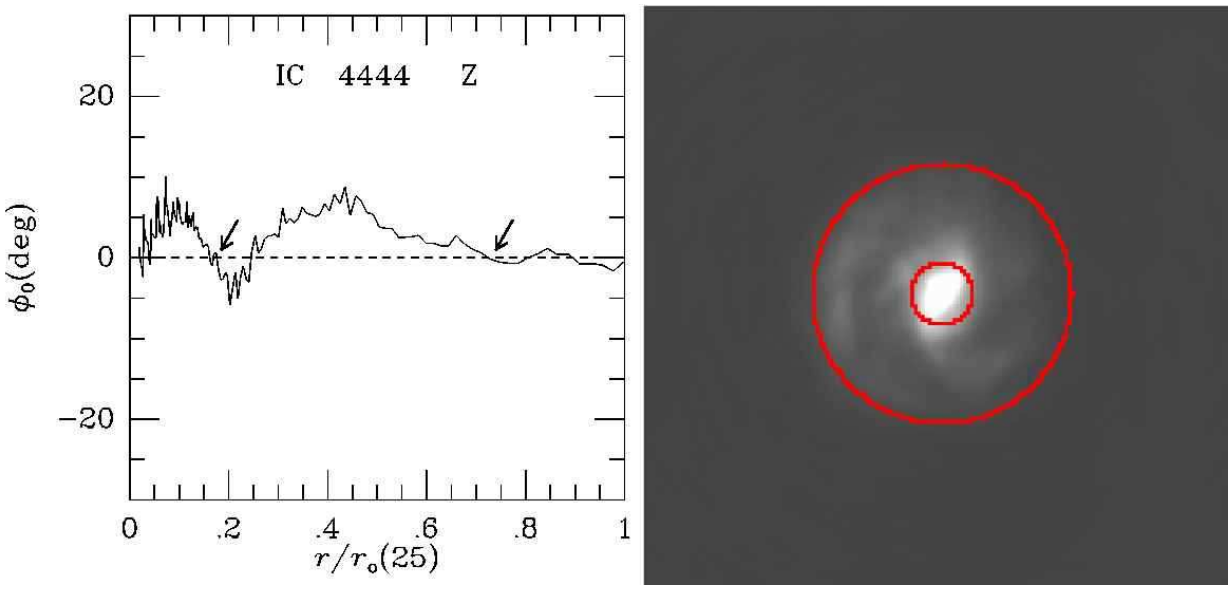

Fig. 2.151.— Same as Figure 2.1 for IC 4444.

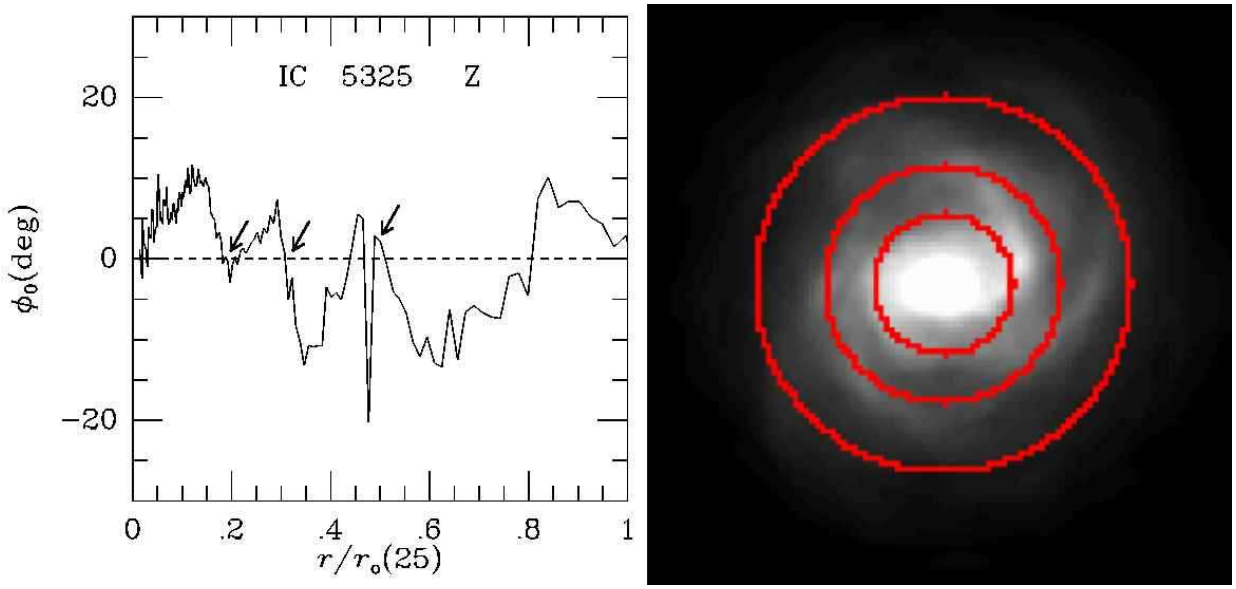

Fig. 2.152.— Same as Figure 2.1 for IC 5325.

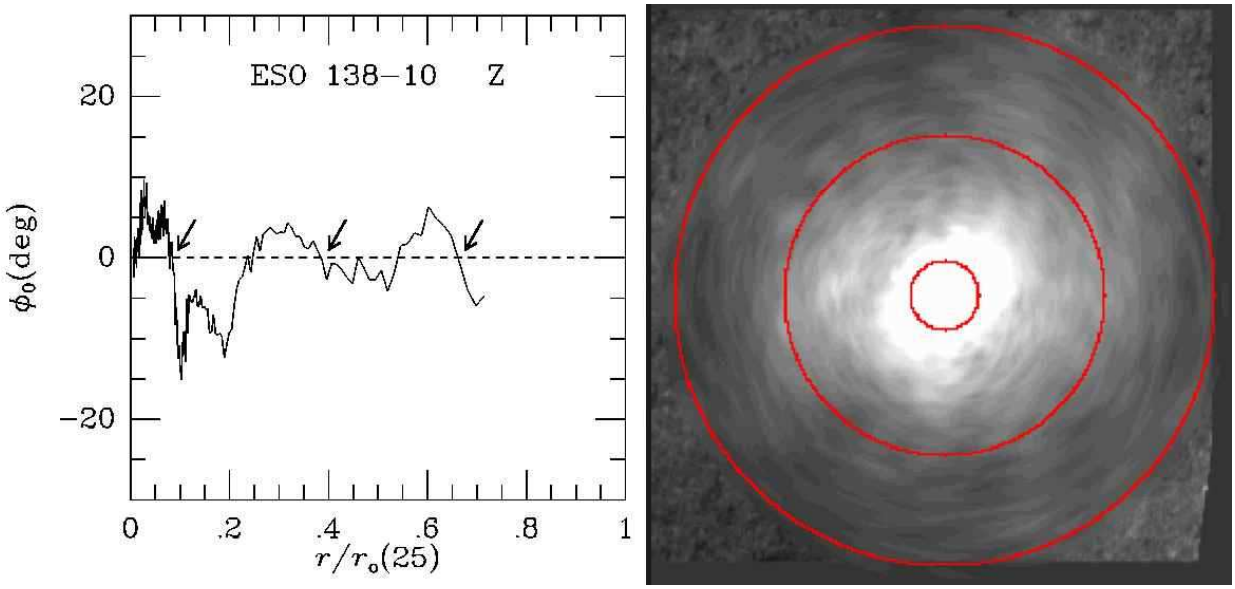

Fig. 2.153.— Same as Figure 2.1 for ESO 138−10.

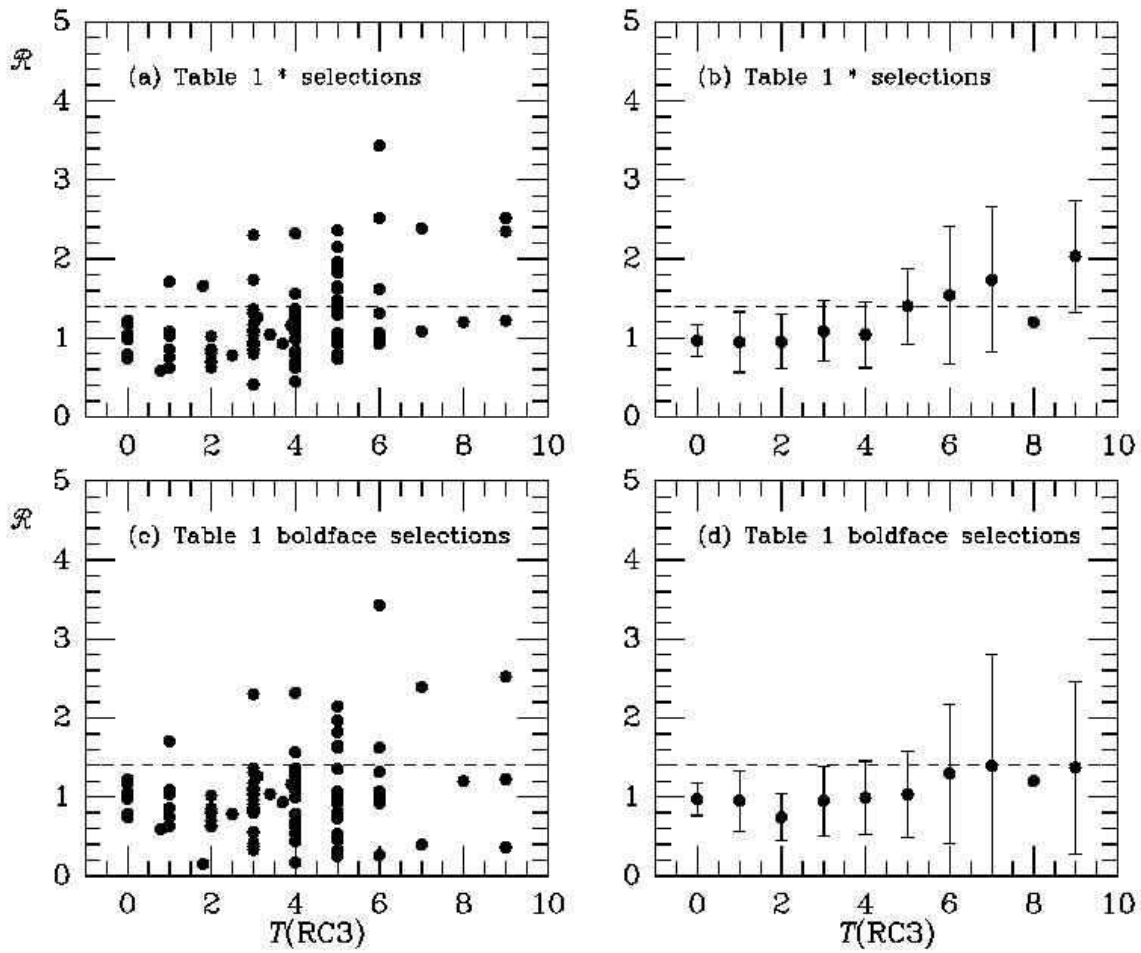

Fig. 3.— Corotation to bar radius, $\mathcal{R} = r(CR)/r(bar)$, for the OSUBGS galaxies having a "Fourier bar" (Laurikainen et al. 2004), plotted versus numerical RC3 stage index. (a),(b) Individual points and means with standard deviations based on the asterisked CR radii in Table 1. (c),(d) Same as (a),(b) but using the boldfaced CR radii in Table 1 as alternative interpretations. The dashed horizontal line is set at the value 1.4, used to delineate a boundary between fast and slow bars (Debattista & Sellwood 2000).

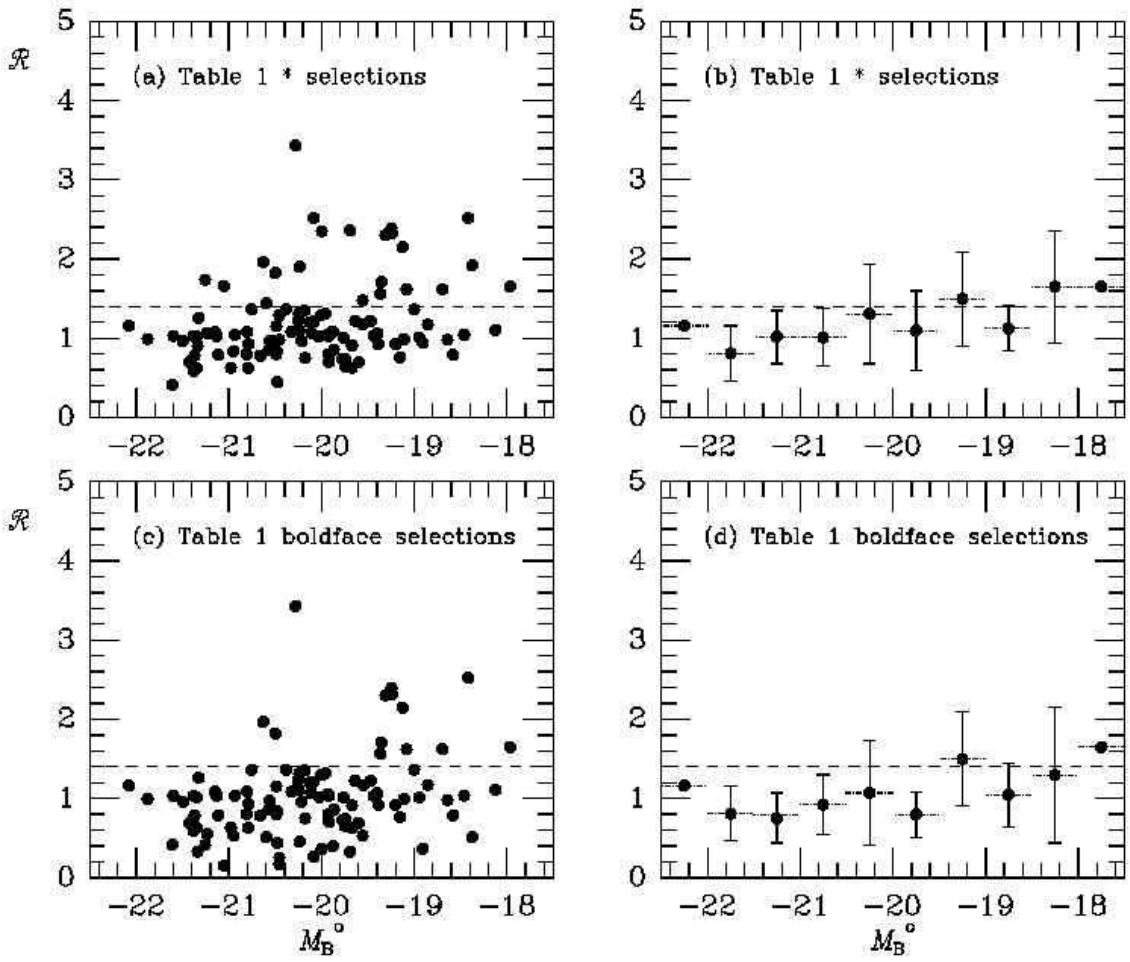

Fig. 4.— Same as Figure 3 plotted versus absolute blue magnitude, based on RC3 parameters. Left: individual points. Right: Means in bins of 0.5 mag with standard deviations. The short dotted horizontal lines indicate the ranges in absolute magnitude used for the averages. The dashed horizontal line is set at the value 1.4, used to delineate a boundary between fast and slow bars (Debattista & Sellwood 2000).

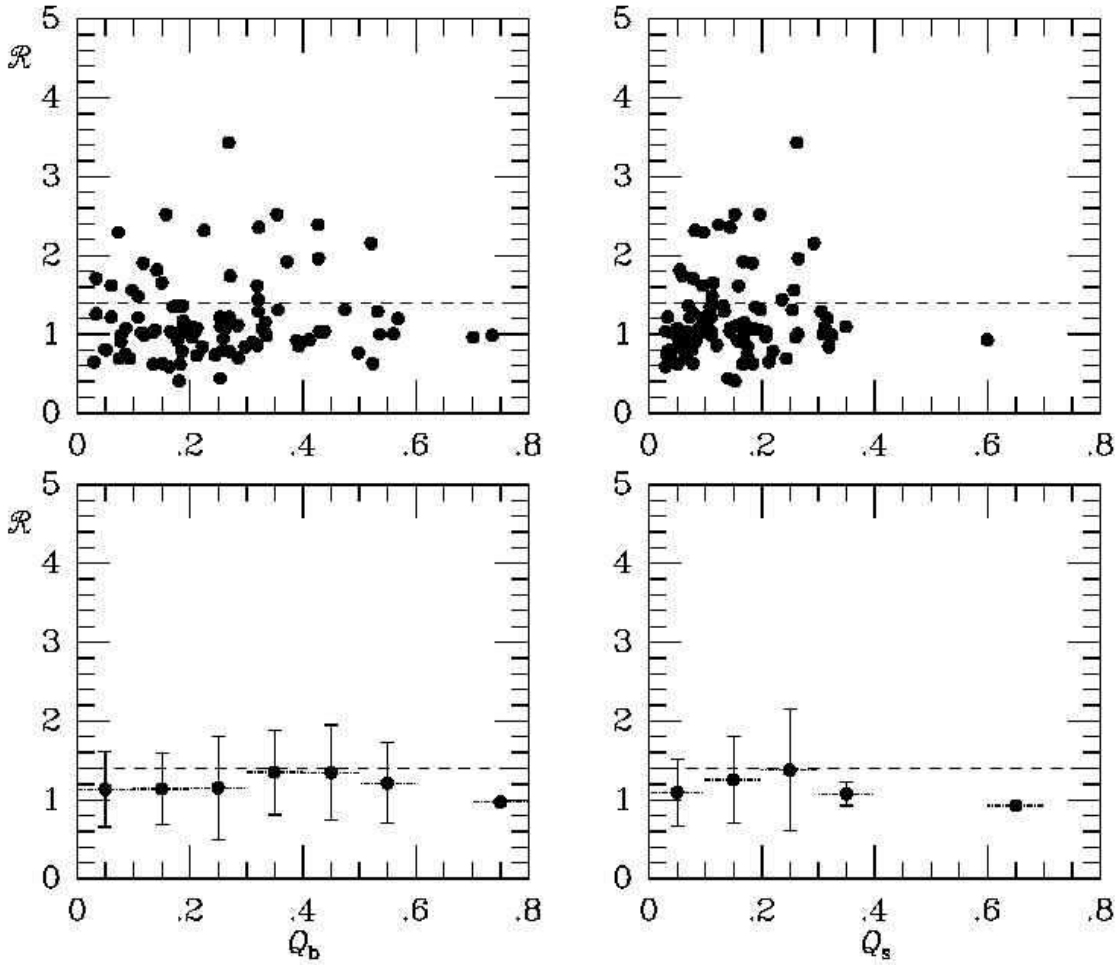

Fig. 5.— $\mathcal{R} = r(CR)/r(bar)$ versus bar and spiral torque strengths from Buta et al. (2005). Only the values for the asterisked radii in Table 1 were used for these plots. In the lower panels, the vertical lines are standard deviation error bars, while the short dotted horizontal lines simply indicate the range in Q_b and Q_s used for the averages. The dashed horizontal line is set at the value 1.4, used to delineate a boundary between fast and slow bars (Debattista & Sellwood 2000).

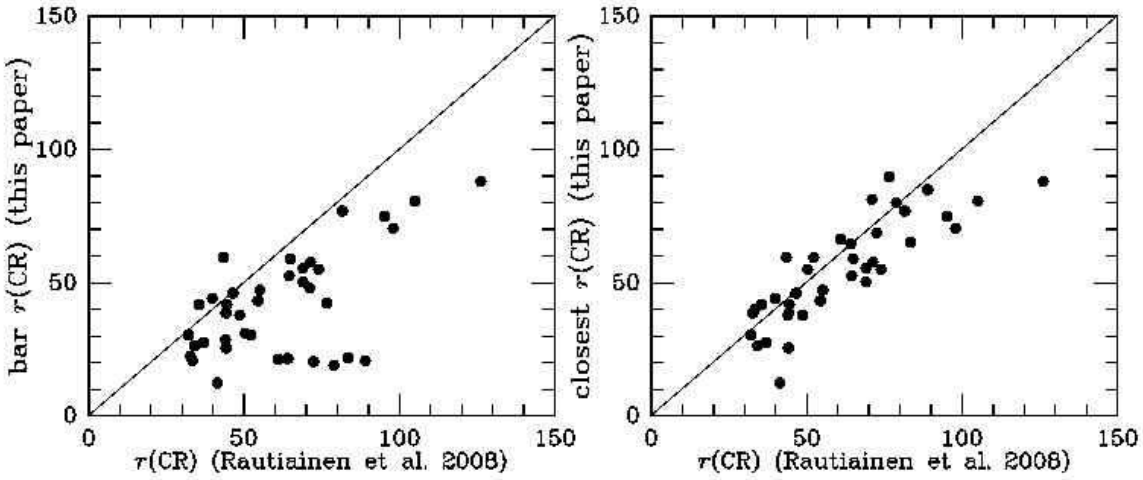

Fig. 6.— Comparisons of phase-shift method CR radii (in arcseconds) with those estimated from numerical simulations by RSL05/RSL08. (a) Comparison between our selected bar CR radii (Table 1, asterisked values) and theirs. (b) Comparison between the phaseshift CR radii closest in absolute value to theirs.

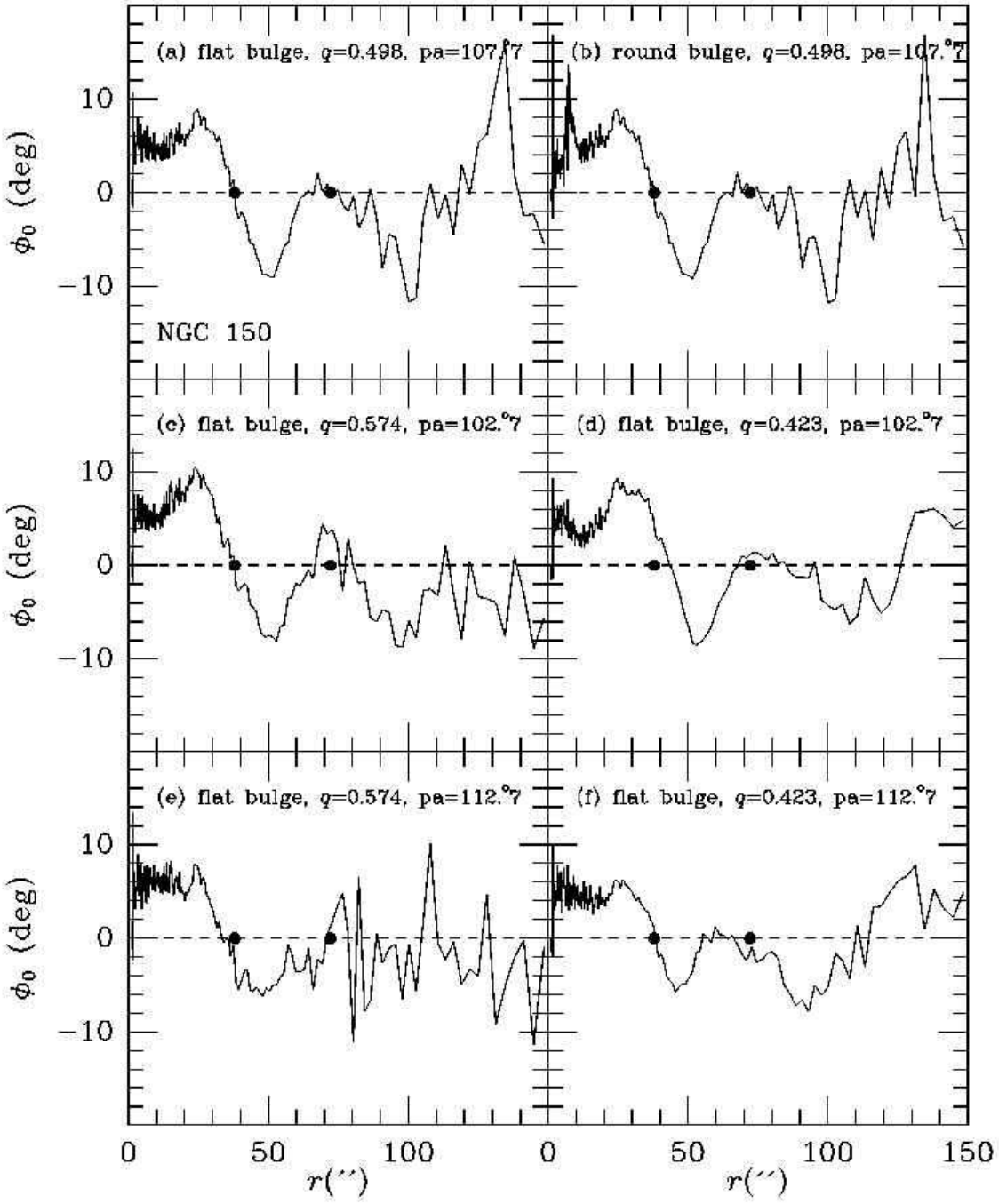

Fig. 7.— Phase-shift distribution for NGC 150 for different orientation parameters and assumed bulge flattenings, as indicated. For comparison, the solid circles show the CR radii from Table 1.

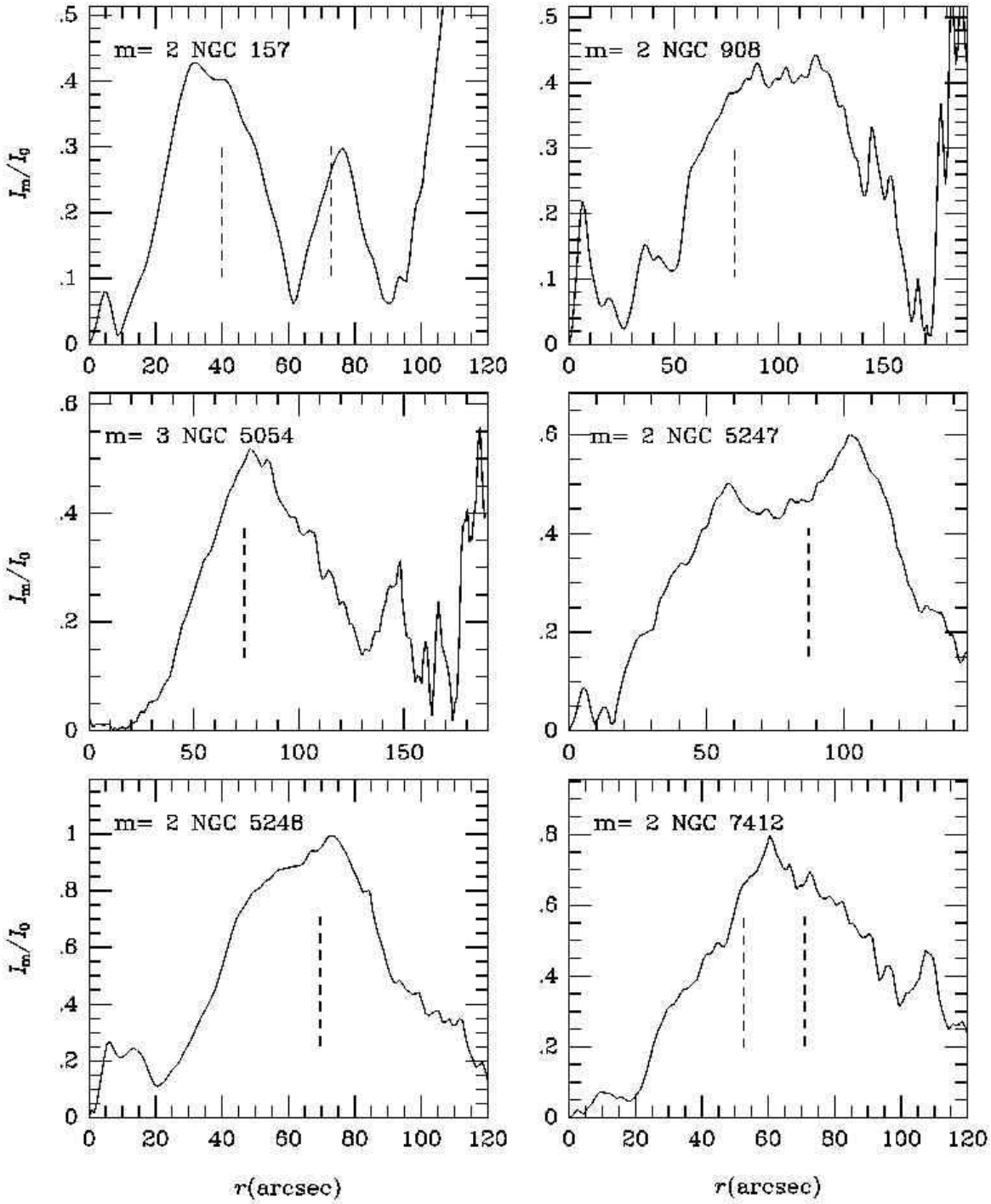

Fig. 8.— Plots of relative Fourier m=2 or 3 amplitudes for six grand-design spirals. The vertical dashed lines indicate the locations of main corotation radii based on phase-shift crossings.

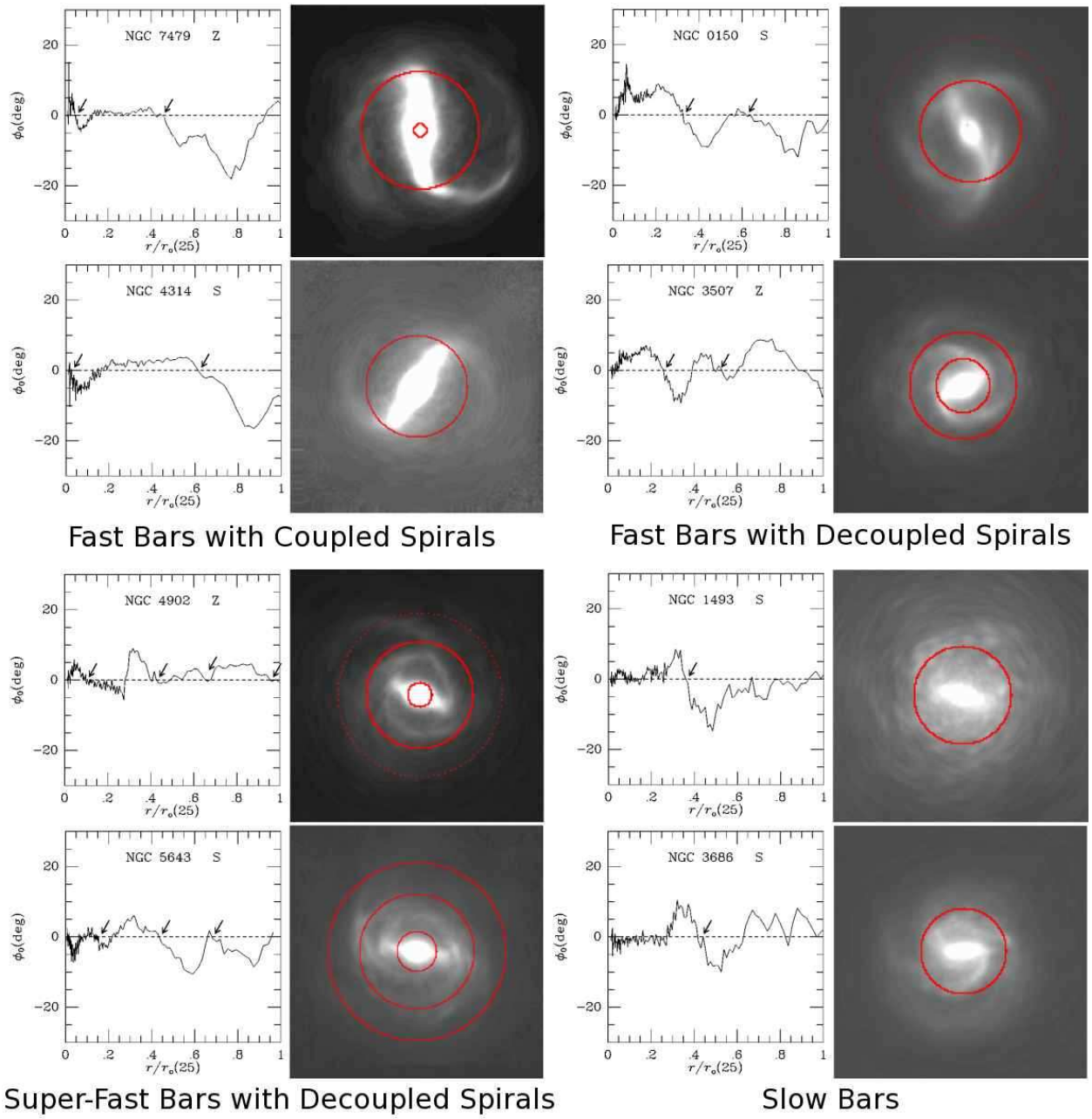

Fig. 9.— Montage showing examples of bars in different categories. Fast bars with coupled spirals are cases where the bar and spiral probably have the same pattern speed. Fast bars with decoupled spirals are cases where the bars extend to near their CR radius, but the spiral has a different CR radius. Super-fast bars with decoupled spirals are very unusual cases where the CR of the bar is likely to be well inside the ends of the bar. Slow bars are cases where $\mathcal{R} > 1.4$.